Mapping of NORMs and Heavy Metals in Central District (Botswana): Evaluation of Long-term Impact of Mining Activities on Water Quality of Letsibogo Dam

Machel Mashaba

orcid.org/0000-0001-7862-3804

Thesis submitted in fulfilment of the requirements for the degree *Doctor of Philosophy in Physics* at the North-West University

Promoter: Prof V.M Tshivhase

Co-promoter: Prof A Faanhof

Examination: August 2018

Student number: 16839609

Declaration

I hereby declare that this research thesis entitled, "Mapping of NORMs and Heavy Metals in Central District (Botswana): Evaluation of Long-term Impact of Mining Activities on Water Quality of Letsibogo Dam" is my own work, carried out at the Centre for Applied Radiation Science and Technology (CARST) at the North-West University, South Africa, between July 2015 and June 2018 under the guidance and supervision of Prof. V.M. Tshivhase and Prof. A. Faanhof for the degree of Doctor of Philosophy in Physics. This thesis has not been submitted for any degree at any other university or institution before, and all the sources of data used, have been fully indicated and duly acknowledged by means of complete references.

Full name: Machel Mashaba Date: June 2018

Signed: 

Acknowledgement

First of all I would like to express my deepest appreciation to several individuals who contributed to the development and success of this project. I wish to thank my promoter Prof Victor Tshivhase for his comprehensive scientific information and also for his guidance, support and encouragement throughout this work. Very special thanks also go to my co-promoter, Prof Arnaud Faanhof for his insightful extensive scientific knowledge, expertise, wisdom and being always available for guidance.

My sincere appreciation also go to the Centre for Applied Radiation Science and Technology (CARST) of North-West University (NWU) for providing me with a conducive nuclear practical research working environment. I am very much indebted to the University of Botswana (UB) for the financial support during my studies. Without the support of UB, this work could not have been possible. I would also like to thank the Eco-Analytica laboratory group of NWU for the analysis of the samples using ICP-MS. Many thanks to my PhD fellows and colleagues especially Mr. Thulani Dlamini for helping during measurements of the samples using gamma spectrometry. I am also very thankful to CARST staff members for their inspiring support especially Mr. Sam Thaga, CARST Administrative Officer, for the logistic support.

I would also like to acknowledge the locals of the study area for assisting with locating the sampling points since we were unfamiliar with the place especially Mr. Moeteledi Seaka for his voluntary efforts and also for helping with foodstuff and bucket dust sampling. I would like to express my gratitude to my family for the support and encouragement throughout this research journey. Above all I praise the Lord for giving me the strength and ability towards a successful completion of this research.

Abstract

The study was carried out in the central district of Botswana around Letsibogo dam and the surrounding communities of the new uranium mine. Mining has been identified as one of the main potential sources of exposure to naturally occurring radioactive materials (NORM) and heavy metals. All human activities within this area may lead to the rise of anthropogenic pollutants. NORMs and heavy metals in environmental samples are of crucial importance in the case of radiological impact studies in any environmental compartment. For this reason, valuable information is needed for the determination of NORMs and heavy metals in environmental samples to ascertain the level of natural and/or man-made radioactivity from a particular area and this requires accurate measurement techniques. The study was conducted with the aim of providing the baseline information on natural radioactivity and heavy metals in the central district of Botswana by evaluation of the long-term impact of mining activities on the water quality of Letsibogo dam and generate baseline data on environmental parameters that might affect radiological and toxicological health-related issues towards humans. In this investigation, identification and quantification of natural radioactivity and heavy metals in environmental samples were evaluated through the use of gamma spectrometry for the identification of the most likely nuclides that contribute to the activity of NORM-nuclides in environmental soil, sediments and vegetable samples, ICP-MS for the identification of heavy metals in all environmental samples and LSC for the quantitative determination of the gross α- and β-activities in water samples. The results were used to map the current level of NORMs and heavy metals in the study area. Some evaluations are made to the potential radiological and chemical hazard that the NORM-nuclides and heavy metals may impose on people living in the study area. The calculated absorbed dose values (D_R) in soil samples ranged from 23.5 ± 1.2 to 103 ± 6 nGy/h, with an average value of 62.3 ± 2.41 nGy/h, which is comparable to the worldwide average value of 59 nGy/h. The radium equivalent (Ra_{eq}) calculated varied from 41.0 ± 2.1 to 224 ± 11 Bq/kg with an average value of 134 ± 5 Bq/kg, which is well below the permissible limit of 370 Bq/kg. The average values of external hazard index (H_{ex}) and the annual effective dose equivalent (AEDE) for soil samples were found to be 0.360 ± 0.014 and 0.080 ± 0.003 mSv/y respectively, which are both below the permissible limit of 1 mSv/y. For foodstuff, the results revealed that the levels of radioactivity in almost food samples are insignificant and will not pose any radiological hazard from consumption except for ^{232}Th and ^{40}K which indicated elevated values in vegetable samples that are above the world average value of 290 μSv/y. The cancer risk for people living in the study area, as a result of heavy

metal in soil, water, foodstuff and dust was also evaluated. For non-carcinogenic risk, the HI values were found to be 1.5, 27.5 and 1.5 for As, Cr and Cu respectively. These values are greater than 1, which indicate a potential health risk of As, Cr and Cu to the residents of the study area. The ingestion pathway was the greatest contributor to non-carcinogenic risk with an HI value of 27.5 driven by Cr in food samples. For carcinogenic risk, the ingestion pathway was found to be the greatest contributor. Cr was observed to be the major contributor to the risk with a total cancer risk value of 4.1×10^{-2}, which is greater than the maximum permissible limit of 1×10^{-4}, indicating a potentially large carcinogenic risk. The gross-α and gross-β activity concentrations in the water samples were also evaluated. The results of this study show that all values of the gross-α and gross-β activity are below the WHO recommended guideline values of 0.5 and 1 Bq/l respectively. The results of this study will be used as a baseline for the surveillance of any possible change in the future.

Table of Contents

List of Figures

List of Tables

List of abbreviations

ADI	Average daily intake
AEDE	Annual effective dose equivalent
ASTM	The American Standard for Testing and Materials
CSF	Cancer slope factor
DCF	Dose conversion factor
DWAF	Department of water affairs (South Africa)
GPS	Geographical Positioning System
H_{ex}	External hazard index
H_{in}	Internal hazard index
HPGe	Hyper pure germanium
HQ	Hazard Quotient
H_T	Equivalent dose
IAEA	International Atomic Energy Agency
ICP-MS	Inductively Coupled Plasma-Mass Spectrometry
ICRP	International Commission for Radiological Protection
L_c	Critical level
L_D	Detection limit
LSC	Liquid scintillation counter
MCA	Multichannel analyser
MDA	Minimum detection activity
NORM	Naturally Occurring Radioactive Materials
PMT	Photomultiplier tube
PSA	Pulse Shape Analyser
Q-value	Decay energy
Ra_{eq}	Radium equivalent
RfD	Reference dose
SQP(E)	Quench parameter
TENORM	Technologically enhanced naturally occurring radioactive material
UNSCEAR	United Nations Scientific Committee on the effects of atomic radiation
USEPA	United States Environmental Protection Agency
WHO	World Health Organization
WRC	Water Research Commission (South Africa)

Chapter 1: Introduction

1.1 General background

Radionuclides and heavy metals are present naturally on the earth's crust (Friedlander, et al., 1981; Pöschl & Nollet, 2007). They are found on the earth's surface, in the soil, the atmosphere, water, building materials, and in plant and animal tissue (UNSCEAR, 2000). All living organisms including human beings are exposed to different radioactive sources and heavy metals subject to the surroundings thereof (APPEA, 2002; Ochiai, 2014; Jaishankar, et al., 2014). Due to natural evolution, all living organisms have adapted to certain amounts of radioactivity and heavy metals without suffering any harmful effects (Kovalchuk, et al., 2001). A major concern arises when certain human activities such as testing of nuclear weapons, mineral exploration, and agriculture significantly enhance exposures of humans and the environment to alarming levels of radioactivity and heavy metals (Ahmed & El-Arabi, 2005).

1.2 Impact of mining activities on the environment

Mining is an important activity that boosts the economies of many countries worldwide (Walser, 2002). However, it has the potential to disrupt and damage the environment by producing large quantities of waste that can have long term deleterious effects to humans and the environment. Hazards caused by mining activities include: land degradation, deforestation, ground and surface water pollution, air pollution, noise pollution, damage to forest flora and fauna, wildlife habitat destruction, and so forth (Ahanger, et al., 2014). Waste disposal of over burden, for example, can result in land degradation whilst the discharge of mine water and acid mine drainage can cause ground and surface water pollution (Sahu & Dash, 2011). Air pollution, on the other hand, can result from the release of toxic gaseous waste and dust (Sahu & Dash, 2011). Mining activities can thus pose a threat to the health of those individuals who are occupationally exposed and the members of the public who live in the vicinity of mining areas (Sahu & Dash, 2011).

Most mining activities utilise toxic chemicals to extract valuable minerals from their ores, and such chemicals include heavy metals like mercury (Hg) (Sahu & Dash, 2011). After the extraction of a mineral from its raw ore, the solid waste residues from the crushed ore and utilised chemicals are piled as tailings into large slime dams (Sahu & Dash, 2011). Acid mine drainage (AMD) can dissolve and transport harmful heavy metals like Hg, arsenic (As), and lead (Pb) from the mine tailings, underground tunnels and other openings (Sahu & Dash, 2011). Therefore, these toxic heavy metals may end up leaching into rivers and streams and hence

pose a threat to aquatic life and the health of human beings (MINEO, 2000). AMD emanates from the exposure of sulphide-bearing minerals like pyrites to oxygen and moist conditions (Jennings, et al., 2008). The most dominant component of AMD is sulphuric acid (Jennings, et al., 2008).

The fact that mining activities involve minerals that contain low levels of radioactive isotopes that become concentrated in mine tailings is well established (Pandey, et al., 2014). These isotopes can be released to the environment as dust through drilling, blasting, overburden loading and unloading, and transport materials (Sahu & Dash, 2011). The transport of these isotopes to the environment is enhanced when the dust gets blown off the mining sites by wind (Sahu & Dash, 2011). In this manner, mining activities lead to increases in concentrations of particulate air pollutants that deteriorate the quality of air in the atmosphere (Pandey, et al., 2014). The radioactive isotopes produced by mining activities can also leak into surface and ground water (Sahu & Dash, 2011. Once integrated into the ecosystem, the radioactive isotopes accumulate in agricultural soils, food crops and water thereby posing a potential health detriment (Sahu & Dash, 2011.

1.3 Natural sources of radionuclides and heavy metals

1.3.1 Naturally occurring radionuclides

Naturally occurring radioactive materials (NORMs) in the environment can be categorised into primordial and cosmogenic radionuclides (Pöschl & Nollet, 2007). Primordial radionuclides are also known as terrestrial radionuclides. They mainly arise from various levels of singly decaying isotopes like potassium-40 (^{40}K) and Rubidium-87 (^{87}Rb), and the decay daughters of Uranium-238 (^{238}U), Thorium-232 (^{232}Th), and Uranium-235 (^{235}U) (Pöschl & Nollet, 2007; UNSCEAR, 2000; Eisenbud & Gesell, 1997). Primordial radionuclides are believed to have been formed concurrently with the universe, and they are found predominantly on the earth's crust (Friedlander, et al., 1981; Watson, et al., 2005). They are long lived and have half-lives in the order of hundreds of millions of years, which makes their presence to be still detected in measurable quantities (Pöschl & Nollet, 2007; UNSCEAR, 2000; Baskaran, 2011). The most important radionuclides in the environment that may be of significance for radiological analysis are ^{238}U and its decay series, ^{232}Th and its decay series, and ^{40}K (Erdi-Krausz, et al., 2003).

Cosmogenic radionuclides are found mainly in the atmosphere and are induced by nuclear reactions that arise from cosmic radiation (Pöschl & Nollet, 2007; Lieser, 2008). They

comprise of radioactive isotopes of lighter elements and have considerably varied half-lives (Pöschl & Nollet, 2007; UNSCEAR, 2000). The primary components thereof are high-energy alpha (α)-particles and protons, which induce nuclear reactions when they impact on the nuclei of the atmospheric atoms (Cember & Johnson, 2009). Cosmogenic radionuclides are mostly attached to aerosol particles and get deposited on the ground (UNSCEAR, 2000). Examples of such radioactive nuclear species include radiocarbon (^{14}C) and tritium (^{3}H) (UNSCEAR, 2000). Otherwise, other cosmogenic radionuclides that have been identified are sodium-22 (^{22}Na) and beryllium-7 (^{7}Be) (Pöschl & Nollet, 2007). From a radiological point of view, the main cosmogenic radionuclides are ^{3}H, ^{7}Be, ^{14}C and ^{22}Na (Pöschl & Nollet, 2007; Watson, et al., 2005). The most significant of these is ^{14}C, which can be taken up by plants and enter the food chain (Pöschl & Nollet, 2007; Watson, et al., 2005).

Apart from primordial and cosmogenic radionuclides, there are other radionuclides such as; ^{137}Cs, ^{90}Sr, that do not occur naturally in the environment (Pöschl & Nollet, 2007). These arise from human activities such as the mining of uranium ores, nuclear reactor accidents, the testing of nuclear weapons, and the manufacture of radioisotopes (UNSCEAR, 2000). Such human activities may thus aggravate the presence of Technologically Enhanced Naturally Occurring Radioactive Materials (TENORMs) or anthropogenic sources (Pöschl & Nollet, 2007).

1.3.2 Heavy metals

Heavy metals belong to a group of metals that have been associated with environmental contamination and potential toxicity (Singh, et al., 2011). They include: copper (Cu), arsenic (As), mercury (Hg), cadmium (Cd), lead (Pb), zinc (Zn), and so on (Oladoye & Adewuyi, 2014; Singh, et al., 2011). Heavy metals comprise of elements that have atomic densities greater than $5g/cm^3$and they are a natural component of the earth's crust (Oladoye & Adewuyi, 2014; Duruibe, et al., 2007). With the assumption that heaviness and toxicity are inter-related, heavy metals can be harmful even at low levels of exposure (Tchounwou, et al., 2012). Ideally, their concentrations in natural environments would pose no threat to human life (Kamunda, 2016). However, anthropogenic or human activities such as mining have impacted significantly and caused environmental health detriments in the forms of pollution and contamination of surface soils and ground waters (Nazir, et al., 2015; Tchounwou, et al., 2012). These activities have led to a wide distribution of heavy metals in the environment, thereby increasing concerns over their possible effects on human health and the environment (Mahurpawar, 2015).

The accumulation of heavy metals and NORMs in the environment can propagate into food chains, which is a potential pathway to human exposure (Jeje & Oladepo, 2014; IAEA, 1989). NORM and heavy metal contaminations in aquatic systems, for example, can affect the quality of surface and ground waters, and hence restrict water usage and infiltrate food chains (IAEA, 1989). The uptake of NORMs and heavy metals by plants in terrestrial systems is the key route for contamination entering into the food chain (Zhuang, et al., 2009; IAEA, 1989). When NORMs and heavy metals accumulate in plants, for example, they can be ingested by animals and spread contamination to higher levels of the food chain (Jeje & Oladepo, 2014; Zhuang, et al., 2009; Fisher, 2005).

1.4 Rationale of this research

The exposure of human beings to environmental radioactivity and heavy metals is often complex (O'Brien & Cooper, 1998). A quantitative understanding of such exposure involves information from a wide variety of scientific displines such as radiation physics, biology, chemistry, meteorology, hydrology, and so forth (Eisenbud & Gesell, 1997). There are many ways by which human beings are exposed to environmental radioactivity (Saad, et al., 2014). The relevant routes of exposure to humans are internal ingestion of water and food as well as the inhalation of dust and aerosols (O'Brien & Cooper, 1998; Tchounwou, et al., 2012). Particles deposited on the Earth's surface can cause direct radiation exposure or even be resuspended by wind action and be inhaled or transpoterd to different locations depending on the wind's direction (Pöschl & Nollet, 2007). The environment is engulfed with physical, chemical and biological potential pathways that lead to its contamination (Faanu, 2011).

Mining activities are a potential source of exposure to NORMs and heavy metals (UNSCEAR, 2000). They yield large volumes of mine tailings that tend to contain enhanced levels of natural radionuclides (O'Brien & Cooper, 1998). Some of the NORMs and heavy metals contained in the mine tailings are soluble in water and have the tendency to leach into water bodies (Sahu & Dash, 2011). They also get carried away in the form of wind-blown dust to contaminate the environment (Sahu & Dash, 2011). Their presence in the environment can lead to radiation doses that may pose some health detriments from a radiological point of view (Till & Meyer, 1983). The discovery of uranium deposits in the Serule area in Botswana should thus be of concern. This area has been identified as a potential hub for the commercial extraction of uranium (IAEA & OECD, 2014). The radioactivity levels in enviromental matrices like drinking water bodies found in this area should be evaluated prior to, during and periodically

after the mining of the uranium to assess the associated health hazards posed to the public (Faanu, et al., 2016). The government of Botswana has already enacted plans to extract the uranium from the Serule area (IAEA & OECD, 2014). Should uranium mining finally take place in this area, which is about 40 km west from the Letsibogo dam, the radionuclide and heavy metal contamination of surface and ground water and the atmosphere is certain to occur (Till & Meyer, 1983).

Uranium isotopes such as ^{238}U, ^{234}U, and ^{235}U have a low level of radiation toxicity, but some of the daughter nuclides in the decay series of these isotopes and ^{232}Th are extremely toxic (Nwankwo, 2010; Ahmed, 2004). The most radiotoxic daughter nuclides are lead-210 (^{210}Pb) and polonium-210 (^{210}Po) both from ^{238}U decay series; protactinium-231 (^{231}Pa) and actinium-227 (^{227}Ac) from ^{235}U decay series; and radium-228 (^{228}Ra) from ^{232}Th decay series (Ahmed, 2004). The presence of these elements in environmental matrices like drinking water can be highly hazardous to humans, and requires particular attention (IAEA, 2003). An environmental radioactivity study for Letsibogo dam will thus yield baseline data that can be used to weigh the adverse effects of the proposed Serule mine and hence take remedial actions in advance. This dam supplies Gaborone, the capital of Botswana, as well as other major villages along the pipeline to Gaborone. Of yet another concern the copper-nickel mine that is located 25 km east of Letsibogo dam. This mine produces large volumes of tailings and waste that may also contain some heavy metals which may be transported to the dam either as a solution in water or as wind-blown dust (Till & Meyer, 1983; Ye, et al., 2011). It is thus crucial to have a comprehensive database of the level of NORMs and heavy metals of the Letsibogo dam to weigh their long term implications to the environment.

1.4.1 Previous studies relevant to this work

Several investigations have been carried out pertaining NORMS and heavy metals (Faanu, et al., 2016; Altıkulaç, et al., 2015; Sultana, et al., 2017). Most of these studies assessed the potential health risks thereof in soil, water, air and foodstuffs, and they provided data on the nature and levels of radioactivity in a particular area (Faanu, et al., 2016; Altıkulaç, et al., 2015; Sultana, et al., 2017).

One such study was carried out in Ghana to ascertain baseline radiation levels prior to the concession of the new mine (Faanu, et al., 2016). The study was based on gamma (γ) dose rate measurements by using γ-spectrometry to determine the activtiy concentration of radionuclides

of ^{238}U, ^{232}Th and ^{40}K in rock, soil, and ore samples, in addition to gross alpha/beta (α/β) analysis in water samples (Faanu, et al., 2016). The obtained results of the study were within the acceptable natural background radiation when compared with other studies and the total annual effective doses were less than 1 mSv. Another related study was undertaken in Nigeria to estimate the baseline data of natural radioactivity in soil, vegetation and water in the industrial district of the Federal Capital Territory (FCT) Abuja (Umar, et al., 2012). Results of this study revealed that there was a location within this disctrict that exceeded the world average activity concentration for ^{40}K in soil (Umar, et al., 2012). There was thus a potential health risk to the people who resided in this area (Umar, et al., 2012).

A preliminary study of gross α/β activity concentrations in drinking water was carried out in Albania (Cfarku, et al., 2014). The analyzed drinking water samples were found to be fit for human consumption (Cfarku, et al., 2014). Study results also complied well with World Health Organization (WHO) recommendations of less than 0.5 Bq/*l* for gross α and 1 Bq/*l* for gross β in drinking water (Cfarku, et al., 2014). Similar investigations on the concentrations of natural and artificial radionuclides in drinking water samples were also carried out in Turkey to evaluate the associated radiological hazards (Altıkulaç, et al., 2015). Results of this study showed that the annual effective doses from all water samples were below the individual dose criterion recommened by WHO (Altıkulaç, et al., 2015). This indicated that the water was safe for human consumption (Altıkulaç, et al., 2015).

Heavy metal concentrations in various vegetables were also investigated in Saudi Arabia (Ali & Al-Qahtani, 2012). Samples collected to assess the concentrations of Fe, Mn, Cu, Zn, Pb, Cd and Hg in four major industrial and urban cities in the Kingdom of Saudi Arabia revealed high levels compared to those recommended by a Joint FAO/WHO Committee on Food Additives (Ali & Al-Qahtani, 2012). This study also showed that more attention was needed towards monitoring toxic substances in farm food stuffs in order to assure food safety for consumers (Ali & Al-Qahtani, 2012). A similar study was conducted in Bangladesh to assess the health risk of heavy metals in vegetables and fruits (Sultana, et al., 2017). It was found that agricultural fields located near the industrial areas of Bangladesh suffered from various heavy metal pollution sources (Sultana, et al., 2017). It was concluded that the study area was not suitable for growing leafy and root vegetables due to the risk of higher heavy metal intakes if eaten (Sultana, et al., 2017).

A case study was undertaken in Keffi, North Central of Nigeria, to determine the level of heavy metals in water, fish and soil samples from the Antau river (Adewumi, et al., 2014). This study revealed that all of the samples were contaminated with high levels of Pb, Ni, Cr and Mn concentrations well above the acceptable limits specified by WHO (Adewumi, et al., 2014). The Antau river was found to be heavly polluted with heavy metals (Adewumi, et al., 2014). In a similar study, a radiological assessment of dam water and sediments for natural radioactivity was carried out in the Abeokuta area South-West of Nigeria (Ibikunle, et al., 2016). It transpired that there were very low possibilities of radiological hazard to human health from radioactivity in the sediments, though the water was unsafe for human consumption (Ibikunle, et al., 2016). The high radioactivity of the water was seen to have arised from the sediments and other sources such as radioactive waste disposal into rivers that fed the dam (Ibikunle, et al., 2016).

Knowledge of NORM and heavy metal concentrations and distributions in the environmemnt may help to provide useful information when assessing the associated health risks. Enhanced radioactivity levels in some environments can arise from discharges of radioactive nuclides and heavy metals by human activities (Carvalho, et al., 2007). It is thus crucial to consider all of the significant sources of radioactive nuclides and heavy metals in the environment. A determination of these radionuclides and heavy metals is essential to establish baseline data and predict possible future changes due to their presence in the environment (Ramli, 1997).

1.5 Research aims and objectives

1.5.1 Research aim

The aim of this study was to provide baseline information on natural radioactivity and heavy metals in the central district of Botswana for evaluation of the long-term impact of mining activities on the water quality of the Letsibogo dam and generate baseline data on environmental parameters that might affect radiological and toxicological health-related issues towards humans as a result of the mining activities

1.5.2 Research objectives

The objectives of this research work were to:

(i) determine the activity concentrations of NORMs and their progeny in soil, water, dust, and food samples obtained from the mining area in the central district of Botswana

(ii) determine the concentrations of heavy metals in soil, water, dust and food samples obtained from the mining area in the central district of Botswana

(iii) assess the potential risks to members of the public that reside in the vicinity of the mining area through radiological indices such as the absorbed dose rate and annual effective dose equivalent for the various exposure pathways

(iv) map the radiological properties of soil and water in a bid to establish areas that may be impacted by NORMs and heavy metals associated with mining, more especially the typical exposure pathways in remote communities reliant on surface and ground water, and

(v) study seasonal variations of the selected sample sources.

Chapter 2: Basic principles of radioactivity

2.1 Introduction

The 1895 discovery of X-rays by Wilhelm Conrad Roentgen was succeeded by that of radioactivity in the following years (Friedlander, et al., 1981; Saad, et al., 2014; Khoo, 1981). Since then, several scientists continued to study the radioactivity phenomena and discovered several elements that emit radiation when the nuclei of their atoms disintegrate or decay (Friedlander, et al., 1981). Such elements are said to be radioactive and they have unstable nuclei that try to change into stable forms by decaying or by emitting excess energy in the form of alpha (α), beta (β) and gamma (γ) radiation that results in the formation of the new nuclei (Friedlander, et al., 1981; Saad, et al., 2014). In this section, three primary decay types of interest to the current work, namely; α, β, and γ decays are discussed.

2.1.1 Alpha Decay

Alpha (α) particles are identified as the nucleus of the helium-4 isotope, consisting of two protons and two neutrons with no electron revolving around the nucleus (Knoll, 2000; Cember & Johnson, 2009). These particles are mostly emitted by naturally occurring radionuclides that have atomic number (Z) between 81 and 92 in which the initial nuclear parent loses its atomic mass number (A), mass and charge (A, Z) by 4 and 2 respectively to form a daughter nuclide (Ralph & Howard, 1955).

During the emission of these particles, energy is released in order for the decay to take place (Knoll, 2000; Cember & Johnson, 2009. The emitted α-particle energies are always high and range between ~4 and 10 MeV. The energy released during an α-decay process is called the decay energy Q-value and is equal to the difference in mass-energy between the parent nuclide and its progenies and appears as kinetic energy shared among all particles (Knoll, 2000).

An example of this type of decay is the decay of radium-226 (^{226}Ra) to form radon-222 (^{222}Rn) shown in equation 2.1 (Turner, 2007). The equation shows the change of A and Z and the Q-value of 4.87 MeV as indicated in equation 2.1.

$$^{226}_{88}Ra \rightarrow {}^{222}_{86}Rn + {}^{4}_{2}\alpha + 4.87MeV \qquad (2.1)$$

In addition to α-particle emissions, parent nuclides do not always decay directly to the ground state of the daughter product, but may have a probability of leaving the daughter nuclide in an excited state for certain α transitions, because their intensities bear a certain relation with one

another (Knoll, 2000). For most α-decaying nuclides, the highest energetic emission of these particles usually leaves the final product in the lowest energy state or the ground state. An α-decay that releases lower energy α-particles will leave the final product in an excited state (Cember & Johnson, 2009). As a result, the final daughter nuclide may reach the ground state by releasing the energy through the emission of γ-radiation (Cember & Johnson, 2009). To understand these energy and intensity considerations, one must understand the concept of radioactive decay schemes, which is a diagram of energy (vertical axis) against the proton number Z (horizontal axis) (Knoll, 2000). Figure 2.1 shows an α-decay scheme of ^{226}Ra to form ^{222}Rn. The figure shows the α-particle energy with the highest emission probability (94.4%) is at a Q-value of 4.785 MeV followed by 4.602 MeV (5.5%). It can then be seen in this figure that the γ-emission is due to transitions from the excited level at 0.186 MeV to the ground state of ^{222}Rn. The figure also shows the change of A and Z as indicated by equation 2.1.

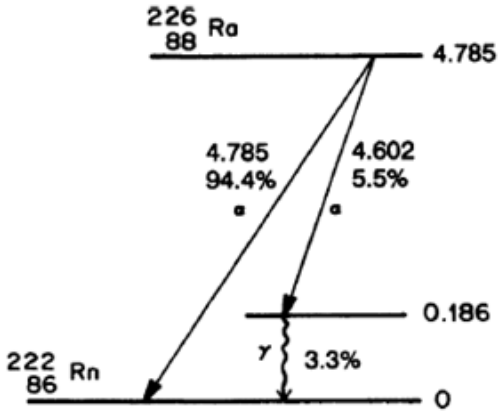

Figure 2.1: Schematic diagram of ^{226}Ra nuclear decay (Turner, 2007).

2.1.2 Beta Decay

Beta (β) particles are the most dominant mode of decay for lighter radionuclides (Lehto & Hou, 2011). These particles are much lighter compared to α-particles (Krane, 1988). In β-decay process, the mass number (*A*) remains unchanged but the atomic number (Z) and the neutron number (N) of the nucleus each change by one unit (Krane, 1988; Friedlander, et al., 1981). There are three forms of β-decay, namely; beta minus (β^-) decay, beta plus (or positron) (β^+) decay and electron capture (EC) (Krane, 1988).

2.1.2.1 Beta minus (β^-) decay

β- decay occurs for nuclides that have extra neutrons in the nucleus (Krane, 1988). In this process a neutron is converted into a proton (Krane, 1988). Both the atomic number (Z) and

the neutron number (N) change by one unit but retain the same mass number (A) (Ralph & Howard, 1955; Krane, 1988).

An example of this decay (β^--decay) is the decay of cobalt-60 (^{60}Co) to form nickel-60 (^{60}Ni) as shown in equation 2.2 (Turner, 2007). The equation clearly shows the constant A and the change of Z.

$$^{60}_{27}Co \rightarrow ^{60}_{28}Ni + ^{0}_{-1}\beta + \bar{\nu}_e \qquad (2.2)$$

The nuclear reaction in equation 2.2 can be represented by the decay scheme as shown in figure 2.2. The figure indicates that the main decay mode is by negative emission (β^-). The two arrows drawn slanting down to the right show the two modes of β^- decay along with the β^- particle energies. The slanting arrows are drawn towards the right to indicate the increase in atomic number (Z) by one unit that results from β^- decay. For α-decay and β^+ decay, the slanting arrows are drawn from right to left to indicate the decrease in atomic number (Z) (Turner, 2007). The figure also shows the two main β-decay transitions or two β^- end point energies. The first transition corresponds to the highest emission probability of 99+ % (strongest transition) of 0.318 MeV whereas the second corresponds to the highest β^- endpoint energy of 1.491 MeV on the decay scheme.

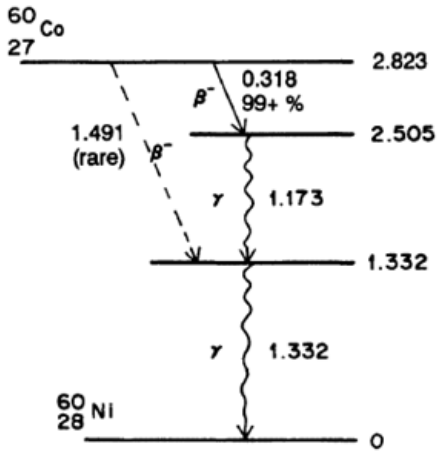

Figure 2.2: Schematic diagram of ^{60}Co nuclear emission to lower state (Turner, 2007).

2.1.2.2 Beta plus (β+) decay

β^+ decay is also called the positron (e^+) decay and is a weak interaction decay process. It occurs when the proton/neutron ratio is excessively higher than many stable isobar of that particular isobaric mass number (A) (Friedlander, et al., 1981). β^+ decay can occur only when the transformation energy is greater than 1.022 MeV. The mass of both the positron and electron

are converted to γ -rays each having the energy of 0.511 MeV (L'Annunziata, 2003). In this process, a proton is transformed into a neutron, positron and a neutrino. As a result, a nuclear charge (Z) is decreased by one unit.

An example of these decay (β^+ decay) is the decay process of $^{22}_{11}Na$ to form $^{22}_{10}Ne$ in equation 2.3. The equation shows a decrease in atomic number and a constant mass number.

$$^{22}_{11}Na \rightarrow {}^{22}_{10}Ne + \beta^+ + v_e \qquad (2.3)$$

The radioactive decay scheme of equation 2.3 is shown in Figure 2.3. The figure also shows a decrease in atomic number and a constant mass number, as well as the energy of 1.820 MeV greater than the energy (1.022 MeV) of the allowed transformation occurrence. The arrows are drawn slanting to left to indicate the decrease in atomic number (*Z*).

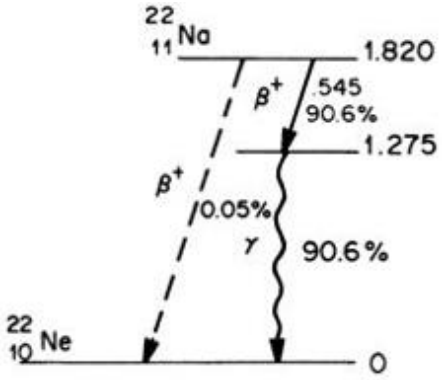

Figure 2.3: Decay scheme of ^{22}Na (Turner, 2007).

Unlike α-particles, which are monoenergetic or emitted with sharp and well defined energies from a given source, β-particles have a continuous distribution of energies ranging from zero up to the maximum allowed by the *Q*-value which is called the endpoint (E_{max}) (Krane, 1988). Figure 2.4 shows the different shaped spectra for continuous distribution of energy for both β^- emission and β^+ emission from a radioactive decay of ^{64}Cu from 0 up to the maximum allowed *Q*-value of 0.5782 MeV emitted from β^- particle and 0.6525MeV from β^+ particle.

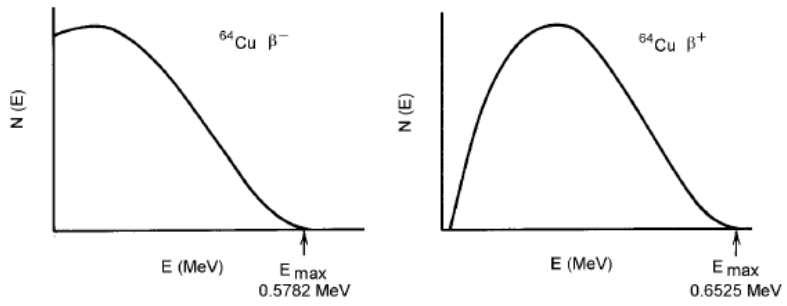

Figure 2.4: Continuous distribution of energy of β-particle from ^{64}Cu decay (Martin, 2013).

2.1.2.3 Electron Capture

In this process, the parent nucleus absorbs an electron from the innermost orbit and converts a proton into a neutron. Electron capture (EC) is an alternative decay process to β^+ decay and often competes with it when neutron to proton ratio is low (Krane, 1988). If a nuclide is unable to meet the energy requirements of β^+ decay, then the decay occurs by EC (Krane, 1988). The decay scheme for ^{22}Na in Figure 2.3 shows that 90% of the decay of ^{22}Na occurs by β^+ emission. The remaining 10% is by EC. ^{22}Na undergoes the EC process by going to a metastable state of the nucleus of ^{22}Ne at the energy of 1.275 MeV. Whenever a nuclide decays by EC, X-rays are always emitted. In EC, no particle is emitted, therefore EC produces undetectable energy from the nucleus (Harvey, 1962). Equation 2.4 (Krane, 1988) is an example of an EC process where no particle is emitted.

$$^{54}_{25}Mn + {}^{0}_{-1}e \rightarrow {}^{54}_{24}Cr + 0.835MeV \qquad (2.4)$$

2.1.3 Gamma Decay

Gamma (γ) radiation is a monochromatic electromagnetic radiation and has no electric charge (Cember & Johnson, 2009; L'Annunziata, 2003). The γ-decay occurs due to radioactive transition between various nuclear levels, resulting in the emission of γ-rays of discrete energy (Krane, 1988). Most of α and β decays leave the final nucleus in an excited state (Krane, 1988). These excited states can decay to a lower or more stable state by the emission of γ-rays (Krane, 1988). The energies of γ-rays cover a range of 0.1 to 10 MeV (Krane, 1988; Lilley, 2001).

An example of this decay (γ-decay) is the decay of ^{60}Co to form ^{60}Ni as shown in Figure 2.2. It can then be seen that γ-emission at 1,173 MeV is due to transitions from the excited level at 2.505 MeV to the level at 1.332 MeV following the most probable β^- emission of 0.318 MeV. Another γ-emission can be seen at 1.332 MeV due to transitions from the excited level at 1.332 MeV to the ground state of ^{60}Ni (Turner, 2007).

2.1.4 Internal conversion

There is another electromagnetic process that competes with γ-decay called internal conversion (IC) (Cember & Johnson, 2009). The IC process is always possible whenever γ-decay is possible (Krane, 1988). In an IC process, the excitation energy does not result in the emission of a photon but instead the electromagnetic multipole fields of the nucleus interact with the orbital electrons and cause one of the electrons to be ejected from the atom (Krane, 1988). For this reason, electrons resulting from IC are different from the β- particles because they are

newly created in the decay process itself (Krane, 1988). The amount of energy given to the emitted electron is nearly equal to the difference between the energy of the transition involved and the binding energy of the electron in the atom (Cember & Johnson, 2009; Turner, 2007).

An example of IC is the decay of Cesium-137 (^{137}Cs) to form Barium-137 (^{137}Ba) plus a β-particle (Martin, 2013). Figure 2.5 illustrates a simplified IC decay of ^{137}Cs through a metastable ^{137m}Ba. The figure indicates that 94.4 % of the emission probability goes to an excited state of ^{137m}Ba of 0.6617 MeV. The excited ^{137m}Ba then emits γ-rays in 90.1% of emissions with a Q-value of 0.6617 MeV and 7.66% by IC from the K shell electrons (Martin, 2013).

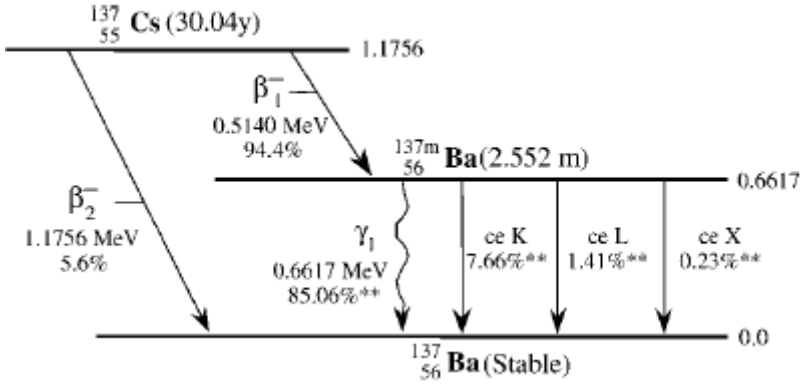

Figure 2.5: IC of ^{137m}Ba in the radioactive decay of ^{137}Cs through ^{137m}Ba to ^{137}Ba (Martin, 2013).

The IC process can be related to γ-decay process by the IC coefficient (α) which is defined by equation 2.5 (Cember & Johnson, 2009; Krane, 1988);

$$\alpha = \frac{N_e}{N_\gamma} \tag{2.5}$$

where; N_e is the rate of conversion electrons and N_γ is the rate of γ-ray emission observed from a decaying nucleus. The IC coefficient values depend on the multipolarity, transition energy and atomic number (Krane, 1988). It also depends on the multipolarity increasing rapidly with increasing multipole order (l) (Krane, 1988) and decreasing with increasing transition energy (ΔE) (Turner, 2007; Krane, 1988).

2.2 Branching ratio

Some nuclides may decay through one single mode to a final state, and some may undergo different radioactive competitive processes to reach final state. There is always some

probability of multiple decay modes taking place simultaneously (Krane, 1988). In branched decay, a parent nuclide has a probability of decaying to more than one daughter nuclear species (Krane, 1988). The relative probability of decay to each type of daughter is called a branching ratio (Krane, 1988). An example of this is the decay of ^{40}K as shown in Figure 2.6 (Pradler, et al., 2013). This has a 10.75 % probability of decay to argon-40 (^{40}Ar) by β^+ and by EC, 89.25 % of decays go to calcium-40 (^{40}Ca) by β^- decay.

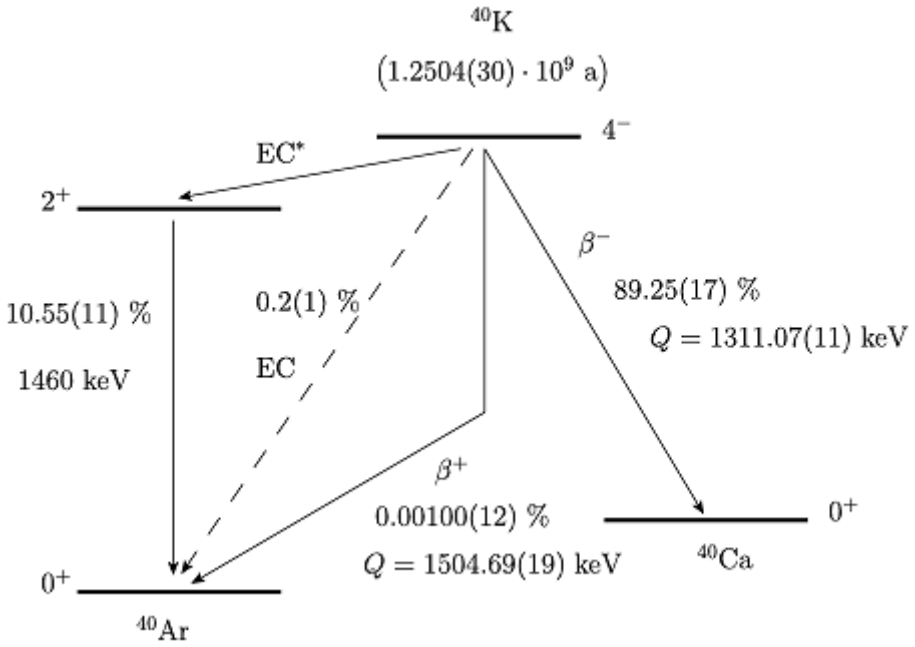

Figure 2.6: Schematic diagram of ^{40}K nuclear decay to daughter nuclides ^{40}Ar and ^{40}Ca (Pradler, et al., 2013).

2.3 Radioactive Decay Rate

In section 2.1, radioactive transformation modes has been discussed. The types of particles emitted and the released energy during decay process are very important for radiation protection because they determine the level of radiation available to cause radiation effects (Cember & Johnson, 2009). Similarly, an important concept to these transformation modes is the strength / activity of the radioactive sample or source which is the rate of decay or the number of nuclei decaying per unit time (L'Annunziata, 2003; Turner, 2007). The probability of a nucleus decaying per unit time is called the decay constant (λ) and if there are a number of nuclei (N) decaying in a sample, the activity of the radioactive sample is calculated by equation 2.6. (Knoll, 2000; Lilley, 2001; Turner, 2007). The unit of activity is the Becquerel (Bq), which is one disintegration per second (Knoll, 2000).

$$A = \frac{dN}{dt} = -\lambda N \tag{2.6}$$

where, the negative sign indicates that N is decreasing with time. If the nucleus decays to other several different states, then (λ) is the sum of the decay probabilities of all states, expressed in equation

$$N = N_0 e^{-\lambda t} \tag{2.7}$$

where N_0 is the number of nuclei present at time $t = 0$. Another useful term for radionuclide decay rate is the half-life ($T_{1/2}$) (Turner, 2007), equation 2.8, and is expressed in-terms (λ). The half-life is defined as the time required for a radionuclide to lose half of its activity (Harvey, 1962) as indicated in Figure 2.7.

$$T_{1/2} = \frac{ln\, 2}{\lambda} \tag{2.8}$$

If the Activity (A) concentration of a radioactive sample is proportional to the number of atoms present, then activity can be represented by equation 2.9, where (A_0) is the activity at time (t = 0).

$$A = A_0 e^{-\lambda t} \tag{2.9}$$

Figure 2.7, illustrates schematically how the activity decays exponentially as a function of time (Turner, 2007). The function of equation 2.9 (Activity) is plotted against the function of equation 2.8 (half-life) in Figure. 2.7, to illustrate how the activity of the radionuclide drops by factors of one-half, as shown by the figure. T represent the half-life.

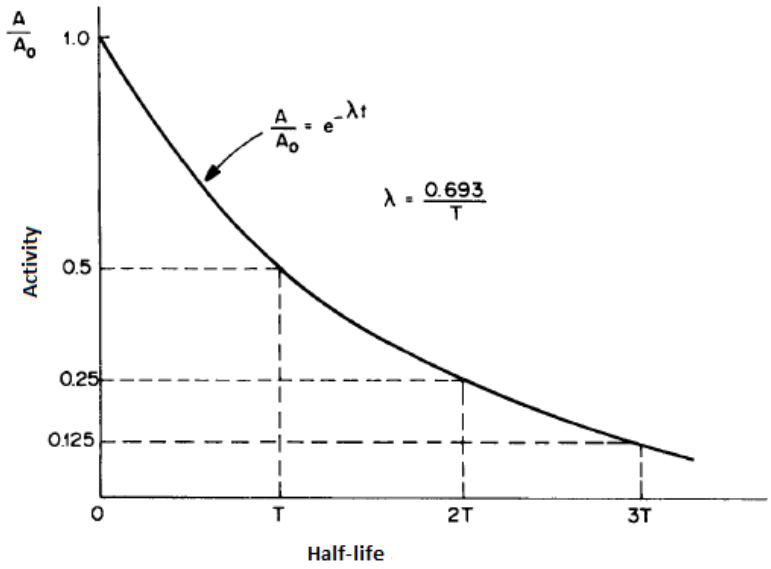

Figure 2.7: Proportion of activity remaining as a function of time (Turner, 2007).

2.4 Radioactive Decay Series

Some radioactive parent nuclides decay directly to a stable daughter nuclide with a simple single decay process (L'Annunziata, 2003). An example is the decay process of ^{36}Cl to form a stable ^{16}Ar daughter nuclide as shown in equation 2.10,

$$^{36}_{17}Cl \rightarrow {}^{36}_{18}Ar + {}^{0}_{-1}\beta + \bar{\nu}_e \tag{2.10}$$

For a more complicated radioactive decay series in which the original parent radioactive nuclide decays to form a daughter nuclide, and the daughter nuclide also decays to form another nuclide, the sequence continues until the last stable nuclide is reached at the end of the series (Krane, 1988) (See Table 2.1, 2.2, 2.3, in section 2.6). The result is a complicated decay series. These relationship between an initial parent nuclide decaying to a second, third, and so on to the last stable daughter nuclide as in equation 2.11 form various decay constants as λ_1, λ_2 and (Krane, 1988; Evans, 1955)

$$1 \xrightarrow{\lambda_1} 2 \xrightarrow{\lambda_2} 3 \tag{2.11}$$

From equation 2.6, the parent nuclei number (N) decreases with time (Krane, 1988). The number of daughter nuclei increases as a result of decay of the parent and decreases as a result of its own (Krane, 1988; Cetnar, 2006);

$$dN_2 = \lambda_1 N_1 dt - \lambda_2 N_2 dt \tag{2.12}$$

The number of initial parent nuclei can then be calculated from equation 2.7. Equation 2.12 can then be solved by using the initial condition of a second daughter $N_2(0)=0$ to become; (Friedlander, et al., 1981; Martin, 2013)

$$N_2 = N_1^0 \frac{\lambda_1}{\lambda_2 - \lambda_1}\left(e^{-\lambda_1 t} - e^{-\lambda_2 t}\right) \tag{2.13}$$

For the last daughter nuclides or last numerous nuclides such as $N_4, N_5 \ldots N_n$, the parent nuclide is so long lived that it decays at a constant rate then the number nuclei for the last nuclei is obtained by equation 2.14 (Friedlander, et al., 1981; Martin, 2013);

$$N_n = C_1 e^{-\lambda_1 t} + C_2 e^{-\lambda_2 t} + \ldots C_n e^{-\lambda_n t}, \tag{2.14}$$

Where

$$C_1 = \frac{\lambda_1 \lambda_2 \ldots \lambda_{n-1}}{(\lambda_2 - \lambda_1)(\lambda_3 - \lambda_1)\ldots(\lambda_n - \lambda_1)} N_1^0, \qquad C_2 = \frac{\lambda_1 \lambda_2 \ldots \lambda_{n-1}}{(\lambda_1 - \lambda_2)(\lambda_3 - \lambda_2)\ldots(\lambda_n - \lambda_2)} N_1^0, \text{ and}$$

$$C_n = \frac{\lambda_1 \lambda_2 \ldots \lambda_{n-1}}{(\lambda_1 - \lambda_n)(\lambda_2 - \lambda_n)\ldots(\lambda_{n-1} - \lambda_n)} N_1^0$$

2.5 Radioactive Equilibrium

The term radioactive equilibrium is normally used to describe the condition of relative activity of a radioactive parent nuclide and its radioactive daughter products as they decay in a decay series (Prince, 1979). There are three conditions of radioactive equilibrium, namely; secular, transient and non-equilibrium (Turner, 2007). During the decay process, the amount of activity varies for each stage of equilibrium condition (Turner, 2007).

2.5.1 Secular equilibrium

Secular equilibrium is a condition where the radioactive parent nuclide half-life is much longer than that of the daughter nuclides $\left(T_{1/2}[1] >> T_{1/2}[2]\right)$ (Cember & Johnson, 2009; Turner, 2007). An example is the decay of ^{226}Ra with a half-life of 1600 years to ^{222}Rn with half-life of 3.82 days in ^{238}U decay series (Cember & Johnson, 2009).

In this condition, the daughter nuclide decays more rapidly than the parent nuclide and reaches secular equilibrium after ~7$T_{1/2}$ as indicated in Figure 2.8. Figure 2.8 shows the activity (A_2) of the relatively short-lived daughter nuclide $\left(T_{1/2}[1] >> T_{1/2}[2]\right)$ as a function of time with the initial activity condition of, (for example if N_{20} represents the number of atoms of a daughter nuclide or nuclide 2), then $A_{20} = 0$. Activity of the daughter nuclide builds up to that of a parent nuclide in above ~7$T_{1/2}$. Thereafter the daughter nuclide decays at the same rate as it is produced, and secular equilibrium is reached. When secular equilibrium is reached, the parent nuclide and all its emerging daughter nuclides have the same activity; $A_1 = A_2$ (Cember & Johnson, 2009; Turner, 2007).

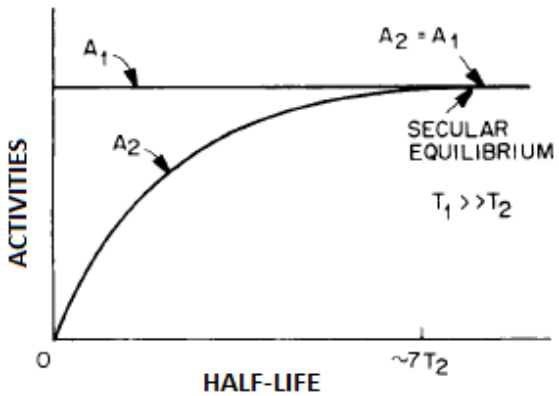

Figure 2.8: Schematic diagram of secular equilibrium (Turner, 2007).

2.5.2 Transient equilibrium

Transient equilibrium occurs when the parent nuclide has a slightly longer half-life than the daughter nuclide $\left(T_{1/2}[1] > T_{1/2}[2]\right)$ (L'Annunziata, 2003). This condition is reached when the half-life of the parent is approximately 10 times greater than the half-life of the daughter. For example, ^{212}Pb with half-life of 10.64 hours decays to ^{212}Bi which has a half-life of 60.55 minutes. Figure 2.9 is an example of a transient equilibrium (Turner, 2007). The Figure shows activities as functions of time when $T_{1/2}[1]$ is slightly greater than $T_{1/2}[2]$ $\left(T_{1/2}[1] \geq T_{1/2}[2]\right)$ (Turner, 2007). Activity of the daughter nuclide builds up to that of a parent nuclide (Turner, 2007). Transient equilibrium is finally reached, in which all activities decay with the half-life $T_{1/2}$ of the parent nuclide (Turner, 2007). Accordingly, the daughter nuclide activity is always higher than that of the parent nuclide after transient equilibrium attainment (Johansson, 1976).

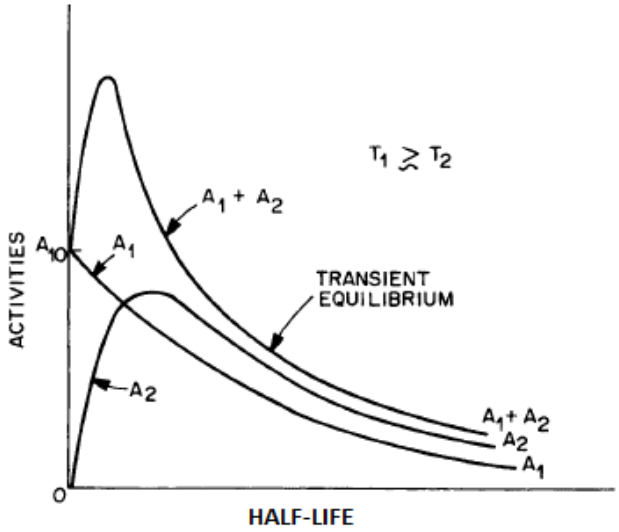

Figure 2.9: Schematic diagram of transient equilibrium (Turner, 2007).

2.5.3 Non-equilibrium state

The non-equilibrium state occurs when the daughter nuclide has a longer half-life than that of the parent nuclide $\left(T_{1/2}[1] < T_{1/2}[2]\right)$ (Turner, 2007). An example is the decay of ^{218}Po with a half-life of 3.1 minutes to ^{214}Pb which has a half-life of 26.8 minutes; hence the parent nuclide (^{218}Po) will decay faster, leaving behind the daughter nuclide (^{214}Pb) alone to decay at its specific half-life (Cember & Johnson, 2009). An example of the non-equilibrium state is shown in Figure 2.10. This Figure shows activities as functions of time when $T_{1/2}[2]$ is greater than

$T_{1/2}[1]$, $(T_{1/2}[1] < T_{1/2}[2])$. No radioactive equilibrium is attained. Lastly, only the daughter nuclide activity remains (Krane, 1988).

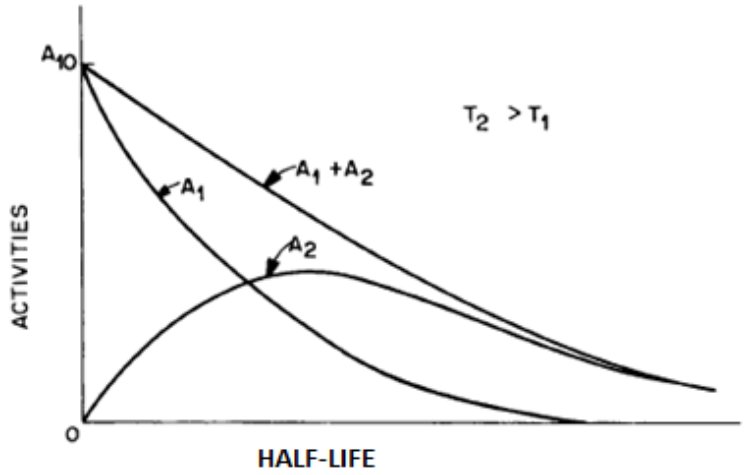

Figure 2.10: Schematic diagram of the state of no equilibrium (Turner, 2007).

2.6 Decay details of the Uranium and Thorium series

The heavy naturally occurring radioelements can be divided into three radioactive decay series namely; Uranium, Thorium, and Actinium series (Lilley, 2001; Martin, 2013). These decay series are found in nature and account for most of the NORMs of primordial (terrestrial) origin (Martin, 2013). They are led by the heavy isotopes of uranium (U) and thorium (Th), and have a wide range of half-lives that are long relative to the age of the earth and finally reach a stable isotope of lead (Pb) at the end of the decay series (Martin, 2013). The decay schemes of three radioactive series and the details of each radionuclide within the series are shown in Table G1 to G3 in annexure G.

2.7 Interaction of Radiation with Matter

The interaction of radiation with matter or medium is very important especially for the determination of biological effects (damage in the cellular Deoxyribonucleic acid, DNA) due to ionizing radiation, or for medical uses of ionizing radiation etc (Turner, 2007). When ionizing radiation (energetic charged particles (α, β particles) and photons (γ-rays)) pass through the medium or matter, they lose energy by ionizing the matter or by exciting the matter(Turner, 2007). To detect the type of ionizing radiation, ionizing radiation has to interact with a matter of a detector (Turner, 2007). This section summarizes how α, β particles and γ-rays interact with matter.

2.7.1 α-particle Interactions

Alpha (α)-particles can interact with either nuclei or orbital electrons in any absorbing medium such as air, water, tissue or metal (Knoll, 2000). They react strongly with matter because they are relatively heavy when compared to the other particles and have a charge, producing many ions per unit length of their path (Lilley, 2001). These particles do not scatter with medium atoms and their path is direct. As a result, they lose all of their energy within a very short distance (Lilley, 2001). The range of α-particles in air is only for few centimetres even the most energetic of these particles. For example, an α-particles with an energy of 5 MeV will only travel about 3.6 cm in air and 0.0033cm in water (Lehto, 2017; Mittal, 2016). For those α-particles observed in nature, the range in air varies between about 4 and 10 cm (Krane, 1988).

2.7.2 β-particle Interactions

In principle, the process of losing energy by ionization and excitation of medium atoms in α-particles is the same as for β-particles, but the different is that β-particles range is much larger than that of α-particles making them more penetrating than α-particles. These particles are small in size compared to α-particles, and hence the probability of collision per unit length of their path is lower compared to α-particles. As noted in section 2.7.1 the range of 5 MeV α-particles is 3.6 cm in air, a β-particle with an energy of 3.5 MeV (< 5 MeV of α-particles) will travel about 11m in air much greater than α-particles. In β-radiation, each particle track varies very much from one particle to another unlike in α-particles where particle track is straightforward.

There are other interaction processes involved in β-radiation such as Bremsstrahlung and Cherenkov radiation. Bremsstrahlung is the electromagnetic energy that is generated when an electron interacts with the electric field of an atomic nucleus. The energy of a β-particle decreases by the amount of energy of the generated photon. At higher β-energies the proportion of energy loss by bremsstrahlung increases. The proportion of energy loss of β-radiation for the emission of bremsstrahlung is, however, very small. For example, only 1% of the energy of the 1 MeV β-particles is absorbed (e.g. in aluminium) for the emission of bremsstrahlung and the remaining almost exclusively by ionization and excitation.

Cherenkov radiation is a blue light, created by a β-particle travelling through the medium at a speed faster than that of light. In water, β-particle energy must be at least 263 keV to exceed the speed of light. In the absorption of β-radiation energy the formation of Cherenkov radiation

forms only a small fraction, less than 0.1%. Cherenkov radiation may, however, be used to measure high energy (E_{max} >700 keV) β-radiation with a liquid scintillation counter.

2.7.3 γ-ray Interactions

β and α particles continue to lose their energies until all of their energy is transferred to the absorbing medium (Knoll, 2000; Attix, 1986). On the other hand, the energy of γ-rays cannot be completely absorbed as they travel long distances. Their energies can only reduce exponentially in intensity. The interaction of γ-rays with matter involves several distinct processes, but only three major mechanisms play an important role in interactions with γ-ray detectors to transfer their energy partially to the absorbing / detecting medium (Knoll, 2000; Attix, 1986). These three most significant γ-ray interaction mechanisms include photoelectric absorption, Compton scattering, and pair production (Knoll, 2000; Attix, 1986).

2.7.3.1 Photoelectric Effect

In the photoelectric effect, a photon undergoes an interaction with the absorber / detector medium atoms in which the photon is totally absorbed. As a result, an energetic photoelectron is ejected by the atom in its place (Knoll, 2000; Attix, 1986). If the energy for γ-rays is sufficient enough, the photoelectron is likely to originate from the most tightly inner orbit of the atom. The schematic diagram of the photoelectric absorption mechanism is illustrated in Figure 2.11. The incoming photon of energy hv is clearly shown interacting with an atomic shell electron bound to an atom with binding energy E_b. The photon disappears, giving a kinetic energy of $E_{e^-} = hv - E_b$ to the electron (Lilley, 2001).

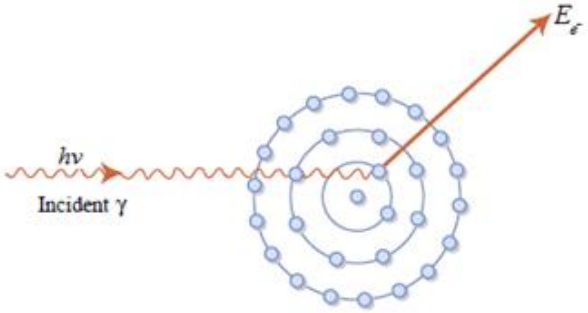

Figure 2.11: Schematic diagram of Photoelectric effect process (Pillalamarri, 2005).

2.7.3.2 Compton Effect

The process of Compton scattering occurs when the interaction takes place between the incident γ-ray photon and weakly bound or free electron in the absorbing material. The incoming γ-ray photon of energy *hv* from the left interact with an electron bound to an atom creating an electron known as a recoil electron, with an amount of kinetic energy *E* and also deflected through an angle θ with respect to its original direction. Figure 2.12 illustrates the Compton scattering process. The Compton process is most important for energy ranging from 100 keV to 10MeV.

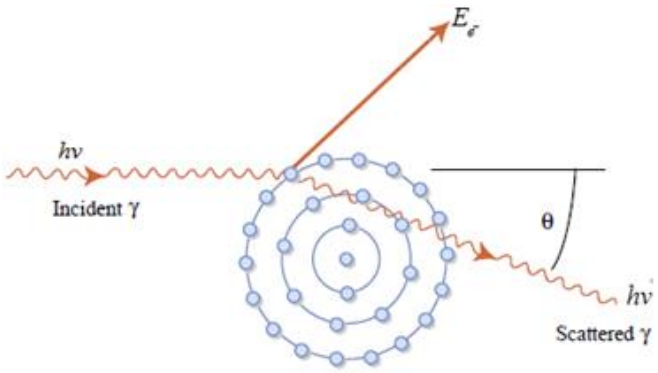

Figure 2.12: Schematic diagram of Compton scattering process (Pillalamarri, 2005).

The energy loss during this process depends on the scattering angle θ of the γ-radiation on the electron. The energies of the scattered photon (*hv'*) and recoil electron (E_e) are related to the angles at which they are emitted, given by equation 2.15 and 2.16; (L'Annunziata, 2003)

$$hv' = \frac{hv}{1+(hv/m_ec^2)(1-cos\,\theta)} \tag{2.15}$$

$$E_e. = hv - hv' = \frac{(hv')^2(1-cos\,\theta)}{m_ec^2+hv(1-cos\,\theta)} \tag{2.16}$$

Where; *hv* is the incident γ-ray photon energy, hv^- is the energy of scattered γ-ray photon, θ is the scattering angle and m_ec^2 is the electron rest mass energy, 511 keV.

2.7.3.3 Pair Production

In a pair production process, the interaction becomes more significant when incident γ-ray energies exceed 1.022 MeV. The interaction of the incident γ-ray photon disappears resulting in the formation of electron-positron pair in its place (Knoll, 2000). Since electron-positron pair formation requires a γ-ray energy photon of 1.022 MeV, any γ-ray energy carried in by γ-ray energy photons exceeding the value of 1.022 MeV, is imparted to and shared equally by

the positron and the electron, and the total kinetic energy of the electron-positron pair is given as, (Turner, 2007)

$$E_{e^-} + E_{e^+} = hv - 2m_0c^2, \tag{2.17}$$

Where E_{e^-} and E_{e^+} are the kinetic energies of the partners, and hv is the photon energy.
After the formation of electron-positron pair, the electron and positron can travel through the medium / detector before losing their kinetic energy in the absorbing material /detector. The positron can then annihilate with another electron in the absorbing material / detector to produce two 511 keV γ –ray photons emitted at 180 degrees to one another. Figure 2.13 illustrates the schematic diagram of the pair production process. The pair production process is most important for energy above 10MeV.

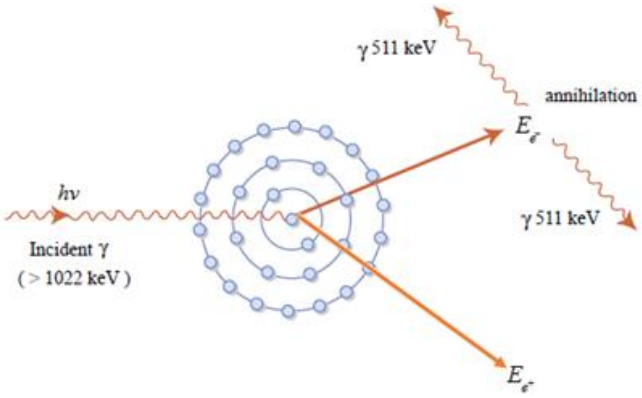

Figure 2.13: Schematic diagram of pair production process (Pillalamarri, 2005).

The interaction of these three mechanisms both depend on the photon energy ($E_\gamma = hv$) and the atomic number Z of the absorber / detection medium (Attix, 1986). Figure 2.14 shows the regions of photon energy and atomic number in which each interaction mechanism predominates. The curves show the values of photon energy and atomic number for which the two neighbouring effects are equally probable. The curves also indicate that photoelectric effect is dominant at lower photon energies while Compton Effect and pair production takes over at medium and higher energies respectively.

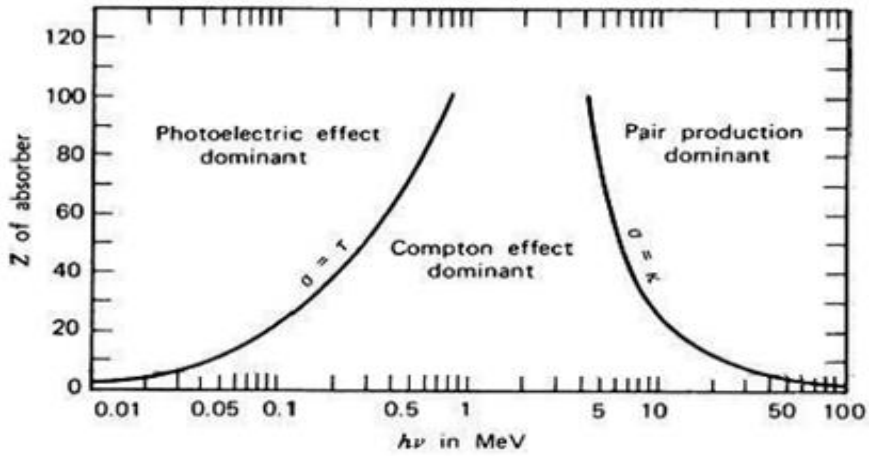

Figure 2.14: Three γ-ray interaction mechanisms and their regions of dominance (Krane, 1988).

2.8 Radiation detection

The detection and measurement of radiation are based on the interactions of α/β-particles and γ-rays emitted in radioactive decay with the detector materials. There are many types of interaction processes, as discussed earlier in section 2.7, but the most predominant processes in radiation detection and measurements are ionization and excitation. The electrons obtained in ionization are amplified to observe pulses representing individual decay processes. In the case of excitation, light is formed in de-excitation process. These light photons are transformed into electrons, which are further amplified to detectable electric pulses. In both cases the pulse rate is proportional to the decay rate and typically the pulse height to the energy of the detected particle or ray. Thus, each pulse obtained from the radiation measurement system represents individual radioactive decay event and the pulse height the energy of detected particle or ray.

There are two methods used to measure radionuclide activities namely radiometric and mass spectrometric. The radiometric method is applied in measurement and detection of radiation emitted by a certain radionuclide whereas the mass spectrometric method is based on counting the number of atoms. The results of these two methods, activity concentration (A) in case of radiometry and number of radioactive atoms (N) in mass spectrometry, can be related to each other by the fundamental law of radioactive decay as indicated in equation 2.6, section 2.3.

There are three types of materials used for radiometric methods (radiation detectors) namely; gas, liquid scintillation and solid material. The exposure of both α/β-particles and γ-rays leads to the production of electrons in this materials.

2.8.1 Gas filled Detectors

Most ionization radiation detectors use electric field to separate ions from recombining with the electrons and count the ions or electrons formed due to the passage of radiation through the detector (Krane, 1988). A gas filled detector can be described as a chamber filled with ionizable gas (for example Kr, Xe, Ar etc.) to which a suitable electrical voltage is applied to produce pulse height that is proportional to the energy of a particular particle (α,β or γ-rays) that passes through the gas (Martin, 2013). Figure 2.15 is a schematic diagram of a gas filled detector indicating a γ-ray path through the gas.

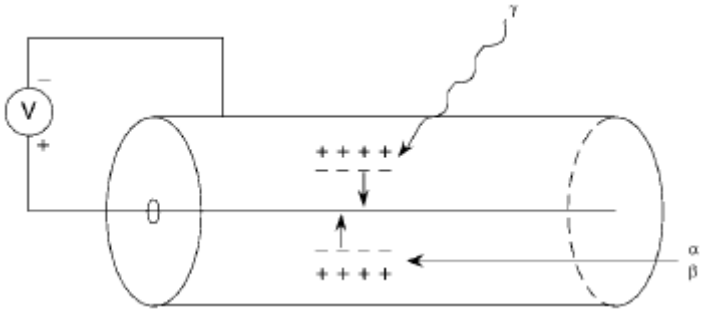

Figure 2.15: Schematic diagram of gas filled detectors (Martin, 2013).

Depending on the electrical voltage applied across the chamber, there are three types of Gas filled detectors namely; ionization chamber, proportional counter, and Geiger counter (Martin, 2013). Ionization chambers operate at very low electric field strength up to about 200 volts. As the electric field is slightly increased to few hundred volts, the region of proportional counter is reached and this counter operates up to electric field of about 700 Volts. When the electric field is further increased to higher voltage, Geiger–Mueller (GM) region is reached. In the GM region the field near the anode is so strong that any initial ionization of the gas results in a pulse and the size being independent of the number of initial ion pairs. Most of these detectors are widely used in measurement of β-radiation especially Proportional and Geiger counters (Martin, 2013).

2.8.2 Scintillation detectors

Some materials, known as scintillators, have the property of flashing light when they absorb ionizing radiation. A scintillator is basically a material that exhibits flashing of light when it absorbs ionizing radiation. These materials, when struck by an energetic incoming α / β particle or γ-ray, absorb its energy and re-emit the absorbed energy in the form of light. The light flashes

are too small to be visualized. A scintillation detector can therefore be used to detect the level of radiation.

A scintillation detector is obtained when a scintillator is coupled to a sensitive light detector such as a photomultiplier tube (PMT). The light flash is detected / absorbed by PMTs. In a PMT (Figure 2.16), the light photon falls on the photocathode of the PMT and releases electrons from the cathode which are then accelerated to a dynode held at an electric field of roughly thousands volts applied across the tube with an incremental biasing of 10V, 100V, 1000V, 10 000V , 100 000V and 1 000 000V. On striking the first dynode, electrons are multiplied by a certain factor and then accelerated to the second dynode. These in turn are multiplied sequentially until the last dynode is reached producing a pulse of millions of electrons that are collected at the anode at the end of the tube. The subsequent multiplication of electrons are converted into an electrical pulse which can be analysed and yields meaningful information about the particle that originally struck the scintillator.

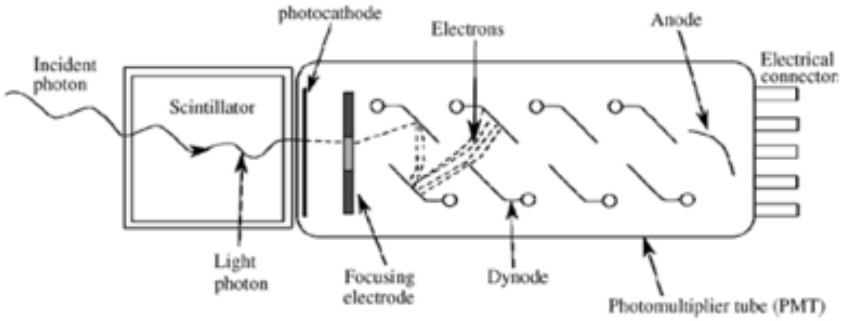

Figure 2.16: Photomultiplier tube coupled to a scintillation detector (Turner, 2007; Lehto & Hou, 2011).

2.8.2.1 Types of Scintillators

There are two types of scintillation detectors namely; inorganic and organic scintillators. The scintillation mechanism for these two types are different.

Inorganic scintillator

Inorganic scintillators are most applicable to the measurement of γ-ray emitting radionuclides. Inorganic scintillator detectors used in γ-detectors are made up of solid transparent crystalline material such as sodium iodide (NaI) containing a small amount of thallium used as a scintillator for the detection of γ-rays. When these detectors are exposed to ionizing radiation, the radiation interacts with the crystal and deposits its energy in that crystal material. Some of

the atoms in the crystal material that absorb energy are ionized, producing free electrons and areas lacking electrons called holes trap free electrons and lock them through the crystal lattice. Heating the crystal causes the lattice to vibrate and release the trapped electrons in the process. The released electrons are lifted from the valence to the conduction band (excited band) releasing the captured energy from ionizing as light. The light is then counted using PMTs.

Organic scintillator

There are various types of organic scintillators such as pure organic crystals, liquid organic solutions and plastic scintillators. Anthracene and stilbene for example, are the most common materials used for organic crystalline scintillators. Anthracene organic materials used for scintillation purposes have the highest efficiency of any organic material while stilbene has a lower efficiency but preferred when PSA is to be used to distinguish different particles emitted by an individual sample. Liquid scintillators are used to count radioactive material that can be dissolved in scintillator solution. A scintillator solution is made of a solvent that dissolves the sample and absorbs the energy of α and β particles or γ-rays. This technique is mostly used for counting low level α-β activities with counting efficiency of nearly 100%. Organic scintillators can also be polymerized to form a solid plastic.

2.8.3 Solid state material (semiconductor detectors)

Solid-state detectors based on semiconductor diode structures are mostly used for γ- and α-spectrometric measurements in radionuclide identification and activity measurement of radionuclides from samples having several γ- and α-emitting nuclides. These detectors are diodes made either of silicon (Si) or germanium (Ge) materials. Silicon is used mainly in α-detectors because of a short range absorption of energy and interfering γ-rays can easily penetrate the detector. Germanium is mainly used in γ-detectors because of the ability to absorb the energy of the very penetrating γ-rays.

The function of semiconductor detectors in principle is based on the electrical properties of Ge and Si. Both of these semiconductor materials (Ge and Si) have got 4 electrons in the valence shell and for them to complete the valence shell they have to share the electrons with the other elements to form four covalent bonds with neighboring atoms of the other elements. All the electrons participating in the conduction band and the valence band would show a filled valence band and an empty conduction band.

Certain impurity materials called dopants are introduced into the semiconductor (Ge and Si) during manufacturing to complete the valence shell of the semiconductor materials. In the doping process, atoms with valence 3 or 5 such as boron (B), phosphorus (P) are used. In the case of a phosphorus atom, which has got 5 electrons in the valence shell, incorporating its atoms into that of Ge or Si, four of the electrons will form covalent bonds with neighboring Ge or Si atoms and the fifth electron from the phosphorus valance shell will easily be excited into the conduction band and form electron donor state or level just below the conduction band. Impurities that behave in this way are called donor impurity. Ge or Si containing extra electrons or donor impurities are called n-type semiconductors (n-for negative) because of the mobile extra negative charge carriers or electrons. A schematic diagram of this situation is shown in Figure 2.17. The dashes represent a normal valence electron involved in a covalent bond.

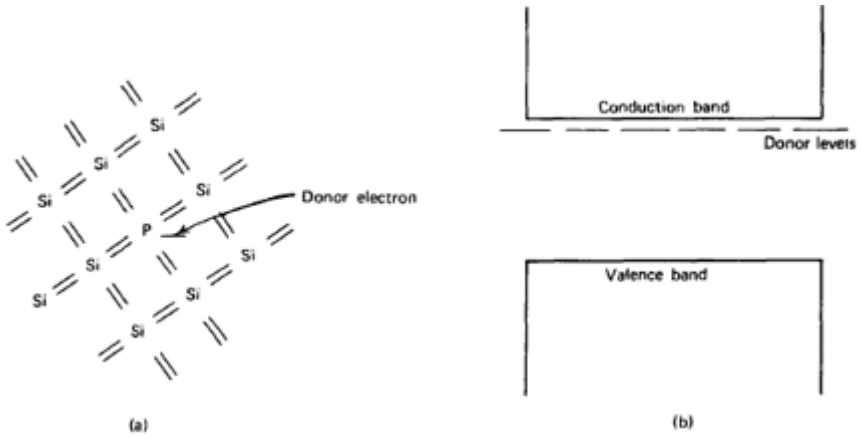

Figure 2.17: (a) Example of an n-type semiconductor (phosphorus donor impurity occupying a substitutional site in a silicon material), (b) donor level created close to the conduction band in the silicon (Knoll, 2000).

Alternatively, doping with valence 3 atoms (Boron atom) to form covalent bonds with four neighboring atoms of Ge or Si will produce a hole in the valence band which is also mobile. The baron valence shell requires an extra electron to complete the covalent bonds with the neighboring atoms of Ge or Si. This hole may be filled by an electron from the bottom valence band, creating another hole in the valence band. The electron that fills the hole caused by boron atom will occupy an energy level just above the valence band as shown in Figure 2.18. These impurity (boron) is called an acceptor impurity. Ge or Si containing missing electrons or acceptor impurities are called p-type semiconductors (p for positive) because boron atoms are effectively a positive charge carrier.

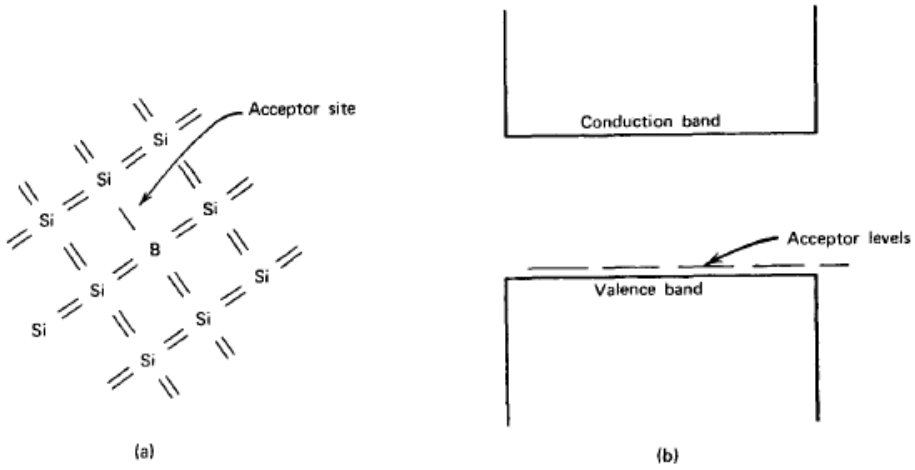

Figure 2.18: (a) Example of a p-type semiconductor (Boron acceptor impurity occupying a substitutional site in a silicon material), (b) Corresponding acceptor level created close to the valence band in the silicon (Knoll, 2000).

When the p-type and the n-type materials are attached together, and the reverse bias electric field is applied across the system, the electrons from the n-type material move across the junction into the p-type material and combine with the holes in the vicinity of the junction neutralizing the charge carriers as shown in Figure 2.19. When radiation (γ-ray or α-particle) interact with the sensitive part of the detector causing ionization through the junction region, electron–hole pairs are formed in the region and the system becomes conducting. The semiconductor is very similar in principle to an ionization chamber. The electric field then produces an electric pulse that can be amplified with an amplifier and converted to a digital form in an analog-to-digital converter (ADC) unit and place the signal according to its specific energy per channel with Multi-channel analyser (MCA). The electric pulse is directly proportional to the energy of γ-ray or α-particle. When used, germanium detectors must be cooled to liquid nitrogen temperatures to reduce electric noise which would considerably increase the background (Knoll, 2000).

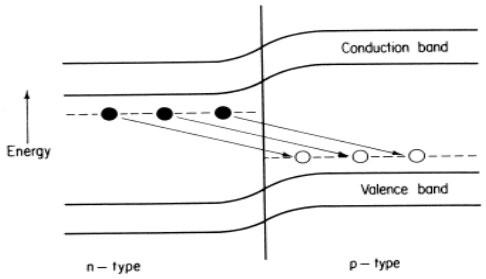

Figure 2.19: Schematic view and function of a p-n junction of a semiconductor detector (Oregon State University , 2017)

2.8.4 Measurement of radionuclides with Mass Spectrometry (ICP-MS)

The alternative method of radiometric for the determination of radionuclide activities is the mass spectrometry (Lehto & Hou, 2011). As mentioned earlier in section 2.8, this technique is based on counting the number of atoms or the measurement of the mass of an element (Vanhaecke & Degryse, 2012; Montaser, 1998). The most widely used instrument today for this purpose is the inductively-coupled plasma mass spectrometry (ICP-MS). The components of this instrument are shown in Figure 2.20. The ICP-MS system combines two techniques; An ICP technique with high sensitivity and good accuracy for ion generation and a low detection limit of quadrupole mass spectrometer (MS) for the separation and detection of these ions (Chajduk, et al., 2012; Montaser, 1998). Instruments designed for ICP-MS consist of many similar components like nebulizer, spray chamber, plasma torch, interface and detector, but differ fundamentally in the design of the mass spectrometer and in particular the mass separation device. Generally, the principle of ICP-MS technique can be subdivided into five parts: (i) sample introduction, (ii) ICP torch (iii) interface, (iv) MS and (v) ion detection (Montaser, 1998).

In ICP-MS, samples in liquid form are introduced into a nebulizer, where samples are transformed into a fine mist (aerosol) with argon gas before being introduced into the ICP. The fine droplets of aerosol then pass into a spray chamber and the spray chamber filters out the larger ones. The fine aerosol produced via nebulation further passes into high temperature ICP to generate positive charged ions (Lehto & Hou, 2011). The newly formed ions then travel through the interface region into the mass spectrometer. After passing through the interface region, the ions are directed by the ion optics into the mass separation analyser. The number of ions emerging from the mass analyzer is finally counted by a counter. The detector converts the ions into electrical pulses, which are processed by the data handling system to obtain the final concentration of elements through ICP-MS calibration standards (Thomas, 2004).

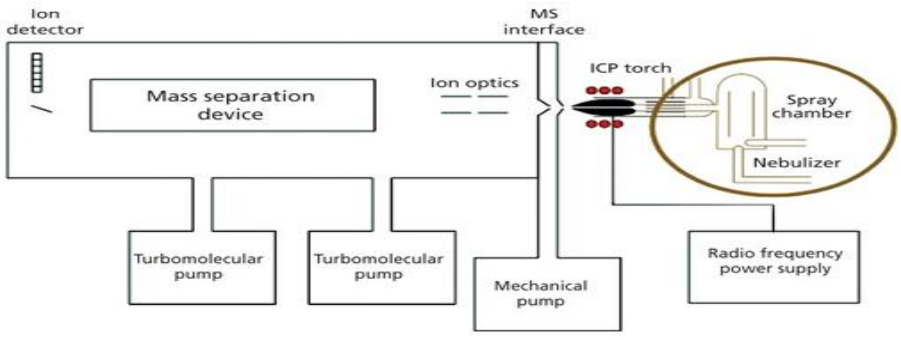

Figure 2.20: Schematic diagram of an ICP-MS instrument (Lehto & Hou, 2011).

Chapter 3: Experimental procedure

3.1 Introduction

In this chapter, the location of the study area, sample collection procedures, sample preparation methods and analysis methods to determine NORMs and heavy metals in all samples are discussed.

3.2 Description of the study area

The study was carried out in Letsibogo dam which is located in the central district of Botswana and the surrounding communities of the initiated uranium mine; Serule, Gojwane, Sese, and Damochojenaa villages. The study area covers a large area of the central district as shown by the area in Figure 3.1. The study area is rural in nature and is representative of natural open grasslands and mopane trees. The area is relatively flat with a slight slope to the east. A map of the study area (Figure 3.1) shows a uranium deposit next to Serule and Gojwane villages. The accumulation of radioactive materials and heavy metals can occur in soils and waters through erosion from the uranium deposits.

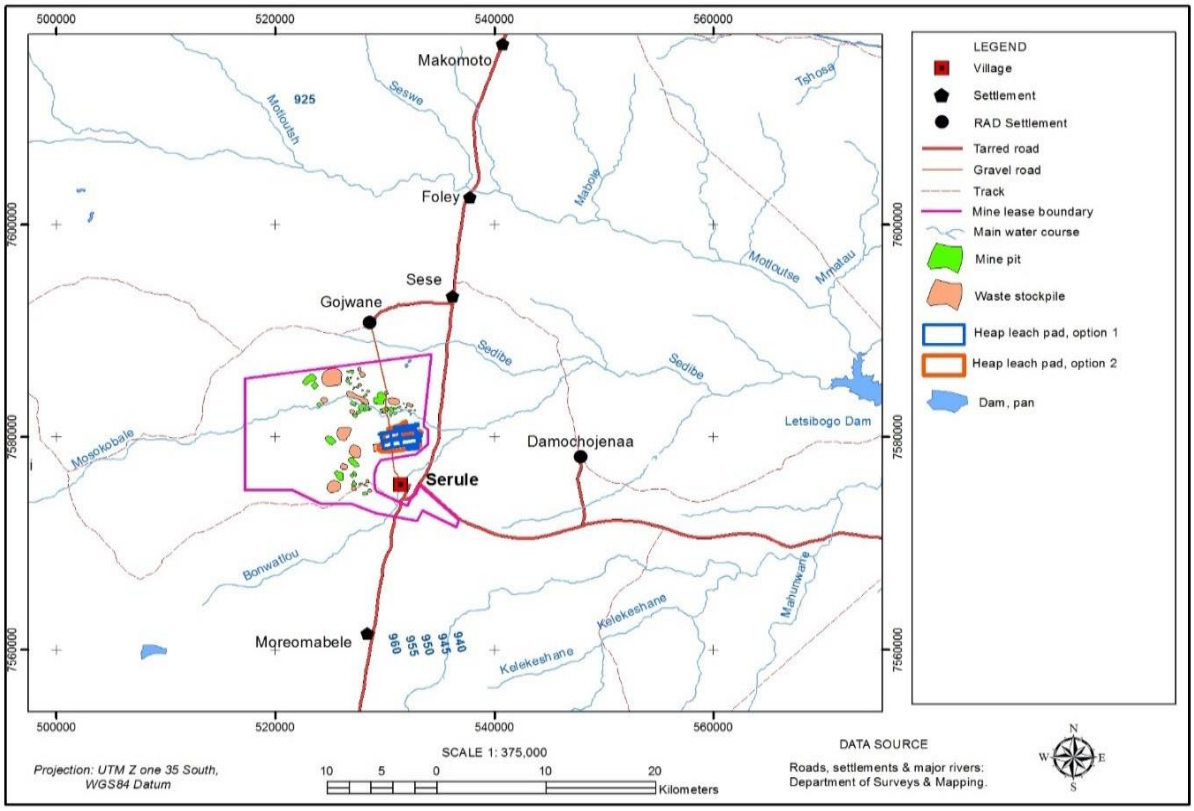

Figure 3.1: Map of sampling area showing initiated mine next to Serule and Gojwane villages (Tego, 2017).

3.3 Climate

The climatic conditions of the study area can be categorized into three seasons; (1) a hot and rainy season with sub-tropical thunderstorms from November to March, (2) a cool season from April to August and (3) a hot dry season with practically no rain from September to November (Likuku, et al., 2013). The winds are mainly predominant from the south-easterly quadrant in all seasons (Likuku, et al., 2013).

3.4 Economic Activities in the Area

The residents of these villages (Serule, Gojwane, Sese and Damochojenaa) are mostly farmers that depend much on agricultural activities especially subsistence farming. Chou Moellier, Essex Rape (Brassica napus) vegetables etc. are amongst the largely grown vegetables for own consumption and sale purposes. The rainfall in this area is generally unreliable and the area is subject to drought seasons. The water sources are therefore very scarce. Due to lack of alternative water sources the villagers, mainly farmers at cattle posts, use groundwater taken from hand-dug wells for drinking and domestic purposes. Since the wells are hand-dug, they are shallow with a depth ranging from approximately less than a metre to 10 m. The water is used without any treatment method. These wells are not regulated, no prior assessment is carried out to determine the suitability of the water for human use hence potentially putting the population at risk. The wells in many instances are uncovered while a few are closed and fitted with a hand pump. Figure 3.2 is an example of a hand-dug well inside the Sedibe River.

Figure 3.2: Hand-dug well in the Sedibe non-perennial river, Botswana.

3.5 Selection of the Study Area

The Letsibogo dam is located in an area with intense human activities. A map of the sampling area (Figure 3.1) shows uranium deposit next to Serule, Gojwane and Sese villages. These villages are also characterized mostly by catchment degradation, poor farming methods leading to soil erosion and siltation into water bodies and so forth. All human activities within this area may lead to anthropogenic pollutants being transported in the streams, rivers and other community or private drainage water systems; either dissolved in water or attached to suspended matter and eventually gets into the Letsibogo dam. In addition, the ground water flow indicates the direction from the proposed uranium mining area in the direction of the Letsibogo Dam, which is one of the main water sources for Gaborone (Capital city of Botswana) and many more along the pipeline. Also the Mosokobale and Bonwatloa rivers pass the initiated mine area on their way to the dam. This can cause elevated levels of NORMs and heavy metals in particular areas and potentially affect people who reside in these areas. Therefore, the entire region between the mining area up to the Letsibogo dam was chosen for this study.

3.6 Sample collection

In order to evaluate the levels of NORMs and heavy metals in the study area, different environmental samples were collected at random positions from different selected locations. The sampling frequency was divided into three seasons; (1) a hot and rainy season (March), (2) a cool season (August) and (3) a hot dry season with practically no rain (November) as indicated in section 3.3. During a field survey, five sampling sites namely Letsibogo dam, Serule, Gojwane, Sese and Damochojenaa villages were identified (Figure 3.1). But for the soil samples, some of these sites were combined and divided into three regions; the upper, middle and lower regions. The lower and middle regions had one site each (Letsibogo dam and Damochojenaa village as well as Damochojenaa surrounding cattle posts), while the upper region had three sites (Serule, Gojwane, Sese villages and their surrounding cattle posts). The five sampling sites were chosen to represent different sub basins that drain into the dam in order to understand the influence of natural and human activities on the dam (Figure 3.1). The sampling points for soil, water, sediments and dust samples are shown in Figure 3.3. The sampling points were selected based on the accessibility within the study area. It was difficult to reach some of the initially intended sampling points due to nonexistence of tracks to reach

them. The sampling points/coordinates of soil, sediments, water and dust samples are presented in Tables D1, D2, D3, and D4 respectively, in annexure D.

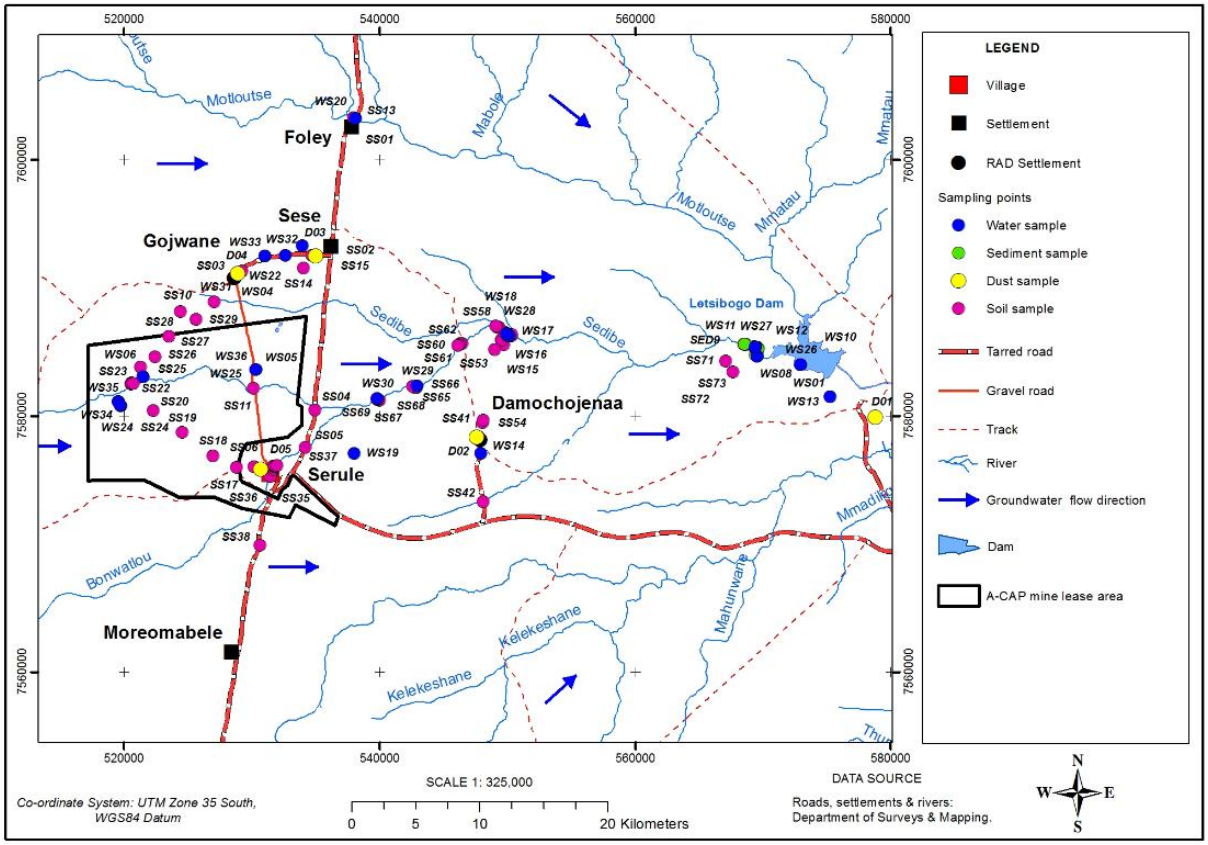

Figure 3.3: Sampling points for soil (purple), water (blue), sediments (green) and dust (yellow) within the study area.

3.6.1 Soil sampling

The sampling strategy adopted from the International Atomic Energy Agency (IAEA) for soil samples was random sampling (IAEA, 2004). The selection of the sampling locations was based on the accessibility to the public. The geological map of the area was used to identify the locations where samples were taken. The locations of the sampling area were marked using a Geographical Positioning System (GPS) (Figure 3.4). The top 5 cm surface soil along with vegetation cover was removed prior taking the sample. The soil samples were taken using a soil auger tool to a depth of 20 cm. The tools used for soil sampling are shown in Figure 3.4 and 3.5. About 2 kg of soil samples were collected from selected areas. These samples were packed into polyethylene bags and marked for later identification. The samples were transported to the laboratory for preparation and analysis.

Figure 3.4: The Geographical Positioning System (GPS) from the Apple Ipad App.

Figure 3.5: Illustration of the use of a hand auger tool for soil sampling

3.6.2 Water sampling

Since the project is focused on establishing baseline data for the level of NORMs and heavy elements, the selection of sampling sites that are suitable for collecting a representative set of water samples were based on domestic use, water consumed by livestock and/or used for irrigation purposes, which can be a potential source of radionuclides and toxic elements in foods. Surface water and groundwater along the selected area were collected for further analysis in two and a half litres (2.5 L) plastic bottles and labelled.

3.6.2.1 Groundwater

The selection of boreholes for ground water samples were based on use for domestic or irrigation purposes. There are different approaches for groundwater sampling depending on the objective of the study. The following method was used for this study, adopted from the Department of Water Affairs (DWA) and the Water Research Commission (WRC) water sampling guide (WRC, 2000). If the borehole water is directly used by the community, the sampling point was then placed at the first tap (or line-opening) in the system after the borehole (WRC, 2000).

3.6.2.2 Surface water

Surface water can be described as water that is found at a source on the surface of the earth, such as a river, stream, dam or lake. The sampling method used for surface water was adopted also from the DWA and WRC water sampling guide (WRC, 2000). The samples were taken by holding the bottle container near the base and plunged the sample bottle neck downward, below the water surface and then turning the bottle neck slightly upward to fill the bottle with water.

3.6.3 Dust sampling

The dust sampling method was based on the standard test method for collection and measurement of dustfall (settleable particulate matter) according to the American Standard for Testing and Materials (ASTM D1739:98) (ASTM, 2004). The addition of a known volume of water was done to the ASTM D1739:98 version dust bucket at the beginning of the sampling period. The bucket samplers were placed on an elevated platform of 1.5 m high away from obstructions and used to sample the dust from the villages of Serule, Gojwane, Sese, Damochojenaa and at the Letsibogo dam. The buckets were firstly rinsed with distilled water before sampling to remove all the dust in the buckets and then they were exposed to the field for a period of 28 to 33 days. The sample buckets were labelled properly using a permanent marker and all the necessary information such as sampling date, volume of water, sample name were documented in a “sample log-book”.

3.6.4 Food sampling

The selection of foodstuff was based on different matrices and pathways relevant to the analysis of radionuclides and toxic elements in foods and those environmental materials that are part of

the immediate pathways leading to contamination of food. About 2 kg of the food products locally grown or mostly harvested/consumed in the study area were sampled from different farms and transported in polyethylene bags to the laboratory for analysis. Other environmental samples such as grass and leaves that may be a possible pathway towards human exposure through animal grazing were also sampled.

3.7 Analytical methods

In this section, the analytical procedures and techniques are described for the determination of radionuclide as well as element concentrations. The available techniques were selected to suit the available resources and research objectives of this study.

3.7.1 Gamma spectrometry

Gamma (γ) spectrometry is the most widely used analytical method for quantifying nuclide specific radioactivity in a variety of matrices. This method can provide data of specific γ-emitting radionuclides in the sample. There are many types of γ-ray spectrometers such as inorganic scintillators; NaI(Tl), CsI(Na), CaI_2(Eu), and semiconductors such as high purity germanium (HPGe) (discussed in chapter 2 section 2.8) used today for detecting γ-emitting radionuclides. Of these, NaI(Tl) and HPGe detectors are the most commonly used. In this study, the activity concentration of the radionuclides in the environmental samples collected were analysed using an HPGe detector manufactured by Canberra, coupled to a computer based MCA and γ-ray spectrum analysis software, GENIE 2000. Figure 3.6 is a schematic diagram of an HPGe detector system. Its function is to collect the electrons produced in the detector from the γ-source, process pulses and sort them by intensity and energy. The charge created within the detector after the photon interaction with the detector, is collected by the preamplifier. The amplifier serves to shape the pulses as well as further amplify them. The MCA performs the essential functions of collecting the data, providing a visual image, and producing output, either in the form of final results or data for later analysis.

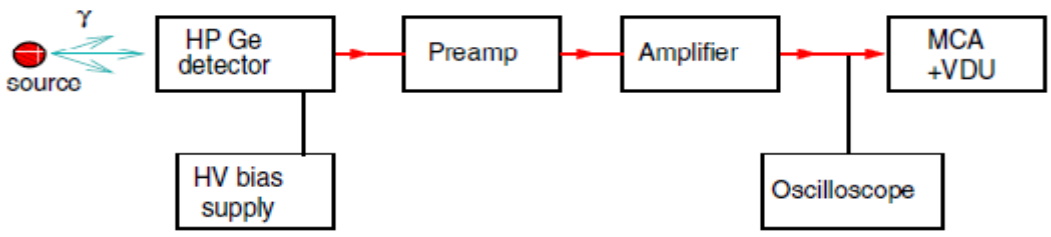

Figure 3.6: Schematic diagram of an HPGe detector system. (Royal Holloway, 2007)

3.7.1.1 Energy calibration of the γ-spectrometer

Energy and efficiency calibration of the HPGe detector were performed before sample measurements. Quality control and quality assurance procedures were performed to check the instrument performance for all the measurements. These include calibration source measurements as well as regular background check-up. The calibration of the detector is normally done according to the procedure recommended by the IAEA using reference materials traceable to IAEA certified standard reference materials such as RGU-1, RGTh-1 and RGK-1 (Oyedele, 2006). In this study, the HPGe detector was calibrated with respect to energy and efficiency using a mixture of ^{152}Eu and ^{133}Ba certified standard reference material for energy calibration and IAEA-RGU-1 certified standard reference material for efficiency calibration. The certified standard reference materials emit photons that cover the desired energy range in order to calibrate the energy-to-channel number. The channel number of every full-energy peak was determined accurately, and accordingly the energy of the photon plotted against the channel number. The curve produced for energy calibration was used to determine the energy of a photon that is responsible for a peak in the spectrum of the sample. The corresponding energy calibration is shown in Figures 3.7 with correlation of $R^2 = 1$. The plot fitted a linear function, which indicates that the detector system is performing well for the certified standard reference material used for the energy calibration.

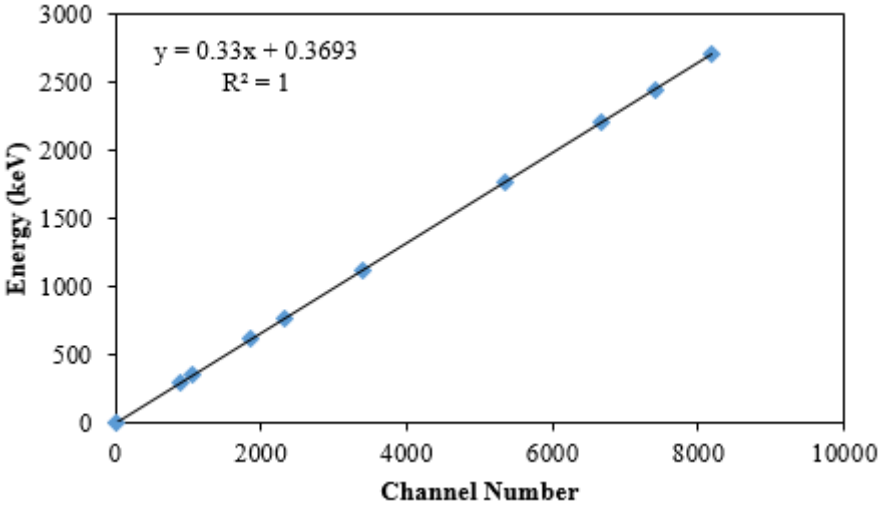

Figure 3.7: Energy calibration curve using a mixture of ^{152}Eu and ^{133}Ba certified standard reference material.

3.7.1.2 Efficiency calibration of the γ-spectrometer

The efficiency calibration curve is shown in Figure 3.8 with correlation coefficients of R^2 = 0.9988 and R^2 = 0.9998 respectively for low energy radionuclides (blue trend line) between 50 to 150 keV and for high energy radionuclides (orange trend line) between 150 to 2500 keV. The best fit of the curves was obtained by applying polynomial trend line resulting in equations (A) and (B) in Figure 3.8.

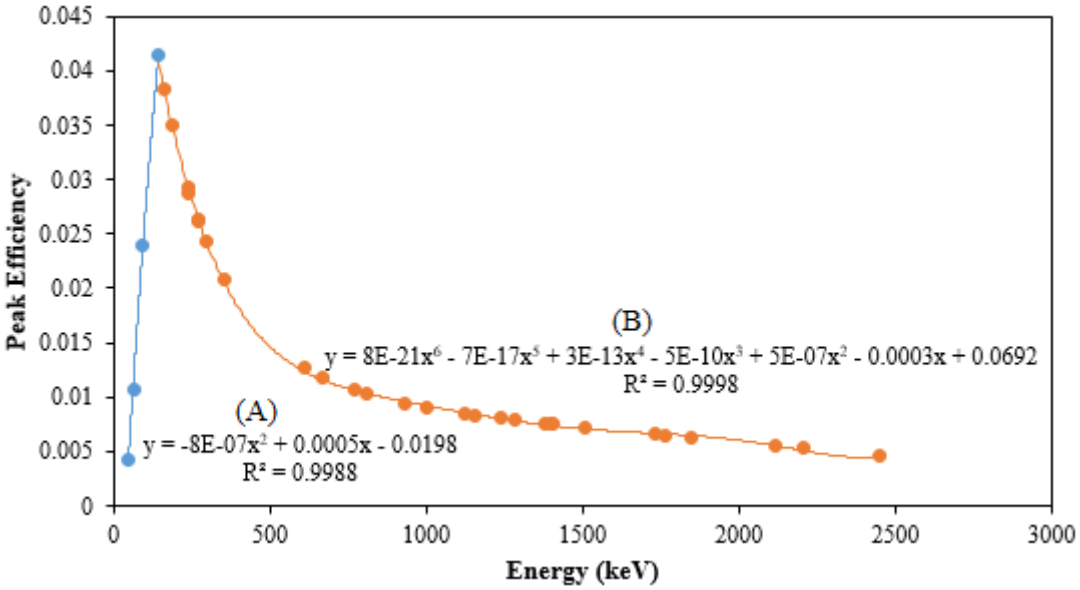

Figure 3.8: Efficiency calibration curve as a function of γ-ray energy for the HPGe-detector used in this work.

3.7.1.3 Preparation of samples for gamma spectrometry

Soil samples

Prior to analyses in the laboratories, the samples were air dried in trays for about a week to ensure that any significant moisture is removed from the samples and then crushed into a fine powder using a pestle and mortar (Figure 3.9). The soil samples were sieved through a 2 mm pore size sieve fitted with a collecting pan and transferred into labelled 1 litre Marinelli beakers. The Marinelli beakers were covered, sealed with a taped lid and stored for about one month to allow ^{226}Ra and its daughters, i.e. gaseous radon (^{222}Rn, half-life 3.8 days) and its short lived decay daughters (^{214}Bi and ^{214}Pb), from the ^{238}U decay series to reach equilibrium. The soil samples were counted with the γ-detector (HPGe) for 12 hours each, and the activity concentrations of the radionuclides of interest in the samples were reported on a dry weight basis in Bq/kg.

Figure 3.9: The apparatus for sample preparation: (A) a weighing scale, (B) a sealed sample inside a Marinelli beaker, (C) a mortar and pestle for crushing and homogenising samples and (D) a sieve of 2 mm mesh size.

Food Samples

In the laboratory, the food samples were air dried for about a week and crushed to fine powders and sieved through a 2 mm mesh into a Marinelli beaker and the dry weight of the sample was recorded. The samples were counted with an HPGe detector for 12 hours and the activity concentrations of the radionuclides of interest in the samples were reported on a dry weight basis in Bq/kg.

3.7.1.4 Determination of activity concentrations

The activity concentrations of ^{238}U, ^{232}Th and ^{40}K in samples were calculated using equation 3.1 (Darko, et al., 2010; Dovlete & Povinec, 2004; Kamunda, et al., 2016).

$$A = \frac{N}{\varepsilon_f P_\gamma t_S m K} \qquad (3.1)$$

where $N = (N_S - N_B)$ is the corrected net counts of the corresponding full-energy peak, N_S and N_B are the counts in the spectrum of the sample and the background spectrum obtained from counting an empty Marinelli beaker, ε_f is the counting efficiency at the photo peak energy under consideration, P_γ is the probability of the γ-ray emission corresponding to the peak energy, t_s is the sample counting time in seconds, m is the sample mass in kg, K is the decay correction factor.

3.7.1.5 Activity uncertainty

The uncertainty of the calculated activity of the individual samples were calculated using equation 3.2 and 3.3; (Canberra, 2004)

$$\sigma_c = c.\sqrt{\left(\frac{\sigma_R}{100}\right)^2 + \left(\frac{\sigma_S}{S}\right)^2 + \left(\frac{\sigma_M}{M}\right)^2 + \left(\frac{\sigma_{\varepsilon'}}{\varepsilon'}\right)^2 + \left(\frac{\sigma_K}{K}\right)^2 + \left(\frac{\sigma_y}{y}\right)^2} \quad (3.2)$$

where c is the calculated activity, σ_R is relative uncertainty in the calibration due to uncertainty of activity of the reference source, S is the net peak area and σ_S its uncertainty, M is the sample mass and σ_M its uncertainty, ε' is the attenuation corrected efficiency and $\sigma\varepsilon'$ its uncertainty defined by equation 3.3, K is the decay correction factor and σ_K its uncertainty, and y is the branching ratio and σ_y its uncertainty,

$$\sigma_{\varepsilon'} = \varepsilon'\sqrt{\left(\frac{\sigma_\varepsilon}{\varepsilon}\right)^2 + \left(\rho t \cdot \sigma_{\mu(E)}\right)^2 + \left(\mu(E) \cdot \sigma_{\rho t}\right)^2} \quad (3.3)$$

where ε is the non-attenuation detection efficiency at the peak in question and σ_ε its uncertainty, ρt is the average sample mass per unit area and $\sigma_{\rho t}$ its uncertainty, and μ(E) is the mass attenuation in units of cm^2/g at γ-energy (E) and $\sigma_{\mu(E)}$ its uncertainty.

3.7.1.6 Interference of peaks

The most serious interferences seen in HPGe γ-spectrometry are probably spectral overlaps. They are mostly caused by other NORM-nuclides peaks that are very close in γ-energy values. An example of such peaks, is the interference of ^{235}U at the γ-energy of 185.7 keV and ^{226}Ra at the γ-energy of 186.2 keV. The branching ratios of ^{235}U and ^{226}Ra are 57.2% and 3.59% respectively. Assuming that secular equilibrium exists between the parent nuclide and its daughters, the activity of the parent can be obtained through daughter nuclides that have more appropriate γ-transitions, e.g. ^{226}Ra and its progenies ^{214}Pb and ^{214}Bi following an in-growth period of at least 30 days after the samples were sealed (Ebaid, 2009).

The contribution of ^{226}Ra through its γ-ray at the energy of 186.2 keV at the branching ratio 3.59% can be calculated by employing the spectral mathematical interference correction equations (De Corte, et al., 2004) using the least spectrally disturbed peak (reference peak) at 295.2 keV from the decay of ^{214}Pb. The net peak area or net counts of ^{226}Ra at the line 186.2 keV can be extracted using equation 3.4 (Yücel, et al., 2009) taking into consideration γ-ray intensities I_γ and peak detection efficiencies ε_p of the reference peak:

$$N_p\left[186.2keV, {}^{226}Ra\right] = \frac{\left[I_\gamma \varepsilon_p F_{COI} F_S\right]_{186.1keV}}{\left[I_\gamma \varepsilon_P F_{COI} F_S\right]_{295.2keV,Ref}} \times N_p\left[295.2keV, {}^{214}Pb\right]_{Ref} \quad (3.4)$$

where Np is the net counts, I_γ is γ-ray emission probability, ε_p is the full-energy peak efficiency. F_{COI} and Fs are the correction factors of the true coincidence summing peak and self-absorption. The effect of the true coincidence summing peak and self-absorption were considered to be negligible in the current work.

3.7.1.7 Detection Limit

The detection abilities related to counting and analysing of radioactive levels vary according to the instrumentation and analytical techniques used (Klement, 1982). For a low-level radiation counting, it is crucial to determine the Detection Limit (L_D) of the system. The Detection Limit can be defined as the level that significant net counts can be detected above the acceptable level (L_C) when a possibility of real activity is present. The concept of a decision level or critical-level and detection limit was established in 1968 by Currie (Currie, 1968).

The critical level (L_C) can be defined as a decision level above which the net counts present some detected activity with a certain degree of confidence. A net count less than L_C indicates that the sample does not contain any measurable activity where as if the net count exceeds L_C, it is assumed that some real and/or excess activity is present (Currie, 1968). The L_C can be expressed as:

$$L_C = 2.36\sigma_{N_B} \tag{3.5}$$

where σ_{N_B} is the standard deviation of the number of counts in a blank sample. The decision limit is usually not significant for the activity measurement and therefore the detection limit (L_D) is introduced, and can be represented mathematically by equation 3.6 (Currie, 1968):

$$L_D = 2.706 + 4.653\sigma_{N_B} \tag{3.6}$$

The minimum detection activity (MDA) can be described as a performance criterion in γ-ray spectrometry (Currie, 1968). The MDA depends on the values of the L_D and the efficiency of a counting system. The MDA can be calculated using equation 3.7.

$$MDA = \frac{L_D}{\varepsilon_f P_\gamma T} \tag{3.7}$$

where ε_f is the absolute efficiency, $P\gamma$ is a γ-emission probability and T is the time of measurement in seconds.

3.7.1.8 Evaluation

The activity concentration of ^{238}U and ^{232}Th were determined by measuring the counts of γ – ray energies of daughter nuclides assuming that secular equilibrium exist in the decay chain. The ^{232}Th activity concentration was calculated as the weighted mean value of ^{228}Ra and ^{228}Th concentration. ^{228}Ra was measured as ^{228}Ac using the 209.3, 270.2, 911.1 and 969.0 keV γ-rays while ^{228}Th was measured through ^{212}Pb using the 238.6 keV γ-ray line, ^{212}Bi using the 727.3 keV γ-ray, and ^{208}Tl using the 583.2 keV γ-ray corrected for the branching ratio of 0.36. The ^{238}U content was determined from the corrected ^{235}U concentration assuming a natural

$^{238}U/^{235}U$ activity ratio of 20.7. The ^{235}U content was based on the spectral interference of ^{226}Ra at of 186.2 keV and ^{235}U at 185.7 keV as given in equation 3.4. ^{40}K was determined directly from its γ -ray energy at 1460.8 keV. Table 3.1 shows the γ –ray energies used in the determination of the activity concentrations.

Table 3.1: γ-ray energies and their associated intensities used in the determination of activity concentrations.

Parent	Daughter	γ-ray Energy (keV)	γ-ray Intensity (%)
^{238}U	^{226}Ra	186.2	3.59
	^{214}Pb	295.2	19.3
		351.9	37.6
	^{214}Bi	609.3	46.1
		768.4	4.89
		1120.3	14.91
		1238.1	5.79
		1377.7	3.97
		1729.6	2.84
^{232}Th	^{228}Ac	209.2	3.89
		270.2	3.55
		911.1	25.8
		969.0	15.9
	^{212}Pb	238.6	43.3
	^{212}Bi	727.3	6.65
	^{208}Tl	583.2	84.5
^{40}K		1460.8	10.67

3.7.2 Liquid scintillation counting

Liquid scintillation counting (LSC) is a technique mostly used for quantitative analysis of α- and β-emitting radionuclides. The principle of LSC is based on a scintillation liquid, called scintillation cocktail, which dissolves the sample during the analysis process. The process of scintillation and the amount of light produced for both α- and β-decay events are different. α -particles interact with the scintillation cocktail to produce light of about 1 photon per keV of the original energy, while about 10 photons per keV of the β-particle energy are produced. The

advantage of using this technique is the capability of measuring α and β particles simultaneously by using a special electronic device called a pulse shape analyzer (PSA),which can identify and separate the pulses of α and β particles because of the scintillation process and light produced by α- and β-decay events.

In this study the gross α/β activity concentrations of environmental water samples were measured using the LSC Quantulus 1220^{TM} manufactured by PerkinElmer coupled to a computer based MCA. The block diagram of an LSC used to acquire data is shown schematically in Figure 3.10. The LSC technique has two photomultiplier tubes (PMT 1 and PMT 2), connected in coincidence mode to convert flashes of light into measurable electrical pulses. After the coincidence unit, the output pulses of the PMTs are summed, further amplified and converted to a digital form in an ADC unit. Finally, the digital pulses are sorted according to their heights in an MCA and go into their distinct channels. In this way, a complete spectrum of radionuclides in a sample is obtained.

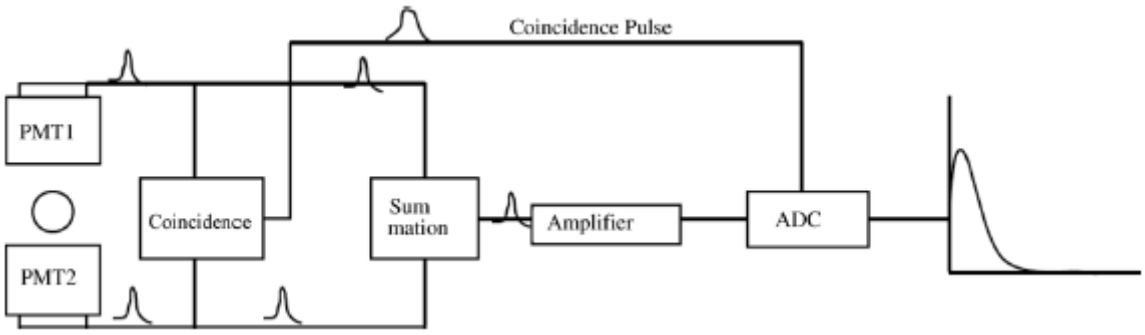

Figure 3.10: Schematic diagram showing the mechanism of an LSC (Lehto & Hou, 2011).

3.7.2.1 LSC Interference

There are many interferences encountered in liquid scintillation counting such as quenching, chemiluminescence, background radiation, heterogeneous samples and so forth (Kessler, 1989). The most common interference found in LSC is quenching (Kessler, 1989). Quenching is defined as the reduction of counting efficiency of the scintillation process (Lehto & Hou, 2011). It can be caused by a number of parameters such as the color of the sample, chemicals that are in the scintillation cocktail and so forth. Highly quenched samples result in the reduction of the observed pulse height and the count rate of the sample. As a result, the spectrum peaks detected appear to shift towards lower channel number and pulse heights. An example of the quench effect is shown for a ^{226}Ra α-spectra in Figure 3.11, showing how the

α-spectrum is shifted to lower channels by quenching. To overcome this interference the PSA must be optimized accurately to discriminate α- or β-particles and store them in their separate channels of an MCA.

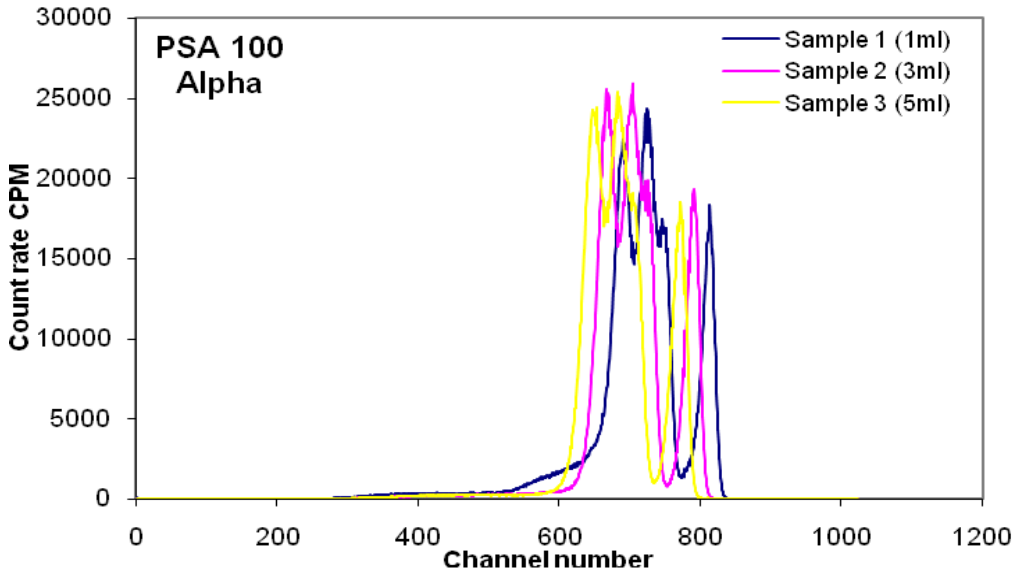

Figure 3.11: ^{226}Ra α-spectrums measured at a constant PSA level of 100. Sample 1 is the least quenched and sample 3 is the most quenched (Mashaba, 2011).

3.7.2.2 PSA calibration

The pulse shape analysis (PSA) level setting is set to minimize the spillover. Based on the work done by Mashaba in 2011 to optimize the LSC equipment, a formula for optimized PSA setting was obtained (Mashaba, 2011). This equation is achieved by plotting α-emitting standard spillover and β-emitting standard spillover against the PSA. ^{241}Am as an α-emitting and ^{90}Sr as the β-emitting standard were used to get the spillovers of α and β respectively. Different volumes of distilled water were spiked with the respective standards to obtain different quench values. The spillover (X) values were calculated using equation 3.8 and 3.9.

$$X_\alpha = \frac{MCA_{11}}{MCA_{12}+MCA_{11}} \tag{3.8}$$

$$X_\beta = \frac{MCA_{12}}{MCA_{12}+MCA_{11}} \tag{3.9}$$

where; X_α is the fraction of counts observed in β-channel (MCA_{11}) with respect to the counts observed in α- and β-channel (MCA_{12} + MCA_{11}) when the ^{241}Am standard is measured and (X_β) is the fraction of counts observed in the α channel (MCA_{12}) with respect to the counts observed

in the α and β channels (MCA_{12} + MCA_{11}) when ^{90}Sr is measured. MCA_{11} contains pure sample β counts while MCA_{12} contains pure sample α counts.

The percentage spillovers obtained by ^{241}Am (α spillover) and ^{90}Sr (β spillover) were plotted against the PSA level. Where the spillover curves cross it is assumed that the spills are equal. This data were used to plot the PSA setting against the quench parameter SQP(E) to obtain the optimal PSA settings (Figure 3.12), and can be presented through the linear regression given in equation 3.10;

$$Y = 0.2787x - 120.59 \tag{3.10}$$

where Y is the optimum PSA setting and x is the measured quench value (SQP(E)) of the unknown sample. This relationship was used to find the optimum PSA setting of unknown samples once the quench value has been determined of each individual environmental sample (from an arbitrary PSA level).

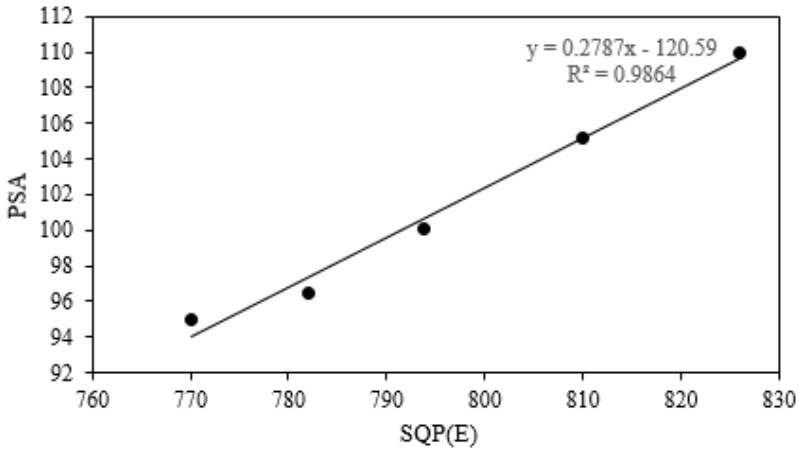

Figure 3.12: Relation between SQP(E) and the optimized PSA setting.

3.7.2.3 Detection Limit

The detection limit values for α/β particles using LSC technique are determined based on the SQP(E) values of the α/β background count rates. For the final results of the α/β calculations, the background values (Table 3.3) are subtracted according to the actual quench parameter of the measured sample. The determination of the MDA values are calculated using equation 3.11 and expressed as a function of the L_D according to ISO 11929 as defined in equation 3.12.

$$MDA(Bq/ml) = \frac{(k_{1-\alpha}+k_{1-\beta})}{60 \cdot \varepsilon \cdot V}\sqrt{R_b\left(\frac{2}{t}\right)} \tag{3.11}$$

$$L_D = (k_{1-\alpha} + k_{1-\beta})\sqrt{R_b\left(\frac{2}{t}\right)} \quad (3.12)$$

where t is the measurement time coinciding with the measurement time of the sample; $k_{1-\alpha} = k_{1-\beta} = 1.645$ for error probabilities α = β = 0.05, R_b is the net count rate, V is the sample volume, ε is the detection efficiency and 60 is the correcting measuring time (Varlam, et al., 2009).

Table 3.2: α / β background as a function of quench.

Quench SQP(E)	**MCA_{12} (A)**		**MCA_{11} (A)**	
	Count rate	Count rate Error	Count rate	Count rate Error
826.340	0.644	0.047	5.464	0.136
811.720	0.590	0.045	5.531	0.137
806.940	0.511	0.042	5.589	0.138
793.060	0.478	0.035	0.658	0.047

3.7.2.4 Preparation of water samples for LSC

A 5 ml portion of the surface and ground water samples was pipetted into a polyethylene counting vial and thereafter 15 ml of the Ultima Gold AB cocktail was also pipetted into the vial and mixed vigorously through shaking. The samples were analysed using the Quantulus 1220^{TM} LSC-system. Background samples were prepared the same way as the real samples using distilled water instead. All samples were counted for 18 000s each. The α- and β-activity concentrations were reported in Bq/*l*.

3.7.2.5 Gross α/β measurements in water samples

Gross α/β analysis is the first step in determining the level of radioactivity in drinking water (World Health Organization, 2008; Kahraman, et al., 2015). This method serves as a preliminary screening procedure and determines whether more sensitive radionuclide specific analyses are required. According to World Health Organization (WHO), water is considered adequate for human consumption when the screening level for gross α activity is below 0.5 Bq/*l* and gross β activity is below 1.0 Bq/*l* (World Health Organization, 2008), while European Union (EU) recommended screening levels of 0,1 Bq/*l* for gross α activity and 1,0 Bq/*l* for β activity in each member state (EU, 2013). When the gross values exceed the recommended

practical screening values further analysis should be carried out to identify specific radionuclides producing this activity according to WHO (World Health Organization, 2008).

The routine method normally used for gross α/β activity analysis is the "EPA 900.0: Gross α and Gross β Radioactivity in Drinking Water" standard method (USEPA, 1980). This method relies on gas-flow proportional counting (GFPC). However, several studies have suggested the use of LSC instead of GFPC due to its advantages of higher detection efficiency and faster analyzing time (Kahraman, et al., 2015).

In literature, there are many options for calculating gross α-β activities from the raw counts obtained (Mashaba, 2011; Kahraman, et al., 2015). In the current study (Mashaba, et al., 2017), the gross activity concentrations (A_α and A_β) was determined using the expression in equation 3.13 and 3.14;

$$A_\alpha = \frac{(MCA_{12(G\alpha)} - MCA_{12(B\alpha)})}{V \cdot T \cdot} \tag{3.13}$$

$$A_\beta = \frac{(MCA_{11(G\beta)} - MCA_{11(B\beta)})}{V \cdot T \cdot} \tag{3.14}$$

where $MCA_{12(G\alpha)}$ and $MCA_{11(G\beta)}$ are the count rate recorded in the α and in β window, respectively, for the sample vial, $MCA_{12(B\alpha)}$ and $MCA_{11(B\beta)}$ are the background count rate recorded in the α and in β window, respectively, for the blank vial. A_α and A_β are the α and β activities (Bq/*l*) of the sample respectively. *V* is the volume of the sample analyzed (*l*) and *T* is the corrected measuring time from minutes to seconds (60).

The uncertainty of the calculated activity of the individual samples was calculated using a confidence level of 95% (k = 2) using equation 3.15 (Varlam, et al., 2009).

$$\sigma(Bq/ml) = \frac{2}{60 \cdot \varepsilon \cdot V}\sqrt{\frac{MCA12_{G\alpha} + MCA_{B\alpha}}{t}}, \tag{3.15}$$

where *t* is the counting time in minutes.

3.7.3 Inductively Coupled Plasma-Mass Spectrometry

Inductively coupled plasma-mass spectrometry (ICP-MS) is an instrumental technique used for analysing isotopes and trace elements (Vanhaecke & Degryse, 2012; Montaser, 1998). This technique is based on the measurement of the mass of an element as discussed earlier in section

2.8.4. Samples were analysed using the NexION 300Q ICP-MS to determine the concentrations of heavy metals. Prior to the measurement, the instrument was calibrated to get accurate results.

3.7.3.1 Calibration of ICP-MS

The NexION Dual Detector calibration solutions manufactured by PerkinElmer containing various elements such as Cr, Co, Fe, Mn, As, Mo, Cd, Pb, Bi, U, etc. were used for the calibration of the ICP-MS. The liquid calibration standards are prepared in the same manner as used in ICP-OES analysis by adding the same amount of different elements into a vial, for example; 2, 10, 20, 50 and 100 ppm standard into diferent vials for 4 or 5 point calibration curve and forced through zero. These standards are analyzed to generate the calibration curve. The unknown sample concentration of each element is determined by comparing the counts measured for a selected isotope to an external calibration curve that was generated for that element. Figure 3.13 shows an example of a calibration curve for the determination of uranium (U) using 5 standards.

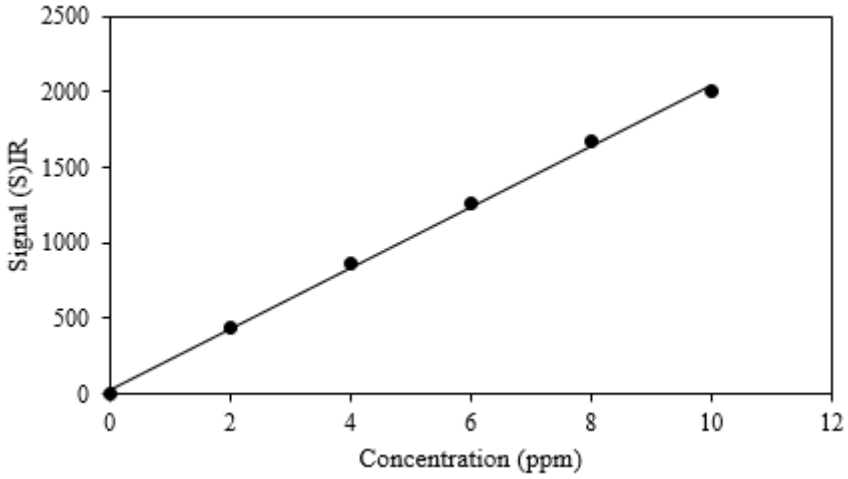

Figure 3.13: Calibration curve for Uranium using 5 standards.

3.7.3.2 Detection limit

The detection limit is the lowest quantity that can be distinguished from a blank (background, distilled water) within a stated confidence limit. It is estimated from the mean of the blank, the standard deviation (σ) of the blank and the confidence factor. It is defined as 3σ where σ is the standard deviation in the concentration of the elements obtained by extrapolation of the calibration plot. Table 3.3 shows the obtained detection limit of some of the major elements in the blank used in this study.

Table 3.3: Major elements of the blank

Element	Na	Mg	Al	K	Ca	Fe
DL in µg/*l*	32.81	5.61	12.49	48.05	90.02	67.69

3.7.3.3 Preparation of samples for ICP-MS

Digestion of Soil and Dust Samples

The method used for samples was the Microwave digestion (EPA method 3052 on Multiwave 3000) method (Mangum, 2009). In this method, one gram (1g) of each soil and dust sample was weighed into a crucible and 3 ml of 70% concentrated nitric acid (HNO_3) and 9 ml of hydrochloric acid (HCl) were added. The crucible was then placed on a hot plate at a temperature of 120°C for about 20 minutes for digestion to occur. Afterwards, all the digested samples were transferred into 100 ml volumetric flask and topped up with deionised water to the volume mark. The digested samples were left to settle overnight and thereafter the samples were filtered through a Whatman filter paper prior to analysis.

Digestion of food Samples

For food samples, 1 g was weighed and dried overnight in an oven at a temperature of 106°C until a constant weight was obtained. Then the samples were allowed to cool in a desiccator. The dried samples were re-weighed and ashed overnight in an oven. The samples were cooled in a desiccator and re-weighed. Digestion of the food samples was done by adding 1 ml of HNO_3 and 10 ml of HCl in a crucible. Thereafter the food digestion method followed the same procedure as for soil samples.

Chapter 4: Health risk assessment

4.1 Radiological Risk Assessment of NORMs

Radiological assessment refers to the process of estimating dose and risk to humans from radioactive materials in the environment (Grogan & Till, 2008). Radioactive materials are generally released from sources of man-made or natural type that may be transported through the environment and appear as concentrations in environmental media (Grogan & Till, 2008). These concentrations can be converted to dose and risk by making assumptions about exposure to people. The activity of a radioactive material and the radiation dose are the two main basic quantities in the assessment of radiation levels. Activity of a radioactive material is defined as the number of nuclear disintegrations per unit time (with unit of Becquerel (Bq) (Grupen, 2010; Turner, 2007). One Becquerel is one disintegration per second (Grupen, 2010; Turner, 2007). The term radiation dose can serve several terms, such as; absorbed dose, equivalent dose or effective dose.

The dose or risk to an individual is influenced by a number of exposure factors, such as time, location, transport of radionuclides through the environment, and the traits of the individual like physiological parameters (e.g., breathing rate), type of dietary consumption of various foods, living habits, use of local resources like agricultural resources, and so forth.

In radiological assessment, a definite set of these characteristics is referred to as an exposure scenario. The radiological assessment target may be of real individuals or representative individuals. Real individuals are those who are or were actually exposed. Their characteristics should be defined as closely as possible to those that actually exist. Representative, or hypothetical, individuals are not characterized by specific persons but have characteristics similar to individuals in the area who are or were exposed in the past or who may be exposed in the future.

4.1.1 Exposure

Exposure is one of the important fundamental quantities and is normally used to express the level of radiation exposure to humans due to radioactive substances. It is defined for γ and X-rays in terms of the amount of ionization they produce in air (Turner, 2007; Grupen, 2010). The symbol of exposure is X, and is defined as the quotient of ΔQ by Δm, where the value of ΔQ is the absolute value of the total charge of the ions of one sign produced in air when all the

electrons liberated by photons in air of mass Δm are completely stopped in air (Turner, 2007; ICRU, 2011).

$$X = \frac{\Delta Q}{\Delta m} \tag{4.1}$$

The unit used to express radiation exposure is called the roentgen (R) and was introduced at the Radiological Congress in Stockholm in 1928 (Turner, 2007). It was initially defined as that amount of γ or X radiation that produces in air 1 esu of electrical charge of either sign in 1 cm^3 or 0.001293g of air at standard temperature and pressure (Turner, 2007). Since 1 esu is equivalent to 3.34 x 10^{-10}coulomb (C) (Turner, 2007; Grupen, 2010), the S.I unit of radiation exposure can now be defined as

$$1R = \frac{1esu}{cm^3} = \frac{3.34\times10^{-10}C}{0.001293g\times10^{-3}kg.g^{-1}} = 2.58 \times 10^{-4}C.kg^{-1} \tag{4.2}$$

From the perspective of radiological protection, exposure to radiation can be divided into two main categories, depending on whether the source of radiation is inside or outside the human body.

Internal exposure

Internal exposure is caused by the intake of radionuclides by inhalation and ingestion (UNSCEAR, 2008). Doses due to inhalation result from radionuclides in air (free and/or part of dust particles). These radionuclides are present in air because of noble gas emission (radon/thoron) and/or the re-suspension of soil particles. Doses due to ingestion arise from consumption of food and drinking water that contain radionuclides. The ingestion of radionuclides depends on the consumption rates of food and water, and on their radionuclide concentrations. The concentrations of radionuclides in food vary because of the differences in the background levels in soil, the climate and the agricultural conditions that prevail. Most of the primordial radionuclides such as ^{238}U, ^{232}Th, and ^{40}K can eventually find their ways into foodstuffs and drinks (Pöschl & Nollet, 2007).

External exposure

External irradiation is caused by radioactivity present in the soil and in any other material surrounding our bodies, including the air. Information on external exposure comes from direct measurements of the dose rate or from evaluations based on measurements of radionuclide concentrations in soil (UNSCEAR, 2008).

4.1.2 Absorbed Dose

A number of specialized dosimetric quantities are used for radiation assessment purposes. Since the exposure unit does not reflect the biological significance of the radiation, another useful unit is the absorbed dose, which considers the energy imparted by ionising radiation to any kind of material and was introduced by the International Commission for Radiological Protection (ICRP) (UNSCEAR, 1993). The quantity absorbed dose is of very fundamental importance in radiological protection for calculating radiation dose. The unit of absorbed dose is given in joule per kilogram, and has a special name called gray (Gy) since 1Gy is equal to 1 joule per kilogram. The relationship of this fundamental quantity to the risk of biological effects is described by the weighted dose quantities recommended by ICRP for the various types and energies of radiation incident or emitted from within the body and for selected tissues and organs (Cember & Johnson, 2009; Turner, 2007; UNSCEAR, 1993). Table 4.1 shows a list of radiation weighting factors for various types of ionizing radiation.

Table 4.1: Weighing factor (W_R) for different radiations (Knoll, 2000; Turner, 2007).

Type of Radiation	Energy range	Weighting factor (W_R)
Photons (X, γ-rays, β)	All energies	1
Neutrons	< 10 keV	5
	10 - 100 keV	10
	100 keV - 2 MeV	20
	2 - 20 MeV	10
	> 20 MeV	5
Protons and charged pions	< 20 MeV	2
α-particles, fission fragments, heavy nuclei		20

4.1.3 Equivalent Dose

It is established that the absorbed dose needed to achieve a given level of biological damage, for example, 50% of cell killing is different for different kinds of radiation. Radiation with a high linear energy transfer (LET) is usually more damaging to a biological system per unit dose than radiation with a low LET. The term linear energy transfer (LET) is used to characterize the distribution of ionizing events along the path of impinging radiation (Turner, 2007). Since

the high-LET radiations are capable of causing more damage per unit absorbed dose, the International Commission for Radiological Protection (ICRP), the National Council on Radiation Protection and Measurements (NCRP), and the International Commission on Radiation Units and Measurements (ICRU) introduced the concept of equivalent dose for radiation-protection purposes. The equivalent dose, symbolized by the letter H_T, can be defined as the product of the absorbed dose D_T and a dimensionless quality factor Q_R, absorbed over a tissue or organ (T), which depends on the LET (Turner, 2007; Cember & Johnson, 2009) and is given by equation 4.3.

$$H_T = \sum_R W_R . D_{T,R} \tag{4.3}$$

where H_T is the equivalent dose absorbed by tissue T, $D_{T,R}$ is the absorbed dose in tissue T by radiation type R and W_R is the radiation weighting factor defined by regulation.

The unit of H_T is expressed in sievert (Sv), when the absorbed dose is expressed in gray (Gy), thus one sievert is also equal to one joule per kilogram. An older unit of the H_T is the rem (radiation equivalent man) with the absorbed dose expressed in units of rad (Turner, 2007) and 1 Sv equals to 100 rem (Knoll, 2000; Lilley, 2001; Turner, 2007).

4.1.4 Effective dose

In addition, towards the latter fundamental quantities to the risk of biological effects due to radiation, the biological effect to radiation is concerned with the sensitivities of tissues or organs (T) that are irradiated. The variation of radiation sensitivity of each organ is taken into account in the contribution of the H_T in all tissues and organs involved. In this case, ICRP introduced a new term, called the effective dose, to indicate the combination of different doses to several different tissues or organs (ICRP, 2007). The effective dose (E) can be defined as the summation of tissue equivalent doses (H_T), each multiplied by the appropriate tissue weighting factor (W_T) of a specific tissue type (the values assigned to weighing factors are giving in Table 4.2 according to ICRP (ICRP, 2012)) to indicate the combination of different doses to several different tissues (equation 4.4) (Cember & Johnson, 2009; ICRP, 2012). The SI unit for effective dose is the sievert (Sv)

$$E = \sum_T w_T . H_T \tag{4.4}$$

Considering equations 4.3 and 4.4, Effective dose (E) can be presented as;

$$E = \sum_T w_T \sum_R W_R . D_{T,R} \tag{4.5}$$

Table 4.2: Tissue Weighting factor (W_T) for different body tissues (Cember & Johnson, 2009; ICRP, 2012; Turner, 2007).

Type of Tissue	Weighting factor (W_T)	Sum of W_T values
Gonads	0.20	0.20
Bone-marrow (red), Colon, Lung, Stomach	0.18	0.48
Bladder, Breast, liver, liver, esophagus, thyroid	0.05	0.25
Skin, Bone surface	0.01	0.02
Remainder	0.05	0.05
Whole body total	-	**1.00**

4.1.5 Biological effects of radiation

The human body is made up of an integrated assembly of organ systems (e.g. the skeletal, digestive, urinary system etc.) whose structures are in consensus with their functions (Cember & Johnson, 2009). The organ system is made up of different types of tissues (e.g. tendons, muscle tissues etc.) (Cember & Johnson, 2009). Each tissue involves specialized cells that perform specific functions. Exposure to ionizing radiation can damage a normal operating cell. The damage occurs when radiation strikes critical areas like the DNA of the cell, inhibiting the cell from dividing due to the breakdown of DNA molecules.

Radiation exposure can be categorized into chronic and acute exposure. Chronic exposure can be described as exposure that occurs over a long period of time (i.e. months or years). In Chronic exposure, a low radiation dose is delivered slowly over a long time, hence giving cells a high chance of recovering. This radiation exposure occurs mostly for members of the public from NORMs. Acute exposure occurs over a short period of time (i.e. within minutes, hours or several days at most) making it difficult for the cells to recover due to relatively fast damage due to high radiation doses within a short time. Mostly acute exposure occurs in accident situations.

In addition to the cell damage, if the cells do not repair themselves, permanent effects of radiation damage can be seen as biological changes in tissues and organs. These changes may be expressed as medical symptoms, which are classified into deterministic or stochastic effects.

Deterministic Effects (non-stochastic)

Deterministic effects exist when there is a threshold below which no detrimental effects are noticed, and the percentage response, known as severity, depends on the dose. The effect increases with increasing radiation dose. The Deterministic effects occur only if the radiation dose is substantial (e.g. in an accident). Below the threshold level there is no effect observed, and it is difficult to predict what the risk is to an individual and whether it will occur if the radiation dose exceeds a threshold level. This type of effect is also called threshold effect because of the minimum radiation dose that has to be exceeded before any sign of effect to the individual. Curve A in Figure 4.1 (S shaped curve) is the distinctive shape of a biological effect that reveals a threshold dose-point a. The spread of the curve from the threshold at point a, until 100% response is thought to be due to biological variability around the mean dose, point c, which is called the 50% dose.

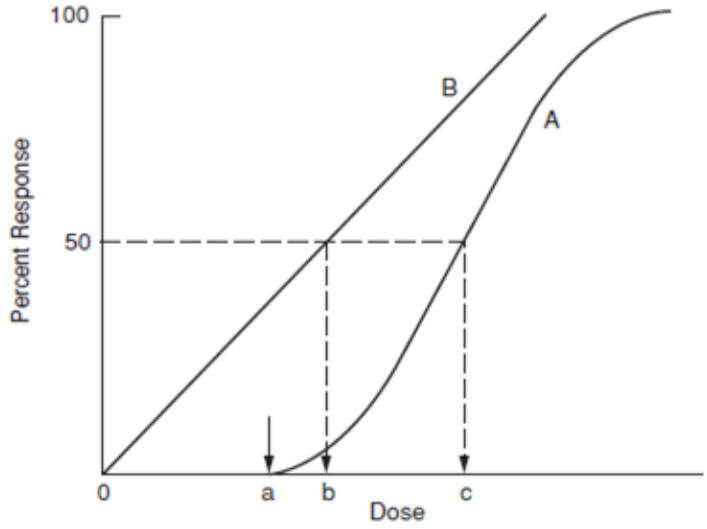

Figure 4.1: Dose-response curves. (Graph A shows the deterministic effect while graph B shows the stochastic effect) (Cember & Johnson, 2009).

An example of a deterministic effect is cataract, which is an opacification of the lens of the eye (Cember & Johnson, 2009). The exposure to a low radiation dose level of the lens of the eye for patients treated with X-rays (ionizing radiation) is estimated at about 2 Gy (Cember & Johnson, 2009). Exposure to ionizing radiation above the threshold dose level (2 Gy) may cause severe damage or can even lead to blindness (Cember & Johnson, 2009).

Another example of this effect is erythema (skin reddening). Below the threshold radiation dose, exposure to a low level of ionizing radiation dose cannot cause skin reddening. But if the radiation dose is increased above the threshold radiation dose level the skin will redden. And

if the dose is further increased, severe burn, blistering, or ulceration may occur (Cember & Johnson, 2009). Death may occur if high levels of ionizing radiation are exposed to the whole body, which may damage the body organs and eventually stop them from functioning (US.EPA, 2008).

Stochastic Effects

In the case of the stochastic effect, radiation effects occur without a threshold level of the dose, and the severity of the damage is independent of the quantity of the dose causing it (IAEA, 1996). Unlike deterministic effects, the amount of radiation exposure does not change the severity (of e.g. cancer) but it does alter the chance of getting cancer. For the purpose of radiation protection, it is assumed that the probability of stochastic effect increases linearly as the dose increases and that there is no threshold dose (see Figure 4.1; curve B). If there is no threshold dose then it is considered that even small doses of radiation might cause an effect. Curve B represents a zero- threshold, linear response. According to the linear, zero-threshold model, every increment in radiation, no matter how small, carries with it a corresponding increased probability of the stochastic effect.

4.1.6 Dose Assessment

In order to assess any radiological hazard, the exposure to radiation arising from NORMs that give rise to both internal and external human radiation doses, can be determined in terms of many parameters. A direct connection between radioactivity concentrations of NORMs and human exposure is known as the absorbed dose rate in the air at 1 metre above the ground level. The activity concentrations of ^{226}Ra, ^{232}Th and ^{40}K (Bq.kg^{-1}) representing the main external sources of natural radiation to the human body are used to calculate the absorbed dose rate (UNSCEAR, 2000; Singh, et al., 2005);

Dose rate

The absorbed dose rate *D,* outdoors due to terrestrial γ-rays at 1 meter above the ground surface can be calculated from the mean activity concentration of ^{226}Ra, ^{232}Th and ^{40}K in the soil and are given by equation 4.6 (UNSCEAR, 2000; Faheem, et al., 2008);

$$D = \sum_x Ax.Cx, \tag{4.6}$$

where *Ax* is the mean specific activity of ^{226}Ra, ^{232}Th or ^{40}K in Bq/kg, while *Cx* is is the corresponding dose conversion factor (DCF) in nGy/h as reported by (UNSCEAR, 2000;

Faheem, et al., 2008) and given as 0.462, 0.604 and 0.0417 respectively. Equation 4.6 can be re-written as:

$$D = 0.462A_{Ra} + 0.604A_{Th} + 0.0417A_K \quad (4.7)$$

Radium equivalent activity

The Radium equivalent (Ra_{eq}), is used to assess hazards associated with materials containing ^{226}Ra, ^{232}Th and ^{40}K nuclides (UNSCEAR, 2000). The values were calculated on the assumption that 370 Bq/kg of ^{226}Ra or 259 Bq/kg of ^{232}Th or 4810 Bq/kg of ^{40}K produce the same γ dose rate (Kamunda, et al., 2016; UNSCEAR, 1993; Ademola, et al., 2015) and can be given as:

$$Ra_{eq} = A_{Ra} + (A_{Th} \times 1.43) + (A_K \times 0.077), \quad (4.8)$$

where A_{Ra}, A_{Th}, and A_K are the specific activities in Bq kg^{-1} of ^{226}Ra, ^{232}Th and ^{40}K, respectively. The published permissible maximum value for Ra_{eq} is 370 Bq/kg (UNSCEAR, 2000; Asaduzzaman, et al., 2015) and corresponds to an effective dose of 1 mSv for the general public (Ajayi, 2009).

External hazard index

The external hazard index (H_{ex}) is used to evaluate the hazard of natural γ radiation (Ibrahim, 1999; Al-Kinani, et al., 2015) and its purpose is to limit the radiation dose to the permissible dose equivalent limit of 1 mSv/y (UNSCEAR, 2000; Asaduzzaman, et al., 2015). In order to determine this index, a model proposed in previous studies is defined and given by equation 4.9 (Kamunda, et al., 2016; Al-Kinani, et al., 2015; Asaduzzaman, et al., 2015; Faheem, et al., 2008)

$$H_{ex} = \frac{A_{Ra}}{370} + \frac{A_{Th}}{259} + \frac{A_K}{4810} < 1, \quad (4.9)$$

where A_{Ra}, A_{Th}, and A_K are the specific activities in Bq.kg^{-1} of ^{226}Ra, ^{232}Th and ^{40}K, respectively. The value of H_{ex} must be less than unity in order to keep the radiation hazard insignificant. The criterion considered by the model is that the maximum value of the external hazard due to γ-rays corresponds to a maximum Ra_{eq} activity of 370 Bq/kg for the material (UNSCEAR, 2000; Asaduzzaman, et al., 2015).

Annual Effective Dose Equivalent (AEDE)

The Annual effective dose equivalent (*AEDE*), in mSv/y, is the dose received by an adult given an average worldwide outdoor occupancy factor of about 20% (UNSCEAR, 2000), and is

derived from the absorbed dose rate in air (equation 4.6) using a conversion factor of 0.7 Sv/Gy. The *AEDE* is given by equation 4.10 (Kamunda, et al., 2016; Taqi, et al., 2016; El-Taher & Al-Zahrani, 2014)

$$AEDE = D\left(\frac{10^9 Gy}{h}\right) \times 24\frac{h}{day} \times 365\frac{day}{y} \times \frac{10^{-6} mGy}{10^9 Gy} \times 0.7\frac{Sv}{Gy} \times 0.2$$

$$AEDE = D \times 1.23 \times 10^{-3} mSvy^{-1} \quad (4.10)$$

The world average *AEDE* from outdoor terrestrial γ-radiation is 460 μSv/y (UNSCEAR, 2000).

In the case of the food samples, the average annual effective doses (E_{av}) were estimated from the activity concentrations of each individual NORM nuclide (^{238}U, ^{232}Th and ^{40}K) and applying the yearly food consumption rate for the adult members of the community and the dose conversion factors of 4.50×10^{-8}, 2.30×10^{-7} and 5.90×10^{-9} Sv/Bq for ^{238}U, ^{232}Th and ^{40}K, respectively (UNSCEAR, 2000; IAEA, 1996) using equation 4.11. Generally in Botswana, the average consumed weight in grams per meal is approximately 260g of vegetables, 100g of fish, and 200g of beef liver once a day. Therefore, based on this information and the non-availability of well-accepted consumption rates of these foodstuffs, an annual consumption rate of 100kg/y was assumed for all vegetables, 35 kg/y for fish and 70 kg/y for beef liver in this work.

$$E_{ave} = I_p \times D_i \times A_i, \quad (4.11)$$

where I_p is the consumption rate from intake of NORMs in foodstuff, D_i is the ingestion dose conversion factor and A_i is the activity concentration of the NORM nuclide in the food sample.

The annual α / β committed effective dose (AED) associated with radiation exposure through ingestion of water was estimated to assess the health risk to adult members of the public. The expression for the AED is provided in equation 4.12 (Mangset, et al., 2014).

$$AED_{(\alpha/\beta)} = A_{(\alpha/\beta)} \times W \times DC, \quad (4.12)$$

where; AED (α/β) is the gross annual α / β committed effective dose due to the consumption, of water, $A_{(\alpha/\beta)}$ is the gross α / β activity (Bq/*l*) concentration in the water, *W* is the consumption rate of water, set at 730 *l*/year for adults (World Health Organization, 2008), and *DC* is the ingestion dose coefficient of 4.50×10^{-8} Sv/Bq for adults (WHO, 2011).

4.2 Risk assessment due to heavy metals

The risk assessment process is based on recommendations by several American publications that describe a group of interconnected processes that include four basic steps; hazard identification, exposure assessment, dose-response assessment (toxicity assessment), and risk characterization (US.EPA, 2005; US.EPA, 2014; US.EPA, 2004). In this current study, risk assessment was used to evaluate the heavy metal hazard in the study area.

Hazard Identification basically aims to investigate chemicals that make a significant contribution to exposure and risk of a study area. In this study, certain heavy metals such as As, Pb, Cd, Cr, Cu, Co, Zn, Th and U were selected to generate baseline data on environmental parameters that could affect toxicological health-related issues towards people in the study area.

The purpose of exposure assessment is to evaluate the pathways by which people could be exposed to elements present at a certain study area. In this study, the exposure assessment evaluation was done by calculating the average daily intake (ADI) of heavy metals (As, Pb, Cd, Cr, Cu, Co, Zn, Th and U) through three exposure pathways namely; ingestion, inhalation, and dermal contact (US.EPA, 2004). The residents of the study area were divided into children and adults due to the behavioural and physiological differences (Kamunda, 2016).

Toxicity assessment evaluates the level of toxicity of certain elements of concern identified at the study area. There are two essential toxicity indices used to estimate the level of toxicity namely; the cancer slope factor (CSF), which is a carcinogen potency factor and a non-carcinogenic threshold called the reference dose (RfD) (US.EPA, 1992; US.EPA, 2004).

Risk characterization incorporates all information gathered from the latter three steps (hazard identification, dose-response assessment and exposure assessment) to evaluate potential cancerous and non-cancerous health risk of children and adults in the study area.

The potential exposure pathways in environmental samples for heavy metals were calculated based on recommendations by American publications USEPA, 1992, 2004, 2005. The exposure of humans to heavy metals in environmental matrices can occur via oral ingestion, inhalation, and direct dermal exposure pathways. These routes of exposure were considered for carcinogenic and non-carcinogenic risk effects of heavy metals present in environmental samples around the study area. The calculations for the ADI of contaminants via various exposure pathways in soil samples were calculated using the exposure Equations 4.13 and 4.14

(US.EPA, 1992; US.EPA, 2004). While equations 4.15 and 4.16 were used to calculate ADI in water (US.EPA, 2004; Wu, et al., 2009), equation 4.16 was used for ADI calculation in vegetable samples (Liu, et al., 2013).

The detailed explanation for all the exposure parameters used for health risk assessment exposure scenario through ingestion, inhalation, and dermal contact exposure pathways are listed in Table 4.3 (US.EPA, 2004)**.**

Table 4.3: Exposure parameters used in this study for the health risk assessment for ingestion, inhalation, and dermal contact exposure pathways for soil (US.EPA, 2004; Kamunda, et al., 2016; Naveedullah, et al., 2014; Wu, et al., 2009).

Parameter	**Unit**	**Child**	**Adult**
Body weight (*BW*)	kg	15	70
Exposure frequency (*EF*)	days/year	350	350
Exposure duration (*ED*)	years	6	30
Ingestion rate (*IR*)	mg/day	200	100
Inhalation rate (IR_{air})	m^3/day	10	20
Skin surface area (*SA*)	cm^2	2100	5800
Soil adherence factor (*AF*)	mg/cm^2	0.2	0.07
Dermal Absorption factor (*ABS*)	none	0.1	0.1
Dermal exposure ratio (*FE*)	none	0.61	0.61
Particulate emission factor (*PEF*)	m^3/kg	1.3×10^9	1.3×10^9
Conversion factor (*CF*)	kg/mg	10^{-6}	10^{-6}
Average time (*AT*) For carcinogens For non-carcinogens	days	 365 × 70 365 × ED	 365 × 70 365 × ED

4.2.1 Dermal contact with soil

$$ADI_{Dermal(soil)} = \frac{C_s \times SA \times FE \times AF \times ABS \times EF \times ED \times CF}{BW \times AT}, \quad (4.13)$$

where $ADI_{Dermal\ (soil)}$ is the exposure dose via dermal contact in mg/kg-day. C_s is the concentration of heavy metal in mg/kg for soil. *SA* in cm^2 is the exposed skin surface area; *FE* is the fraction of the dermal exposure ratio; *AF* in mg/cm^2 is the soil adherence factor; *ABS* is

the fraction of the applied dose absorbed across the skin, *EF* in days/year is the exposure frequency, *ED* is the exposure duration in years, *CF* is the conversion factor in kg/mg, BW is the body weight of the exposed individual in kg, and *AT* is the time period over which the dose is averaged in days.

4.2.2 Inhalation via re-suspended soil particulates

$$ADI_{Inhale(soil)} = \frac{C_S \times IR_{Air} \times EF \times ED}{PEF \times BW \times AT}, \quad (4.14)$$

where $ADI_{Inhale\ (soil)}$ is the average daily intake of inhaled re-suspended soil in mg/kg-day; IR_{Air} in m^3/day is the inhalation rate; PEF is the particulate emission factor in m^3/kg. C_s *EF, ED, BW* and *AT* are as defined in Equation 4.13.

4.2.3 Ingestion of heavy metals via oral intake of water

For water samples, the calculations for ADI of contaminants via various exposure pathways were calculated using Equation 4.15 and 4.16 (US.EPA, 2004; Wu, et al., 2009).

$$ADI_{Oral(water)} = \frac{C_{Oral} \times IR_{Oral(water)} \times ABS \times EF \times ED}{BW \times AT}, \quad (4.15)$$

Where $ADI_{Oral\ (water)}$ is the average daily intake of oral intake of water in *l*/day. C_{Oral} in *l*/day is the concentration for water. $IR_{Oral(water)}$ is the water ingestion rate in *l*/day (2 *l*/day ingestion rate was used in the current study). *EF, ABS, ED, BW* and *AT* are as defined earlier in Equation 4.13 and 4.14.

4.2.4 Dermal contact with water

$$ADI_{Dermal(water)} = \frac{C_{water} \times ET_{shawer} \times EF \times ED \times SA \times AF \times ABS \times CF}{BW \times AT}, \quad (4.16)$$

where $ADI_{Dermal\ (water)}$ is the exposure dose via dermal contact in mg/kg-day. C_{water} in mg/kg is the concentration for water; *ET* is exposure time (in this study: 0.6 h/day for adults and 1 h/day for children (Wu, et al., 2009)), while *EF*, *ED*, *SA*, *AF*, *ABS*, *CF*, *BW* and *AT* are as defined earlier in Equation 4.13 before. Table 4.4 states details of exposure parameters used for health risk assessment exposure scenario through ingestion, inhalation, and dermal contact exposure pathways (US.EPA, 2004).

Table 4.4: Exposure parameters used for the health risk assessment through different exposure pathways for water (US.EPA, 2004; Kamunda, et al., 2016; Naveedullah, et al., 2014; Wu, et al., 2009).

Parameter	**Unit**	**Child**	**Adult**
Body weight (*BW*)	kg	15	70
Exposure frequency (*EF*)	days/year	350	350
Exposure duration (*ED*)	years	6	70
Ingestion rate (*IR*)	mg/day	1.8	2.2
Skin surface area (*SA*)	cm^2	2100	5800
Soil adherence factor (*AF*)	mg/cm^2	0.2	0.07
Dermal Absorption factor (*ABS*)	none	0.001 0.03 for As	0.001 0.03 for As
Exposure Time	h/day	1	0.6
Conversion factor (*CF*)	kg/mg	10^{-6}	10^{-6}
Average time (*AT*) For carcinogens For non-carcinogens	days	 365 × 70 365 × ED	 365× 70 365 × ED

4.2.5 Ingestion of heavy metals via intake of vegetables

For diet samples, the calculations for ADI of contaminants were calculated using equation (4.17) (Liu, et al., 2013).

$$ADI_{Vegetable} = \frac{C_{vegetable} \times IR_{vegetable} \times EF \times ED}{BW \times AT}, \quad (4.17)$$

where $ADI_{Vegetable}$ is average daily intake of heavy metals from vegetable in mg/kg-day. $C_{vegetable}$ in mg/kg is the concentration for vegetable. $IR_{vegetable}$ in kg/day is the vegetable ingestion rate (in this study: 0.345 kg/day) while *EF*, *ED*, *BW* and *AT* are as defined earlier in Equation 4.13.

4.2.6 Carcinogenic Risk Assessment

The carcinogenic risks are estimated as the incremental probability of an individual developing cancer over a lifetime as a result of exposure to the potential carcinogen. The excess lifetime cancer risk is calculated using equation 4.18;

$$Risk_{pathway} = \sum_{k=1}^{n} ADI_K CSF_K, \quad (4.18)$$

where $Risk_{pathway}$ is a probability of an individual developing cancer over a lifetime from carcinogens. ADI_K (mg/kg-day) and CSF_K (mg/kg-day)$^{-1}$ are the average chronic daily intake (CDI) and the CSF, respectively for the kth heavy metal, for n number of heavy metals. The summation sign converts the estimated daily intake of the heavy metal averaged over a lifetime of exposure directly to incremental risk of an individual developing cancer (US.EPA, 1989; Liu, et al., 2013). The acceptable risk for regulatory purposes ranges between 1×10^{-6} and 1×10^{-4} (Liu, et al., 2013)

The total excess lifetime cancer risk for an individual is calculated from the average contribution of the individual heavy metals for different exposure pathways using equation 4.19;

$$Risk_{(total)} = Risk_{(ing)} + Risk_{(inh)} + Risk_{(dermal)}, \quad (4.19)$$

where $Risk_{(ing)}$, $Risk_{(inh)}$, and $Risk_{(dermal)}$ are risks contributions through ingestion, inhalation and dermal pathways through different media (soil, water, dust and foodstuff).

4.2.7 Non-Carcinogenic Risk Assessment

For non-carcinogenic risk, the risk is expressed by a term called hazard quotient (HQ). HQ is expressed as the ratio of exposure from carcinogens. It is defined as the quotient of dose (ADI) divided by the chronic reference dose (RfD) of toxicant in mg/kg-day of a specific heavy metal as shown in Equation 4.20 (US.EPA, 1989; Liu, et al., 2013; Wu, et al., 2009);

$$HQ = \frac{ADI}{RfD} \quad (4.20)$$

The sum of more than one HQ due to an individual heavy metal or multiple exposure pathways introduce a new term called the chronic Hazard Index (HI) as defined by the United States Environmental Protection Agency (USEPA) document (US.EPA, 1989). The mathematical representation of this parameter is shown in equation 4.21;

$$HI = \sum_{k=1}^{n} HQ_k = \sum_{k=1}^{n} \frac{ADI_k}{RfD_k}, \quad (4.21)$$

where HQ_k, ADI_k and RfD_k are the values of heavy metal *k*. If the value of HI exceeds one, then there may be concern for potential non-carcinogenic effects and when the value of HI is less than one, then the reverse applies (US.EPA, 1989; Liu, et al., 2013).

The carcinogenic and non-carcinogenic risk assessment of heavy metals are estimated using RfD and CSF values derived from the Department of Environmental Affairs (South Africa) and the USEPA as shown in Table 4.5.

Table 4.5: Reference doses (RfD) in mg/kg-day and Cancer Slope Factors (CSF) for the different heavy metals (Liu, et al., 2013; Wu, et al., 2009; US.EPA, 1989; DEA, 2010).

Heavy Metal	**Oral CSF**	**Dermal CSF**	**Inhalation CSF**	**Oral RfD**	**Dermal RfD**	**Inhalation RfD**
As	1.5	1.5	15.0	0.3×10^{-3}	0.3×10^{-3}	0.3×10^{-3}
Pb	8.5×10^{-3}	-	4.2×10^{-2}	3.6×10^{-3}	-	-
Cd	-	-	6.3	0.5×10^{-3}	0.5×10^{-3}	5.7×10^{-5}
Cr (VI)	0.5×10^{-2}	-	41.0	0.3×10^{-2}	-	0.3×10^{-4}
Co	-	-	9.8	3.7×10^{-2}	5.7×10^{-6}	5.7×10^{-6}
Cu	-	-	-	0.3×10^{-2}	2.4×10^{-2}	-
Zn	-	-	-	0.2×10^{-3}	7.5×10^{-2}	-
Th	-	-	-	-	-	-
U	-	-	-	0.6×10^{-3}	-	-

4.2.8 Biological Effects of Heavy Metals

Certain heavy metals such as iron (Fe), copper (Cu), manganese (Mn), molybdenum (Mo), and zinc (Zn) have been reported to be important to human life because of their irreplaceable roles in the working of body organs (Singh, et al., 2011; Iqbal & Shah, 2013). All living organisms require certain amounts of heavy metals, but become toxic when their levels increase to higher concentrations (Singh, et al., 2011). Other heavy metals like mercury (Hg), plutonium (Pu), and lead (Pb) have been reported to have no useful role or beneficial effect in the human metabolic system and other living organisms, and exposure to these metals even at very low concentrations can be toxic (Singh, et al., 2011; Iqbal & Shah, 2013)

Human beings and other living organisms are exposed to heavy metals as a result of transport along various environmental pathways. Once absorbed, for example through ingestion of food and drinking water, they are distributed in tissues and organs and thereby disrupt functions in vital organs and glands such as the heart, brain, kidneys, bone, liver etc. and may result in

adverse health effects varying from shortness of breath to different types of cancers (Iqbal & Shah, 2013).

Arsenic (As) for example, is considered a human carcinogen even from very low levels of exposure (ATSDR, 2007). After its absorption, arsenic exposure affects almost the entire body system (Kesici, 2016). It is distributed in the cardiovascular, nervous, hepatobiliary, gastrointestinal, renal, dermatologic and respiratory systems (Kesici, 2016). Severe exposure to arsenic can cause, vomiting, diarrhea, nausea, stomach ache, muscle cramps, abnormal heart rhythm and burning of the mouth and throat (NRC, 1999). Chronic exposure of arsenic results in an unusual pattern of skin changes, such as patches of darkened skin and the appearance of small corn or warts on the palms, soles, and torso. Skin cancer has also been associated with arsenic exposure (UNEP, 2002).

Lead (Pb) is also identified as toxic even at extremely low concentrations and is considered as a human mutagen and probable carcinogen (Podsiki, 2008). Pb in large doses can cause chronic damage to the central nervous system resulting in health effects such as high blood pressure problems, hearing problems, headaches, reproductive problems in men and women, digestive problems, muscle and joint pain. Pb is considered as number one health threat to children. Children and developing foetuses appear to be particularly vulnerable to the neurotoxic effects of Pb. Epidemiologic studies have also revealed that low-level Pb exposure in children under five years of age results in deficit in intellectual development (ATSDR, 2007).

Cadmium (Cd) on the other hand, is generally classified as a toxic element even at low concentration levels and is regarded as a probable carcinogen. Acute exposure to Cd may result in health problems such as coughing, headaches, vomiting, emphysema, bronchiolitis and alveolitis (Kamunda, et al., 2016). High levels of ingested Cd may accumulate in the liver and kidneys, causing kidney dysfunctions and reproductive deficiencies or even cancer (Khan, et al., 2013.).

Chromium (Cr) compounds in excess amounts are toxic (Podsiki, 2008). Inhalation of high levels of Cr has been considered as a potential cause of lung cancer. Long term exposure may cause damage to liver, kidney, circulatory and nerve disorders, as well as skin irritation. Cr often accumulates in aquatic life, adding also to the danger of eating fish that may have been exposed to high levels of Cr.

Additionally, extreme intake of zinc (Zn) and copper (Cu) may cause non-carcinogenic effects to humans, even though they are important substances to human life (Cao, et al., 2010). Chronic

exposure to Cu may result in the development of anemia, liver and kidney damage (Salem, et al., 2000). High copper exposure can also cause diarrhea to young children. Zn also produces adverse nutrient interactions with Cu. Higher doses of Zn can also diminish growth and reproduction (Kamunda, et al., 2016).

Chapter 5: Results and discussion

5.1 Activity concentrations, absorbed dose rates and annual effective dose equivalent

5.1.1 Sediments and soil

The results of the activity concentrations of the ^{238}U and ^{232}Th chains and ^{40}K in all of the sediment and soil samples are presented in Figure 5.1 and 5.2, respectively.

5.1.1.1 Sediment samples

From Figure 5.1 (and/or Table A3: Annexure A), it is observed that the ^{238}U-, ^{232}Th- and ^{40}K-concentrations are fairly constant over the entire region, indicating that there is no specific trend observed indicating contamination from the operational area of the mine. The exceptions are sediment sample SED02 with relatively low ^{238}U-, ^{232}Th- and ^{40}K-concentrations. A possible explanation for this could be attributed to low colloidal of sediment SED02. In addition, SED06 has the lowest activities of ^{238}U and ^{232}Th. But both samples (SED02 and SED06) appear to have the same deposition of sediments which could also be attributed to the same mobility characteristic of these nuclides.

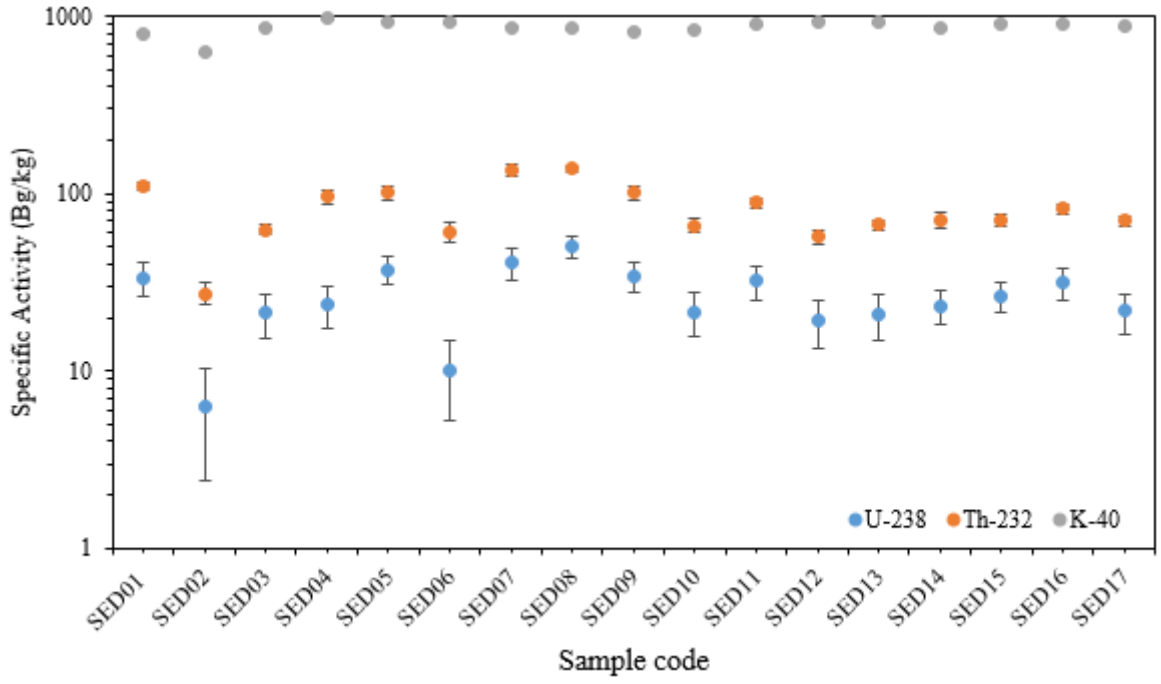

Figure 5.1: The overall activity concentration of ^{238}U, ^{232}Th and ^{40}K in all measured sediments samples

5.1.1.2 Soil samples

In Figure 5.2, the three regions (upper, middle and lower) identified for soil sampling in the study area as described in section 3.6 are indicated. From this it can be observed that there is a steady trend for an increasing ^{40}K-concentration from the upper to the lower region, which to a lesser extend also holds for ^{238}U and ^{232}Th. This can most likely be attributed to the geological deposits in the area, and as such should not be an indication of the mining activity in the upper area. A clear exception is SS53 with relatively low ^{238}U-, ^{232}Th- and ^{40}K-concentrations. A possible explanation for this could be due to the soil type variances that attribute to the differences of this sample. The full detailed results of the activity concentrations data of selected γ-ray transitions and weighted mean activity are presented in Annexure A (Table A1 – A7).

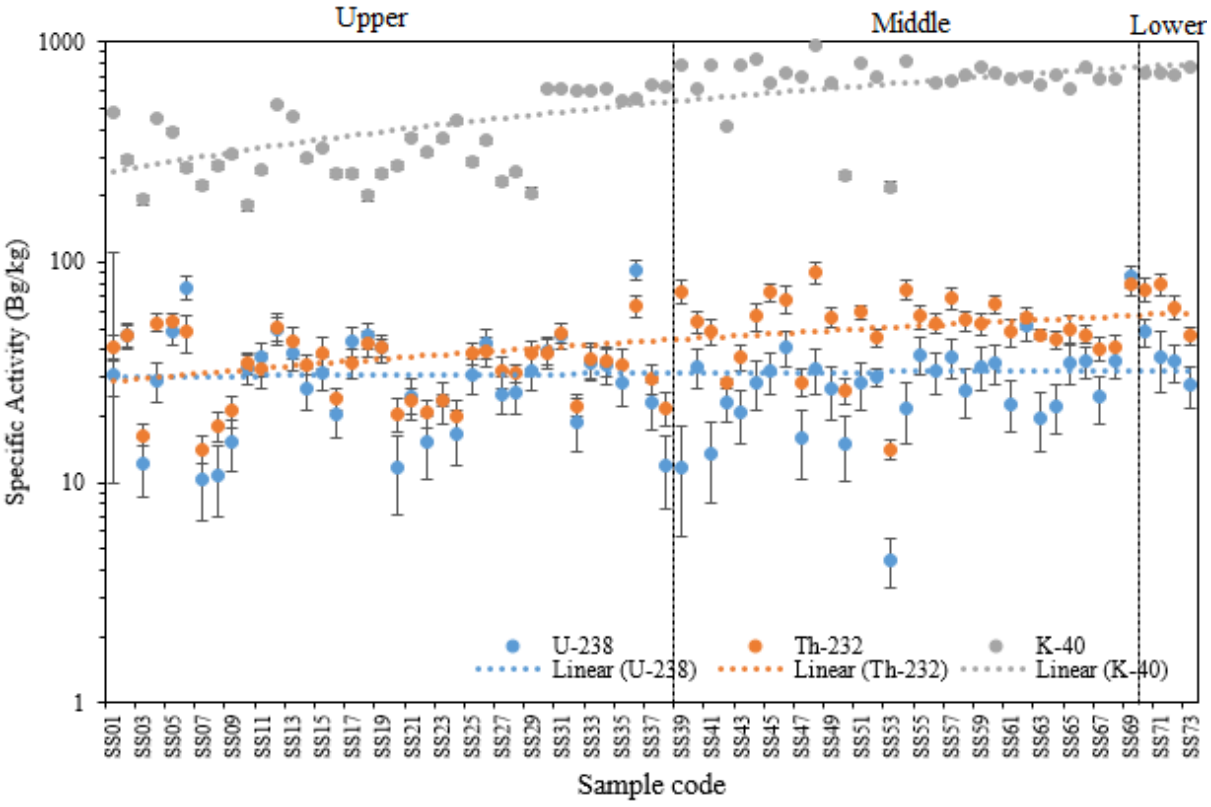

Figure 5.2: The overall activity concentration of ^{238}U, ^{232}Th and ^{40}K in the collected soil samples.

5.1.1.3 Comparison of activity concentrations of ^{238}U, ^{232}Th and ^{40}K in soil and sediments

The average values of activity concentration of naturally occurring radionuclides (^{238}U, ^{232}Th and ^{40}K) in sediment and soil samples are presented in Table 5.1. The average activity of ^{238}U in soil and sediments are 31.3 ± 1.8 Bq/kg and 26.7 ± 2.7 Bq/kg respectively, which indicates that there is statistically no difference between the two matrices. The same conclusion can be drawn for thorium as the measured activity of ^{232}Th in soil and sediments are 43.9 ± 2.0 Bq/kg and 56.1 ± 4.6 Bq/kg respectively. Potassium seems to be somewhat higher in the sediments as the ^{40}K activity in soil averages at 519 ± 25 Bq/kg, while for sediments the measured activity averages of 787 ± 18 Bq/kg, which can be attributed to long-term leaching of potassium from the soil and deposition in the sediments.

Table 5.1: Average activity concentrations of ^{238}U, ^{232}Th and ^{40}K in soil and sediment samples.

Sample type	No. of Samples	Parameter	Activity concentrations (Bq/kg)		
			^{238}U	^{232}Th	^{40}K
Sediment	17	Min	6.3 ± 3.9	21.0 ± 3.9	600 ± 8
		Max	50.3 ± 7.2	95.8 ± 11.4	878 ± 11
		Average	26.7 ± 2.7	56.0 ± 4.6	787 ± 18
Soil	73	Min	10.3 ± 3.6	14.1 ± 1.4	180 ± 3
		Max Average	91.9 ± 9.5	89.1 ± 10.1	958 ± 13
			31.3 ± 1.8	43.9 ± 2.0	519 ± 25
Average Sediment + soil	90	Min	6.3 ± 3.9	14.1 ± 1.4	180 ± 3
		Max	91.9 ± 9.5	95.8 ± 11.4	958 ± 13
		Average	30.4 ± 1.6	46.2 ± 1.9	572± 24

The results of the present study are comparable to the published data from other countries and world average values as shown in Table 5.2.

Table 5.2: Comparison of natural radioactivity (^{238}U, ^{232}Th and ^{40}K) levels in soil and air absorbed with those in other countries (Thabayneh & Jazzar, 2012; UNSCEAR, 2000).

Country	Activity concentration (Bq/kg) (Soil)					
	^{238}U		^{232}Th		^{40}K	
	Range	**Average**	**Range**	**Average**	**Range**	**Average**
Egypt	5 - 64	17	2 - 96	18	29 -650	320
Nigeria	9 - 18	14	1 - 38	19	712 - 1098	896
Malaysia	38 - 94	67	63 - 110	82	170 - 430	310
USA	8 - 160	40	4 - 130	35	100 - 700	370
China	2 - 440	32	1 - 360	41	9 - 1800	440
Japan	6 - 98	33	2 - 88	28	15 - 990	310
India	7 - 81	29	14 - 160	64	38 - 760	400
Iran	8 - 55	28	5 - 42	22	250 - 980	640
Poland	5 - 120	26	4 - 77	21	110 - 970	410
Romania	8 - 60	32	11 - 75	38	250 - 1100	490
Spain	6 - 250	32	2 - 210	33	25 - 1650	470
Luxembourg	6 - 52	35	7 - 70	50	80 - 1800	620
Worldwide average	17 - 60	35	11 - 64	30	140 - 850	400
Present Study	10 - 92	31	14 - 89	44	180 -958	519

5.1.1.4 Determination of the secular equilibrium in soil and sediment samples

The activity ratios of $^{238}U/^{226}Ra$ and $^{228}Ra/^{228}Th$ as presented in Table A1 – A7 (Annexure A) were used to determine the levels of secular equilibrium in the ^{238}U and ^{232}Th decay series, respectively. The average activity ratios in soil and sediment samples in each series are shown in Table 5.3, from which it can be seen that the average activity ratios in the ^{238}U and ^{232}Th decay series is consistent with unity indicating of secular equilibrium in the two matrices. For more source of information on activity ratios of all sediment and soil samples, Table A5- A6 (Annexure A) is referred to and the comments on each individual sample are stated also.

Table 5.3: Activity Ratios of the nuclides in ^{238}U and ^{232}Th decay series**.**

Sample	Activity ratio			
	Sediment		Soil	
	^{238}U-series	^{232}Th-series	^{238}U-series	^{232}Th-series
	$^{238}U/^{226}Ra$	$^{228}Ra/^{228}Th$	$^{238}U/^{226}Ra$	$^{228}Ra/^{228}Th$
Min	0.6 ± 0.3	0.9 ± 0.2	0.7 ± 0.2	0.9 ± 0.2
Max	1.6 ± 0.4	1.1 ± 0.3	1.6 ± 0.4	1.2 ± 0.3
Average	1.1 ± 0.1	1.0 ± 0.2	1.0 ± 0.3	1.0 ± 0.2

5.1.1.5 Radiological maps of soil samples of the study area: (^{238}U, ^{232}Th, and ^{40}K)

The activity concentration maps of ^{238}U, ^{232}Th and ^{40}K are shown in Figure 5.3, 5.4 and 5.5 respectively. These maps indicate the spatial distribution of these nuclides from the measured soil samples. The Geosoft® (Oasis montaj software) was used to produce these maps.

From these maps one can deduce a heterogeneous distribution of natural radiation across the study area. The purple colour indicate the highest activity concentration of ^{238}U, ^{232}Th and ^{40}K in the study area while the blue colour shows the lowest activity concentration of these radionuclides. The white colour with square shape shows the area that was not sampled. In Figure 5.3 for example, the activity concentration of ^{238}U is found to be higher across the upper region compared to the middle region. This is also expected since the uranium deposits have been discovered within the Serule area.

These distribution maps are significant for future studies to observe any long-term surface contamination due to the mining and mineral processing activities in the area.

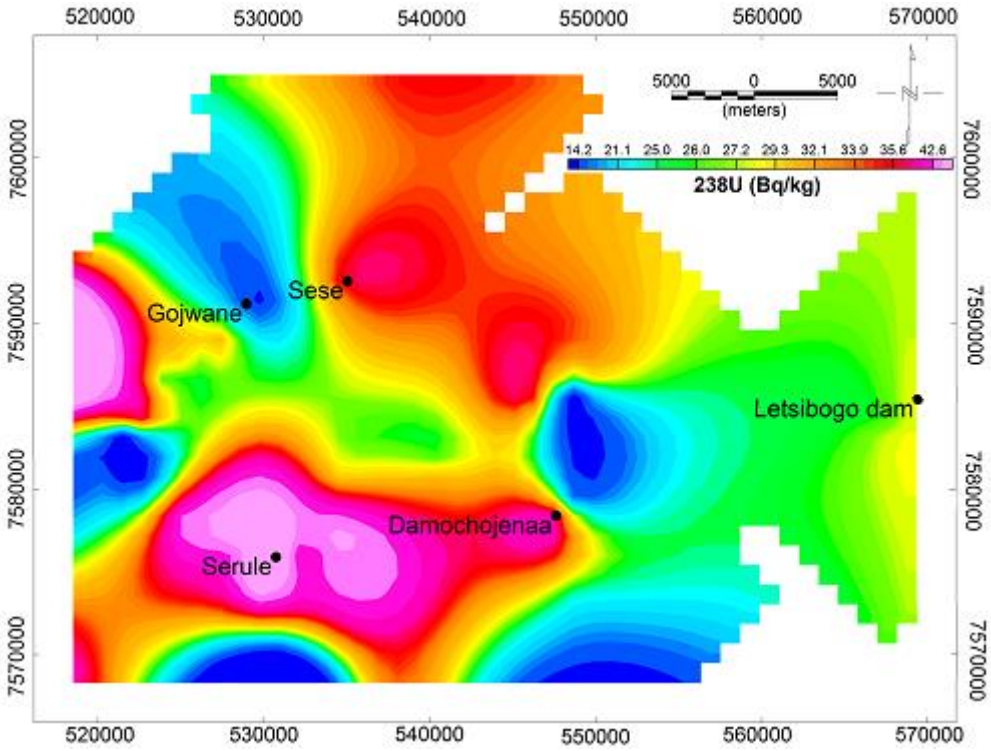

Figure 5.3: Radiation map of the study area showing the current activity concentration distribution of ^{238}U.

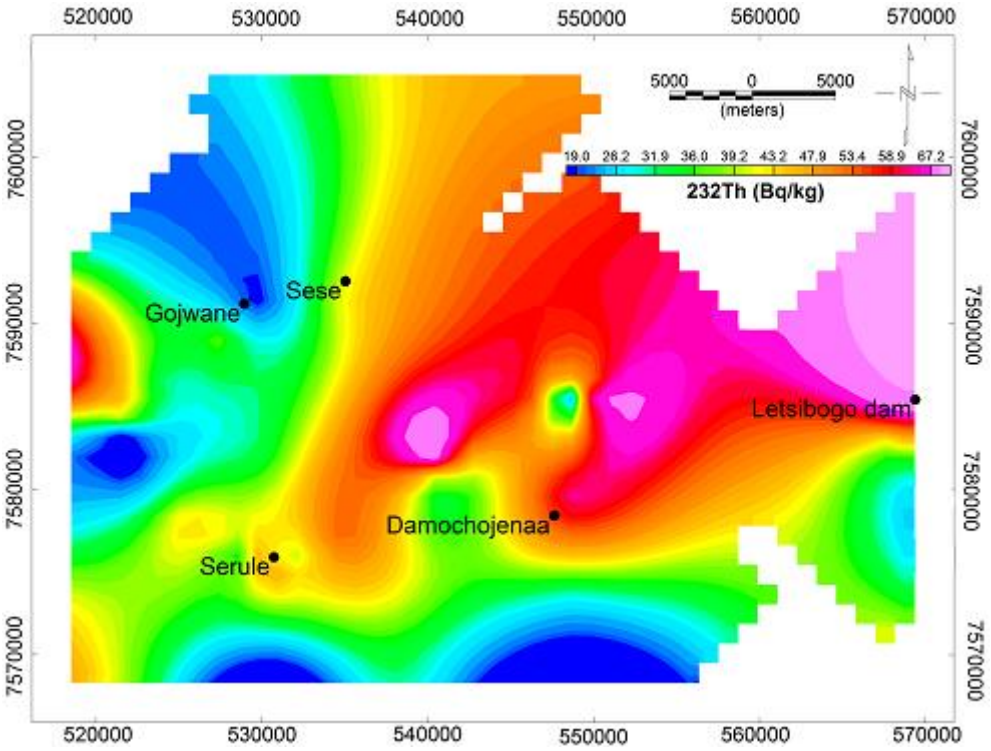

Figure 5.4: Radiation map of the study area showing the current activity concentration distribution of ^{232}Th.

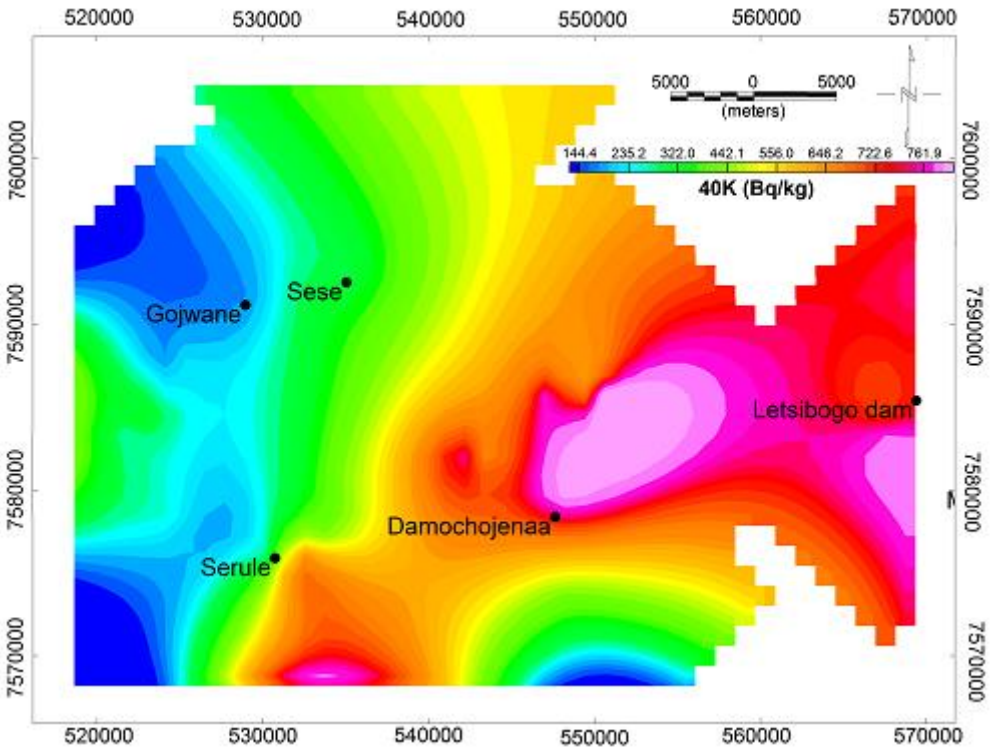

Figure 5.5: Radiation map of the study area showing the current activity concentration distribution of ^{40}K.

5.1.1.6 Radiological risk assessment for soil samples.

The radiological effects parameters such as; Calculated Radium Equivalent Activity (Ra_{eq}), Absorbed Dose Rate in air (D_R), Annual Effective Dose Equivalent (AEDE) and External Hazard Index (H_{ex}) of soil samples were used to assess the radiation effect to people living in the study area. The only direct external dose is due to the soil; sediment samples were not assessed because the local people are not really directly exposed to the sediments of the study area. The results of the radiological assessment are shown in Table 5.4. Detailed information on all soil samples regarding radiological risk is given in Table A7 (Annexure A).

Table 5.4: Calculated D_R, Ra_{eq}, H_{ex} and AEDE of all soil samples from the study area.

Soil	**D_R (nGy/h)**	**Ra_{eq} (Bq/kg)**	**H_{ex} (mSv/y)**	**AEDE (mSv/y)**
Min	23.5 ± 1.2	41.0 ± 2.1	0.11 ± 0.01	0.02 ± 0.001
Max	103 ± 6	224 ± 11	0.60 ± 0.04	0.13 ± 0.006
average	62.2 ± 2.4	133 ± 5	0.36 ± 0.02	0.08 ± 0.003
Worldwide				
Average	59	-	-	0.48
Range	18-93	-	-	-
Limit	59	370	1	1

The calculated absorbed dose values (D_R) in the study area vary from 23.5 ± 1.2 to 103 ± 6 nGy/h, with an average value of 62.3 ± 2.41 nGy/h, which is close to the worldwide average value of 59 nGy/h, although some high activity concentrations found in some soil samples (e.g. SS36 and SS48) lead to a slightly higher dose than the worldwide upper-range of 93. From Figure 5.6 it can be seen that the main contributor to the calculated absorbed dose rate in most of the soil samples is ^{232}Th. The averaged contributions of ^{238}U, ^{232}Th and ^{40}K to the total absorbed dose averaged at 24%, 42% and 34%, respectively. Though there are variations in the activity concentrations of ^{238}U, ^{232}Th and ^{40}K the D_R-values are below the safety limits provided by UNSCEAR (UNSCEAR, 2000) and reflect a general radiation background trend.

The Ra_{eq} calculated varied from 41.0 ± 2.1 to 224 ± 11 Bq/kg with an average value of 134 ± 5 Bq/kg, which is well within the permissible limit of 370 Bq/kg.

The external hazard index (H_{ex}) ranges from 0.110 ± 0.001 to 0.600 ± 0.039 with average values of 0.360 ± 0.014, which is all within the permissible limit of 1 mSv/y.

The annual effective dose equivalent (AEDE) varies from 0.020 ± 0.001 to 0.130 ± 0.006 mSv/y with an average of 0.080 ± 0.003 mSv/y, which lie within the world wide average values reported by UNSCEAR, and remain within the dose criterion of 1 mSv/y recommended by ICRP (ICRP, 1991a).

It can therefore be concluded that the study area is safe for human living from a radiological point of view as all values are below the limits set by UNSCEAR (UNSCEAR, 2000).

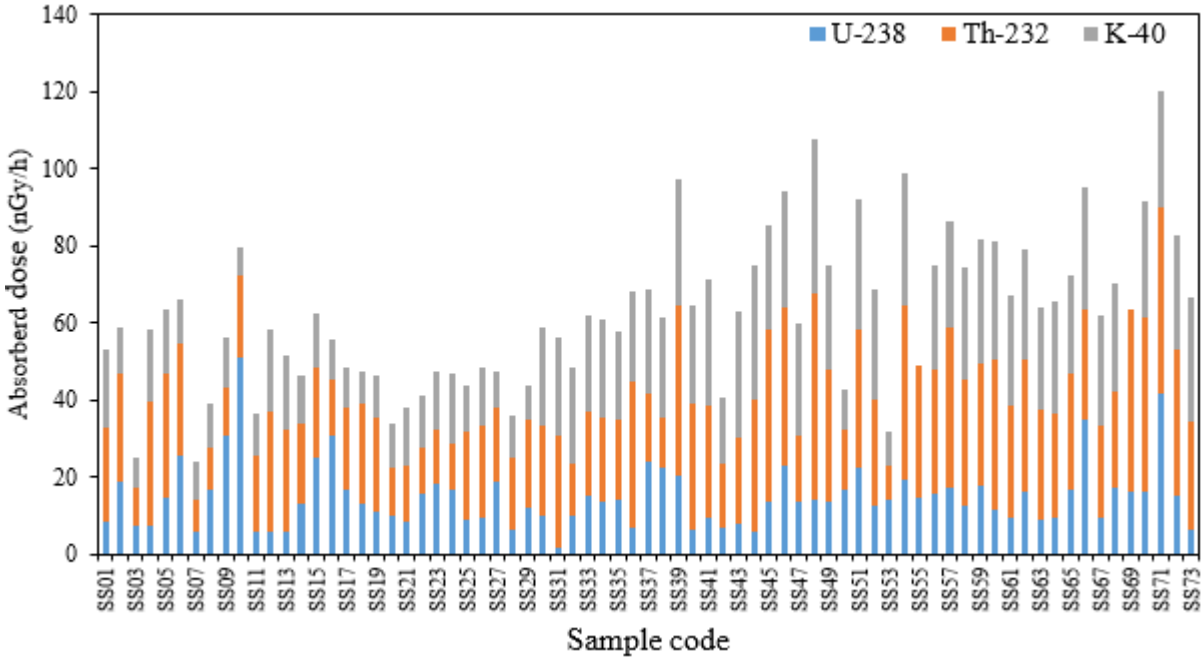

Figure 5.6: The calculated absorbed dose rate from ^{238}U, ^{232}Th and ^{40}K for all the measured soil samples

5.1.2 Foodstuff.

The results of the activity concentrations of NORM nuclides (^{238}U, ^{232}Th and ^{40}K) in the food samples collected in this study are presented in Table 5.5. The activity concentrations values were used to calculate mean activity and annual effective dose as presented in Table 5.6. The information in Table 5.5 is depicted in Figure 5.7. The highest activity concentration is observed in vegetable (spinach, rape and chou-mollier) samples for ^{40}K as indicated in Figure 5.7. In general, the activity concentrations of ^{40}K are significantly high in vegetables (Bolca, et al., 2007). Table 5.6 compares the natural radioactivity of ^{40}K in vegetable samples with those in different studies. The average activity concentration of this study is significantly less compared to the values in Table 5.6. The high activity concentration of ^{40}K in vegetable samples of this study could also be due to the soil that they have been planted on in the study area as it was also indicated on Figure 5.2 that the soil samples of this area contain high levels of ^{40}K activity. This may be a major contributing factor in the abundance of ^{40}K in the vegetables. Another possible reason could be the use of certain agricultural fertilizers such as nitrogen, phosphorus and potassium fertilizer (NPK) added to the soil during the plantation of the seeds. The effect of fertilization on uptake and distribution in vegetables has not been studied and need to be studied in future.

Table 5.5: Activity concentrations of ^{238}U, ^{232}Th and ^{40}K in food samples.

Activity concentration (Bq/kg)				
Categories	**Food**	**^{238}U** (From ^{214}Bi)	**^{232}Th** **(**From ^{208}Tl **)**	**^{40}K**
Fish				
F1	Burs	4.6 ± 2.3	4.2 ± 3.9	363 ± 29
F2	Kappa	4.2 ± 2.5	14.7 ± 4.3	300 ± 34
F3	Bream	9.6 ± 2.8	3.4 ± 1.6	251± 15
F4	Catfish	5.4 ± 2.7	8.5 ± 2.9	283 ± 38
Average		**6.0 ± 2.2**	**7.7 ± 4.5**	**299 ± 41**
Vegetables				
V1	Spinach	16.0 ± 1.9	17.9 ± 6.8	1441 ± 70
V2	Rape	19.8 ± 5.1	21.4 ± 2.7	1088 ± 67
V3	Chou-mollier	17.4 ± 5.7	18.1 ± 5.9	1576 ± 73
Average		**17.7 ± 1.6**	**19.1 ± 1.6**	**1368 ± 206**
Meat	Beef liver	< 6.1	5.9 ± 3.4	351 ± 30

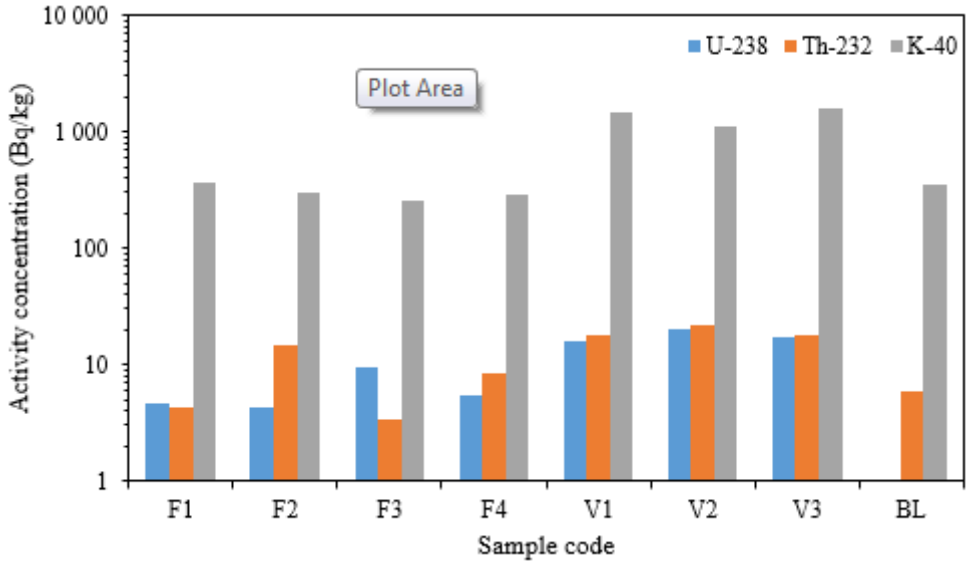

Figure 5.7: The Activity concentrations of ^{238}U, ^{232}Th and ^{40}K for all the measured food samples.

Table 5.6: Comparison of average activity concentration of ^{40}K in vegetable samples measured in this study and from different studies (Bolca, et al., 2007).

Study (Author)	^{226}Ra	^{232}Th	^{40}K
Ekdal (2003-2005)	10.1	17.4	4375
Bolca (2007)	27.7	10.2	1498
Present study	17.7	19.1	1368

5.1.2.1 Radiological risk assessment for food samples

The activity intake and annual effective dose of each radionuclide was calculated based on the average values obtained for each sample group. The results of the mean activity intake and annual effective dose are presented in Table 5.7. The artificial radionuclide (^{137}Cs) activity concentration were not included in the annual effective dose rate calculations since its activity concentration values were found to be negligible in all food samples. The analyses of food samples were based on dry weight in Bq/kg. The annual effective dose rate calculations of ^{238}U, ^{232}Th and ^{40}K were calculated on the basis of the assumptions made in section 4.1.6. The results implies that the levels of radioactivity in almost all food samples are insignificant and will not pose any radiological hazard from consumption except for ^{232}Th and ^{40}K which indicated elevated values in vegetable samples that are above the world average value of 290 μSv/y (UNSCEAR, 2000; Canbazoglu & Dogru, 2013). This elevated values could be caused by the consumption rate values (chapter 4, section 4.1.6) used for calculating annual effective dose. Generally, the ingestion of ^{232}Th and ^{40}K dose in vegetable samples can be considered to be low when compared with natural external exposures of about 2000 μSv/ y. Among the natural radionuclides in food samples of the study area, ^{40}K showed the highest concentration, possibly due to high activity concentrations of ^{40}K in the soil of the study area that can be taken up by vegetables. All the food samples investigated in this study are normally cooked before been consumed and this was not considered at this time in this work. However, future work on different food products in the study area need to consider the form in which they are ingested, to investigate the effect of boiling may have on the cooked product.

Table 5.7: Effective dose coefficient and annual effective dose in µSv/y for ^{238}U, ^{232}Th and ^{40}K.

Radionuclides	Activity Intake (Bq)	Effective Dose coefficient (µSv/Bq) (ICRP, 1996)	Effective Dose (µSv/y)	
			Range	Average
Fish				
^{238}U	208 ± 43	0.05	6.7 ± 4 - 15.1 ± 4.4	9.4 ± 1.9
^{232}Th	269 ± 90	0.23	27.5 ± 12.5 - 118 ± 34	62.0 ± 20.8
^{40}K	10406 ± 833	0.01	51.7 ± 0.1 - 75.0 ± 0.2	61.4 ± 4.9
Vegetables				
^{238}U	1770 ± 111	0.05	71.6 ± 3.0 - 88.9 ± 8.0	79.7 ± 5.0
^{232}Th	1912 ± 112	0.23	412 ± 0.6 - 491 ± 0.2	440 ± 26
^{40}K	136833 ± 14548	0.01	642 ± 0.4 - 930 ± 0.4	807 ± 86
Beef liver				
^{238}U	427 ± 21	0.05	-	19.2 ± 0.9
^{232}Th	413 ± 117	0.23	-	94.9 ± 27.0
^{40}K	24584 ± 30	0.01	-	145 ± 17

Note: - sign shows that there is no effective dose range for ^{238}U, ^{232}Th and ^{40}K in beef liver.

5.2 Heavy Metal Concentrations in soil, water, foodstuff and dust samples

5.2.1 Soil and Sediments

The average concentrations of heavy metals and radiotoxic elements in soil and sediments samples are presented in Table 5.8 and 5.9 respectively. Detailed results and additional metals of all samples in this study can be found in annexure B. The values in Table 5.8 were used to calculate average daily intakes for the carcinogenic and non-carcinogenic risk assessment in sections 5.3 and 5.4 respectively.

Table 5.8: Average concentrations (mg/kg) of selected heavy metals in soil samples from the three regions; the upper, middle and lower region.

Location	Average concentrations of heavy metals in soil samples (mg/kg)								
	As	Pb	Cd	Cr	Cu	Zn	Co	Th	U
Upper	2.0	30.4	0.7	108	22.3	29.4	6.8	9.1	1.6
Middle	1.3	14.4	0.5	75.9	18.0	27.7	14.3	9.8	1.3
Lower	2.2	36.9	0.5	84.3	20.9	19.0	21.2	12.3	1.5
Average	1.8	27.2	0.6	89.3	20.4	25.4	14.1	10.4	1.5

Table 5.9: Average concentrations (mg/kg) of selected heavy metals and radiotoxic elements in sediment samples from the dam.

Location	Average concentrations of heavy metals in sediments samples (mg/kg)								
	As	Pb	Cd	Cr	Cu	Zn	Co	Th	U
Dam	0.7	7.4	0.2	59.3	12.5	8.1	9.7	5.0	0.9

The results presented in Table 5.8 showed that the average concentrations of the heavy metals in soil are in the order of Cr, Pb, Zn, Cu, Co, Th, As, U and Cd. This observation is illustrated in Figure 5.8.

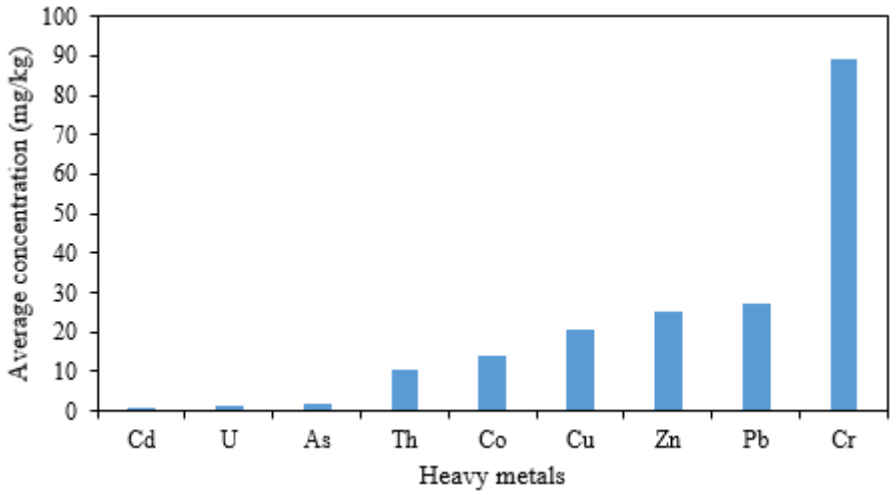

Figure 5.8: Average Concentrations of Heavy Metals and Radiotoxic elements in Soil

To further understand the status of heavy metals in the study area, the presented results were compared with those of other countries as shown in Table 5.10. The average concentrations of

most heavy metals in the soil samples were lower than the maximum allowable limits. These results suggest that the soil of this area is not polluted with heavy metals.

Table 5.10: Maximum allowable limits in soil (mg/kg) for different countries (Dragovic, et al., 2006; Kamunda, et al., 2016)

Country	**Maximum allowable limit of the concentrations of heavy metals in soil (mg/kg) for different countries**								
	As	**Pb**	**Cd**	**Cr**	**Cu**	**Zn**	**Co**	**Th**	**U**
Germany	50	70	1	60	40	150	-	-	-
Poland	-	100	3	100	100	300	50	5.19	2.08
Australia	20	300	3	50	100	200	-	1.3	2.2
Taiwan	60	300	5	250	200	600	-	10.8	2.4
Bulgaria	10	26	0.4	65	345	88	20	7.41	3.2
Canada	20	200	3	250	150	500	-	11.9	4.1
China	30	80	0.5	200	100	250	-	15.2	-
Tanzania	1	200	1	100	200	150	-	-	-
South Africa	5.8	20	7.5	6.5	16	240	300	7.77	2.29
World average	30	140	2.8	120	139	275	125	11.08	2.67
Present study	1.83	27.23	0.56	89.30	20.40	25.38	14.14	10.40	1.47
FAO/WHO Guidelines	20	100	3	100	100	300	50	-	1.4

NOTE: - not reported

5.2.2 Water

The average concentrations (mg/*l*) of heavy metals in water samples are presented in Table 5.11. Detailed results and additional metals of all analysed water samples can be found in Table B3, Annexure B. The results were compared with those of international guidelines for permissible limits of heavy metals in drinking water. The average concentrations of most heavy metals in the water samples were lower than the permissible limits. The results showed that the average concentrations of the heavy metals in water were lower than the WHO permissible limit for all selected heavy metals indicating safe water drinking for the residents of the study area. A point of concern to be investigated further is the elevated cadmium concentration in the dam, as this water source is the major supplier to the capital of Botswana.

Table 5.11: The average heavy metals concentrations (mg/*l*) in water samples for all seasons and comparison with permissible limit in drinking water (WHO, 2011).

Water source	**Average concentrations of heavy metals in different water sources in mg/*l* ($\times 10^{-3}$)**								
	As	**Pb**	**Cd**	**Cr**	**Cu**	**Zn**	**Co**	**Th**	**U**
Dam	0.9	7.7	10.9	21.5	17.5	90.6	3.3	0.04	0.7
Borehole 1	12.5	1.8	0.3	16.2	17.4	41.2	0.6	<0.001	13.0
Borehole 2	8.9	1.2	5.8	24.3	26.8	16.2	<0.002	<0.001	0.15
Borehole 3	2.2	1.6	0.2	24.1	31.9	39.3	0.1	<0.001	11.2
Pond	0.5	1.4	<0.1	10.6	12.7	13.5	0.2	<0.001	4.2
Well	0.8	3.348	0.448	35.0	42.6	81.2	1.4	<0.001	0.1
average all samples	4.3	2.8	2.9	22.0	24.8	71.2	0.9	0.01	4.9
WHO	10	10	3	50	2000	3000	100	-	15

5.2.3 Foodstuff

Table 5.12 presents the average concentrations of heavy metals in food samples. Additional results of analysed food samples in this study can be found in Table B4, Annexure B. The average concentration values were further used to calculate average ADI and cancer risk for children and adults in the study area.

Table 5.12: Average concentrations (mg/kg) of selected heavy metals in food samples.

Sample type	**Average concentrations of heavy metals in food samples (mg/kg)**								
	As	**Pb**	**Cd**	**Cr**	**Cu**	**Zn**	**Co**	**Th**	**U**
Fish	0.2	0.4	0.1	40.9	2.3	10.4	0.4	0.02	0.02
Vegetable	0.2	0.3	0.1	39.5	7.3	7.9	0.6	0.04	0.07
Beef liver	0.1	0.5	0.1	41.1	183	40.5	0.5	0.01	<0.01
Average	0.2	0.4	0.1	40.5	64.2	19.6	0.5	0.02	0.04

The results in Table 5.12 were compared with those of international guidelines for permissible limits (Table 5.13) of heavy metals in foodstuffs. Table 5.12 revealed that the highest heavy metal concentrations were found in beef liver because the liver is the major organ involved in

xenobiotic metabolism. Organisms retain metals through specific binding proteins known as metallothioneins in their liver. Metallothioneins play an important role in metal homeostasis and in protection against heavy-metal toxicity. Despite having high concentrations of heavy metals, Cu was found to have exceeded the permissible limits of beef liver samples. From the permissible limits set by international guidelines, consumers of beef liver from this study areas are likely to be prone to Cu toxicity.

For fish samples, the results showed that the levels of heavy metals in muscles of the four fish species were within the acceptable limits set by international standards for fish human consumption permissible limit except for Pb and Cr which were slightly above the permissible limit. The results suggest that consumers of the fishes from this study areas are also likely to be liable to Cr toxicity. The overall obtained results suggest that the fishes of the Letsibogo dam are suitable for human consumption. For vegetable samples, Pb was found to have slightly exceeded the permissible limit. The results suggest consumers of vegetables from the study area may face danger of Pb toxicity as at the time of study.

Table 5.13: Permissible Limits of Heavy Metals in food samples (Commission Regulation, 2006; Baharom & Ishak, 2015).

Foodstuff	**Heavy metals concentration in various foodstuff (mg/kg)**								
	As	**Pb**	**Cd**	**Cr**	**Cu**	**Zn**	**Co**	**Th**	**U**
Fish	1	0.30	0.05	2	30	100	-	-	
Vegetable	0.5	0.10	0,20	-	40	60	0.01	-	-
Beef liver	1	0,50	0,50	-	50	50		-	-
WHO	-	5.0	0.01	-	0.2	2.0	-	-	-

-: not reported

5.2.4 Dust

Table 5.14 presents the heavy metal and radiotoxic element concentrations in dust samples in mg/l. These values were used to calculate ADI for carcinogenic and non-carcinogenic risk for the residents of the study area. The results were also compared with those of other cities in developed countries for heavy metals in dust. The average concentrations of heavy metals in dust samples were lower than those determined in other cities. The results of these villages in this study suggest that the natural sources dominate the composition of dust samples in the study area as at the time of study.

Table 5.14: The heavy metal concentrations (mg/kg) of selected heavy metals in dust samples and comparison with different countries values from literature (Ferreira-Baptista & Miguel, 2005).

Locality	**Average concentrations of heavy metals in different locations (mg/kg)**								
	As	**Pb**	**Cd**	**Cr**	**Cu**	**Zn**	**Co**	**Th**	**U**
Serule	1.3	2.5	0.1	21.0	13.8	124	1.5	3.1	0.5
Sese	1.2	16.1	0.2	43.1	43.2	86.5	3.1	3.2	0.5
Gojwane	3.4	13.8	0.2	37.6	11.5	139	3.5	2.7	0.5
Damochoje-naa	0.5	5.3	0.1	37.5	22.3	135	2.5	2.9	0.4
Mmadinare	0.8	16.7	0.1	37.0	54.3	116	3.4	3.5	0.4
Average	1.5	10.9	0.1	35.2	29.0	120	2.8	3.1	0.5
London	-	1030	3.5	-	155	680	-	-	-
Luanda	5	351.3	1.2	25.7	41.8	317	2.9	1.7	1.0
Madrid	-	1927	-	61	188	476	-	-	-
Oslo	-	180	1.4	-	123	412	-	-	-
Ottawa	-	68	0.6	59	188	184	-	-	-

Note: - sign indicates that there was no data reported these countries.

5.3 Non-carcinogenic risk assessment of heavy metals through soil, water, foodstuff and dust exposure routes

The assessment of non-carcinogenic risk for heavy metals on individual members of the public were calculated based on the RfD values shown in Table 4.5 and the calculated ADI values of the measured samples. The ADI values via various exposure pathways (ingestion, inhalation and dermal) were calculated using the exposure equations, 4.13 to 4.17. These results were further presented in terms of the hazard quotient (HQ) and hazard index (HI) for different exposure pathways using equations 4.20 and 4.21 in chapter 4. The expressions of HQ and HI are important parameters used to assess the level of non-carcinogenic risks. If the value of HQ and/or HI is less than 1, then there is no obvious risk to individual members of the public, but if the HI value is greater than 1, there may be concern for potential non-carcinogenic health effects (US.EPA, 1989; DEA, 2010).

5.3.1 Non-carcinogenic risk assessment of heavy metals through soil exposure routes

Table 5.15 presents the ADI values used for non-carcinogenic risk calculations due to soil samples while Table 5.16 shows the HQ and HI values. Inhalation and Dermal were the only exposure pathways considered for soil samples. The HQ values for each constituent were summed to obtain HI. The results presented in Table 5.16 show that the total HQ values (HI) is less than 1 indicating no risk to individual members of the public.

Table 5.15: Average daily intake (ADI) values (mg/kg/day) for adults and children in all regions due to soil for non-carcinogenic risk calculations.

Heavy metals	Pathway (Child)			Pathway (Adult)		
	Inhalation ($\times 10^{-8}$)	Dermal ($\times 10^{-5}$)	Total ($\times 10^{-5}$)	Inhalation ($\times 10^{-9}$)	Dermal ($\times 10^{-6}$)	Total ($\times 10^{-6}$)
As	0.1	0.3	0.3	0.4	0.6	0.6
Pb	1.3	4.5	4.5	5.7	9.2	9.3
Cd	0.1	0.1	0.1	0.1	0.2	0.2
Cr	4.4	14.6	14.6	18.8	30.3	30.3
Cu	1.0	3.3	3.3	4.3	6.9	6.9
Zn	1.3	4.2	4.2	5.4	8.6	8.6
Co	0.7	2.3	2.3	3.0	4.8	4.8
Th	0.5	1.7	1.7	2.2	3.5	3.5
U	0.1	0.2	0.2	0.3	0.5	0.5
Total	9.4	31.2	31.2	40.2	64.7	64.7

Table 5.16: Hazard quotient (HQ) values and corresponding hazard Indices (HI) for heavy metals in soil.

ADI (mg/kg-day)						
Heavy metals	**Pathway (Child) ($\times 10^{-3}$)**			**Pathway (Adult) ($\times 10^{-3}$)**		
	Inhalation (HQ)	**Dermal (HQ)**	**Total (HI)**	**Inhalation (HQ)**	**Dermal (HQ)**	**Total (HI)**
As	0.003	10.0	10.0	0.001	2.1	2.1
Pb	-	12.4	12.4	-	2.57	2.6
Cd	1.8	1.8	1.8	0.002	0.38	0.4
Cr	68.7	48.8	68.7	8.6	10.11	18.7
Cu	-	1.4	1.4	-	0.29	0.3
Zn	-	0.1	0.1	-	0.03	0.03
Co	2.6	2.3	2.6	0.1	0.48	0.6
Th	-	-	-	-	-	-
U	-	-	-	-	-	-
Total	73.1	76.9	97.1	8.7	15.93	24.7

Note: - sign in the table indicates that no reference dose values were available.

5.3.2 Non-carcinogenic risk assessment of heavy metals through water exposure routes

The ADI values used for non-carcinogenic risk assessment in water samples are presented in Table 5.17. The non-carcinogenic risk parameters, HQ and HI values, are shown in Table 5.18. The exposure pathways considered were ingestion and dermal. The total HQ values (HI) in Table 5.18 is less than 1 indicating no risk to the people in the study area.

Table 5.17: ADI values and the cancer risk values through ingestion and dermal contact of heavy metals for individual members of the public for water.

ADI (mg/kg-day)						
Heavy metals	**Pathway (Child)**			**Pathway (Adult)**		
	Ingestion ($\times10^{-5}$)	**Dermal ($\times10^{-8}$)**	**Total ($\times10^{-5}$)**	**Ingestion ($\times10^{-4}$)**	**Dermal ($\times10^{-8}$)**	**Total ($\times10^{-4}$)**
As	2.7	0.9	2.7	0.7	5.9	0.7
Pb	5.4	1.7	5.4	1.37	11.7	1.3
Cd	0.3	0.1	0.4	0.1	0.7	0.1
Cr	21.5	6.8	21.5	5.4	46.8	5.4
Cu	26.9	8.5	26.9	6.7	58.5	6.7
Zn	130	41.0	130	32.5	283	325
Co	4.6	1.4	4.6	1.1	9.9	1.1
Th	0.04	0.01	0.04	0.01	0.1	0.01
U	8.9	2.8	8.9	2.2	0.2	2.2

Table 5.18: Hazard quotient (HQ) values and corresponding hazard indices (HI) for heavy metals in water.

HQ Values						
Heavy metals	**Pathway(Child)**			**Pathway(Adult)**		
	Ingestion ($\times10^{-2}$)	**Dermal ($\times10^{-5}$)**	**Total (HI) ($\times10^{-2}$)**	**Ingestion ($\times10^{-2}$)**	**Dermal ($\times10^{-5}$)**	**Total (HI) ($\times10^{-2}$)**
As	9.1	2.9	9.1	22.7	19.8	22.7
Pb	1.5	-	1.5	3.7	-	3.7
Cd	0.6	0.2	0.6	1.5	1.3	1.5
Cr	7.2	-	7.2	17.9	-	17.9
Cu	0.1	0.4	0.1	0.2	2.4	0.2
Zn	6.5	0.6	6.5	16.3	3.8	16.3
Co	0.1	252	0.4	0.3	1740	2.1
Th	-	-	-	-	-	-
U	-	-	-	-	-	-

Note: - sign in the table indicates that no reference dose values were available for calculation.

5.3.3 Non-carcinogenic risk assessment of heavy metals through foodstuff exposure routes

The results of ADI values used together with their corresponding HQ and HI values for food samples are presented in Table 5.19. The only exposure pathway considered for food samples was the ingestion. The calculated HI values exceeded the safety limit of 1 for As, Cr and Cu for children and adults, indicating a potential non-carcinogenic health risk to residents in the study area.

Table 5.19: Average daily intake (ADI) for adults and children and their corresponding hazard quotient (HQ) values due to ingestion of heavy metals in foodstuff samples.

ADI (mg/kg/day) and HQ						
Heavy metals	**Pathway, (Child)**			**Pathway, (Adult)**		
	$ADI_{(ing)}$ ($\times 10^{-4}$)	**$RfD_{(ing)}$ ($\times 10^{-3}$)**	**HQ (HI) ($\times 10^{-1}$)**	**$ADI_{(ing)}$ ($\times 10^{-4}$)**	**$RfD_{(ing)}$ ($\times 10^{-3}$)**	**HQ (HI) ($\times 10^{-1}$)**
As	3.5	0.3	11.8	3.8	0.3	12.6
Pb	7.4	3.6	2.1	1.7	3.6	2.2
Cd	1.6	0.5	3.1	8.0	0.5	3.3
Cr	764	3.0	2.6	819	3.0	273
Cu	505	37.0	13.7	541	37.0	14.6
Zn	249	301	0.8	267	301	0.9
Co	8.8	20.0	0.4	9.4	20.0	0.5
Th	0.5	-	-	0.5	-	-
U	0.8	-	-	0.8	-	-

Note: - sign in the table indicates that no reference dose values were available for calculation.

5.3.4 Non-carcinogenic risk assessment of heavy metals through dust exposure routes

Table 5.20 presents results of ADI values used together with their corresponding HQ and HI values for dust samples. The only pathway considered was the inhalation pathway. The calculated HI values are less than unit showing no risk to individual members of the public according to USEPA and South African guidelines. (US.EPA, 1989; DEA, 2010).

Table 5.20: Average daily intake (ADI) and their corresponding hazard quotient (HQ) and HI values due to inhalation of heavy metals in dust.

ADI (mg/kg/day) and HQ						
Heavy metals	**Pathway (Child)**			**Pathway (Adult)**		
	$ADI_{(inh)}$ ($\times 10^{-10}$)	**$RfD_{(inh)}$ ($\times 10^{-5}$)**	**HQ (HI) ($\times 10^{-6}$)**	**$ADI_{(inh)}$ ($\times 10^{-10}$)**	**$RfD_{(inh)}$ ($\times 10^{-5}$)**	**HQ (HI) ($\times 10^{-6}$)**
As	0.6	30.0	0.2	1.3	30.0	0.4
Pb	4.6	-	-	9.8	-	-
Cd	0.1	5.7	0.1	0.1	5.7	0.2
Cr	14.9	3.0	49.5	31.8	3.0	106
Cu	12.2	0.6	214	26.2	0.6	459
Zn	50.6	-	-	108	-	-
Co	1.2	-	-	2.5	-	-
Th	1.3	-	-	2.8	-	-
U	0.2	-	-	0.4	-	-

Note: - sign in the table indicates that no reference dose values were available for calculation.

5.3.5 Summary of non-carcinogenic risk assessment of heavy metals for all samples

A summary of the non-carcinogenic risk of heavy metals for the various exposure pathways considered in this study in all the sample matrices is presented in Table 5.21. The HI values were obtained by adding up an individual heavy metal values of various samples of the same exposure pathway components. The HI value were found to be 1.5, 2.8×10^{1} and 1.5 for As, Cr and Cu respectively. These values are greater than 1, indicating a potential health risk of As, Cr and Cu to the residents of the study area. The values in Table 5.21 were also used to evaluate the exposure pathway and the sample type that contributed the most risk to non-carcinogenic in Figure 5.12 and Figure 5.13 respectively.

Table 5.21: Summary of HQ values and HI in all samples matrices for adults in the study area.

	Soil		Water		Food	Dust	Total Risk, HI
	Inhalation ($\times10^{-4}$)	**Dermal ($\times10^{-4}$)**	**Ingestion ($\times10^{-2}$)**	**Dermal ($\times10^{-4}$)**	**Ingestion ($\times10^{-1}$)**	**Inhalation ($\times10^{-5}$)**	**($\times10^{-1}$)**
As	0.01	20.7	22.7	2.0	12.6	0.04	14.9
Pb	-	25.7	3.7	-	2.2	-	2.6
Cd	0.02	3.8	1.5	0.1	3.3	0.02	3.5
Cr	85.5	101	17.9	-	273	10.6	27.5
Cu	-	2.9	0.2	0.2	14.6	45.9	14.6
Zn	-	0.3	16.3	0.4	0.9	-	2.5
Co	1.0	4.8	0.3	174	0.5	-	0.7
Th	-	-	-	-	-	-	-
U	-	-	-	-	-	-	-

Note: - sign indicates that no reference dose values were available for calculation

The values in Table 5.21 were depicted in Figure 5.9 and Figure 5.10 to determine the exposure pathway (Figure 5.9) and the sample type (Figure 5.10) that contributed the most risk to non-carcinogenic. In Figure 5.9, it can be seen that the greatest contributor to non-carcinogenic risk is the ingestion pathway with an HI value of 2.8×10^{1} driven by Cr. This was primarily because Cr is an essential trace element occurring in food products of both plant and animal origins. Although Cr plays a vital role in various metabolic processes, their HI values for food samples were higher than the toxicity threshold doses for the ingestion pathway, thereby becoming more hazardous compared to the other heavy metals. It can also be seen in Figure 5.10 that food samples had the greatest contribution with an HQ value of 2.7×10^{1}. Cr again was realized to contribute the most to the non-carcinogenic risk.

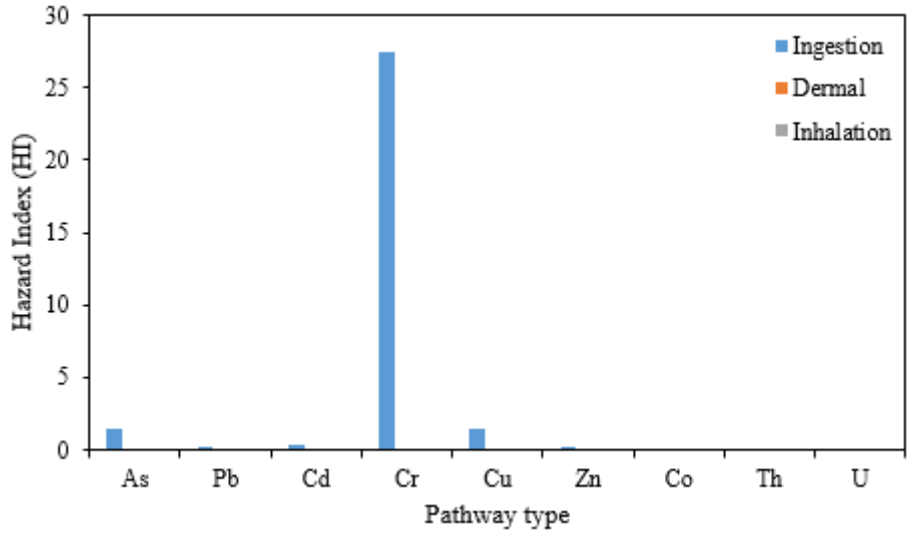

Figure 5.9: Hazard Quotient for Heavy Metals through various exposure pathways.

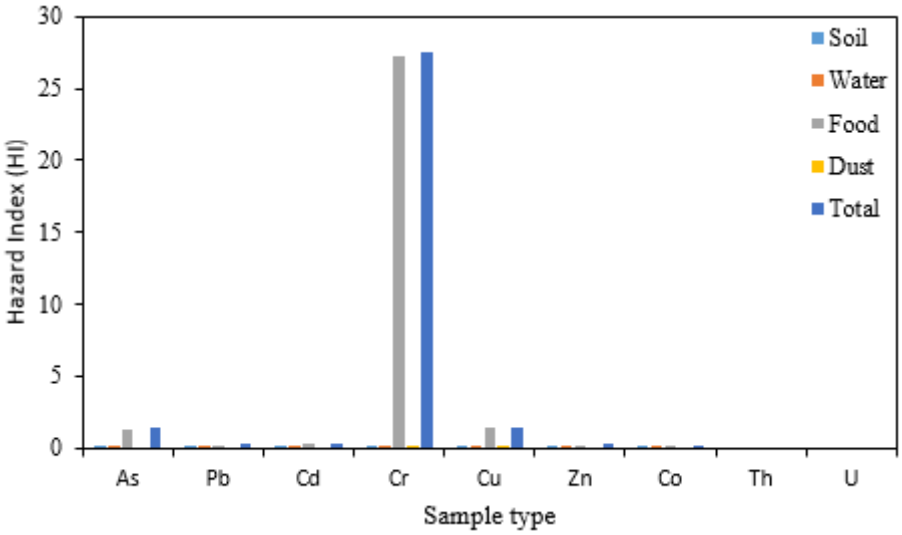

Figure 5.10: Hazard quotient for heavy metals through different samples**.**

5.4 Carcinogenic risk assessment of heavy metals through soil, water, foodstuff and dust exposure routes

For carcinogenic risk, the exposure assessment evaluation was done by calculating the average daily intake (ADI) of heavy metals of As, Pb, Cd, Cr and Co as these metals are known to induce carcinogenic effects. The ADI values for different exposure pathways were calculated using the exposure equations 4.12 to 4.16 in chapter 4. According to regulatory bodies, the acceptable range of risk in terms of radiological safety is 1×10^{-6} to 1×10^{-4} (Hu, et al., 2017). A carcinogenic risk of less than or equal to 1×10^{-6} represents essential safety, and a

carcinogenic risk of equal to or greater than 1×10^{-4} indicates a potentially great risk (Hu, et al., 2017).

5.4.1 Carcinogenic risk assessment of heavy metals through soil exposure routes

The ADI values used for carcinogenic risk calculations for soil are presented in Table 5.22. These values were further used in cancer risk assessment as shown in Table 5.23. The assessed carcinogenic risk associated with exposure to soil contaminated with heavy metals was 1.5×10^{-6} and 6.9×10^{-7} for children and adults respectively. The children and adult's values are almost equal and/or less than the acceptable value for risk of 1×10^{-6} indicating no threat to children and adults in the study area.

Table 5.22: Average daily intake (ADI) values used for carcinogenic risk calculations in soil.

ADI (mg/kg/day) ($\times 10^{-6}$)						
Heavy metals	**Pathway (Child)**			**Pathway (Adult)**		
	Inhalation	**Dermal**	**Total**	**Inhalation**	**Dermal**	**Total**
As	1.2	0.3	1.5	0.6	0.3	0.9
Pb	16.3	3.8	20.2	8.8	4.0	12.7
Cd	0.4	0.1	0.5	0.2	0.1	0.3
Cr	67.1	12.5	79.6	35.9	13.0	48.9
Co	7.7	2.0	9.7	4.1	2.1	6.2
Total	92.8	18.6	11.1	49.7	19.4	69.0

Table 5.23: Cancer risk values of heavy metals for individual members of the public through Soil.

Risk values						
Heavy metals	**Pathway (Child)**			**Pathway (Adult)**		
	Inhalation	**Dermal**	**Total**	**Inhalation**	**Dermal**	**Total**
As	0.1×10^{-9}	4.7×10^{-7}	4.7×10^{-7}	3.1×10^{-11}	5.0×10^{-7}	5.0×10^{-7}
Pb	6.5×10^{-11}	-	6.5×10^{-11}	1.9×10^{-7}	-	1.9×10^{-7}
Cd	1.3×10^{-10}	-	1.3×10^{-10}	1.6×10^{-11}	-	1.6×10^{-11}
Cr	1.0×10^{-6}	-	1.0×10^{-6}	6.1×10^{-11}	-	6.1×10^{-11}
Co	8.8×10^{-9}	-	8.8×10^{-9}	4.6×10^{-10}	-	4.6×10^{-10}
Total	1.0×10^{-7}	4.7×10^{-7}	1.5×10^{-6}	1.96×10^{-7}	5.02×10^{-7}	6.9×10^{-7}

Note: - sign indicates that no reference dose values were available for calculation.

5.4.2 Carcinogenic risk assessment of heavy metals through water exposure routes

The ADI values used for carcinogenic risk calculations in water samples are presented in Table 5.24. These values were used to calculate cancer risk in Table 5.25. The results shown in this table indicate that the total cancer risk was 1.5×10^{-4} and 3.7×10^{-4} for children and adults respectively. The results are within the acceptable radiological safety range of 1×10^{-6} to 1×10^{-4} indicating no risk to children and adults in the study area exposed to water.

Table 5.24: ADI values and the cancer risk values through ingestion and dermal contact of heavy metals for individual members of the public for water.

ADI and the Cancer Risk Values						
Heavy metals	**Pathway (Child)**			**Pathway (Adult)**		
	Ingestion ($\times 10^{-5}$)	**Dermal ($\times 10^{-8}$)**	**CSF_{ing} ($\times 10^{-2}$)**	**Ingestion ($\times 10^{-5}$)**	**Dermal ($\times 10^{-8}$)**	**CSF_{derm} ($\times 10^{-2}$)**
As	2.7	0.9	150	6.8	5.9	150
Pb	5.4	1.7	0.9	13.4	11.7	-
Cd	0.3	0.1	-	0.7	0.7	-
Cr	21.5	6.8	50.0	53.8	0.5	-
Co	4.6	1.4	-	11.4	9.9	-

Note: - sign indicates that no reference dose values were available for calculation.

Table 5.25: Cancer risk values of heavy metals for individual members of the public through water.

Risk values						
Heavy metals	**Pathway (Child)**			**Pathway (Adult)**		
	Ingestion ($\times 10^{-5}$)	**Dermal ($\times 10^{-8}$)**	**Risk ($\times 10^{-5}$)**	**Ingestion ($\times 10^{-4}$)**	**Dermal ($\times 10^{-8}$)**	**Risk ($\times 10^{-4}$)**
As	4.1	1.3	4.1	1.0	8.9	1.0
Pb	0.1	-	0.1	0.01	-	0.01
Cd	-	-	-	-	-	-
Cr	10.8	-	10.8	2.7	-	2.7
Co	-	-	-	-	-	-
Total	14.9	1.3	14.9	3.7	8.9	3.7

Note: - sign indicates that no reference dose values were available for calculation.

5.4.3 Carcinogenic risk assessment of heavy metals through foodstuff exposure routes

For food samples, the results of the carcinogenic risks presented in Table 5.26 revealed that the total carcinogenic risk due to consumption of the foodstuff was found to be 3.9×10^{-2} and 4.2×10^{-2} for children and adults respectively, mainly driven by Cr. These values are higher than the guideline value indicating carcinogenic risk for both children and adults of the study area.

Table 5.26: ADI values and the cancer risk values through ingestion of heavy metals for individual members of the public for foodstuff.

ADI (mg/kg/day) and cancer risk values						
Heavy metals	**Pathway (Child)**			**Pathway (Adult)**		
	$ADI_{(ing)}$ ($\times 10^{-4}$)	**$CSF_{(ing)}$ ($\times 10^{-2}$)**	**Risk ($\times 10^{-4}$)**	**$ADI_{(ing)}$ ($\times 10^{-4}$)**	**$CSF_{(ing)}$ ($\times 10^{-2}$)**	**Risk ($\times 10^{-4}$)**
As	3.5	150	5.3	3.8	150	5.7
Pb	7.4	0.9	0.1	8.0	0.9	0.1
Cd	1.6	-	-	1.7	-	-
Cr	764	0.1	382	819	0.1	410
Co	8.8	-	-	9.4	-	-
Total	785		387	842		415

Note: - sign indicates that no reference dose values were available for calculation.

5.4.4 Carcinogenic risk assessment of heavy metals through dust exposure routes

Table 5.27 presents the ADI and carcinogenic risk results for dust samples. The total carcinogenic risk for children and adults was found to be 6.3×10^{-8} and 1.4×10^{-7}, respectively, all of which were less than the acceptable value for risk of 1×10^{-6} making dust samples safe to people of the study area. Inhalation was considered the main pathway of carcinogenic risk to human health.

Table 5.27: Average ADI values and the cancer risk values through inhalation of heavy metals for individual members of the public for dust.

ADI (mg/kg/day) and cancer risk values						
Heavy metals	**Pathway (Child)**			**Pathway (Adult)**		
	$ADI_{(inh)}$ ($\times 10^{-10}$)	**$CSF_{(inh)}$ ($\times 10^{0}$)**	**Risk ($\times 10^{-9}$)**	**$ADI_{(inh)}$ ($\times 10^{-10}$)**	**$CSF_{(inh)}$ ($\times 10^{0}$)**	**Risk ($\times 10^{-9}$)**
As	0.6	15.0	0.9	1.3	15.0	2.0
Pb	4.6	0.04	0.02	9.8	0.04	0.04
Cd	0.1	6.3	0.03	0.1	6.3	0.1
Cr	14.9	41.0	61.1	31.8	41.0	130
Co	1.2	9.8	1.2	2.5	9.8	2.5
Total	21.3	72.1	63.2	45.6	72.1	135

5.4.5 Summary of carcinogenic risk assessment of heavy metals for all samples

A summary of the carcinogenic risk for the various exposure pathways considered in all the sample matrices is presented in Table 5.28. These values were used to determine the exposure pathway and the sample type that contributed most to the risk of carcinogenic exposure, and are shown in Figure 5.11 and Figure 5.12 respectively.

Table 5.28: Summary of cancer risk values of heavy metals through soil, water, foodstuff and dust exposure routes for adults of the study area.

	Soil		**Water**		**Food**	**Dust**	**Total Risk**
	Inhalation ($\times 10^{-10}$)	**Dermal ($\times 10^{-7}$)**	**Ingestion ($\times 10^{-4}$)**	**Dermal ($\times 10^{-8}$)**	**Ingestion ($\times 10^{-4}$)**	**Inhalation ($\times 10^{-9}$)**	
As	0.3	5.0	1.0	8.9	5.7	2.0	6.7×10^{-4}
Pb	1850	-	0.01	-	0.1	0.04	8.1×10^{-6}
Cd	0.2	-	-	-	-	0.1	9.0×10^{-11}
Cr	0.6	-	2.7	-	410	130	4.1×10^{-2}
Co	4.6	-	-	-	-	2.47	2.9×10^{-9}

Note: - sign indicates that no reference dose values were available for calculation

In Figure 5.11, it can be clearly seen that the greatest contributor to carcinogenic risk is the ingestion pathway. Cr was realized to be the major contributor to the risk of carcinogenic with the total cancer risk value of 4.1×10^{-2}, which is greater than the maximum permissible limit of 1×10^{-4}, indicating a great potentially carcinogenic risk. It was also observed that the food samples in Figure 5.12 contributed the most of Cr to the carcinogenic risk.

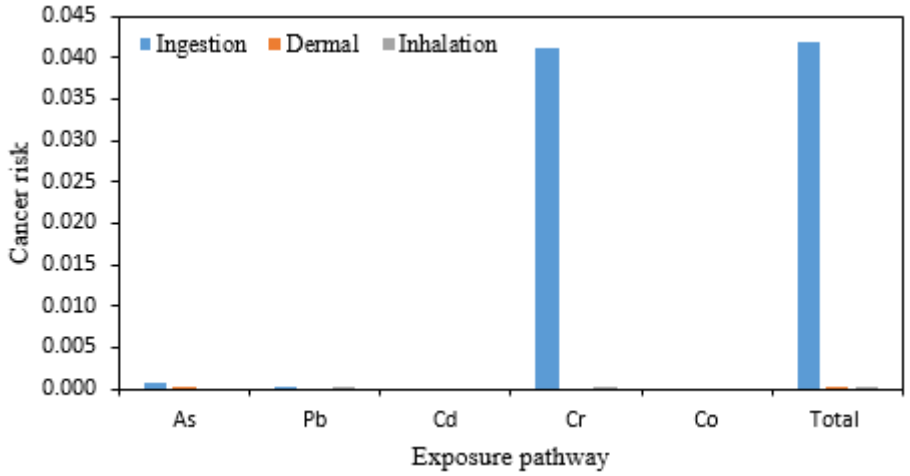

Figure 5.11: Cancer risk values for heavy metals through different pathways.

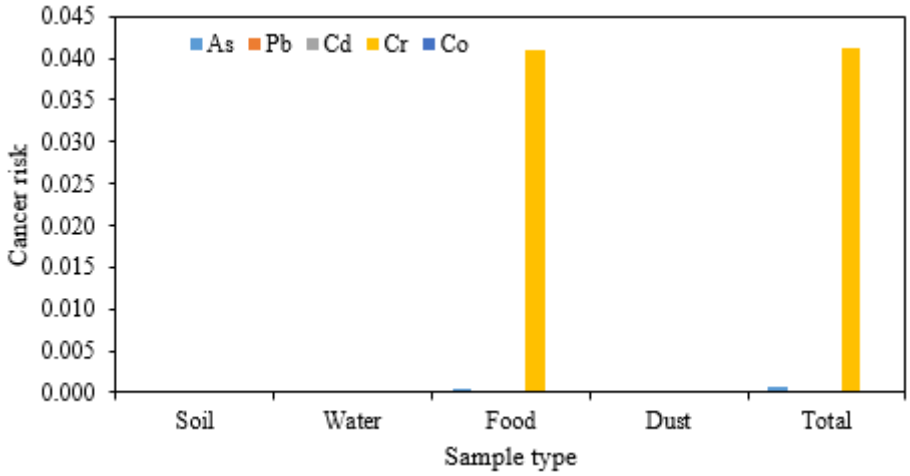

Figure 5.12: Cancer risk values for heavy metals through different matrices.

5.5 Seasonal variation for heavy metals in water.

The seasonal variation concentrations of heavy metals in different water sources are presented in Tables 5.29 to 5.32 and depicted in Figures 5.13 to 5.16. Without going into the details of every individual element, four heavy metals i.e., As, Pb, Cd and Cr were selected for the

assessment of seasonal dynamics in water samples. The figures were plotted using a clustered column chart type to show how heavy metals change in concentration over a period of time.

Analysis of water samples showed a slightly higher average concentration of As, Pb, Cd and Cr in the dry season compared to the other seasons. This is likely due to high temperatures in the dry season that lead to a high rate of evaporation especially for surface water bodies and a prolonged period of no rain fall, leading to the concentration of heavy metals in water bodies. The rainy season will cause dilution and lower the concentration of heavy metals in water bodies as it was observed in most of the water bodies.

Table 5.29: As- concentration (mg/*l*) for cool, rainy and dry seasons in different water sources.

Season	Dam	Borehole1	Borehole2	Borehole3	Pond	Well
Cool	< 0.00001	0.0107	0.0249	0.0006	-	0.0008
Rainy	0.0010	0.0055	0.0008	0.0006	0.0005	< 0.00001
Dry	0.0008	0.0212	0.0009	0.0055	-	0.0007

Note: - and < signs indicate that there was no water during this seasons and below detection limit, respectively.

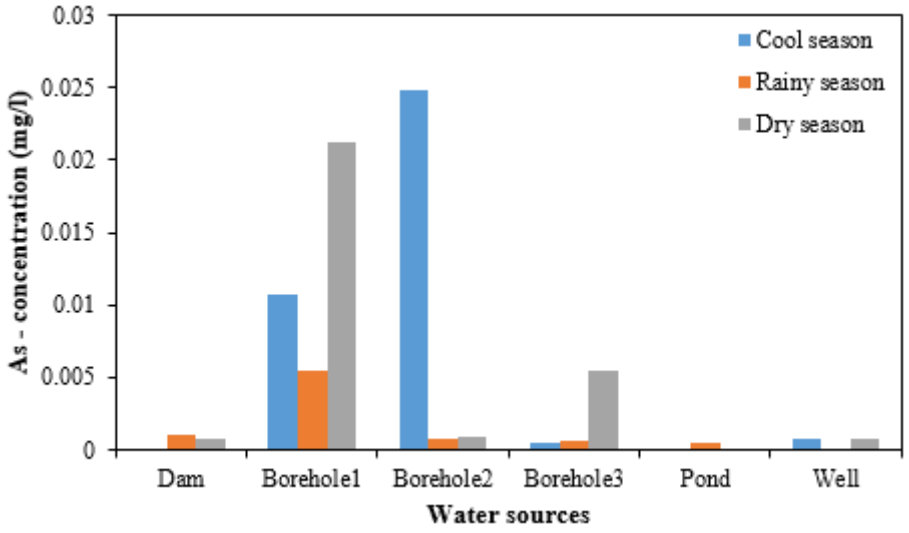

Figure 5.13: Seasonal variations of As in different water sources.

Table 5.30: Pb- concentration (mg/*l*) for cool, rainy and dry seasons in different water sources.

Season	Dam	Borehole1	Borehole2	Borehole3	Pond	Well
Cool	0.0157	0.0022	< 0.000001	0.0016	-	0.0043
Rainy	0.0037	0.0009	0.0011	0.0013	0.0014	< 0.000001
Dry	0.0037	0.0024	0.0014	0.0018	-	0.0024

Note: - sign indicates that there was no water during this seasons.

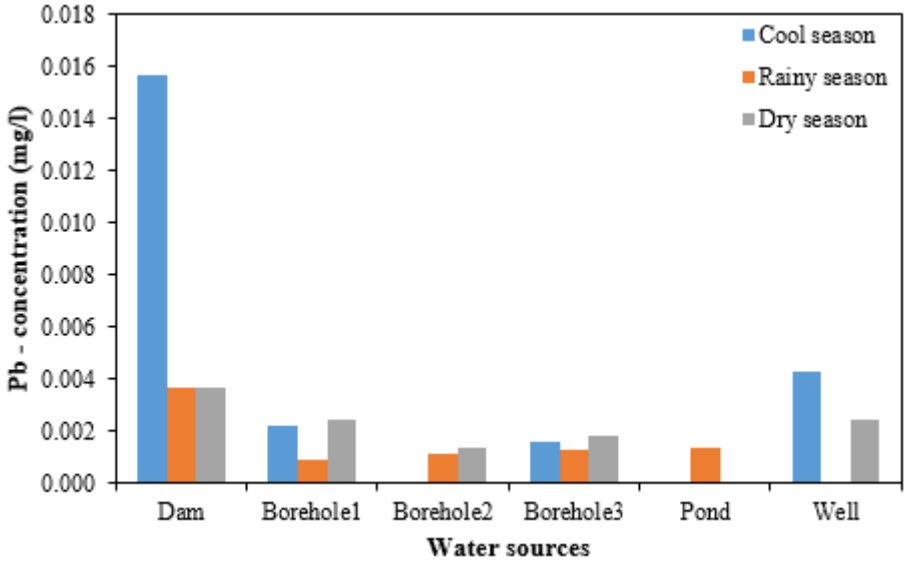

Figure 5.14: Seasonal variation for Pb in different water sources.

Table 5.31: Cd- concentration (mg/*l*) for cool, rainy and dry seasons in different water sources.

Season	Dam	Borehole1	Borehole2	Borehole3	Pond	Well
Cool	0.0109	0.0008	0.0116	0.0006	-	0.0008
Rainy	< 0.00003	0.00004	< 0.00003	0.00003	< 0.00003	< 0.00003
Dry	< 0.00003	0.00003	0.00004	0.0001	-	0.0001

Note: - sign indicates that there was no water during this seasons.

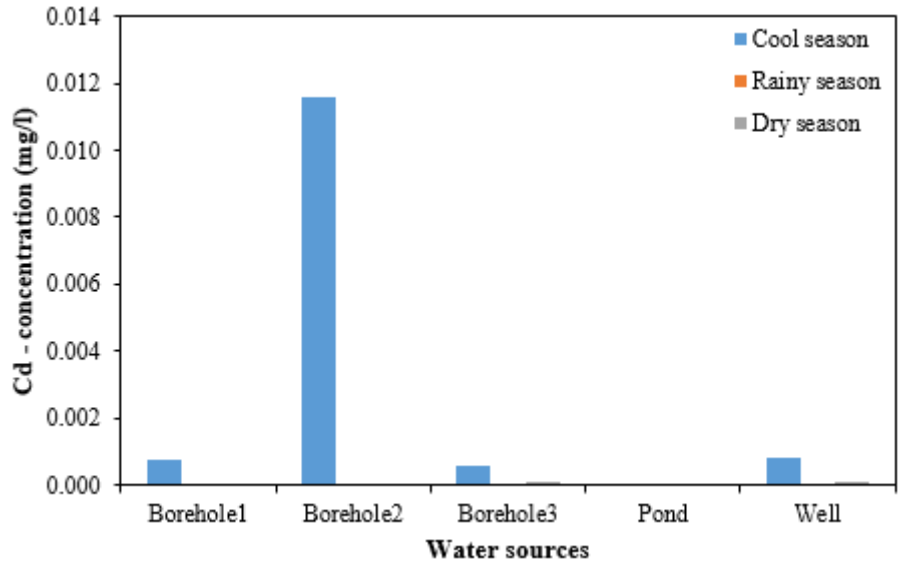

Figure 5.15: Seasonal variation for Cd in different water sources.

Table 5.32: Cr- concentration (mg/*l*) for cool, rainy and dry seasons in different water sources.

Season	Dam	Borehole1	Borehole2	Borehole3	Pond	Well
Cool	< 0.0009	0.0125	< 0.0009	0.0209	-	0.0532
Rainy	0.0214	0.0189	0.0215	0.0214	0.0106	< 0.0009
Dry	0.0215	0.0172	0.0272	0.0300	-	0.0168

Note: - sign indicates that there was no water during this seasons.

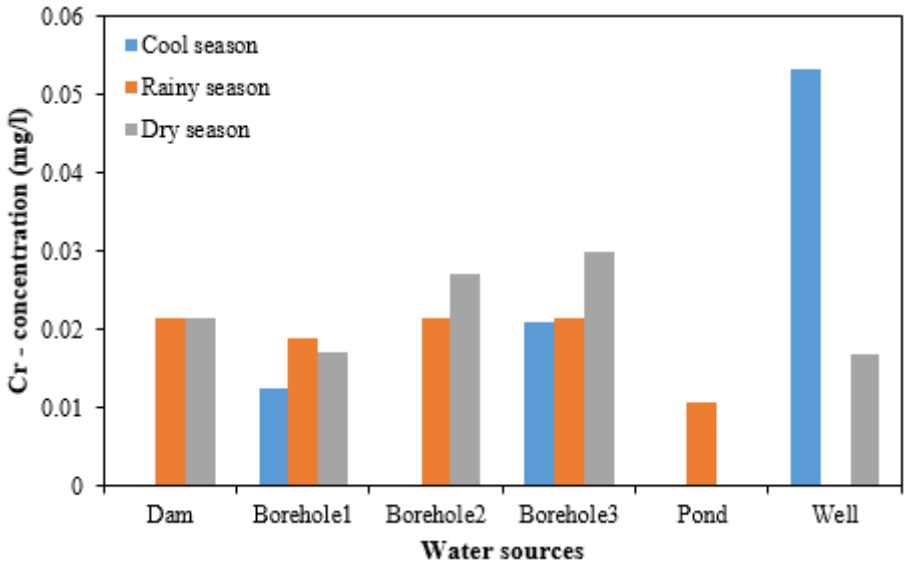

Figure 5.16: Seasonal variation for Cr in different water sources.

5.6 Comparison between γ-spectroscopy and ICP-MS methods for the measurement of ^{238}U and ^{232}Th concentration (Bq/kg) in sediment samples.

The comparison of the ^{238}U and ^{232}Th concentrations obtained by γ-spectrometry and ICP-MS are presented in the Table 5.33 and 5.34 and depicted in Figure 5.17and 5.18. As clearly shown in the Table 5.33 and 5.34 and Figure 5.17 and 5.18, the ^{238}U/^{238}U and ^{232}Th/^{232}Th ratios by γ-spectrometry and ICP-MS, are found to be almost similar and close to a unit. This indicates secular equilibrium attainment in the case of γ-spectrometry analysis. The obtained results illustrate the good agreement between the two techniques for analysis of these nuclides in sediments and soil samples. The elevated ratios could be due to the nature of the studied samples and the dilution factor in preparing the solids into solutions. For additional source of information on comparison of concentration ratios of all soil samples obtained by γ-spectrometry and ICP-MS, Annexure C (Table C1 and C2) is referred to.

Table 5.33: Comparison between γ-spectroscopy and ICP-MS methods for the measurement of ^{238}U concentration (Bq/kg) in sediment samples.

Sample code	^{238}U by γ-spec	^{238}U by ICP-MS	Ratio
SED01	33.3 ± 7.3	30.3 ± 5.5	1.1 ± 0.3
SED02	6.3 ± 3.9	16.1 ± 4.0	0.4 ± 0.3
SED03	21.2 ± 5.7	21.4 ± 4.6	1.0 ± 0.3
SED04	23.7 ± 6.5	38.8 ± 6.2	0.6 ± 0.2
SED05	37.2 ± 6.7	21.3 ± 4.6	1.8 ± 0.5
SED06	10.1 ± 4.5	8.8 ± 3.0	1.2 ± 0.7
SED07	40.7 ± 7.9	26.0 ± 5.1	1.6 ± 0.4
SED08	50.3 ± 7.2	50.1 ± 7.1	1.0 ± 0.2
SED09	34.6 ± 6.6	36.8 ± 6.1	0.9 ± 0.2
SED10	21.6 ± 5.9	29.3 ± 5.4	0.7 ± 0.2
SED11	32.1 ± 6.9	24.9 ± 5.0	1.3 ± 0.4
SED12	19.1 ± 5.8	21.9 ± 4.7	0.9 ± 0.3
SED13	21.0 ± 6.2	18.1 ± 4.3	1.2 ± 0.4
SED14	23.2 ± 5.0	25.6 ± 5.1	0.9 ± 0.3
SED15	26.4 ± 5.0	20.7 ± 4.6	1.3 ± 0.4
SED16	31.5 ± 6.5	39.2 ± 6.3	0.8 ± 0.2
SED17	21.7 ± 5.5	36.1 ± 6.0	0.6 ± 0.2

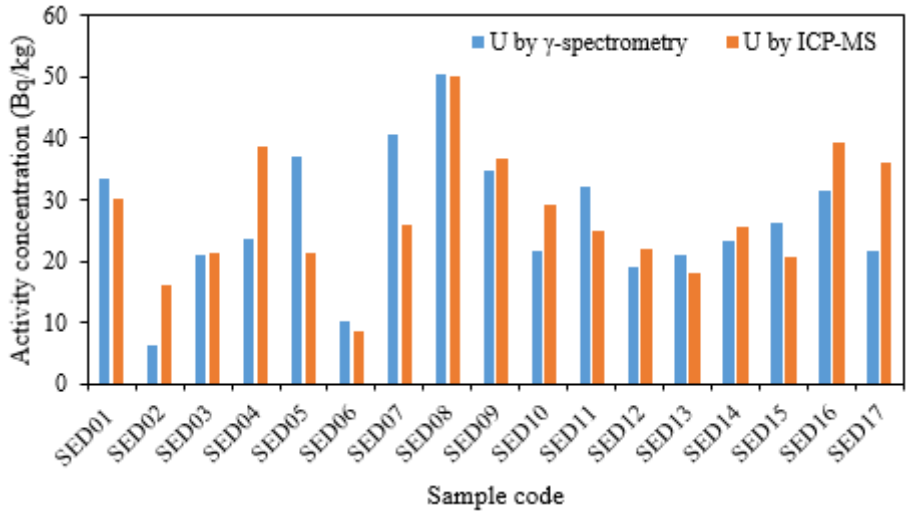

Figure 5.17: Comparison of ^{238}U activity concentration obtained by γ-spectroscopy and ICP-MS methods in sediment samples.

Table 5.34: Comparison between γ-spectroscopy and ICP-MS methods for the measurement of ^{232}Th concentration (Bq/kg) in sediment samples.

Sample code	^{232}Th by γ-spec	^{232}Th by ICP-MS	Ratio
SED01	78.0 ± 5.8	85.1 ± 9.2	0.9 ± 0.1
SED02	21.0 ± 3.9	67.2 ± 8.2	0.3 ± 0.1
SED03	41.7 ± 4.6	59.2 ± 7.7	0.7 ± 0.1
SED04	71.9 ± 9.0	70.3 ± 8.4	1.0 ± 0.2
SED05	63.9 ± 8.7	23.0 ± 4.8	2.8 ± 0.7
SED06	50.9 ± 8.2	22.2 ± 4.7	2.3 ± 0.6
SED07	95.8 ± 11.4	30.4 ± 5.5	3.2 ± 0.7
SED08	86.9 ± 6.0	65.2 ± 8.1	1.3 ± 0.2
SED09	66.2 ± 9.1	54.3 ± 7.4	1.2 ± 0.2
SED10	44.5 ± 6.1	49.3 ± 7.0	0.9 ± 0.2
SED11	56.4 ± 5.4	37.6 ± 6.1	1.5 ± 0.3
SED12	37.7 ± 5.0	36.2 ± 6.0	1.0 ± 0.2
SED13	46.2 ± 4.4	30.4 ± 5.5	1.5 ± 0.3
SED14	48.0 ± 7.4	48.7 ± 7.0	1.0 ± 0.2
SED15	44.5 ± 5.7	39.2 ± 6.3	1.1 ± 0.2
SED16	50.6 ± 5.7	46.6 ± 6.8	1.1 ± 0.2
SED17	48.2 ± 4.1	51.4 ± 7.2	0.9 ± 0.2

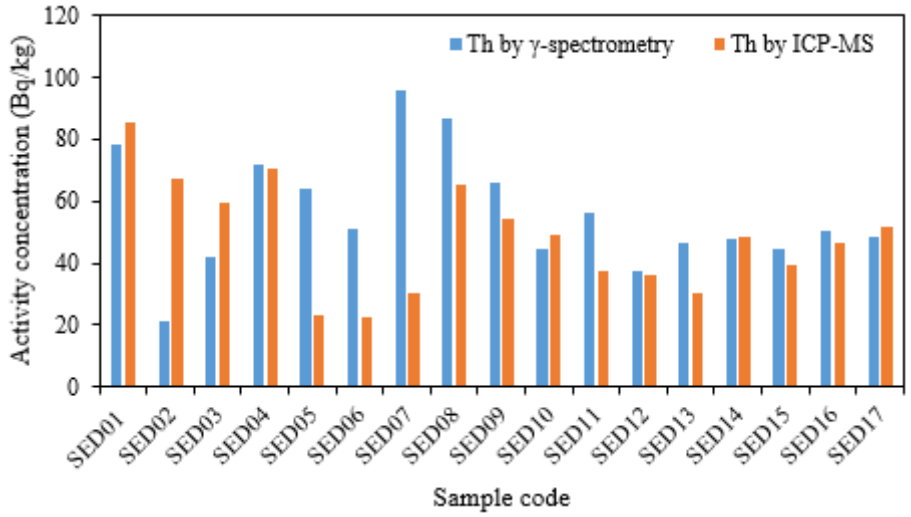

Figure 5.18: Comparison of ^{232}Th activity concentration obtained by γ-spectroscopy and ICP-MS methods in sediment samples.

5.7 Gross α/β activity concentrations

5.7.1 Water

The activity concentrations of gross-α and gross-β in water samples are shown in Table D1 (Annexure D). These water samples are used in various communities of the study area for consumption and domestic purposes. The activity concentrations of gross-α in the water samples varied from 0.06 ± 0.02 Bq/*l* to 0.34 ± 0.03 Bq/*l* with an average value of 0.21 ± 0.02 Bq/*l*. For the gross-β, the activity concentrations varied from 0.16 ± 0.06 Bq/*l* to 0.54 ± 0.06 Bq/*l* with an average value of 0.36 ± 0.03 Bq/*l*. The WHO recommended guideline values for drinking water below which no further action is required are 0.5 Bq/*l* for gross-α and 1.0 Bq/*l* for gross-β [WHO, 2004]. Comparing the results of this study with the WHO guidelines shows that all gross-α and gross-β activities are lower than the guideline values. The guideline values also ensure an exposure lower than 0.1 mSv/y assuming a water consumption rate of 2 litre /day. The average annual effective dose of this study is 0.07 mSv/y for gross-α and 0.1 mSv/y for gross-β, lower than the recommended limit of 0.1 mSv/y. This indicates that all the water sources in the study area, which are designated for drinking and domestic purposes do not pose any significant radiological hazard. These data can be used as baseline for future investigations.

5.8 Seasonal variation

The seasonal variation in the concentrations of gross-α in water samples is shown in Figure 5.19**.** This Figure was plotted based on the samples that were sampled repeatedly within the same water source for all seasons during investigation period. The seasonal variation in the gross-α concentrations indicates a slightly higher concentration in the dry season, which may be attributed to a prolonged period of no rain fall, leading to lowering of water table concentrating α-emitting nuclides like uranium and radium.

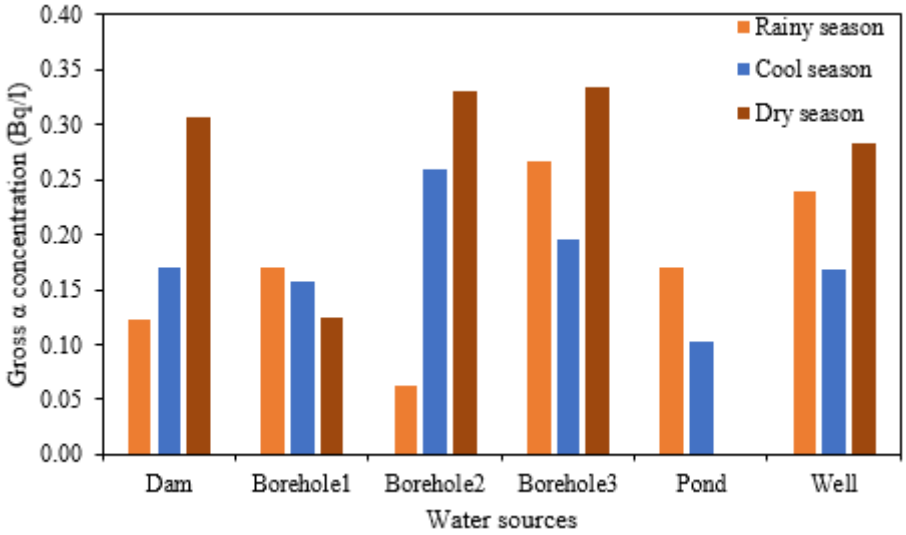

Figure 5.19: Gross α concentrations as a function of seasonal variations in different types of water sources.

Chapter 6: Summary, Conclusions and Recommendation

6.1 Summary and Conclusions

The aim of this study was to provide baseline information on natural radioactivity and heavy metals in the central district of Botswana for evaluation of the long-term impact of mining activities on the water quality of the Letsibogo dam and generate baseline data on environmental parameters that might affect radiological and toxicological health-related issues towards humans as a result of the mining activities. The study considered four (4) potential exposure pathways namely;

- direct external gamma ray exposure from natural radioactivity concentrations in soil,
- internal exposure from drinking water containing natural radioactivity and heavy metals,
- internal exposure due to ingestion of food containing ^{238}U and ^{232}Th nuclides and heavy metals, and
- internal exposure due to inhalation of dust containing ^{238}U and ^{232}Th nuclides and heavy metals.

The covered areas in this work include the communities of Serule village, Sese, Gojwane, Damochojenaa as well as the surrounding cattle posts of these villages and the Letsibogo dam. The study was motivated by the fact that no data are available on the radiological risk and the effects of NORMs and heavy metals to members of the public in this area. The research work is therefore to provide useful information on the levels of NORM and heavy metal concentration for future evaluation of mining activities in this area.

In this study work, the investigated samples used for the radiation maps showed that primordial radionuclides of ^{238}U and ^{232}Th decay chains and ^{40}K are contained in all type of samples.

The activity concentrations of the soil samples were found to be on average;

- 31.3 ± 1.8 (range: 10.3 ± 3.6 to 91.9 ± 9.5) Bq/kg for ^{238}U,
- 43.9 ± 2.0 (range: 14.1 ± 1.4 to 89.1 ± 10.1) Bq/kg for ^{232}Th, and
- 519 ± 25 (range: 180 ± 3 to 958 ± 13) Bq/kg for ^{40}K.

The obtained results of the average activity concentrations of ^{232}Th and ^{40}K were found to be higher than the worldwide average activity concentration values of 30 and 400 Bq/kg respectively due to high concentration values found in some soil samples. However, the obtained values are comparable to the published data from other countries and those of

UNSCEAR (2000) and fall within the range of corresponding world values, while the ^{238}U average activity concentration were within the acceptable worldwide average activity concentration value of 35 Bq/kg.

The activity ratios between parent and daughter nuclides $^{238}U/^{226}Ra$ and $^{228}Ra/^{228}Th$ were used to validate the assumption of secular equilibrium in the ^{238}U and ^{232}Th decay series, respectively. The average activity ratios of $^{238}U/^{226}Ra$ and $^{228}Ra/^{228}Th$ were found to be close to unity, indicating that the state of secular equilibrium has been attained in most of the area surveyed. In addition, the activity concentration in Bq/kg of ^{238}U and ^{232}Th obtained by γ-spectrometry were converted into the elemental concentrations in terms of ppm (parts per million) and compared with results obtained by ICP-MS for ^{238}U and ^{232}Th to assess the accuracy of the two techniques in the collected soil and sediments samples. The correlations between the elemental concentrations were considered in terms of elemental ratios. The $^{238}U/^{238}U$ and $^{232}Th/^{232}Th$ ratios by γ-spectrometry and ICP-MS were found to be close to unity. The obtained results shows that the two techniques are in good agreement for the analysis of this nuclides. In the case of γ-spectrometry analysis, the results also indicate that secular equilibrium has been attained.

In food samples, the total average activity concentrations of ^{238}U, ^{232}Th and ^{40}K for fish samples were found to be;

- 6.0 ± 0.2 (range: 4.2 ± 2.5 to 9.6 ± 2.8) Bq/kg for ^{238}U,
- 7.7 ± 1.2 (range: 3.4 ± 1.6 to 14.7 ± 4.3) Bq/kg for ^{232}Th, and
- 299 ± 10 (range: 251 ± 15 to 363 ± 29) Bq/kg for ^{40}K.

For vegetable samples, the average activity concentration was;

- 17.7 ± 2.0 (range: 16.0 ± 1.9 to 19.8 ± 5.1) Bq/kg for ^{238}U,
- 19.1 ± 2.1 (range: 17.9 ± 6.8 to 21.4 ± 2.7) Bq/kg for ^{232}Th, and
- 1368 ± 3 (range: 1088 ± 67 to 1576 ± 73) Bq/kg for ^{40}K,

and for beef liver the activity was < 6.1 Bq/kg for ^{238}U, 5.9 ± 3.4 Bq/kg for ^{232}Th, and 351 ± 30 Bq/kg for ^{40}K.

The activity concentrations of ^{40}K were found to be elevated in the vegetable samples but still comparable to values from other countries. This could have been influenced by geological structure variation and/or high utilisation of fertilizers.

The radiological hazard from ^{238}U, ^{232}Th and ^{40}K nuclides in soils and foodstuffs to the people of the study area was also evaluated. For soil the estimated absorbed dose rate (D_R) ranged from 23.5 ± 1.2 to 103 ± 6 nGy/h with an average value 62.3 ± 2.4 nGy/h, which is similar to the world average value of 59 nGy/h. The main contributor to D_R in most of the soil samples measured was found to be ^{232}Th, contributing about 42% of the total dose.

The calculated Ra_{eq} ranged from 41.0 ± 2.1 to 224 ± 11 Bq/kg with an average value of 134 ± 5 Bq/kg, which is lower than the accepted international value of 370 Bq/kg as recommended by the Organisation for Economic Cooperation and Development (OECD). The calculated H_{ex} ranged from 0.110 ± 0.001 to 0.600 ± 0.039 with average values of 0.360 ± 0.014. The H_{ex} values are less than the permissible dose equivalent limit of 1 mSv/y recommended by ICRP 60. The calculated AEDE varied from 0.020 ± 0.001 to 0.130 ± 0.006 mSv/y with an average value of 0.080 ± 0.003 mSv/y and these results were within the world wide average values reported by UNSCEAR and the dose criterion of 1mSv/y recommended by ICRP 60. The values of the radiation hazard parameters from this current study are not extremely high compared to the world averages and therefore unlikely to cause additional radiological health risks to the people living in the areas studied.

For foodstuff, the annual effective dose of ^{238}U, ^{232}Th and ^{40}K was estimated based on the average value obtained for each sample group, at an annual intake of spices that is proposed on section 4.1.6 and the net radiological impact of these radionuclides were compared with the world average value of 290 μSv/y. The net radiological impact of ^{238}U, ^{232}Th and ^{40}K were found to be;

- 133 ± 22 μSv/yr (9.4 ± 1.9, 62.0 ± 20.8 and 61.4 ± 4.9) Bq/kg for fish samples
- 1327 ± 90 μSv/yr (79.7 ± 5.01, 440 ± 26 and 807 ± 86) Bq/kg for vegetables and
- 667 ± 38 μSv/yr (427 ± 21, 94.9 ± 27.0 and 145 ± 17) Bq/kg for beef liver.

The results revealed that the levels of radioactivity in almost food samples are insignificant and will not pose any radiological hazard from consumption except for ^{232}Th and ^{40}K which indicated elevated values in vegetable samples that are above the world average value of 290 μSv/y. This could be caused by high activity concentration of the soil that they have been planted on in the study area as it was also indicated on chapter 5, Figure 5.2 that the soil samples

of this area contain high levels of ^{40}K activity and also the consumption rate values used for calculating annual effective dose. Generally, the ingestion of ^{232}Th and ^{40}K dose in vegetable samples can be considered to be low when compared with natural external exposures of about 2000 μSv/ y.

The average concentrations of heavy metals in soil, water, food and dust samples were also measured. These values were also compared with the international guidelines and other countries for permissible limits for an individual sample type. In some cases, the average concentrations exceeded the guideline values. For soil samples, the average concentrations were lower than the maximum allowable limits indicating that soil of the study area is free for any application. For the water samples, the average concentration of most heavy metals were lower than the permissible limits indicating that the water is safe for drinking. For the average concentrations of heavy metals determined in food samples, it was found that the highest heavy metal concentrations were observed in beef liver and found to have exceeded the permissible limits for some elements; e.g. Cu. For fish samples, the results showed that the levels of heavy metals were within the acceptable limits set by international standards for fish except for Pb and Cr. For vegetable samples, Pb was found to have slightly exceeded the permissible limit. For dust samples, the results were compared with those of other cities in developed countries. The measured average concentrations in dust samples were found to be lower than those determined in other cities indicating that the natural sources dominate the composition of dust samples in the study area.

The cancer risk for people living in the study area, as a result of heavy metal in soil, water, foodstuff and dust was also evaluated. The average concentrations of heavy metals were used to calculate the average daily intake for carcinogenic and non-carcinogenic risk. The daily intakes values (ADI) were also used to determine the exposure pathway and the sample type that contributes the most to carcinogenic and non-carcinogenic risk. For non-carcinogenic risk, the HI values were found to be 1.5, 27.5 and 1.5 for As, Cr and Cu respectively. These values are greater than 1, which indicate a potential health risk of As, Cr and Cu to the residents of the study area. The ingestion pathway was the greatest contributor to non-carcinogenic risk with an HI value of 27.5 driven by Cr in food samples.

For carcinogenic risk, the ingestion pathway was found to be the greatest contributor. Cr was observed to be the major contributor to the risk with a total cancer risk value of 4.1×10^{-2}, which is greater than the maximum permissible limit of 1×10^{-4}, indicating a potentially large

carcinogenic risk. It was also observed that for food samples Cr contributed the most to the carcinogenic risk. This study considers that the ingestion of food could be the most significant mode of exposure in the study area. But, based on the results from this study, the consumption of food does not pose any significant hazard to the people of the study area except for the elevated levels of Cr, which could lead to negative effects like spinal/joint degeneration, depressed immune system and lymphatic swelling.

The gross-α and gross-β activity concentrations in the water samples as well as the seasonal variation of gross-α activity concentrations were also evaluated. The results of this study show that all values of the gross-α and gross-β activity are below the WHO recommended guideline values. The results indicate that all the water sources in the study area, which are designated for drinking and domestic purposes do not pose any significant radiological hazard. The seasonal variation in gross-α/β and heavy metal concentrations were also found to be less significant in all the water samples. The results from this study data can be used as a baseline for future investigations.

6.2 Recommendations

From the outcomes of this study, the following recommendations should be considered for future investigation;

- Additional soil samples need to be collected within a small grid interval in order to obtain more accurate data.
- More water samples from different boreholes need to be collected to accommodate the assessment of seasonal variation.
- Future studies could consider physico-chemical factors such as pH, temperature, electrical conductivity, chemical composition that can affect the mobility of radionuclides and heavy metals.
- This work can be expanded to cover a range of environmental matrices like crop, pasture, livestock analysis and all other foodstuff to determine the impact of consumption.
- The analysis performed for dust samples in this work was only carried out using large particles of dust. Even though it will take time in sample preparation and analysis for this thesis, it would be valuable to investigate different sizes of dust particles, for example, 5 µm, 3 µm, and 1 µm, if possible. Because dust particles of these sizes are

far more likely to become airborne and remain suspended long enough for people to inhale them, and particles of these sizes can penetrate deeper into the lungs, giving people a larger exposure. This also requires more advanced equipment for dust sampling.

- Direct determination of isotope ratios for Uranium in dust samples in the study area using radiochemical separation and alpha spectrometry should be considered also in future work.
- The measured activity concentration of all sample matrices in this study was done only once due to time constraints and thus subsequent measurements should be repeated in order to obtain better statistics.

In conclusion, based on the study the general recommendation is continuous monitoring of the study area to allow future evaluations of potential changes once the mining and mineral processing operations are in full swing.

References

Ademola, A. K., Olaoye, M. A. & Abodunrin, P. O., 2015. Radiological safety assessment and determination of heavy metals in soil samples from some waste dumpsites in Lagos and Ogun state, south-western, Nigeria. *Radiation Research and Applied Sciences,* Volume 8, pp. 148-153.

Adewumi, D., Daniyan, I. & Adeodu, A., 2014. Determination of heavy metals in water, fish and soil samples from Antau River in Keffi, Nasarawa State, Nigeria: a case study of Antau River in Keffi, Nasarawa North Central Nigeria. *International Journal of Science and Research,* 3(3), pp. 701-705.

Ahanger, F. A., Sharma, H. K., Rather, M. A. & Rao, R. J., 2014. Impact of mining activities on various environmental attributes with specific reference to health impacts in Shatabdipuram, Gwalior, India. *International Research Journal of Environment Sciences,* pp. 81-87.

Ahmed, N. K., 2004. Natural Radioactivity of Ground and Drinking Water in Some Areas of Upper Egypt. *Turkish Journal of Engineering and Environmental Sciences,* Volume 28, pp. 345-354.

Ahmed, N. K. & El-Arabi, A. G. M., 2005. Natural radioactivity in farm soil and phosphate fertilizer and its environmental upper Egypt. *Journal of Environmental Radioactivity,* pp. 51 - 64.

Ajayi, O. S., 2009. Measurement of activity concentrations of 40K, 226Ra and 232Th for assessment of radiation hazards from soils of the southwestern region of Nigeria. *Radiation Environmental Biophysics*, Volume 48, p. 323–332.

Ali, M. & Al-Qahtani, K., 2012. Assessment of some heavy metals in vegetables, cereals and fruits in Saudi Arabian markets. *The Egyptian Journal of Aquatic Research,* 38(1), pp. 31-37.

Al-Kinani, A., Hushari, M., Al-Sulaiti, H. & Alsadig, I., 2015. Norm in soil and sludge samples in Dukhan oil Field, Qatar state. *Brazilian Journal of Radiation Sciences,* 03(01), pp. 01-15.

Altıkulaç, A., Turhan, Ş. & Gümüş, H., 2015. The natural and artificial radionuclides in drinking water samples and consequent population doses. *Journal of Radiation Research and Applied Sciences,* 8(4), pp. 578-582.

APPEA, 2002. *Guidelines for naturally occurring radioactive materials,* s.l.: Canberra.

Asaduzzaman, K. et al., 2015. Assessment of Natural Radioactivity Levels and Potential Radiological Risks of Common Building Materials Used in Bangladeshi Dwellings. *PLOS One TENTH annivessary.*

ASTM, 2004. *Standard Test Method for Collection and Measurement of Dustfall (Settleable Particulate Matter),* United States: Designation: pp 1739-98.

ATSDR, 2007. *Agency for Toxic Substances and Disease Registry (U.S. Public Health Service).* [Online] Available at: https://www.atsdr.cdc.gov/toxprofiles/guidance/set_21_guidance.pdf [Accessed 4 July 2017].

Attix, F. H., 1986. *Introduction to Radilogical Physics and Radiation Dosimetry.* Madison, Wiscosin: Wiley-VCH.

Baharom, Z. S. & Ishak, M. Y., 2015 . Determination of heavy metal accumulation in fish species in Galas River, Kelantan and Beranang mining pool, Selangor. *Procedia Environmental Sciences,* Volume 30, pp. 320-325.

Baskaran, M., 2011. *Handbook of Environmental Isotope Geochemistry.* Heidelberg: Springer.

Bevington, P. R. & Robinson, K. D., 2003. *Data Reduction and Error Analysis for the Physical Sciences.* 3rd ed. New York: McGraw-Hill.

Bolca, M. et al., 2007. Radioactivity in soils and various foodstuffs from the Gediz river basin of Turkey. *Radiation Measurements,* Volume 42, pp. 263-270.

Canbazoglu, C. & Dogru, M., 2013. A preliminary study on 226Ra, 232Th, 40K and 137Cs activity concentrations in vegetables and fruits frequently consumed by inhabitants of Elazıg˘ region, Turkey. *Radioanalysis Nuclear Chemistry,* Volume 295, pp. 1245-1249.

Canberra, 2004. *Genie 2000 3.1 Customization Tools Manual. ISO 9001 System certified.* s.l.:s.n.

Cao, H. et al., 2010. Heavy metals in rice and garden vegetables and their potential health risks to inhabitants in the vicinity of an industrial zone in Jiangsu, China. *Journal of Environmental Sciences,* 22(11), pp. 1792-1799.

Carvalho, F., Oliveira, J., Lopes, I. & Batista, A., 2007. Radionuclides from past uranium mining in rivers of Portugal. *Journal of Environmental Radioactivity,* 98(3), pp. 298-314.

Cember, H. & Johnson, T. E., 2009. *Intoduction to Health Physics (Fourth Edition).* New York: McGraw-Hill.

Cetnar, J., 2006. General solution of Bateman equations for nuclear transmutations. *Annals of Nuclear Energy,* pp. 640-645.

Cfarku, F. et al., 2014. A preliminary study of gross alpha/beta activity concentrations in drinking waters from Albania. *Journal of Radioanalytical and Nuclear Chemistry,* 301(2), pp. 435-442.

Chajduk, E., Kalbarczyk, P., Dudek, J. & Polkowska-Motrenko, H., 2012. Isotope ratio measurements for uranium by quadrupole-based inductively coupled plasma mass spectrometry. Application in thorium fuel research.. *Procedia Chemistry,* Volume 7, pp. 660-665.

Commission Regulation, E. N. 1., 2006. *assurance.redtractor.org.uk.* [Online] Available at: https://www.fsai.ie/uploadedFiles/Consol_Reg1881_2006.pdf [Accessed 21 07 2018].

Currie, L. A., 1968. Limits for qualitative detection and quantitative determination. *Application to Radiochemistry,* 40(3), pp. 586-593.

Darko, E. O. et al., 2010. Public exposure to hazards associated with natural radioactivity in open-pit mining in Ghana. *Radiation Protection Dosimetry,* 138(1), pp. 45-51.

De Corte, F., Umans, H., Vandenberghe, D. & De Wispelaere, A., 2004. *Direct gamma-spectrometric measurement of the 226Ra 186.1 keV line for detecting 238U/Ra disequilibrium in determining the environmental dose rate for luminescence dating of sediments.* s.l., Abstracts 8th International Conference on Applications of Nuclear Techniques.

DEA, 2010. *South African Waste Information Centre.* [Online] Available at: http://sawic.environment.gov.za/documents/562.pdf [Accessed 03 July 2017].

Dovlete, C. & Povinec, P., 2004. *Quantification of Uncertainty in Gamma-spectrometric Analysis of Environmental Samples,* Vienna, Austria: IAEA-TECDOC-1401 Quantifying uncertainty in nuclear analytical measurements.

Dragovic, S., Lj. Jankovic, L., Onjiac, A. & Bacic, G., 2006. Distribution of primordial radionuclides in surface soils from Serbia and Montenegro. *Radiation Measurements,* Volume 41, pp. 611-616.

Duruibe, J. O., Ogwuegbu, M. O. C. & Egwurugwu, J. N., 2007. Heavy metal pollution and human biotoxic effects. *International Journal of Physical Sciences,* 2(5), pp. 112-118.

Ebaid, Y., 2009. Use of gamma-ray spectrometry for uranium isotopic analysis in environmental samples. *Romanian Journal of Physics,* 55(1-2), pp. 69-74.

Eisenbud, M. & Gesell, T., 1997. *Environmental Radioactivity from Natural, Industrial, and Military Sources.* San Diego: Elsevier.

El-Taher, A. & Al-Zahrani, J., 2014. Radioactivity measurements and radiation dose assessments in soil of Al-Qassim region, Saudi Arabia. *Indian Journal of Pure & Applied Physics,* Volume 54, pp. 147-154.

Erdi-Krausz, G. et al., 2003. *Guidelines for radioelement mapping using gamma ray spectrometry data: also as open access e-book.,* Vienna: International Atomic Energy Agency (IAEA).

EU, C. D., 2013. Laying down requirements for the protection of the health of the general public with regard to radioactive substances in water intended for human consumption. *Official Journal of the European Union,* Volume 2013/51/EURATOM, pp. 1-10.

Evans, R. D., 1955. *The Atomic Nucleus.* Bombay New Delhi: McGraw-Hill, Inc.

Faanu, A., 2011. *Assessment of public exposure to naturally occurring radioactive materials from mining and mineral processing activities of Tarkwa Goldmine in Ghana.* Thesis ed. Kumasi: Kwame Nkrumah University of Science and Technology.

Faanu, A. et al., 2016. Natural radioactivity levels in soils, rocks and water at a mining concession of Perseus gold mine and surrounding towns in Central Region of Ghana. *SpringerPlus,* 5(98), pp. 1-16.

Faheem, M., Mujahid, S. & Matiullah, 2008. Assessment of radiological hazards due to the natural radioactivity in soil and buildingmaterial samples collected from six districts of the Punjab province-Pakistan. *Radiation Measurements,* Volume 43, pp. 1443-1447.

Ferreira-Baptista, L. & Miguel, E., 2005. Geochemistry and risk assessment of street dust in Luanda, Angola: A tropical urban environment. *Atmospheric Environment,* Volume 39, pp. 4501-4512.

Fisher, A. B., 2005. Heavy metals in the food chain-lead, cadmium and mercury in foodstuff and population exposures. *Indian National Science Academy,* Volume 4, pp. 109-143.

Friedlander, G., Kennedy, J. W., Macias, E. S. & Miller, J. M., 1981. *Nuclear and Radiochemistry (3rd Edition).* New York, Chichester, Brisbane, Toronto: John Wiley & Sons.

Grogan, H. A. & Till, J. E., 2008. *Radiological Risk Assessment and Environmental Analysis.* New York: Oxford University press.

Grupen, C., 2010. *Iintroduction to Radiation Protection.* Verlag Berlin Heidelberg: Springer.

Harvey, B. G., 1962. *Introduction to Nuclear Physics and Chemistry (Second edition).* New Jersey: Prentice-Hall, Inc.

Hu, B. et al., 2017. Assessment of heavy metal pollution and health risks in the soil-plant-human system in the Yangtze river delta, China. *Environmental Research and Public Health,* Volume 14, pp. 1-18.

IAEA, 1989. *Measurement of Radionuclides in Food and the Environment: A Guidebook,* Vienna, Austria: s.n.

IAEA, 1996. *International Basic Safety Standards for Protection against Ionising Radiation and for the safety of radiation sources, Safety Series No. 115,* Vienna, Austria: s.n.

IAEA, 2003. *Extent of Environmental Contamination by Naturally Occurring Radioactive Material (NORM) and Technological Options for Mitigation,* Vienna: IAEA, Technical Reports SeriEs No. 419.

IAEA, 2004. *Soil sampling for environmental contaminants. IAEA-TECDOC-1415,* Vienna, Austria: s.n.

IAEA & OECD, 2014. *Uranium 2014: Resources, Production and Demand,* s.l.: Nuclear energy agency organisation for economic cooperatin and development.

Ibikunle, S., Ajayi, O., Arogunjo, A. & Salami, A., 2016. Radiological assessment of dam water and sediments for natural radioactivity and its overall health detriments. *Ife Journal of Science,* 18(1), pp. 551-559.

Ibrahim, N., 1999. Natural activities of 238U, 232Th and 40K in building materials. *Environmental Radioactivity,* Volume 43, pp. 255-258.

ICRP, 1991a. *1990 Recommendations of the International Commission on Radiological Protection.* Pergamon Press ed. Oxford: ICRP Publication 60, Annals of the ICRP.

ICRP, 1996. *Age-dependent Doses to Members of the Public from intake of Radionuclides: Part 5 Compilation of Ingestion and Inhalation Dose Coefficients,* s.l.: Elsevier Science.

ICRP, 2007. *The 2007 Recommendations of the International Commission on Radiological Protection,* s.l.: Elsevier.

ICRP, 2012. *Compedium of Dose Coefficients Based on ICRP Publication 60,* s.l.: Elsevier.

ICRU, 2011. *Fundamental Quantities and Units for Ionizing Radiation,* s.l.: Oxford University Press.

Jaishankar, M. et al., 2014. Toxicity, mechanism and health effects of some heavy metals. *Interdisciplinary Toxicololgy,* 7(2), pp. 60-72.

Jeje, J. & Oladepo, K. T., 2014. Assessment of Heavy Metals of Boreholes and Hand Dug Wells in Ife North Local Government Area of Osun State, Nigeria. *International Journal of Science and Technology,* 3(4), pp. 209-214.

Jennings, S., Neuman, D. & Blicker, P., 2008. *Acid mine drainage and effects on fish health and ecology: a review. ,* Alaska: Reclamation Research Group Publication, Bozeman, MT.

Johansson, L., 1976. . Determination of Pb-210 and Po-210 in aqueous environmental samples. MSc Dissertation. Von der Naturwissenschaftlichen Fakultat der Gottfried Wilhelm Leibniz Universitat Hannover zur Erlangung des Grades. Frandefors, Schweden.

Kahraman, G., Aslan, N., Sahin, M. & Yüksek, S., 2015. Radioactivity measurement method for environmental monitoring gross alpha/beta activities in drinking water in Turkey. *Acta Chimimica Slovenica,* Volume 62, pp. 595-604.

Kamunda, C., 2016. *Human Health Risk Assessment of Environmental Radionuclides and Heavy Metals around a Gold Mining Area in Gauteng Province, South Africa.* Thesis ed. Mafikeng: North-West University.

Kamunda, C., Mathuthu, M. & Madhuku, M., 2016. An Assessment of Radiological Hazards from Gold Mine Tailings in the Province of Gauteng in South Africa. *Environmental Research and Public Health,* 13(138), pp. 1-10.

Kamunda, C., Mathuthu, M. & Madhuku, M., 2016. Health Risk Assessment of Heavy Metals in Soils from Witwatersrand Gold Mining Basin, South Africa. *International Journal of Environmental Research and Public Health,* 13(663), pp. 1-11.

Kesici, G. G., 2016. Arsenic ototoxicity. *Journal of Otology,* Volume 11, pp. 13e17.

Kessler, M. J., 1989. *Liquid Scintillation Analysis,* U.S.A: Packard Instrument Company, Publication No. 169-3052.

Khan, K. et al., 2013.. Heavy metals in agricultural soils and crops and their health risks in Swat District, northern Pakistan.. *Food and Chemical Toxicology ,* Volume 58, pp. 449-458.

Khoo, F., 1981. *X-rays in Singapore, 1896-1975.* s.l.:Singarepore University Press.

Klement, A. W., 1982. *Handbook of Environmental Radiation.* Florida: CRC Press, Inc..

Knoll, G. E., 2000. *Radiation Detection and Measurement (Third Edition).* Third ed. New York: John Wiley & Sons.

Kovalchuk, I., Kovalchuk, O. & Hohn, B., 2001. Biomonitoring the genotoxicity of environmental factors with transgenic plants.. *Trends in plant science,* 6(7), pp. 306-310.

Krane, K. S., 1988. *Introductory Nuclear Physics.* New York: John Wiley & sons.

L'Annunziata, M. F., 2003. *Handbook of Radioactivity Analysis. 2nd Edition.* San Diego: Academic Press.

Lehto, J., 2017. *Basics of Nuclear Physics and of Radiation Detection and Measurement: An open-access textbook for Nuclear and Radiochemistry students.* Finland: s.n.

Lehto, J. & Hou, X., 2011. *Chemistry and Analysis of Radionuclides.* Weinheim: Wiley-VCH.

Lieser, H. K., 2008. *Nuclear and Radiochemistry: fundamentals and applications.* New York: John Wiley & Sons.

Likuku, A. S., Mmolawa, K. B. & Gaboutloeloe, G. K., 2013. Assessment of Heavy Metal Enrichment and Degree of Contamination Around the Copper-Nickel Mine in the Selebi Phikwe Region, Eastern Botswana. *Environment and Ecology Research,* 1((2)), pp. 32-40.

Lilley, J., 2001. *Nuclear Physics: Principles and applications.,* Baffins Lane, Chichester: John Wiley & Sons.

Liu, X. et al., 2013. Human health risk assessment of heavy metals in soil–vegetable system: A multi-medium analysis. *Science of the Total Environment*, 463(464), pp. 530-540.

Mahurpawar, M., 2015. Effects of heavy metals on human health. *International Journal of Research-Granthaalayah*, pp. 1-7.

Mangset, E. et al., 2014. Gross alpha and beta radioactivity concentrations and estimated committed effective dose to the general public due to intake of groundwater in mining areas of Plateau State, North Central Nigeria. *Advances in Physics Theories and Applications*, Volume 38, pp. 30-38.

Mangum, S. J., 2009. *PerkinElmer*. [Online] Available at: https://www.perkinelmer.com/lab-solutions/resources/docs/APP_MicrowaveDigestionMultiwave.pdf [Accessed 16 March 2017].

Martin, J. E., 2013. *Physics for Radiation Protection.* Third ed. Weinheim, germany: Wiley-VCH Verlag & Co. KGaA.

Mashaba, M., 2011. *Direct Quantitative Gross αβ-Measurements of Environmental Water Contaminated with Nuclides from the Uranium, Thorium and Actinium Decay Series and Semi-Qualitative Identification of Nuclides Concerned*, Mafikeng: North-west University.

Mashaba, M., Kotze, D., Tshivhase, V. M. & Faanhof, A., 2017. *Gross Alpha and Beta Measurements of Water Samples from the Wonderfonteinspruit Catchment Area in the Gauteng Province (South Africa), using Liquid Scintillation Counting.* s.l., LSC.

MINEO, 2000. *MINEO project.* [Online]
Available at: http://www2.brgm.fr/mineo/UserNeed/IMPACTS.pdf

Mittal, A., 2016. A study on interaction of alpha particles with nuclei. *National Journal of Multidisciplinary Research and Development*, 1(1), pp. 27-29.

Montaser, A., 1998. *Inductively Coupled Plasma Mass Spectrometry.* New York: Wiley-VCH.

Naveedullah, et al., 2014. Concentrations and Human Health Risk Assessment of Selected Heavy Metals in Surface Water of the Siling Reservoir Watershedin Zhejiang Province, China. *Polish Journal of Environmental Studies*, 23(3), pp. 801-811.

Nazir, R. et al., 2015. Accumulation of Heavy Metals (Ni, Cu, Cd, Cr, Pb, Zn, Fe) in the soil, water and plants and analysis of physico-chemical parameters of soil and water Collected from Tanda Dam kohat. *Journal of Pharmaceutical Sciences and Research*, 7(3), pp. 89-97.

NRC, N. R. C., 1999. *Arsenic in drinking water.* s.l.:National Academies Press.

Nwankwo, L. I., 2010. Annual effective dose due to combined concentration of 226Ra and 228Ra in the groundwater system: A case study of the University of Ilorin main campus, Nigeria.. *Facta Universitatis. Working and Living Environmental Protection,* 7(1), pp. 53-58.

O'Brien, R. S. & Cooper, M. B., 1998. Technologically Enhanced Naturally Occurring Radioactive Material (NORM): Pathway Analysis and Radiological Impact. *Applied Radiation lsotopes,* 49(3), pp. 227-239.

Ochiai, E., 2014. *Juniata College.* [Online] Available at: https://www.juniata.edu/offices/juniata-voices/media/ochiai-radiation.pdf [Accessed 23 01 2018].

Oladoye, P. O. & Adewuyi, O. O., 2014. Comparative assessment of lead and zinc in the Coastal Areas of Niger Delta. *Journal of Research in Environmental Science and Toxicology,* 3(3), pp. 39-45.

Oregon State University , 2017 . *Oregon State University.* [Online] Available at: http://oregonstate.edu/instruct/ch374/ch418518/Chapter%2018%20Radiation%20Detectors.pdf [Accessed 17 January 2018].

Oyedele, J., 2006. Assessment of the natural radioactivity in the soils of Windhoek city, Namibia, Southern Africa.. *Radiation protection dosimetry,* 121(3), pp. 337-340.

Pandey, B., Agrawal, M. & Singh, S., 2014. Assessment of air pollution around coal mining area: Emphasizing on spatial distributions, seasonal variations and heavy metals, using cluster and principal component analysis. *Atmospheric Pollution Research* , Volume 5, pp. 79-86.

Pillalamarri, I., 2005. *Massachusetts Institute of Technology.* [Online] Available at: http://ocw.mit.edu/courses/earth-atmospheric-and-planetary-sciences/12-091-trace-element-analysis-of-geological-biological-environmental-materials-by-neutron-activation-analysis-an-exposure-january-iap-2005/lecture-notes/session2a.pdf [Accessed 11 August 2016].

Podsiki, C., 2008. *Podsiki, C., 2008. Heavy metals, their salts, and other compounds: a quick reference guide from AIC and the Health & Safety Committee,* s.l.: AIC news.

Pöschl, M. & Nollet, L. M. L., 2007. *Radionuclide Concentrations in Food and the Environment,* Boca Raton: Taylor & Francis Group.

Pradler, J., Balraj, S. & Itay, Y., 2013. On an unverified nuclear decay and its role in the DAMA experiment. *Physics Letters B,* 720(4), pp. 399-404.

Prince, J. R., 1979. Comments on Equilibrium, Transient Equilibrium, and Secular Equilibrium in Serial Radioactive Decay. *Journal Nuclear Medicine,* Volume 20, pp. 162-164.

Ramli, A., 1997. Environmental terrestrial gamma radiation dose and its relationship with soil type and underlying geological formations in Pontian District, Malaysia. *Applied radiation and isotopes,* 48(3), pp. 407-412.

Royal Holloway, 2007. *Royal Holloway Physics TWiki.* [Online] Available at: http://www.pp.rhul.ac.uk/~ptd/TEACHING/PH2510/np2.pdf [Accessed 16 March 2017].

Saad, M. H., Tamboul, J. Y. & Yousef, M., 2014. Evaluation of natural radioactivity in different regions in Sudan. *Journal of American Science,* Volume 10 (2), pp. 14-18.

Sahu, H. B. & Dash, S., 2011. *Land Degradation due to Mining in India and its Mitigation Measures.* Singapore, Proceedings of second international conference on environmental science and technology.

Salem, H., Eweida, E. & Farag, A., 2000. Heavy metals in drinking water and their environmental impact on human health.. *ICEHM2000, Cairo University, Egypt,* pp. 542-556..

Singh, R., Gautam, N., Mishra, A. & Gupta, R., 2011. Heavy metals and living systems: An overview. *Indian Journal of Pharmacology,* 43(3), pp. 246-253..

Singh, S., Rani, A. & Mahajan, R. K., 2005. 226Ra, 232Th and 40K in a soil samples from some areas of Punjab and Himachal Pradesh, India usinggammaray spectrometry. *Radiation Measurements,* Volume 39, pp. 431-439.

Sultana, M. et al., 2017. Health risk assessment for carcinogenic and non-carcinogenic heavy metal exposures from vegetables and fruits of Bangladesh. *Cogent Environmental Science,* 3(1), p. 1291107.

Taqi, A. H., Al-Ani, L. A. & Ali, A. M., 2016. Assessment of the natural radioactivity levels in Kirkuk oil field. *Journal of Radiation Research and Applied Sciences,* Volume 9, pp. 337-344.

Tchounwou, P. B., Yedjou, C. G., Patlolla, A. K. & Sutton, D. J., 2012. Heavy metals toxicity and the environment. *NIH Public Access,* Volume 101, pp. 133-164.

Tego, F., 2017. *Roads, settlements and major rivers.* [Art] (Department of Surveys and Mapping (DSM)).

Thabayneh, K. M. & Jazzar, M. M., 2012. Natural radioactivity levels and estimation of radiation exposure in environmental soil samples from Tulkarem Province-Palestine. *Open Journal of Soil Science,* Volume 2, pp. 7-16.

Thomas, R., 2004. *Practical Guide to ICP-MS.* Newy ORK Basel: s.n.

Turner, J. E., 2007. *Atoms, Radiation and Radiation Protection.* Weinheim: Willey-VCH Verlag Gmgh & co.KGaA.

Umar, A., Onimisi, M. & Jonah, S., 2012. Baseline measurement of natural radioactivity in soil, vegetation and water in the industrial district of the Federal Capital Territory (FCT) Abuja, Nigeria. *British Journal of Applied Science & Technology,* 2(3), pp. 266-274.

UNEP, 2002. *Chemicals, and Inter-Organization Programme for the Sound Management of Chemicals. Global mercury assessment.*. [Online] Available at: http://fusion4freedom.us/pdfs/UN-EPA-MOU.pdf [Accessed 04 07 2017].

UNSCEAR, 1993. *Sources and Effects of Ionizing Radiation,* New York: United Nations.

UNSCEAR, 2000. *Sources and effects of ionising radiation. United Nations Scientific Committee on the Effects of Atomic Radiation. Exposures from natural sources,* New york: Report to the General Assembly, with Scientific Annexes, United Nations.

UNSCEAR, 2008. *Sources and Effects of Ionizing Radiation,* Vienna: United Nations.

US.EPA, 1989. *Risk Assessment. Guidance for Superfund. Volume I. Human Health Evaluation Manual (Part A),* Washington: U.S. Environmental Protection Agency.

US.EPA, 1992. *Guidelines for Exposure Assessment,* Washington, DC: s.n.

US.EPA, 2004. *Risk Assessment Guidance for Superfund Volume I: Human Health Evaluation Manual (Part E, Supplemental Guidance for Dermal Risk Assessment),* Washington, DC: s.n.

US.EPA, 2005. *Guidelines for Carcinogen Risk Assessment.* [Online] Available at: https://www3.epa.gov/airtoxics/cancer_guidelines_final_3-25-05.pdf [Accessed 22 February 2017].

US.EPA, 2008. *Plan for Review of the National Ambient Air Quality Standards for Carbon Monoxide.* orth Carolina: U. S. Environmental Protection Agency.

US.EPA, 2014. *Framework for Human Health Risk Assessment to inform Decision.* [Online] Available at: https://www.epa.gov/sites/production/files/2014-12/documents/hhra-framework-final-2014.pdf [Accessed 22 February 2017].

USEPA, 1980. *Method 900.0: Gross Alpha and Gross Beta Radioactivity in Drinking Water,* s.l.: www.epa.gov.

Vanhaecke, F. & Degryse, P., 2012. *Isotopic analysis: fundamentals and applications using ICP-MS.* Weiheim: John Wiley & Sons.

Varlam, C. et al., 2009. Applying direct liquid scintillation counting to low level tritium. *Applied Radiation and Isotopes,* Volume 67, pp. 812-816.

Walser, G., 2002. *Walser, G. Economic impact of world mining.,* s.l.: IAEA-CSP-10/P.

Watson, S. J., Jones, A. L., Oatway, W. B. & Hughes, J. S., 2005. *Ionising Radiation Exposure of the UK Population: 2005 Review,* Chilton, Didcot, Oxfordshire OX11 0RQ: Health Protection Agency, Centre for Radiation, Chemical and Environmental Hazards, Radiation Protection Division.

WHO, 2011. *Guidelines for drinking-water quality.*. 4 ed. s.l.:WHO chronicle.

World Health Organization, W. H. O., 2008. *Guidelines for Drinking-water Quality.* Third, Incorporating the First and second Addenda Vol.1, Recommendations ed. Geneva: WHO Library Cataloguing.

WRC, 2000. *Quality of domestic water supplies Volume 2:Sampling Guide,* Pretoria: The Department of Water Affairs and Forestry, Department of Health, Water Research Commission.

Wu, B. et al., 2009. Preliminary Risk Assessment of Trace Metal Pollution in Surface Water from Yangtze River in Nanjing Section, China. *Bulletin Environmental Contamamination and Toxicology,* Volume 82, pp. 405-409.

Ye, C., Li, S., Zhang, Y. & Zhang, Q., 2011. Assessing soil heavy metal pollution in the water-level-fluctuation zone of the Three Gorges Reservoir, China. *Journal of hazardous materials,* 191(1), pp. 366-372.

Yücel, H., Solmaz, A., Köse, E. & Bor, D., 2009. Spectral interference corrections for the measurement of 238 U in materials rich in thorium by a high resolution γ-ray spectrometry.. *Applied Radiation and Isotopes,* 67(11), pp. 2049-2056.

Zhuang, P. et al., 2009. Health risk from heavy metals via consumption of food crops in the vicinity of Dabaoshan mine, South China. *Science of The Total Environment,* 407(5), pp. 1551-1561.

Annexure A: Calculated Activity Concentrations of Soil, sediments and foodstuff samples from the study area.

Table A1: Activity Concentrations of ^{238}U in soil samples derived from ^{235}U assuming activity ratio $^{238}U/^{235}U$ of 20.7:1.

Region	sample code	Activity Concentration (Bq/kg)		
		^{226}Ra (^{214}Pb-^{214}Bi)	^{235}U (Ra-corrected) 186.2 keV	^{238}U (from ^{235}U)
Upper	SS01	31.6 ± 0.3	1.5 ± 0.3	30.6 ± 5.8
	SS02	55.7 ± 0.4	2.3 ± 0.3	46.6 ± 6.1
	SS03	12.4 ± 0.2	0.6 ± 0.2	12.3 ± 3.7
	SS04	35.7 ± 0.3	1.4 ± 0.3	29.1 ± 5.9
	SS05	65.9 ± 0.5	2.3 ± 0.3	48.5 ± 6.8
	SS06	111 ± 0.8	3.7 ± 0.4	76.8 ± 9.0
	SS07	12.0 ± 0.2	0.5 ± 0.2	10.3 ± 3.6
	SS08	13.0 ± 0.2	0.5 ± 0.2	10.8 ± 3.7
	SS09	12.8 ± 0.2	0.7 ± 0.2	15.2 ± 4.0
	SS10	28.6 ± 0.3	1.6 ± 0.2	32.6 ± 4.8
	SS11	54.0 ± 0.4	1.8 ± 0.3	36.8 ± 6.5
	SS12	66.6 ± 0.5	2.4 ± 0.3	49.1 ± 7.0
	SS13	32.4 ± 0.3	1.9 ± 0.3	38.5 ± 6.3
	SS14	29.5 ± 0.3	1.3 ± 0.3	26.9 ± 5.6
	SS15	30.5 ± 0.3	1.5 ± 0.3	31.4 ± 5.6
	SS16	14.4 ± 0.2	1.0 ± 0.2	20.3 ± 4.3
	SS17	51.4 ± 0.4	2.1 ± 0.3	43.8 ± 6.4
	SS18	48.6 ± 0.4	2.3 ± 0.3	46.5 ± 6.5
	SS19	43.5 ± 0.4	2.0 ± 0.3	40.8 ± 5.8
	SS20	14.1 ± 0.2	0.6 ± 0.2	11.6 ± 4.5
	SS21	20.3 ± 0.2	1.2 ± 0.3	24.4 ± 5.3
	SS22	14.2 ± 0.2	0.7 ± 0.2	15.2 ± 4.8
	SS23	16.5 ± 0.2	1.1 ± 0.2	23.5 ± 4.9
	SS24	12.3 ± 0.2	0.8 ± 0.2	16.5 ± 4.5
	SS25	29.9 ± 0.3	1.5 ± 0.3	30.7 ± 5.7

Table A1: Continued

Region	sample code	Activity Concentration (Bq/kg)		
		^{226}Ra (^{214}Pb-^{214}Bi)	^{235}U (Ra-corrected) 186.2 keV	^{238}U (from ^{235}U)
Upper	SS26	49.1 ± 0.4	2.1 ± 0.3	42.8 ± 6.7
	SS27	28.8 ± 0.3	1.2 ± 0.2	25.3 ± 5.0
	SS28	30.3 ± 0.3	1.3 ± 0.3	25.8 ± 5.4
	SS29	29.8 ± 0.3	1.5 ± 0.3	31.9 ± 5.8
	SS30	35.7 ± 0.3	1.9 ± 0.3	39.8 ± 6.0
	SS31	48.2 ± 0.4	2.3 ± 0.3	46.6 ± 6.0
	SS32	19.8 ± 0.2	0.9 ± 0.2	18.8 ± 5.0
	SS33	37.5 ± 0.3	1.7 ± 0.3	35.2 ± 6.1
	SS34	34.6 ± 0.3	1.6 ± 0.3	33.9 ± 6.3
	SS35	34.9 ± 0.3	1.4 ± 0.3	28.1 ± 5.8
	SS36	90.3 ± 0.6	4.4 ± 0.5	91.9 ± 9.5
	SS37	33.2 ± 0.3	1.1 ± 0.3	22.8 ± 5.6
	SS38	14.0 ± 0.2	0.6 ± 0.2	12.0 ± 4.3
Middle	SS39	17.6 ± 0.2	0.6 ± 0.3	11.7 ± 6.1
	SS40	40.3 ± 0.4	1.6 ± 0.3	33.5 ± 7.1
	SS41	15.7 ± 0.2	0.7 ± 0.3	13.5 ± 5.4
	SS42	16.2 ± 0.2	1.1 ± 0.2	23.2 ± 4.4
	SS43	18.5 ± 0.2	1.0 ± 0.3	20.6 ± 5.6
	SS44	33.3 ± 0.3	1.4 ± 0.4	28.4 ± 7.2
	SS45	39.4 ± 0.4	1.5 ± 0.3	31.9 ± 6.6
	SS46	35.9 ± 0.3	2.0 ± 0.4	40.9 ± 7.2
	SS47	19.0 ± 0.2	0.8 ± 0.3	15.8 ± 5.4
	SS48	20.5 ± 0.3	1.6 ± 0.4	32.5 ± 7.7
	SS49	40.5 ± 0.4	1.3 ± 0.3	26.4 ± 7.1
	SS50	13.4 ± 0.2	0.7 ± 0.2	15.1 ± 5.0

Table A1: Continued

Region	sample code	Activity Concentration (Bq/kg)		
		^{226}Ra (^{214}Pb-^{214}Bi)	^{235}U (Ra-corrected) 186.2 keV	^{238}U (from ^{235}U)
Middle	SS51	25.5 ± 0.3	1.4 ± 0.3	28.1 ± 6.9
	SS52	21.2 ± 0.2	1.5 ± 0.1	30.1 ± 2.7
	SS53	3.89 ± 0.3	0.2 ± 0.1	4.4 ± 1.1
	SS54	22.0 ± 0.3	1.1 ± 0.3	21.7 ± 6.7
	SS55	27.1 ± 0.3	1.8 ± 0.4	38.1 ± 7.1
	SS56	30.7 ± 0.3	1.5 ± 0.3	31.8 ± 6.7
	SS57	41.2 ± 0.4	1.8 ± 0.4	37.2 ± 7.8
	SS58	31.6 ± 0.3	1.3 ± 0.3	25.9 ± 6.5
	SS59	34.3 ± 0.3	1.6 ± 0.4	33.5 ± 7.2
	SS60	37.3 ± 0.3	1.7 ± 0.4	35.1 ± 7.2
	SS61	26.5 ± 0.3	1.1 ± 0.3	22.8 ± 6.0
	SS62	38.2 ± 0.3	2.5 ± 0.4	51.3 ± 7.4
	SS63	25.1 ± 0.3	1.0 ± 0.3	19.6 ± 5.9
	SS64	20.1 ± 0.2	1.1 ± 0.3	22.3 ± 5.8
	SS65	35.5 ± 0.3	1.7 ± 0.3	34.8 ± 7.0
	SS66	19.4 ± 0.2	1.7 ± 0.3	35.4 ± 5.8
	SS67	20.7 ± 0.3	1.2 ± 0.3	24.4 ± 6.1
	SS68	35.7 ± 0.3	1.7 ± 0.3	35.3 ± 56.0
	SS69	75.7 ± 0.6	4.2 ± 0.5	86.3 ± 9.3
Lower	SS70	27.1 ± 0.3	1.8 ± 0.4	38.1 ± 7.1
	SS71	30.7 ± 0.3	1.5 ± 0.3	31.8 ± 6.7
	SS72	41.2 ± 0.3	1.8 ± 0.4	37.2 ± 7.8
	SS73	31.6 ± 0.2	1.3 ± 0.3	25.9 ± 6.5
	Min	**3.89 ± 0.3**	**0.2 ± 0.1**	**4.4 ± 1.1**
	Max	**111 ± 0.8**	**4.4 ± 0.5**	**91.9 ± 9.5**
	Average	**32.0 ± 2.1**	**1.5 ± 0.1**	**31.3 ± 1.8**

Table A2: Calculated Activity Concentrations of ^{232}Th in soil samples derived from ^{228}Ra and ^{228}Th daughter nuclides.

Sample code	Activity Concentration (Bq/kg)									
	^{228}Ra				^{228}Th					
	^{228}Ac				^{212}Pb	^{212}Bi	^{208}Tl (Corrected)	^{228}Ra	^{228}Th	Weighted mean
	209.3 keV	270.2 keV	911.2 keV	969.0 keV	238.6 keV	727.3 keV	583.2 keV			
SS01	32.1 ± 3.5	47.4 ± 4.4	42.9 ± 0.9	43.1 ± 1.2	38.2 ± 0.6	46.4 ± 2.9	38.7 ± 0.7	41.3 ± 6.5	41.1 ± 4.6	41.2 ± 5.3
SS02	39.4 ± 3.7	49.1 ± 5.0	49.7 ± 1.0	47.3 ± 1.3	42.2 ± 0.7	54.3 ± 3.3	42.8 ± 1.0	46.4 ± 4.8	46.4 ± 6.8	46.4 ± 5.2
SS03	15.0 ± 2.3	14.1 ± 2.9	17.7 ± 0.5	18.5 ± 0.7	15.5 ± 0.3	18.7 ± 2.0	15.3 ± 0.5	16.3 ± 2.1	16.5 ± 1.9	16.4 ± 1.9
SS04	46.6 ± 3.9	50.8 ± 4.4	58.4 ± 1.2	55.0 ± 1.4	49.9 ± 0.8	59.4 ± 3.0	51.4 ± 1.0	52.7 ± 5.1	53.6 ± 5.1	53.1 ± 4.7
SS05	50.1 ± 4.4	52.2 ± 2.0	58.1 ± 1.2	56.0 ± 1.4	48.6 ± 0.7	60.9 ± 3.5	48.1 ± 1.1	54.1 ± 3.6	52.5 ± 7.3	53.4 ± 5.0
SS06	43.9 ± 4.7	68.0 ± 2.3	48.8 ± 1.4	45.6 ± 1.2	40.6 ± 0.6	50.4 ± 1.5	40.5 ± 0.7	51.6 ± 9.8	43.8 ± 5.7	48.3 ± 9.5
SS07	11.5 ± 2.0	15.2 ± 2.9	16.1 ± 0.7	13.7 ± 0.6	12.8 ± 0.2	16.8 ± 1.9	13.2 ± 0.5	14.1 ± 2.0	14.3 ± 2.2	14.2 ± 1.9
SS08	16.4 ± 2.3	22.8 ± 3.2	19.6 ± 0.7	16.8 ± 0.7	15.9 ± 0.3	19.8 ± 2.0	15.5 ± 0.6	18.9 ± 3.0	17.0 ± 2.4	18.1 ± 2.7
SS09	14.7 ± 2.4	22.2 ± 3.0	23.9 ± 0.6	22.9 ± 0.7	19.3 ± 0.3	25.3 ± 2.2	20.0 ± 0.6	20.9 ± 4.2	21.5 ± 3.3	21.2 ± 3.5
SS10	28.2 ± 3.0	36.2 ± 1.4	36.2 ± 0.8	37.3 ± 1.0	31.7 ± 0.5	39.3 ± 2.6	32.9 ± 0.7	34.5 ± 4.2	34.6 ± 4.1	34.5 ± 3.8
SS11	30.4 ± 3.4	46.0 ± 1.7	33.9 ± 0.8	30.3 ± 1.0	28.9 ± 0.5	32.4 ± 3.1	28.3 ± 0.7	35.1 ± 7.4	29.9 ± 2.2	32.9 ± 6.1
SS12	41.8 ± 4.5	61.9 ± 2.2	55.0 ± 1.1	50.5 ± 1.4	46.0 ± 0.7	55.6 ± 1.6	46.0 ± 1.1	52.3 ± 8.4	49.2 ± 5.5	51.0 ± 7.0
SS13	32.9 ± 3.8	50.5 ± 4.5	47.1 ± 1.4	43.9 ± 1.3	40.0 ± 0.6	51.5 ± 3.8	38.3 ± 1.0	43.6 ± 7.6	43.2 ± 7.2	43.4 ± 6.8
SS14	32.9 ± 3.4	40.8 ± 4.4	35.5 ± 1.1	34.9 ± 1.1	30.8 ± 0.5	33.4 ± 2.8	30.3 ± 0.9	36.0 ± 3.4	31.5 ± 1.7	34.1 ± 3.5

Table A2: Continued

Sample code	Activity Concentration (Bq/kg)									
	^{228}Ra				^{228}Th			^{228}Ra	^{228}Th	Weighted mean
	^{228}Ac				^{212}Pb	^{212}Bi	^{208}Tl			
	209.3 keV	**270.2 keV**	**911.2 keV**	**969.0 keV**	**238.6 keV**	**727.3 keV**	**583.2 keV**			
SS15	29.2 ± 3.6	48.8 ± 4.2	40.5 ± 0.9	41.4 ± 1.2	35.4 ± 0.6	42.6 ± 2.6	34.9 ± 0.8	40.0 ± 8.1	37.6 ± 4.3	39.0 ± 6.4
SS16	22.6 ± 2.7	28.6 ± 3.7	24.6 ± 0.9	22.9 ± 0.8	21.4 ± 0.4	26.3 ± 2.5	21.2 ± 0.7	24.7 ± 2.8	23.0 ± 2.9	23.9 ± 2.7
SS17	28.2 ± 1.5	44.1 ± 4.1	37.2 ± 0.8	35.8 ± 1.1	31.9 ± 0.5	35.8 ± 1.4	30.6 ± 0.9	36.3 ± 6.5	32.7 ± 2.7	34.8 ± 5.2
SS18	33.9 ± 4.3	48.0 ± 1.9	44.8 ± 1.0	45.2 ± 1.3	39.0 ± 0.6	50.0 ± 1.5	39.0 ± 1.0	43.0 ± 6.2	42.7 ± 6.4	42.8 ± 5.8
SS19	34.3 ± 4.0	42.9 ± 1.8	44.1 ± 1.0	41.4 ± 1.2	39.0 ± 0.6	45.9 ± 3.1	38.8 ± 0.8	40.7 ± 4.4	41.2 ± 4.0	40.9 ± 3.9
SS20	13.7 ± 2.4	22.2 ± 3.4	22.0 ± 0.9	21.1 ± 0.8	19.0 ± 0.3	25.4 ± 2.6	20.0 ± 0.6	19.8 ± 4.1	21.5 ± 3.5	20.5 ± 3.6
SS21	19.4 ± 3.2	24.7 ± 4.2	26.3 ± 1.0	24.0 ± 0.9	21.1 ± 0.4	27.4 ± 2.4	20.8 ± 0.8	23.6 ± 3.0	23.1 ± 3.7	23.4 ± 3.0
SS22	18.9 ± 3.1	19.4 ± 3.7	22.4 ± 1.0	20.8 ± 0.8	17.8 ± 0.3	26.6 ± 2.6	18.3 ± 0.6	20.4 ± 1.5	20.9 ± 4.9	20.6 ± 3.1
SS23	23.4 ± 3.4	25.4 ± 3.4	24.4 ± 0.6	24.0 ± 0.9	21.4 ± 0.4	24.7 ± 2.9	21.5 ± 0.7	24.3 ± 0.9	22.5 ± 1.9	23.5 ± 1.5
SS24	15.1 ± 3.0	18.3 ± 3.4	22.7 ± 1.0	21.7 ± 0.8	18.8 ± 0.3	25.3 ± 2.6	18.7 ± 0.7	19.4 ± 3.5	20.9 ± 3.8	20.1 ± 3.4
SS25	34.5 ± 3.5	40.6 ± 4.0	40.4 ± 0.9	38.5 ± 1.2	34.3 ± 0.6	45.9 ± 3.1	34.9 ± 0.9	38.5 ± 2.8	38.4 ± 6.6	38.4 ± 4.3
SS26	32.4 ± 4.2	50.8 ± 2.0	41.3 ± 0.9	40.5 ± 1.2	35.2 ± 0.6	42.7 ± 3.1	35.3 ± 1.0	41.3 ± 7.6	37.7 ± 4.3	39.8 ± 6.2
SS27	22.8 ± 3.0	40.4 ± 4.1	35.0 ± 0.8	31.5 ± 1.0	30.3 ± 0.5	33.1 ± 2.8	29.7 ± 0.8	32.4 ± 7.4	31.0 ± 1.8	31.8 ± 5.4
SS28	29.7 ± 3.3	28.0 ± 4.3	34.3 ± 1.7	33.9 ± 1.1	29.3 ± 0.5	34.6 ± 4.8	28.8 ± 0.9	31.5 ± 3.1	30.9 ± 3.2	31.2 ± 2.9
SS29	29.6 ± 3.6	45.1 ± 4.1	43.4 ± 1.0	39.1 ± 1.2	35.4 ± 0.6	41.3 ± 2.7	34.5 ± 0.9	39.3 ± 6.9	37.1 ± 3.7	38.3 ± 5.5
SS30	30.4 ± 2.9	44.8 ± 4.4	41.6 ± 1.3	38.9 ± 1.2	34.5 ± 0.6	47.4 ± 3.2	33.6 ± 0.9	38.9 ± 6.2	38.5 ± 7.7	38.7 ± 6.2

Table A2: Continued

Sample code	Activity Concentration (Bq/kg)									
	^{228}Ra				^{228}Th			^{228}Ra	^{228}Th	Weighted mean
	^{228}Ac				^{212}Pb	^{212}Bi	^{208}Tl			
	209.3 keV	**270.2 keV**	**911.2 keV**	**969.0 keV**	**238.6 keV**	**727.3 keV**	**583.2 keV**			
SS31	42.1 ± 4.0	49.6 ± 5.4	53.8 ± 1.2	51.3 ± 1.4	44.1 ± 0.7	50.5 ± 3.8	43.1 ± 1.0	49.2 ± 5.0	45.9 ± 4.1	47.8 ± 4.6
SS32	25.4 ± 2.9	24.8 ± 3.4	21.0 ± 0.9	22.5 ± 0.8	19.1 ± 0.3	24.1 ± 2.7	19.6 ± 0.7	23.4 ± 2.0	20.9 ± 2.8	22.3 ± 2.5
SS33	25.6 ± 4.0	38.4 ± 5.1	38.4 ± 0.9	39.0 ± 1.1	32.9 ± 0.5	45.9 ± 3.2	33.4 ± 0.9	35.3 ± 6.5	37.4 ± 7.4	36.2 ± 6.4
SS34	29.3 ± 4.0	47.2 ± 4.7	37.8 ± 0.9	35.9 ± 1.1	33.0 ± 0.5	34.2 ± 4.1	33.4 ± 0.9	37.6 ± 7.4	33.6 ± 0.6	35.9 ± 5.7
SS35	24.8 ± 6.1	42.5 ± 4.5	37.2 ± 0.9	36.3 ± 1.1	31.1 ± 0.5	37.6 ± 7.1	30.9 ± 0.8	35.2 ± 7.4	33.2 ± 3.8	34.3 ± 5.8
SS36	52.2 ± 2.2	75.2 ± 2.6	65.9 ± 1.3	65.5 ± 1.7	57.6 ± 0.9	66.9 ± 1.9	60.8 ± 1.3	64.7 ± 9.5	61.7 ± 4.7	63.4 ± 7.4
SS37	21.5 ± 4.0	30.8 ± 4.8	32.4 ± 1.1	33.0 ± 1.0	27.8 ± 0.5	35.1 ± 1.4	28.1 ± 0.5	29.4 ± 5.4	30.3 ± 4.2	29.8 ± 4.5
SS38	17.6 ± 2.5	26.4 ± 3.5	21.9 ± 0.6	21.9 ± 0.8	18.8 ± 0.3	26.6 ± 2.4	18.7 ± 0.6	21.9 ± 3.6	21.4 ± 4.5	21.7 ± 3.7
SS39	62.2 ± 4.6	69.2 ± 5.0	78.9 ± 1.5	78.0 ± 1.9	69.2 ± 1.0	89.5 ± 3.9	68.3 ± 1.2	72.1 ± 7.9	75.6 ± 12	73.6 ± 9.1
SS40	44.6 ± 4.7	56.4 ± 5.3	59.3 ± 1.2	56.4 ± 1.5	49.9 ± 0.8	61.2 ± 4.0	49.6 ± 1.1	54.2 ± 6.5	53.5 ± 6.6	53.9 ± 6.0
SS41	44.7 ± 3.9	41.0 ± 4.1	53.4 ± 1.1	51.0 ± 1.3	44.8 ± 0.7	58.6 ± 2.8	45.2 ± 0.9	47.5 ± 5.7	49.5 ± 7.8	48.4 ± 6.1
SS42	25.6 ± 2.9	29.0 ± 4.1	29.7 ± 1.1	26.5 ± 0.9	28.5 ± 0.5	28.3 ± 3.0	29.0 ± 0.8	27.7 ± 2.0	28.6 ± 0.4	28.1 ± 1.5
SS43	28.0 ± 3.5	38.2 ± 4.7	41.8 ± 0.9	42.1 ± 1.2	33.8 ± 0.5	41.2 ± 3.0	34.7 ± 0.8	37.5 ± 6.6	36.5 ± 4.1	37.1 ± 5.3
SS44	44.4 ± 4.5	62.6 ± 2.3	61.3 ± 1.3	61.8 ± 1.7	51.7 ± 0.8	65.7 ± 4.0	49.5 ± 1.2	57.5 ± 8.8	55.7 ± 8.8	56.7 ± 8.1
SS45	65.5 ± 4.7	72.0 ± 2.4	81.9 ± 1.6	77.2 ± 1.9	67.3 ± 1.0	80.8 ± 8.5	68.1 ± 1.3	74.1 ± 7.0	72.1 ± 7.6	73.2 ± 6.7
SS46	50.5 ± 2.1	68.2 ± 5.5	75.7 ± 1.5	73.2 ± 1.9	64.1 ± 1.0	78.9 ± 4.0	65.8 ± 1.4	66.9 ± 11	69.6 ± 8.1	68.0 ± 9.4

Table A2: Continued

Sample code	Activity Concentration (Bq/kg)									
	^{228}Ra				^{228}Th			^{228}Ra	^{228}Th	Weighted mean
	^{228}Ac				^{212}Pb	^{212}Bi	^{208}Tl			
	209.3 keV	**270.2 keV**	**911.2 keV**	**969.0 keV**	**238.6 keV**	**727.3 keV**	**583.2 keV**			
SS47	21.7 ± 3.6	27.8 ± 3.6	32.3 ± 1.2	30.8 ± 1.1	27.4 ± 0.5	33.2 ± 2.8	26.2 ± 0.9	28.1 ± 4.7	29.0 ± 3.7	28.5 ± 4.0
SS48	74.5 ± 5.2	85.8 ± 5.4	97.1 ± 1.9	97.2 ± 2.4	83.5 ± 1.3	103 ± 5	82.9 ± 1.6	88.6 ± 11	89.8 ± 11	89.1 ± 10.1
SS49	49.6 ± 4.4	58.6 ± 2.3	60.9 ± 1.3	59.0 ± 1.7	51.9 ± 0.8	63.6 ± 3.9	51.2 ± 1.3	57.0 ± 5.1	55.6 ± 6.9	56.4 ± 5.4
SS50	24.0 ± 3.3	22.7 ± 4.2	28.4 ± 1.1	28.8 ± 1.1	23.5 ± 0.4	31.8 ± 3.0	23.3 ± 0.9	26.0 ± 3.1	26.2 ± 4.8	26.1 ± 3.5
SS51	56.1 ± 5.0	54.3 ± 6.0	65.0 ± 1.4	62.6 ± 1.7	55.3 ± 0.9	64.7 ± 4.7	56.4 ± 1.2	59.5 ± 5.1	58.8 ± 5.2	59.2 ± 4.7
SS52	44.5 ± 3.4	45.5 ± 1.8	46.7 ± 1.0	46.8 ± 1.3	40.3 ± 0.6	51.7 ± 2.9	41.1 ± 1.0	45.9 ± 1.1	44.4 ± 6.3	45.2 ± 3.8
SS53	12.6 ± 0.8	14.8 ± 1.0	14.7 ± 0.3	14.2 ± 0.4	12.7 ± 0.2	16.6 ± 0.8	12.9 ± 0.2	14.1 ± 1.0	14.1 ± 2.2	14.1 ± 1.4
SS54	63.1 ± 5.3	73.7 ± 6.0	81.2 ± 1.6	79.2 ± 2.0	71.2 ± 1.1	84.8 ± 4.6	71.3 ± 1.4	74.3 ± 8.1	75.7 ± 7.9	74.9 ± 7.4
SS55	48.5 ± 4.3	57.1 ± 5.1	57.8 ± 2.4	58.2 ± 1.5	51.4 ± 0.8	70.2 ± 4.3	53.2 ± 1.1	55.4 ± 4.6	58.3 ± 10	56.6 ± 7.0
SS56	44.4 ± 4.4	52.7 ± 5.5	56.4 ± 1.2	57.9 ± 1.5	49.2 ± 0.8	59.8 ± 3.8	49.5 ± 1.1	52.9 ± 6.1	52.8 ± 6.1	52.9 ± 5.5
SS57	58.6 ± 4.9	69.7 ± 6.0	73.2 ± 1.5	71.3 ± 1.8	63.5 ± 1.0	80.1 ± 4.3	63.0 ± 1.3	68.2 ± 6.6	68.9 ± 9.7	68.5 ± 7.3
SS58	51.9 ± 4.7	58.8 ± 4.9	55.8 ± 1.2	53.5 ± 1.4	48.1 ± 0.7	64.0 ± 3.8	48.4 ± 1.1	55.0 ± 3.0	53.5 ± 9.1	54.3 ± 5.7
SS59	42.7 ± 4.1	56.5 ± 5.3	55.6 ± 1.2	56.0 ± 1.5	49.3 ± 0.8	58.2 ± 3.9	48.7 ± 1.1	52.7 ± 6.7	52.1 ± 5.4	52.4 ± 5.7
SS60	56.1 ± 5.1	65.8 ± 5.6	69.7 ± 1.4	66.8 ± 1.7	59.2 ± 0.9	73.5 ± 4.5	60.1 ± 1.1	64.6 ± 5.9	64.3 ± 8.0	64.5 ± 6.2
SS61	42.5 ± 3.9	54.5 ± 4.2	48.6 ± 1.0	47.4 ± 1.3	41.8 ± 0.6	60.4 ± 3.6	41.4 ± 1.0	48.2 ± 4.9	47.8 ± 11	48.1 ± 7.2
SS62	46.2 ± 4.5	63.0 ± 5.6	59.3 ± 1.3	59.7 ± 1.6	51.8 ± 0.8	61.5 ± 4.7	51.8 ± 1.1	57.0 ± 7.4	55.0 ± 5.6	56.2 ± 6.3

Table A2: Continued

Sample code	Activity Concentration (Bq/kg)									
	^{228}Ra				^{228}Th					Weighted mean
	^{228}Ac				^{212}Pb	^{212}Bi	^{208}Tl	^{228}Ra	^{228}Th	
	209.3 keV	**270.2 keV**	**911.2 keV**	**969.0 keV**	**238.6 keV**	**727.3 keV**	**583.2 keV**			
SS63	45.5 ± 4.3	46.2 ± 4.9	50.8 ± 1.1	48.4 ± 1.3	43.7 ± 0.7	48.3 ± 3.5	45.7 ± 1.0	47.7 ± 2.4	45.9 ± 2.3	46.9 ± 2.4
SS64	37.8 ± 3.6	48.5 ± 4.5	47.4 ± 1.0	46.3 ± 1.2	40.8 ± 0.6	47.2 ± 3.3	41.9 ± 0.9	45.0 ± 4.9	43.3 ± 3.4	44.3 ± 4.1
SS65	40.0 ± 4.1	58.0 ± 5.2	52.0 ± 1.1	52.1 ± 1.4	45.6 ± 0.7	57.3 ± 3.6	44.6 ± 1.0	50.5 ± 7.6	49.2 ± 7.1	49.9 ± 6.8
SS66	44.3 ± 6.4	44.9 ± 3.9	51.3 ± 1.1	48.7 ± 1.3	42.9 ± 0.7	53.9 ± 3.5	43.0 ± 1.0	47.3 ± 3.3	46.6 ± 6.3	47.0 ± 4.3
SS67	34.7 ± 3.6	33.9 ± 4.1	43.9 ± 1.0	47.1 ± 1.2	38.6 ± 0.6	44.0 ± 3.1	39.4 ± 0.9	39.9 ± 6.6	40.7 ± 2.9	40.2 ± 5.0
SS68	33.4 ± 3.7	44.5 ± 4.8	42.2 ± 0.9	42.7 ± 1.2	36.3 ± 0.6	49.5 ± 3.6	37.7 ± 0.9	40.7 ± 5.0	41.1 ± 7.3	40.9 ± 5.5
SS69	66.0 ± 5.7	89.1 ± 6.7	82.9 ± 1.6	81.4 ± 2.0	72.1 ± 1.1	87.2 ± 2.2	72.8 ± 1.4	79.9 ± 9.8	77.3 ± 8.5	78.8 ± 8.6
SS70	62.1 ± 4.5	72.3 ± 6.2	81.3 ± 1.6	80.5 ± 2.0	70.2 ± 1.1	88.8 ± 4.2	69.5 ± 1.4	74.1 ± 8.9	76.2 ± 11	75.0 ± 9.0
SS71	70.0 ± 4.7	72.9 ± 5.8	85.9 ± 1.7	86.8 ± 2.1	74.9 ± 1.1	92.6 ± 4.3	74.0 ± 1.4	78.9 ± 8.7	80.5 ± 11	79.6 ± 8.7
SS72	55.0 ± 4.3	63.5 ± 5.7	68.5 ± 1.4	63.3 ± 1.7	56.4 ± 0.9	74.2 ± 4.0	56.1 ± 1.1	62.6 ± 5.6	62.2 ± 10	62.4 ± 7.2
SS73	40.1 ± 3.6	46.6 ± 4.4	51.3 ± 1.1	49.9 ± 1.4	42.9 ± 0.7	50.4 ± 3.8	42.6 ± 0.9	47.0 ± 5.0	45.3 ± 4.4	46.3 ± 4.5
Min	**11.5 ± 2.0**	**14.1 ± 2.9**	**14.7 ± 0.3**	**13.7 ± 0.6**	**12.7 ± 0.2**	**16.6 ± 0.8**	**12.9 ± 0.2**	**14.1 ± 1.0**	**14.1 ± 2.2**	**14.1 ± 1.4**
Max	**74.5 ± 5.2**	**89.1 ± 6.7**	**97.1 ± 1.9**	**97.2 ± 2.4**	**83.5 ± 1.3**	**103 ± 5**	**82.9 ± 1.6**	**88.6 ± 11**	**89.8 ± 11**	**89.1 ± 10**
Average	**37.3 ± 0.5**	**46.6 ± 0.5**	**47.1 ± 0.1**	**45.8 ± 0.2**	**40.3 ± 0.1**	**49.8 ± 0.4**	**40.4 ± 0.1**	**44.2 ± 0.7**	**43.5 ± 0.7**	**43.9 ± 0.7**

Table A3: The results of the mean activity concentrations of ^{238}U, ^{232}Th, ^{40}K and ^{137}Cs in sediments samples.

Sample code	Specific activity (Bq/kg) (Sediment)			
	^{238}U	^{232}Th	^{40}K	^{137}Cs
SED01	33.34 ± 7.30	78.0 ± 5.80	685.4 ± 9.47	0.38 ± 0.07
SED02	6.34 ± 3.90	21.0 ± 3.87	600.4 ± 7.90	< 0.33
SED03	21.17 ± 5.73	41.7 ± 4.56	802.7 ± 10.6	0.52 ± 0.07
SED04	23.67 ± 6.46	71.9 ± 9.00	877.8 ± 11.5	< 0.55
SED05	37.19 ± 6.65	63.9 ± 8.72	827.5 ± 11.1	< 3.87
SED06	10.11 ± 4.86	50.9 ± 8.23	862.5 ± 11.2	< 0.31
SED07	40.68 ± 7.90	95.8 ± 11.38	732.2 ± 10.2	0.22 ± 0.08
SED08	50.34 ± 7.17	86.9 ± 6.00	713.3 ± 9.75	< 0.61
SED09	34.59 ± 6.63	66.2 ± 9.08	721.0 ± 9.76	< 0.57
SED10	21.58 ± 5.87	44.5 ± 6.07	771.6 ± 10.1	< 0.51
SED11	32.08 ± 6.85	56.4 ± 5.36	812.7 ± 10.9	< 0.59
SED12	19.11 ± 5.82	37.7 ± 4.98	871.9 ± 11.3	< 0.53
SED13	21.00 ± 6.24	46.2 ± 4.39	858.8 ± 11.2	0.67 ± 0.08
SED14	23.22 ± 4.97	48.0 ± 7.42	783.9 ± 10.4	1.28 ± 0.09
SED15	26.36 ± 5.01	44.5 ± 5.69	839.4 ± 10.9	0.74 ± 0.08
SED16	31.51± 6.52	50.6 ± 5.71	823.0 ± 10.7	0.20 ± 0.07
SED17	21.70 ± 5.50	48.2 ± 4.14	800.9 ± 10.4	0.47 ± 0.08
Min	**6.34 ± 3.90**	**21.0 ± 3.87**	**600.4 ± 7.90**	**0.20 ± 0.07**
Max	**50.34 ± 7.17**	**95.8 ± 11.38**	**877.8 ± 11.5**	**1.28 ± 0.09**
Average	**25.89 ± 5.98**	**56.0 ± 4.60**	**787.4 ± 18.3**	

Table A4: The results of the mean activity concentrations of ^{238}U, ^{232}Th, ^{40}K and ^{137}Cs in soil samples.

Sample code	Specific activity (Bq/kg) Soil			
	^{238}U	^{232}Th	^{40}K	^{137}Cs
SS01	30.6 ± 5.8	41.2 ± 5.3	482 ± 7	0.30 ± 0.20
SS02	46.6 ± 6.1	46.4 ± 5.2	292 ± 5	< 0.49
SS03	12.3 ± 3.7	16.4 ± 1.9	192 ± 3	0.10 ± 0.03
SS04	29.1 ± 5.9	53.1 ± 4.7	452 ± 6	< 0.45
SS05	48.5 ± 6.8	53.4 ± 5.0	392 ± 6	< 0.50
SS06	76.8 ± 8.9	48.3 ± 9.5	269 ± 5	< 0.55
SS07	10.3 ± 3.6	14.2 ± 1.9	225 ± 4	0.39 ± 0.04
SS08	10.8 ± 3.7	18.1 ± 2.7	276 ± 4	0.75 ± 0.06
SS09	15.2 ± 4.0	21.2 ± 3.5	310 ± 5	0.59 ± 0.06
SS10	32.6 ± 4.8	34.5 ± 3.8	180 ± 3	< 0.23
SS11	36.8 ± 6.5	32.9 ± 6.1	266 ± 4	< 0.44
SS12	49.1 ± 7.0	51.0 ± 7.0	517 ± 7	< 0.53
SS13	38.5 ± 6.3	43.4 ± 6.8	460 ± 7	0.38 ± 0.07
SS14	26.9 ± 5.6	34.1 ± 3.5	296.5 ± 5	0.20 ± 0.06
SS15	31.4 ± 5.6	39.0 ± 6.4	331 ± 5	0.44 ± 0.06
SS16	20.3 ± 4.3	23.9 ± 2.7	251 ± 4	0.43 ± 0.06
SS17	43.8 ± 6.4	34.8 ± 5.2	253 ± 5	0.90 ± 0.07
SS18	46.5 ± 6.5	42.8 ± 5.8	200 ± 4	0.38 ± 0.06
SS19	40.8 ± 5.8	40.9 ± 3.9	254± 5	0.39 ± 0.06
SS20	11.6 ± 4.5	20.5 ± 3.6	273 ± 5	0.48 ± 0.05
SS21	24.4 ± 5.3	23.4 ± 3.0	369 ± 6	2.14 ± 0.09
SS22	15.2 ± 4.8	20.6 ± 3.1	315 ± 5	1.01 ± 0.07
SS23	23.5 ± 4.9	23.5 ± 1.5	363 ± 6	0.95 ± 0.07
SS24	16.5 ± 4.5	20.1 ± 3.4	438 ± 6	0.42 ± 0.13
SS25	30.7 ± 5.7	38.4 ± 4.3	287 ± 5	0.38 ± 0.07

Table A4: Continued

Sample code	Specific activity (Bq/kg) Soil			
	^{238}U	^{232}Th	^{40}K	^{137}Cs
SS26	42.8 ± 6.7	39.8 ± 6.2	355 ± 6	0.93 ± 0.08
SS27	25.3 ± 5.0	31.8 ± 5.4	231± 4	0.87 ± 0.06
SS28	25.8 ± 5.4	31.2 ± 2.9	255 ± 4	0.20 ± 0.05
SS29	31.9 ± 5.8	38.3 ± 5.5	207 ± 4	0.58 ± 0.07
SS30	39.8 ± 6.0	38.7 ± 6.2	616 ± 8	< 0.48
SS31	46.6 ± 6.0	47.8 ± 4.6	613 ± 9	< 0.55
SS32	18.8 ± 5.0	22.3 ± 2.5	595 ± 8	< 0.43
SS33	35.2 ± 6.1	36.2 ± 6.4	604 ± 8	0.51 ± 0.07
SS34	33.9 ± 6.3	35.9 ± 5.7	617 ± 9	0.44 ± 0.07
SS35	28.1 ± 5.8	34.3 ± 5.8	547 ± 8	0.37 ± 0.07
SS36	91.9 ± 9.5	63.4 ± 7.4	551 ± 8	0.39 ± 0.08
SS37	22.8 ± 5.6	29.8 ± 4.5	641 ± 9	0.35 ± 0.07
SS38	12.0 ± 4.3	21.7 ± 3.7	625 ± 8	0.39 ± 0.14
SS39	11.7 ± 6.1	73.6 ± 9.1	786 ± 10	< 0.51
SS40	33.5 ± 7.1	53.9 ± 6.0	609 ± 8	< 0.54
SS41	13.5 ± 5.4	48.4 ± 6.1	785 ± 10	< 0.45
SS42	23.2 ± 4.4	28.1 ± 1.5	415 ± 6	< 0.42
SS43	20.6 ± 5.6	37.1 ± 5.3	783 ± 10	0.46 ± 0.07
SS44	28.4 ± 7.2	56.7 ± 8.1	836 ± 11	1.40 ± 0.10
SS45	31.9 ± 6.6	73.2 ± 6.7	652 ± 9	< 0.61
SS46	40.9 ± 7.2	68.0 ± 9.4	724 ± 10	0.49 ± 0.09
SS47	15.8 ± 5.4	28.5 ± 4.0	701 ± 10	0.45 ± 0.07
SS48	32.5 ± 7.7	89.1 ± 10.1	958 ± 13	< 0.67
SS49	26.4 ± 7.1	56.4 ± 5.4	652 ± 9	< 0.61
SS50	15.1 ± 5.0	26.1 ± 3.5	250 ± 4	< 0.46

Table A4: Continued

Sample code	Specific activity (Bq/kg) Soil			
	^{238}U	^{232}Th	^{40}K	^{137}Cs
SS51	28.1 ± 6.9	59.2 ± 4.7	809 ± 11	1.54 ± 0.10
SS52	30.1 ± 2.7	45.2 ± 3.8	688 ± 9	< 0.49
SS53	4.4 ± 1.1	14.1 ± 1.4	220 ± 3	0.15 ± 0.02
SS54	21.7 ± 6.7	74.9 ± 7.4	826 ± 11	< 0.61
SS55	38.1 ± 7.1	56.6 ± 7.0	< 20.2	0.42 ± 0.08
SS56	31.8 ± 6.7	52.9 ± 5.5	654 ± 9	0.25 ± 0.08
SS57	37.2 ± 7.8	68.5 ± 7.3	666 ± 9	< 0.65
SS58	25.9 ± 6.5	54.3 ± 5.7	705 ± 10	0.68 ± 0.08
SS59	33.5 ± 7.2	52.4 ± 5.7	778 ± 11	< 0.61
SS60	35.1 ± 7.2	64.5 ± 6.2	728 ± 10	< 0.61
SS61	22.8 ± 6.0	48.1 ± 7.2	686 ± 9	0.52 ± 0.08
SS62	51.3 ± 7.4	56.2 ± 6.3	694 ± 10	0.38 ± 0.08
SS63	19.6 ± 5.9	46.9 ± 2.4	636 ± 9	0.46 ± 0.07
SS64	22.3 ± 5.8	44.3 ± 4.1	706 ± 9	< 0.50
SS65	34.8 ± 7.0	49.9 ± 6.8	610 ± 9	0.61 ± 0.08
SS66	35.4 ± 5.8	47.0 ± 4.3	766 ± 10	< 0.51
SS67	24.4 ± 6.1	40.2 ± 5.0	684 ± 9	2.45 ± 0.10
SS68	35.3 ± 6.0	40.9 ± 5.5	< 17.6	< 0.50
SS69	86.3 ± 9.3	78.8 ± 8.6	< 19.9	0.42 ± 0.09
SS70	48.1 ± 7.3	75.0 ± 9.0	719 ± 10	< 0.61
SS71	37.0 ± 11.4	79.6 ± 8.7	728 ± 10	< 0.60
SS72	35.2 ± 6.8	62.4 ± 7.2	709 ± 10	< 0.59
SS73	27.6 ± 6.1	46.3 ± 4.5	775 ± 11	< 0.53
Min	**10.3 ± 3.6**	**14.1± 0.02**	**180 ± 3**	**0.10 ± 0.03**
Max	**91.9 ± 9.5**	**89.20 ± 0.8**	**958± 13**	**2.45 ± 0.10**
Average	**31.3 ± 1.8**	**43.9 ± 2.0**	**519 ± 25**	

Table A5: Isotopic activity ratios of radionuclides $^{238}U/^{226}Ra$ in ^{238}U series and $^{228}Ra/^{228}Th$ in ^{232}Th series of sediments samples.

Sample code	Activity Ratio			
	$^{238}U/^{226}Ra$	**Remarks on ^{238}U-series**	**$^{228}Ra/^{228}Th$**	**Remarks on ^{232}Th-series**
SED01	0.95 ± 0.21	Equilibrium	0.99 ± 0.12	Equilibrium
SED02	0.89 ± 0.55	Equilibrium	1.05 ± 0.27	Equilibrium
SED03	1.05 ± 0.28	Equilibrium	0.94 ± 0.16	Equilibrium
SED04	1.03 ± 0.28	Equilibrium	0.94 ± 0.18	Equilibrium
SED05	1.60 ± 0.44	U-Enriched or Ra-Depleted	0.96 ± 0.20	Equilibrium
SED06	0.57 ± 0.28	Ra-Enriched or U-Depleted	0.93 ± 0.22	Equilibrium
SED07	1.19 ± 0.23	Equilibrium	0.96 ± 0.17	Equilibrium
SED08	1.29 ± 0.19	Equilibrium	1.03 ± 0.12	Equilibrium
SED09	1.17 ± 0.22	Equilibrium	0.96 ± 0.21	Equilibrium
SED10	0.97 ± 0.26	Equilibrium	0.97 ± 0.20	Equilibrium
SED11	1.12 ± 0.24	Equilibrium	0.97 ± 0.15	Equilibrium
SED12	1.20 ± 0.37	Equilibrium	0.99 ± 0.20	Equilibrium
SED13	1.02 ± 0.30	Equilibrium	1.01 ± 0.14	Equilibrium
SED14	0.98 ± 0.21	Equilibrium	1.00 ± 0.23	Equilibrium
SED15	1.27 ± 0.24	Equilibrium	0.97 ± 0.19	Equilibrium
SED16	1.21 ± 0.25	Equilibrium	0.96 ± 0.16	Equilibrium
SED17	0.90 ± 0.23	Equilibrium	1.02 ± 0.13	Equilibrium
Min	**0.57 ± 0.28**		**0.93 ± 0.22**	
Max	**1.60 ± 0.44**		**1.05 ± 0.27**	
Average	**1.08 ± 0.05**	**Equilibrium**	**0.98 ± 0.01**	**Equilibrium**

Table A6: Isotopic activity ratios of radionuclides $^{238}U/^{226}Ra$ in ^{238}U series and $^{228}Ra/^{228}Th$ in ^{232}Th series of soil samples.

Sample code	Activity Ratio			
	$^{238}U/^{226}Ra$	Remarks on ^{238}U-series	$^{228}Ra/^{228}Th$	Remarks on ^{232}Th-series
SS01	0.97 ± 0.19	Equilibrium	1.01 ± 0.19	Equilibrium
SS02	0.84 ± 0.11	Ra-Enriched or U-Depleted	1.00 ± 0.18	Equilibrium
SS03	0.99 ± 0.30	Equilibrium	0.99 ± 0.17	Equilibrium
SS04	0.82 ± 0.17	Ra-Enriched or U-Depleted	0.98 ± 0.13	Equilibrium
SS05	0.74 ± 0.10	Ra-Enriched or U-Depleted	1.03 ± 0.16	Equilibrium
SS06	0.69 ± 0.08	Ra-Enriched or U-Depleted	1.18 ± 0.30	Equilibrium
SS07	0.86 ± 0.30	Equilibrium	0.99 ± 0.21	Equilibrium
SS08	0.83 ± 0.29	Ra-Enriched or U-Depleted	1.11 ± 0.23	Equilibrium
SS09	1.19 ± 0.31	Equilibrium	0.97 ± 0.24	Equilibrium
SS10	1.14 ± 0.17	Equilibrium	1.00 ± 0.17	Equilibrium
SS11	0.68 ± 0.12	Ra-Enriched or U-Depleted	1.18 ±0.26	Equilibrium
SS12	0.74 ± 0.10	Ra-Enriched or U-Depleted	1.06 ± 0.21	Equilibrium
SS13	1.19 ± 0.19	Equilibrium	1.01 ± 0.24	Equilibrium
SS14	0.91 ± 0.19	Equilibrium	1.14 ± 0.12	Equilibrium
SS15	1.03 ± 0.18	Equilibrium	1.06 ± 0.25	Equilibrium
SS16	1.41 ± 0.30	U-Enriched or Ra-Depleted	1.08 ± 0.18	Equilibrium
SS17	0.85 ± 0.13	Equilibrium	1.11 ± 0.22	Equilibrium
SS18	0.96 ± 0.13	Equilibrium	1.01 ± 0.21	Equilibrium
SS19	0.94 ± 0.13	Equilibrium	0.99 ± 0.14	Equilibrium
SS20	0.82 ± 0.32	Ra-Enriched or U-Depleted	0.92 ± 0.24	Equilibrium
SS21	1.20 ± 0.26	Equilibrium	1.02 ± 0.21	Equilibrium
SS22	1.07 ± 0.34	Equilibrium	0.98 ± 0.24	Equilibrium
SS23	1.43 ± 0.30	U-Enriched or Ra-Depleted	1.08 ± 0.10	Equilibrium
SS24	1.34 ± 0.37	Equilibrium	0.93 ± 0.24	Equilibrium
SS25	1.03 ± 0.19	Equilibrium	1.00 ± 0.19	Equilibrium

Table A6: Continued

Sample code	Activity Ratio			
	$^{238}U/^{226}Ra$	Remarks on ^{238}U-series	$^{228}Ra/^{228}Th$	Remarks on ^{232}Th-series
SS26	0.87 ± 0.14	Equilibrium	1.09 ± 0.24	Equilibrium
SS27	0.88 ± 0.17	Equilibrium	1.05 ± 0.25	Equilibrium
SS28	0.85 ± 0.18	Equilibrium	1.02 ± 0.15	Equilibrium
SS29	1.07 ± 0.20	Equilibrium	1.06 ± 0.21	Equilibrium
SS30	1.12 ± 0.17	Equilibrium	1.01 ± 0.26	Equilibrium
SS31	0.97 ± 0.13	Equilibrium	1.07 ± 0.14	Equilibrium
SS32	0.95 ± 0.25	Equilibrium	1.12 ± 0.18	Equilibrium
SS33	0.94 ± 0.16	Equilibrium	0.94 ± 0.25	Equilibrium
SS34	0.98 ± 0.18	Equilibrium	1.12 ± 0.22	Equilibrium
SS35	0.80 ± 0.17	Ra-Enriched or U-Depleted	1.06 ± 0.25	Equilibrium
SS36	1.02 ± 0.11	Equilibrium	1.05 ± 0.17	Equilibrium
SS37	0.69 ± 0.17	Ra-Enriched or U-Depleted	0.97 ± 0.22	Equilibrium
SS38	0.86 ± 0.31	Equilibrium	1.03 ± 0.27	Equilibrium
SS39	0.67 ± 0.35	Ra-Enriched or U-Depleted	0.95 ± 0.18	Equilibrium
SS40	0.83 ± 0.18	Ra-Enriched or U-Depleted	1.01 ± 0.17	Equilibrium
SS41	0.86 ± 0.34	Equilibrium	0.96 ± 0.19	Equilibrium
SS42	1.44 ± 0.28	U-Enriched or Ra-Depleted	0.97 ± 0.07	Equilibrium
SS43	1.12 ± 0.30	Equilibrium	1.03 ± 0.21	Equilibrium
SS44	0.85 ± 0.22	Equilibrium	1.03 ± 0.23	Equilibrium
SS45	0.81 ± 0.17	Ra-Enriched or U-Depleted	1.03 ± 0.15	Equilibrium
SS46	1.14 ± 0.20	Equilibrium	0.96 ± 0.20	Equilibrium
SS47	0.83 ± 0.29	Ra-Enriched or U-Depleted	0.97 ± 0.20	Equilibrium
SS48	1.59 ± 0.38	U-Enriched or Ra-Depleted	0.99 ± 0.17	Equilibrium
SS49	0.65 ± 0.18	Ra-Enriched or U-Depleted	1.03 ± 0.16	Equilibrium
SS50	1.13 ± 0.38	Equilibrium	0.99 ± 0.22	Equilibrium

Table A6: Continued

Sample code	Activity Ratio			
	$^{238}U/^{226}Ra$	Remarks on ^{238}U-series	$^{228}Ra/^{228}Th$	Remarks on ^{232}Th-series
SS51	1.10 ± 0.27	Equilibrium	1.01 ± 0.12	Equilibrium
SS52	1.42 ± 0.13	U-Enriched or Ra-Depleted	1.03 ± 0.15	Equilibrium
SS53	1.14 ± 0.29	Equilibrium	1.00 ± 0.17	Equilibrium
SS54	0.99 ± 0.31	Equilibrium	0.98 ± 0.15	Equilibrium
SS55	1.41 ± 0.27	U-Enriched or Ra-Depleted	0.95 ± 0.19	Equilibrium
SS56	1.04 ± 0.22	Equilibrium	1.00 ± 0.16	Equilibrium
SS57	0.90 ± 0.19	Equilibrium	0.99 ± 0.17	Equilibrium
SS58	0.82 ± 0.21	Ra-Enriched or U-Depleted	1.03 ± 0.18	Equilibrium
SS59	0.98 ± 0.21	Equilibrium	1.01 ± 0.17	Equilibrium
SS60	0.94 ± 0.19	Equilibrium	1.00 ± 0.15	Equilibrium
SS61	0.86 ± 0.23	Equilibrium	1.01 ± 0.25	Equilibrium
SS62	1.34 ± 0.19	U-Enriched or Ra-Depleted	1.04 ± 0.17	Equilibrium
SS63	0.78 ± 0.24	Ra-Enriched or U-Depleted	1.04 ± 0.07	Equilibrium
SS64	1.11 ± 0.29	Equilibrium	1.04 ± 0.14	Equilibrium
SS65	0.98 ± 0.20	Equilibrium	1.03 ± 0.21	Equilibrium
SS66	1.83 ± 0.30	U-Enriched or Ra-Depleted	1.01 ± 0.15	Equilibrium
SS67	1.17 ± 0.29	Equilibrium	0.98 ± 0.18	Equilibrium
SS68	0.99 ± 0.17	Equilibrium	0.99 ± 0.21	Equilibrium
SS69	1.14 ± 0.12	Equilibrium	1.03 ± 0.17	Equilibrium
SS70	1.32 ± 0.20	U-Enriched or Ra-Depleted	0.97 ± 0.18	Equilibrium
SS71	1.30 ± 0.40	U-Enriched or Ra-Depleted	0.98 ± 0.17	Equilibrium
SS72	1.51 ± 0.29	U-Enriched or Ra-Depleted	1.01 ± 0.19	Equilibrium
SS73	1.27 ± 0.28	U-Enriched or Ra-Depleted	1.04 ± 0.15	Equilibrium
Min	**0.65 ± 0.18**		**0.92 ± 0.24**	
Max	**1.59 0.38**		**1.18 ± 0.30**	
Average	**1.03 ± 0.03**	**Equilibrium**	**1.02 ± 0.01**	**Equilibrium**

Table A7: Calculated Ra_{eq}, D_R, AEDE, H_{ex} and H_{in} of soil samples

Sample code	D_R (nGy/h)	Ra_{eq} (Bq/kg)	H_{ex}	AEDE (mSv/y)
SS01	59.6 ± 3.2	128 ± 8	0.34 ± 0.02	0.07 ± 0.004
SS02	65.9 ± 3.1	145 ± 7	0.39 ± 0.02	0.08 ± 0.004
SS03	23.6 ± 1.1	50.6 ± 2.7	0.14 ± 0.01	0.03 ± 0.001
SS04	67.4 ± 2.9	146 ± 7	0.40 ± 0.02	0.08 ± 0.004
SS05	79.1 ± 3.0	173 ± 7	0.47 ± 0.02	0.10 ± 0.004
SS06	91.6 ± 5.7	201 ± 14	0.54 ± 0.04	0.11 ± 0.007
SS07	23.5 ± 1.2	49.6 ± 2.8	0.13 ± 0.01	0.03 ± 0.001
SS08	28.4 ± 1.6	60.1 ± 3.9	0.16 ± 0.01	0.03 ± 0.002
SS09	31.6 ± 2.1	70.0 ± 5.1	0.18 ± 0.01	0.04 ± 0.003
SS10	41.6 ± 2.3	91.9 ± 5.5	0.25 ± 0.02	0.05 ± 0.003
SS11	55.7 ± 3.7	121 ± 9	0.33 ± 0.02	0.07 ± 0.005
SS12	83.1 ± 4.2	179 ± 10	0.48 ± 0.03	0.10 ± 0.005
SS13	60.4 ± 4.1	130 ± 10	0.35 ± 0.03	0.07 ± 0.005
SS14	46.6 ± 2.1	101 ± 5	0.27 ± 0.01	0.06 ± 0.003
SS15	51.4 ± 3.9	112 ± 9	0.30 ± 0.03	0.06 ± 0.005
SS16	31.6 ± 1.7	67.9 ± 3.9	0.18 ± 0.01	0.04 ± 0.002
SS17	55.3 ± 3.2	121 ± 7	0.33 ± 0.02	0.07 ± 0.004
SS18	56.7 ± 3.5	125 ± 8	0.34 ± 0.02	0.07 ± 0.004
SS19	55.4 ± 2.4	122 ± 6	0.33 ± 0.02	0.07 ± 0.003
SS20	30.3 ± 2.2	64.4 ± 5.2	0.17 ± 0.01	0.04 ± 0.003
SS21	38.9 ± 1.8	82.2 ± 4.3	0.22 ± 0.01	0.05 ± 0.002
SS22	32.1 ± 1.9	67.9 ± 4.4	0.18 ± 0.01	0.04 ± 0.002
SS23	37.0 ± 1.0	78.1 ± 2.3	0.21 ± 0.01	0.05 ± 0.001
SS24	36.1 ± 2.1	74.7 ± 4.9	0.20 ± 0.01	0.04 ± 0.003
SS25	49.0 ± 2.6	107 ± 6	0.29 ± 0.02	0.06 ± 0.003
SS26	61.5 ± 3.8	134 ± 9	0.36 ± 0.02	0.08 ± 0.005
SS27	42.2 ± 3.3	92.1 ± 7.7	0.25 ± 0.02	0.05 ± 0.004
SS28	43.5 ± 1.8	94.6 ± 4.2	0.26 ± 0.01	0.05 ± 0.002

Table A7: Continued

Sample code	D_R (nGy/h)	Ra_{eq} (Bq/kg)	H_{ex}	AEDE (mSv/y)
SS29	45.5 ± 3.3	101 ± 8	0.27 ± 0.02	0.06 ± 0.004
SS30	65.5 ± 3.8	139 ± 9	0.37 ± 0.02	0.08 ± 0.005
SS31	76.7 ± 2.8	164 ± 7	0.44 ± 0.02	0.09 ± 0.003
SS32	47.5 ± 1.6	97.6 ± 3.7	0.26 ± 0.01	0.06 ± 0.002
SS33	64.4 ± 3.9	136 ± 9	0.37 ± 0.03	0.08 ± 0.005
SS34	63.4 ± 3.4	133 ± 8	0.36 ± 0.02	0.08 ± 0.004
SS35	59.7 ± 3.5	126 ± 8	0.34 ± 0.02	0.07 ± 0.004
SS36	103 ± 4	224 ± 11	0.60 ± 0.03	0.13 ± 0.006
SS37	60.1 ± 2.8	125 ± 7	0.34 ± 0.02	0.07 ± 0.003
SS38	45.6 ± 2.2	93.1 ± 5.3	0.25 ± 0.01	0.06 ± 0.003
SS39	85.3 ± 5.5	183 ± 13	0.49 ± 0.04	0.10 ± 0.007
SS40	76.6 ± 3.6	164 ± 9	0.44 ± 0.02	0.09 ± 0.004
SS41	69.2 ± 3.7	145 ± 9	0.39 ± 0.02	0.09 ± 0.005
SS42	41.7 ± 0.9	88 ± 2.2	0.24 ± 0.01	0.05 ± 0.001
SS43	63.6 ± 3.2	132 ± 8	0.36 ± 0.02	0.08 ± 0.004
SS44	84.5 ± 4.9	179 ± 12	0.48 ± 0.03	0.10 ± 0.006
SS45	89.7 ± 4.1	194 ± 10	0.52 ± 0.03	0.11 ± 0.005
SS46	87.9 ± 5.7	189 ± 13	0.51 ± 0.04	0.11 ± 0.007
SS47	55.2 ± 2.4	114 ± 6	0.31 ± 0.02	0.07 ± 0.003
SS48	103 ± 6	222 ± 15	0.60 ± 0.04	0.13 ± 0.008
SS49	80.0 ± 3.3	171 ± 8	0.46 ± 0.02	0.10 ± 0.004
SS50	32.3 ± 2.1	69.9 ± 5.1	0.19 ± 0.01	0.04 ± 0.003
SS51	81.3 ± 2.9	173 ± 7	0.47 ± 0.02	0.10 ± 0.004
SS52	65.8 ± 2.3	139 ± 6	0.37 ± 0.02	0.08 ± 0.003
SS53	19.5 ± 0.9	41.0 ± 2.1	0.11 ± 0.01	0.02 ± 0.001
SS54	89.8 ± 4.5	193 ± 11	0.52 ± 0.03	0.11 ± 0.005
SS55	46.7 ± 4.2	109 ± 10	0.29 ± 0.03	0.06 ± 0.005
SS56	73.4 ± 3.4	157 ± 8	0.42 ± 0.02	0.09 ± 0.004

Table A7: Continued

Sample code	D_R (nGy/h)	Ra_{eq} (Bq/kg)	H_{ex}	AEDE (mSv/y)
SS57	88.2 ± 4.4	190 ± 11	0.51 ± 0.03	0.11 ± 0.005
SS58	76.8 ± 3.5	163 ± 8	0.44 ± 0.02	0.09 ± 0.004
SS59	79.9 ± 3.5	169 ± 8	0.46 ± 0.02	0.10 ± 0.004
SS60	86.5 ± 3.8	186 ± 9	0.50 ± 0.02	0.11 ± 0.005
SS61	69.9 ± 4.3	148 ± 10	0.40 ± 0.03	0.09 ± 0.005
SS62	80.5 ± 3.8	172 ± 9	0.46 ± 0.02	0.10 ± 0.005
SS63	66.5 ± 1.5	141 ± 3	0.38 ± 0.01	0.08 ± 0.002
SS64	65.5 ± 2.5	138 ± 6	0.37 ± 0.02	0.08 ± 0.003
SS65	72.0 ± 4.1	154 ± 10	0.42 ± 0.03	0.09 ± 0.005
SS66	69.3 ± 2.7	146 ± 6	0.39 ± 0.02	0.09 ± 0.003
SS67	62.4 ± 3.0	131 ± 7	0.35 ± 0.02	0.08 ± 0.004
SS68	41.2 ± 3.3	94.2 ± 7.8	0.25 ± 0.02	0.05 ± 0.004
SS69	82.6 ± 5.2	188 ± 12	0.51 ± 0.03	0.10 ± 0.006
SS70	92.0 ± 5.5	199 ± 13	0.54 ± 0.04	0.11 ± 0.007
SS71	91.5 ± 5.2	198 ± 12	0.54 ± 0.03	0.11 ± 0.006
SS72	78.0 ± 4.3	167 ± 10	0.45 ± 0.03	0.10 ± 0.005
SS73	70.3 ± 2.7	148 ± 6	0.40 ± 0.02	0.09 ± 0.003
average	**62.2 ± 2.4**	**133 ± 5**	**0.36 ± 0.02**	**0.08 ± 0.003**
World average	**59**	**370**	**<1**	**0.48**

Annexure B: Concentrations of heavy metals in soil, water, food and dust samples.

Table B1: Concentration of metals in sediments samples

Sediment Code	Metal concentration (mg/kg)															
	Co	**Cr**	**Cu**	**Fe**	**Mg**	**Mn**	**Mo**	**Na**	**Se**	**Zn**	**As**	**Cd**	**K**	**Pb**	**Th**	**U**
SED01	11.8	99.0	35.3	16540	4579	163	1.1	121	1.4	23.4	1.4	0.5	47198	12.5	20.7	1.8
SED02	7.9	78.4	20.5	9410	2437	121	1.0	81.7	1.2	11.9	1.1	0.7	23570	9.2	16.3	1.3
SED03	5.5	62.0	16.6	6748	1620	82.3	1.1	94.0	1.2	9.8	1.2	0.6	18906	9.4	14.4	1.7
SED04	10.9	71.7	30.4	17870	4259	189.3	0.2	107	0.7	28.0	0.9	0.1	57729	10.2	17.2	3.2
SED05	17.4	42.8	10.1	5789	2265	135	3.0	221	0.3	9.0	0.8	0.1	21062	2.0	5.6	1.8
SED06	12.6	52.1	10.0	6405	2083	113	1.3	155	0.1	6.3	0.7	0.1	17016	4.7	5.5	1.8
SED07	11.5	61.5	13.9	8827	3044	188	1.2	155	0.5	7.6	0.4	0.2	41969	8.0	7.5	2.2
SED08	6.5	108	23.8	15980	4118	301	1.5	1112	0.4	13.4	0.8	0.4	38850	16.1	16.0	4.2
SED09	10.1	91.4	17.3	12411	2579	234	1.6	234	0.3	11.8	1.2	0.23	30707	13.2	13.3	3.1
SED10	3.7	63.0	14.6	6209	1019	70.1	0.7	71.7	0.5	6.8	0.8	0.5	15938	5.9	12.1	2.5
SED11	4.2	64.1	14.2	8191	1857	101	0.7	77.6	0.5	9.8	0.8	0.5	21023	6.1	9.2	2.1
SED12	3.4	55.7	13.4	5066	1182	53.0	1.0	60.4	1.0	7.4	1.0	0.6	12375	6.1	8.8	1.8
SED13	2.5	58.5	13.2	4875	803	57.7	0.7	64.9	0.4	5.1	0.6	0.5	11953	4.7	7.4	1.5
SED14	6.1	61.8	17.8	7440	1456	153.	0.7	81.1	0.6	13.1	0.8	0.5	20226	8.0	11.9	2.1
SED15	3.8	60.1	15.2	6284	1004	93.5	0.8	84.9	0.5	7.0	0.7	0.5	15568	5.9	9.6	1.7
SED16	6.6	64.0	20.1	7823	1675	115	1.1	87.3	1.3	11.9	1.3	0.7	21100	10.6	11.3	3.2
SED17	5.8	58.2	20.8	7291	1486	102	1.0	179	1.1	11.4	1.2	0.6	17133	9.9	12.5	2.9

Table B2: Concentration of metals in soil samples

Soil Code	Metal concentration (mg/kg)															
	Co	**Cr**	**Cu**	**Fe**	**Mg**	**Mn**	**Mo**	**Na**	**Se**	**Zn**	**As**	**Cd**	**K**	**Pb**	**Th**	**U**
SS01	7.0	52.3	20.3	7524	1807	136	1.0	63.1	1.1	12.4	1.6	0.7	15302	10.6	10.4	3.4
SS02	8.6	81.1	26.1	10870	2509	180	0.9	52.7	1.4	29.7	4.9	0.7	36590	17.8	13.7	3.7
SS03	4.0	57.9	9.3	4858	377	69.8	1.0	31.1	1.0	5.3	1.3	0.7	7814	6.0	4.1	0.8
SS04	12.8	94.3	60.8	13140	2373	181	1.3	67.4	1.4	13.2	1.6	0.7	25590	13.6	15.4	2.1
SS05	10.6	91.9	35.4	11600	2224	175	1.2	105	1.3	16.9	2.7	0.7	20010	18.1	15.5	5.9
SS06	21.7	80.7	72.4	28980	1471	391	1.8	132	1.8	21.7	2.9	0.7	23149	13.5	13.4	5.1
SS07	5.5	52.1	12.4	5125	1018	90.6	1.2	41.6	1.1	8.6	1.5	0.7	21231	6.6	4.5	1.3
SS08	6.5	68.5	23.8	8377	2427	124	1.0	51.0	1.2	11.1	1.3	0.7	21507	6.7	4.5	1.3
SS09	4.5	63.5	11.0	6605	1393	99.0	1.2	67.4	1.1	9.9	1.8	0.7	29877	8.1	5.6	1.0
SS10	7.3	71.4	28.9	8562	1206	176	1.1	45.3	1.3	14.2	3.5	0.7	22015	17.4	11.3	2.1
SS11	7.8	89.7	23.8	10950	2314	116	1.5	62.2	1.4	14.6	4.0	0.7	23396	13.5	10.1	2.6
SS12	13.5	113	30.2	13590	3255	263	1.5	125.4	1.4	18.3	2.5	0.7	28598	16.7	15.1	4.8
SS13	6.8	63.4	17.1	6527	1335	122	1.1	53.7	1.2	10.9	1.6	0.7	14274	10.5	9.1	3.1
SS14	3.7	65.0	12.9	5439	1001	77.7	0.9	176	0.5	9.8	1.9	0.5	18972	7.5	7.5	2.4
SS15	5.0	64.4	5.0	6488	1509	125	0.9	66.7	0.7	11.5	2.2	0.5	27647	9.7	9.7	3.0
SS16	2.8	46.5	8.4	3080	1920	112	0.4	98.5	0.1	51.2	1.2	0.2	6565	15.1	3.6	1.2
SS17	28.8	86.4	28.8	60750	1278	988	1.7	53.6	1.0	23.3	2.0	0.6	17292	21.2	7.8	5.1

Table B2: Continued

Soil Code	Metal concentration (mg/kg)															
	Co	**Cr**	**Cu**	**Fe**	**Mg**	**Mn**	**Mo**	**Na**	**Se**	**Zn**	**As**	**Cd**	**K**	**Pb**	**Th**	**U**
SS18	1.2	105	13.7	6571	1399	185	0.5	59.4	0.02	45.5	9.4	0.6	5606	56.1	28.8	2.6
SS19	9.2	76.9	21.3	9633	553	177	1.7	34.1	1.20	15.8	4.0	0.7	11326	15.7	9.8	2.4
SS20	0.3	65.0	9.7	5334	1037	122	0.6	73.8	0.04	26.9	0.8	0.3	10678	0.3	4.8	0.8
SS21	0.3	78.8	21.5	8160	2498	262	0.5	92.6	0.01	43.5	0.6	0.5	27726	17.4	6.1	2.6
SS22	1.3	64.7	14.0	6440	1966	170	0.1	55.6	0.06	27.0	0.2	0.3	13250	12.4	5.2	1.9
SS23	2.2	289	24.6	8018	3149	265	1.1	190	0.03	83.7	0.2	0.4	16712	4.9	5.7	2.9
SS24	5.4	42.7	8.1	4703	1053	72.3	19.3	30.5	1.20	2.8	0.8	0.3	13310	26.5	3.3	1.2
SS25	7.3	103	19.6	16607	220	283	3.0	163	0.10	11.8	3.7	0.9	14269	99.0	14.7	4.3
SS26	6.8	92.8	25.9	12831	3411	277	1.6	271	0.03	20.5	3.7	0.8	21188	11.1	11.5	4.1
SS27	6.8	91.3	20.3	12544	2285	234	1.4	195	0.01	16.9	1.1	0.6	7794	50.5	11.0	3.6
SS28	1.9	76.0	18.4	6965	2593	191	0.5	223	0.01	16.3	1.5	0.4	13708	3.3	4.9	2.7
SS29	7.8	119	7.8	8266	829	266	1.0	50.7	0.80	8.1	2.9	0.5	15611	12.7	10.1	1.6
SS30	9.7	87.0	17.1	7932	2451	178	0.6	190	0.07	11.4	1.0	0.4	17010	6.8	8.0	2.5
SS31	3.8	102	17.0	10618	2081	202	0.5	102	0.03	10.2	0.5	0.6	16563	25.1	9.0	2.9
SS32	2.8	80.8	2.8	3983	624	34.3	0.9	35.3	0.30	4.0	0.6	0.5	8542	4.0	4.6	1.4
SS33	1.1	100	14.0	7482	1895	149	0.7	113	0.04	28.6	1.3	0.4	13563	7.8	8.8	2.4
SS34	5.9	68.0	15.6	7313	1386	123	1.0	49.9	0.50	7.8	1.3	0.5	16494	6.8	8.8	2.5

Table B2: Continued

Soil Code	Metal concentration (mg/kg)														
	Co	**Cr**	**Cu**	**Fe**	**Mg**	**Mn**	**Mo**	**Na**	**Se**	**Zn**	**As**	**Cd**	**K**	**Pb**	**Th**	**U**
SS35	5.8	70.4	17.1	7577	1434	127	0.9	51.0	0.4	8.6	1.2	0.5	17462	6.9	8.7	2.6
SS36	6.3	67.5	16.8	7033	1353	147	0.8	237	0.4	8.3	1.1	0.5	17477	6.9	8.4	2.5
SS37	0.2	104	18.2	11924	3201	288	1.1	224	0.1	115	1.0	0.7	35246	18.7	10.7	4.1
SS38	5.4	81.4	14.1	6333	1658	101	1.0	39.6	1.0	8.4	1.1	0.7	14495	8.4	6.0	1.5
SS39	10.8	67.0	19.2	13630	2782	210	1.0	215	1.4	17.5	1.3	0.6	18833	16.1	28.5	1.2
SS40	10.1	84.9	23.1	13160	3710	202	1.2	3056	1.4	20.6	1.7	0.7	33684	13.5	15.3	3.0
SS41	7.0	70.4	19.7	8644	1624	166	1.1	72.7	1.4	12.3	1.2	0.7	22262	12.5	17.0	0.9
SS42	7.1	80.3	16.8	11980	4025	162	0.9	66.9	1.3	14.9	1.3	0.7	32710	10.4	10.6	1.6
SS43	30.1	79.7	24.6	24435	3143	274	14.9	261	0.7	23.8	5.5	1.1	35569	105	29.0	5.6
SS44	22.4	73.0	26.6	12718	4330	257	2.1	407	0.3	28.1	2.3	0.7	18509	6.3	11.4	4.6
SS45	18.8	82.6	26.0	12531	4226	193	1.1	554	0.2	24.1	1.7	0.6	20990	17.1	13.3	4.2
SS46	14.3	72.9	20.2	10881	3181	199	0.9	280	0.3	21.5	1.2	0.6	21006	11.3	9.1	3.4
SS47	20.2	54.6	14.6	6088	2170	134	0.9	248	0.1	20.5	1.2	0.4	11441	1.7	5.6	2.0
SS48	22.9	61.9	15.9	14197	2640	221	0.9	280	0.3	22.5	0.9	0.7	13932	23.5	15.2	4.0
SS49	6.2	80.4	20.8	12840	3400	133	0.9	2114	0.8	17.9	1.2	0.5	40295	8.6	12.3	1.8
SS50	21.3	51.1	17.5	6107	4050	134	1.4	355	0.1	27.2	1.5	0.4	9862	12.4	4.2	2.8
SS51	21.7	55.6	17.4	8620	2615	162	0.7	341	0.2	20.8	1.1	0.5	12539	1.3	9.1	2.8

Table B2: Continued

Soil Code	Metal concentration (mg/kg)															
	Co	**Cr**	**Cu**	**Fe**	**Mg**	**Mn**	**Mo**	**Na**	**Se**	**Zn**	**As**	**Cd**	**K**	**Pb**	**Th**	**U**
SS52	17.8	55.5	16.5	7539	2956	135	0.8	351	0.2	24.7	1.1	0.4	14560	27.1	6.3	2.4
SS53	0.4	73.7	16.5	9422	2780	193	1.4	193	0.1	138	0.9	0.5	10171	23.0	11.6	3.4
SS54	3.5	112	13.0	8246	1765	244	0.3	48.6	0.1	22.9	0.749	0.4	28731	14.4	12.3	2.2
SS55	19.1	68.2	21.2	8614	4117	178	0.9	360	0.2	27.8	1.449	0.5	23337	43.1	6.1	3.2
SS56	8.0	76.3	8.0	10980	2356	204	1.0	130	0.9	14.0	1.3	0.5	34455	10.12	14.7	2.6
SS57	8.2	84.4	8.2	14000	4451	214	0.8	5621	1.0	19.0	1.4	0.5	50265	10.2	17.5	2.2
SS58	5.9	65.7	5.9	6771	1517	152	0.9	122	0.6	7.4	1.0	0.5	17434	8.1	16.5	2.2
SS59	9.0	74.23	9.0	9411	1962	217	1.0	92.3	0.8	12.9	1.1	0.5	24898	10.0	15.9	3.4
SS60	29.2	48.9	15.1	6320	2603	153	0.8	283	0.1	20.2	1.1	0.4	11654	17.5	4.5	2.3
SS61	19.7	76.0	24.5	10543	2459	197	0.7	287	0.3	24.6	1.4	0.6	16453	3.9	10.5	3.3
SS62	10.5	83.0	10.5	12300	2904	237	0.8	330	0.8	16.0	1.6	0.5	29598	12.3	17.7	4.4
SS63	16.2	74.4	10.6	11768	2291	1237	0.5	190	0.3	9.9	0.9	0.6	20212	17.2	12.4	2.9
SS64	22.4	69.8	24.0	9286	2776	212	0.7	286	0.3	28.4	1.2	0.5	26733	3.8	7.5	3.1
SS65	3.8	90.2	14.7	8810	2152	136	1.1	197	1.2	26.7	1.3	0.5	12325	14.5	11.9	2.9
SS66	10.2	89.6	10.2	12660	3459	235	1.1	95.8	0.8	19.4	1.5	0.5	42773	11.8	14.6	3.2
SS67	0.1	97.8	14.8	9361	2108	190	2.5	115	0.1	25.4	1.4	0.5	22770	15.0	11.5	2.7

Table B2: Continued

Soil Code	Metal concentration (mg/kg)															
	Co	**Cr**	**Cu**	**Fe**	**Mg**	**Mn**	**Mo**	**Na**	**Se**	**Zn**	**As**	**Cd**	**K**	**Pb**	**Th**	**U**
SS68	0.5	130	28.4	13563	1822	319	1.2	77.6	0.1	24.9	1.8	0.7	22953	59.0	16.7	3.6
SS69	5.3	97.2	14.3	5542	2382	87.4	1.2	208	0.1	68.1	0.7	0.3	7669	11.1	6.2	2.3
SS70	21.1	102	22.1	14777	3900	300	0.9	379	0.1	15.8	0.9	0.3	29265	17.4	11.6	4.2
SS71	24.3	69.4	15.3	9208	3251	161	0.9	433	0.2	14.0	1.4	0.2	24087	13.3	9.2	2.5
SS72	13.6	109	24.4	15058	3025	277	0.9	247	0.7	18.0	1.1	0.3	26899	16.1	15.9	3.8
SS73	17.0	79.0	19.3	11255	3443	193	1.1	349	0.1	20.3	0.9	0.3	12998	13.6	11.4	3.4

Table B3: Concentration of metals in water samples

Water Code	Metal concentration (mg/*l*) ($\times 10^{-4}$)															
	Co	**Cr**	**Cu**	**Fe**	**Mg**	**Mn**	**Mo**	**Na**	**Se**	**Zn**	**As**	**Cd**	**K**	**Pb**	**Th**	**U**
WS01	< 0.1	< 8.9	2420	18840	13200	14990	< 0.2	10630	< 1.1	1691	< 1.2	109	1964000	457	< 0.1	13.1
WS02	8.3	95.4	829	7021	56320	745	0.9	48660	1.2	384	7.8	7.9	87200	45.7	< 0.1	2.9
WS03	1.9	532	547	12530	49760	607	1.8	32790	4.6	759	8.0	7.9	140000	42.8	< 0.1	1.5
WS04	6.2	125	179	5742	90690	1248	39.4	34990	74.5	255	107	7.5	178100	22.1	< 0.1	83.5
WS05	< 0.1	< 8.9	7612	10610	33690	4075	138	20770	3226	38010	249	116	1338000	< 1.3	< 0.1	< 0.1
WS06	0.2	182	296	8216	37580	985	22.0	< 143	227	344	9.7	10.1	150500	28.2	< 0.1	3.1
WS07	< 0.1	209	220	10660	17110	653	8.5	< 143	205	190	5.5	6.0	100700	16.1	< 0.1	4.6
WS08	< 0.1	< 8.9	4507	43080	12520	66530	< 0.2	54910	< 1.1	< 22.5	< 1.2	< 0.3	1830000	136	< 0.1	< 0.1
WS09	61.9	< 8.9	9227	28020	15250	35710	< 0.2	12200	< 1.1	3240	< 1.2	163	2188000	1014	< 0.1	39.4
WS10	42.0	214	192	57450	53160	2448	< 0.2	44330	1.9	824	10.4	< 0.3	80100	59.6	0.4	3.3
WS11	16.2	185	139	37760	40760	1019	< 0.2	31500	1.9	233	5.7	< 0.3	68460	38.3	< 0.1	2.2
WS12	57.0	217	485	62210	58010	3105	< 0.2	34450	5.5	308	8.9	0.5	80000	78.7	< 0.1	4.5
WS13	< 0.1	< 8.9	1593	23230	24230	12150	547	< 143	1383	2228	1148	< 0.3	4252000	40.6	< 0.1	< 0.1
WS14	< 0.1	110	65.2	242.4	914	78.4	< 0.2	16180	< 1.1	19870	1.7	0.7	7394	10.6	< 0.1	< 0.1
WS15	81.1	135	138	17770	72090	15300	< 0.2	36330	11.1	203	10.0	0.5	241100	36.8	< 0.1	2.9
WS16	< 0.1	< 8.9	8714	26480	98520	27430	279	32000	1016	749.8	< 1.2	< 0.3	4270000	< 1.3	< 0.1	< 0.1
WS17	8.2	111	50.8	1481	47340	2115	3.6	22140	< 1.1	112	11.2	< 0.3	70410	14.0	< 0.1	1.1

Table B3: Continued

Water Code	Metal concentration (mg/*l*)															
	Co	**Cr**	**Cu**	**Fe**	**Mg**	**Mn**	**Mo**	**Na**	**Se**	**Zn**	**As**	**Cd**	**K**	**Pb**	**Th**	**U**
WS18	8.0	114	119	8224	46900	2599	1.6	20300	2.6	250	7.7	< 0.3	79950	14.0	< 0.1	1.1
WS19	2.2	106	127	2850	85720	1790	< 0.2	18310	3.4	135	5.4	< 0.3	174000	25.0	< 0.1	1.6
WS20	2.9	116	194	3361	10310	1616	4.9	47140	1.2	525	12.7	< 0.3	72730	13.7	< 0.1	0.3
WS21	422	286	347	17110	87410	36650	< 0.2	7405	5.8	636	37.6	0.9	193500	12.9	< 0.1	13.9
WS22	< 0.1	189	233	6767	88030	382	33.6	< 143	297	232	54.7	0.4	138400	650	< 0.1	3.4
WS23	< 0.1	214	372	690	14420	46.52	32.9	< 143	192	131	6.2	0.3	104000	8.8	< 0.1	297
WS24	51.7	262	272	70370	49880	3105	< 0.2	38520	8.5	1245	41.2	1.6	348900	13.0	< 0.1	6.1
WS25	< 0.1	215	295	7418	34420	816	21.4	< 143	173	207.2	7.7	< 0.3	138800	82.3	< 0.1	0.5
WS26	23.3	215	143	37270	52200	1238	< 0.2	45690	5.5	202.7	8.4	< 0.3	73810	11.0	< 0.1	1.3
WS27	22.9	196	162	32660	50790	1253	< 0.2	43580	< 1.1	215	7.4	< 0.3	75270	37.0	< 0.1	3.9
WS28	26.9	168	185	17150	36450	2678	< 0.2	32250	< 1.1	928	7.4	0.8	83810	38.6	< 0.1	4.1
WS29	< 0.1	155	533	877	42230	19.9	3.5	28490	13.6	309	11.1	< 0.3	36440	24.0	< 0.1	0.1
WS30	< 0.1	146	108	1935	52770	540	19.7	15510	15.5	416	30.6	< 0.3	35990	16.3	< 0.1	68.9
WS31	< 0.1	172	108	804	38900	20.9	116	37860	22.3	750	212	0.04	47120	16.1	< 0.1	235
WS32	7.7	204	113	3440	11170	2847	47.0	33760	88.6	416	13.8	< 0.3	174600	24.3	< 0.1	9.0
WS33	< 0.1	167	117	938.3	35630	281	15.0	13850	10.2	2088	26.9	< 0.3	54110	15.4	< 0.1	972
WS34	1.2	300	365	7475	81720	533	32.2	< 143	284	859	54.8	0.8	132500	41.4	< 0.1	287

Table B3: Continued

Water Code	Metal concentration (mg/*l*)															
	Co	**Cr**	**Cu**	**Fe**	**Mg**	**Mn**	**Mo**	**Na**	**Se**	**Zn**	**As**	**Cd**	**K**	**Pb**	**Th**	**U**
WS35	< 0.1	272	214	2176	154900	569	26.3	< 143	197	261	6.0	0.4	98260	12.7	< 0.1	7.1
WS36	< 0.1	272	212	4931	375800	974	23.8	< 143	192	2320	9.2	0.3	148900	13.6	< 0.1	1.6

Table B4: Concentration of metals in food samples

Food Code	Metal concentration (mg/kg)															
	Co	**Cr**	**Cu**	**Fe**	**Mg**	**Mn**	**Mo**	**Na**	**Se**	**Zn**	**As**	**Cd**	**K**	**Pb**	**Th**	**U**
F1	0.3	38.1	1.6	43.7	1201	1.0	0.6	2899	1.4	7.8	0.1	0.1	4452	0.3	0.0	0.0
F2	0.3	43.9	2.8	44.6	1312	1.7	0.7	3171	1.5	14.1	0.2	0.1	4291	0.4	0.0	0.0
F3	0.3	42.3	1.3	48.2	1393	1.6	0.6	3017	1.6	8.0	0.2	0.1	4403	0.4	0.0	0.0
F4	0.6	39.5	3.4	60.7	1463	22.2	0.6	2874	0.9	11.6	0.5	0.1	2538	0.6	0.0	0.1
Spinach	0.5	29.3	11.1	116	12540	52.1	0.9	2736	0.7	6.0	0.1	0.1	15600	0.3	0.0	0.1
Rape	0.6	45.9	6.9	91.8	9831	46.0	1.7	6388	1.5	10.0	0.2	0.2	11620	0.3	0.0	0.1
Choumullier	0.7	43.3	3.8	178	7666	23.8	4.3	2528	0.6	7.6	0.2	0.1	18110	0.4	0.1	0.0
Beef liver	0.5	41.1	183.0	162.2	876	5.2	3.6	5947	1.2	40.5	0.1	0.1	3712	0.5	0.0	0.0

Table B5: Concentration of metals in dust samples

Dust Code	**Metal concentration (mg/kg)**														
	Co	**Cr**	**Cu**	**Fe**	**Mg**	**Mn**	**Mo**	**Na**	**Se**	**Zn**	**As**	**Cd**	**K**	**Pb**	**Th**	**U**
D1	1.5	21.0	13.8	3368	1210	45.0	1.1	459	0.5	124	1.3	0.05	57.3	2.5	3.1	0.5
D2	3.1	43.1	43.2	3555	4683	57.7	2.1	429	0.9	86.5	1.2	0.2	636	16.1	3.2	0.5
D3	3.5	37.6	11.5	3735	8530	73.3	2.5	822	0.7	139	3.4	0.16	324	13.8	2.7	0.5
D4	2.5	37.5	22.3	1942	30510	43.4	1.4	157	0.7	135	0.5	0.11	32.1	5.3	2.9	0.4
D5	3.4	37.0	54.3	3493	4609	50.0	0.8	118	0.7	116	0.8	0.13	174	16.7	3.5	0.4

Annexure C: Comparison between γ-spectroscopy and ICP-MS in soil samples.

Table C1: Comparison between γ-spectroscopy and ICP-MS methods for the measurement of ^{238}U concentration (Bq/kg) in soil samples.

Sample code	^{238}U by γ-spec	^{238}U by ICP-MS	Ratio	Sample code	^{238}U by γ-spec	^{238}U by ICP-MS	Ratio
SS01	30.6	38.1	0.8	SS28	25.8	32.1	0.8
SS02	46.6	45.8	1.0	SS29	31.9	19.5	1.6
SS03	12.3	10.1	1.2	SS30	39.8	29.9	1.3
SS04	29.1	25.9	1.1	SS31	46.6	34.4	1.4
SS05	48.5	72.6	0.7	SS32	18.8	16.8	1.1
SS06	76.8	63.5	1.2	SS33	35.2	29.0	1.2
SS07	10.3	15.7	0.7	SS34	33.9	30.3	1.1
SS08	10.8	15.5	0.7	SS29	28.1	31.2	0.9
SS09	15.2	12.8	1.2	SS30	91.9	30.4	3.0
SS10	32.6	25.6	1.3	SS31	22.8	19.9	1.2
SS11	36.8	32.3	1.1	SS32	12.0	18.9	0.6
SS12	49.1	59.8	0.8	SS33	11.8	15.1	0.8
SS13	38.5	37.8	1.0	SS34	33.5	36.5	0.9
SS14	26.9	28.6	0.9	SS35	13.5	10.6	1.3
SS15	31.4	36.1	0.9	SS36	23.2	19.7	1.2
SS16	20.3	14.1	1.4	SS37	20.6	27.3	0.8
SS17	43.8	61.3	0.7	SS38	28.4	55.0	0.5
SS18	46.5	30.7	1.5	SS39	31.9	50.7	0.6
SS19	40.8	29.3	1.4	SS40	40.9	40.7	1.0
SS20	11.6	22.8	0.5	SS41	15.8	23.5	0.7
SS21	24.4	31.1	0.8	SS42	32.5	47.4	0.7
SS22	15.2	22.9	0.7	SS43	25.8	32.1	0.8
SS23	23.5	34.8	0.7	SS44	31.9	19.5	1.6
SS24	16.5	14.6	1.1	SS45	39.8	29.9	1.3
SS25	30.7	51.7	0.6	SS46	46.6	34.4	1.4
SS26	42.8	48.9	0.9	SS47	18.8	16.8	1.1
SS27	25.3	43.4	0.6	SS48	35.2	29.0	1.2

Table C1: Continued

Sample code	^{238}U by γ-spec	^{238}U by ICP-MS	Ratio
SS49	26.4	21.0	1.3
SS50	15.1	33.3	0.5
SS51	28.1	33.8	0.8
SS52	30.1	29.1	1.0
SS53	4.4	40.6	0.1
SS54	21.7	26.2	0.8
SS55	38.1	38.8	1.0
SS56	31.8	30.6	1.0
SS57	37.2	26.5	1.4
SS58	26.0	26.0	1.0
SS59	33.5	40.5	0.8
SS60	35.1	28.0	1.3
SS61	22.8	39.2	0.6
SS62	51.3	52.1	1.0
SS63	19.6	35.0	0.6
SS64	22.3	36.9	0.6
SS65	34.8	34.9	1.0
SS66	35.4	37.6	0.9
SS67	24.4	32.0	0.8
SS68	35.3	43.6	0.8
SS69	86.3	27.7	3.1
SS70	48.1	50.5	1.0
SS71	37.0	30.1	1.2
SS72	35.2	45.8	0.8
SS73	27.6	40.4	0.7

Table C2: Comparison between γ-spectroscopy and ICP-MS methods for the measurement of ^{232}Th concentration (Bq/kg) in soil samples.

Sample code	^{232}Th by γ-spec	^{232}Th by ICP-MS	Ratio	Sample code	^{232}Th by γ-spec	^{232}Th by ICP-MS	Ratio
SS01	41.2	42.7	1.0	SS28	31.2	20.1	1.6
SS02	46.4	56.3	0.8	SS29	38.3	41.3	0.9
SS03	16.4	16.7	1.0	SS30	38.7	32.5	1.2
SS04	53.1	63.3	0.8	SS31	47.8	36.7	1.3
SS05	53.4	63.7	0.8	SS32	22.4	18.6	1.2
SS06	48.3	55.1	0.9	SS33	36.2	35.9	1.0
SS07	14.2	18.5	0.8	SS34	35.9	36.1	1.0
SS08	18.1	18.3	1.0	SS29	34.4	35.6	1.0
SS09	21.2	23.0	0.9	SS30	63.4	34.1	1.9
SS10	34.5	46.6	0.7	SS31	29.8	43.5	0.7
SS11	32.9	41.7	0.8	SS32	21.7	24.8	0.9
SS12	51.0	62.1	0.8	SS33	73.6	117	0.6
SS13	43.5	37.5	1.2	SS34	53.9	62.9	0.9
SS14	34.1	30.4	1.1	SS35	48.4	69.9	0.7
SS15	39.0	39.7	1.0	SS36	28.1	43.4	0.7
SS16	23.9	14.8	1.6	SS37	37.1	118.2	0.3
SS17	34.8	31.8	1.1	SS38	56.7	46.5	1.2
SS18	42.8	89.3	0.5	SS39	73.2	54.4	1.4
SS19	40.9	40.3	1.0	SS40	68.0	37.1	1.8
SS20	20.5	19.7	1.0	SS41	28.5	22.9	1.2
SS21	23.4	24.7	1.0	SS42	89.1	62.1	1.4
SS22	20.6	21.4	1.0	SS43	31.2	20.1	1.6
SS23	23.5	23.3	1.0	SS44	38.3	41.3	0.9
SS24	20.1	13.2	1.5	SS45	38.7	32.5	1.2
SS25	38.4	59.9	0.6	SS46	47.8	36.7	1.3
SS26	39.8	46.8	0.9	SS47	22.4	18.6	1.2
SS27	31.8	44.7	0.7	SS48	36.2	35.9	1.0

Table C2: Continued

Sample code	^{232}Th by γ-spec	^{232}Th by ICP-MS	Ratio
SS49	56.4	50.1	1.1
SS50	26.1	17.1	1.5
SS51	59.2	37.0	1.6
SS52	45.2	25.5	1.8
SS53	14.1	47.3	0.3
SS54	74.9	50.1	1.5
SS55	56.6	24.9	2.3
SS56	52.9	60.0	0.9
SS57	68.5	71.5	1.0
SS58	54.4	67.1	0.8
SS59	52.4	64.7	0.8
SS60	64.5	18.3	3.5
SS61	48.1	42.9	1.1
SS62	56.2	72.3	0.8
SS63	46.9	50.6	0.9
SS64	44.3	30.6	1.5
SS65	49.9	48.4	1.0
SS66	47.0	59.6	0.8
SS67	40.2	46.8	0.9
SS68	40.9	68.0	0.6
SS69	78.8	25.2	3.1
SS70	75.0	47.3	1.6
SS71	79.6	37.7	2.1
SS72	62.4	64.7	1.0
SS73	46.3	46.6	1.0

Annexure D: Gross α/β activity concentrations in water samples.

Table D1: Gross α/β activity concentrations (Bql^{-1}) and their corresponding committed annual effective dose in water samples from the dam and surrounding communities.

Sample number	Type of water	Activity concentration (Bq.l^{-1})		Committed annual effective dose (mSv/y)	
		Gross α	Gross β	Gross α	Gross β
WS01	Dam	0.12 ± 0.02	0.35 ± 0.05	0.04	0.12
WS02	Dam	0.16 ± 0.02	0.44 ± 0.06	0.05	0.14
WS03	Well	0.24 ± 0.02	0.31 ± 0.05	0.08	0.10
WS04	Borehole	0.17 ± 0.02	0.35 ± 0.07	0.06	0.12
WS05	Borehole	0.06 ± 0.02	0.16 ± 0.06	0.02	0.05
WS06	Borehole	0.23 ± 0.03	0.24 ± 0.06	0.08	0.08
WS07	Borehole	0.27 ± 0.02	0.32 ± 0.05	0.09	0.10
WS08	Dam	0.24 ± 0.02	0.25 ± 0.05	0.08	0.08
WS09	Dam	0.10 ± 0.01	0.26 ± 0.04	0.03	0.09
WS10	Dam	0.17 ± 0.02	0.19 ± 0.07	0.06	0.06
WS11	Dam	0.25 ± 0.02	0.39 ± 0.07	0.08	0.13
WS12	Dam	0.20 ± 0.02	0.35 ± 0.07	0.07	0.12
WS13	Pond	0.19 ± 0.02	0.32 ± 0.06	0.06	0.11
WS14	Well	0.17 ± 0.02	0.35 ± 0.06	0.06	0.12
WS15	Well	0.22 ± 0.02	0.30 ± 0.06	0.07	0.10
WS16	Well	0.17 ± 0.02	0.28 ± 0.07	0.05	0.09
WS17	Well	0.27 ± 0.02	0.42 ± 0.06	0.09	0.14
WS18	River water	0.30 ± 0.02	0.32 ± 0.06	0.10	0.11
WS19	Pond	0.23 ± 0.02	0.40 ± 0.06	0.08	0.13
WS20	River water	0.10 ± 0.02	0.33 ± 0.07	0.03	0.11
WS21	Pond	0.22 ± 0.02	0.34 ± 0.06	0.07	0.11
WS22	Borehole	0.16 ± 0.02	0.43 ± 0.07	0.05	0.14
WS23	Borehole	0.20 ± 0.02	0.39 ± 0.07	0.06	0.13

Table D1: continued

WS24	Surface water	0.23 ± 0.02	0.28 ± 0.06	0.07	0.09
WS25	Borehole	0.26 ± 0.03	0.37 ± 0.06	0.08	0.12
WS26	Dam	0.31 ± 0.02	0.47 ± 0.06	0.10	0.15
WS27	Dam	0.15 ± 0.02	0.46 ± 0.06	0.05	0.15
WS28	Well	0.28 ± 0.02	0.48 ± 0.06	0.09	0.16
WS29	Well	0.11 ± 0.02	0.45 ± 0.06	0.04	0.14
WS30	Borehole	0.12 ± 0.02	0.38 ± 0.06	0.04	0.13
WS31	Borehole	0.12 ± 0.02	0.22 ± 0.06	0.04	0.07
WS32	Borehole	0.19 ± 0.04	0.33 ± 0.07	0.06	0.11
WS33	Borehole	0.33 ± 0.03	0.40 ± 0.06	0.11	0.13
WS34	Borehole	0.33 ± 0.03	0.54 ± 0.06	0.11	0.18
WS35	Borehole	0.34 ± 0.03	0.49 ± 0.06	0.11	0.15
WS36	Borehole	0.33 ± 0.03	0.42 ± 0.06	0.11	0.14
Range		**0.06 ± 0.02 - 0.34 ± 0.03**	**0.16 ± 0.06 – 0.54 ± 0.06**	**0.02 - 0.11**	**0.05 - 0.18**
Weighted Average		**0.21 ± 0.02**	**0.36 ± 0.03**	**0.07**	**0.10**
WHO recommended limit		**0.50**	**1.00**		

Annexure E: Sampling points of the study.

Table E1: The details of sources of soil from the selected 5 different sampling areas.

Sample code	Latitude	Longitude	Sample code	Latitude	Longitude
SS01	-21.673135	27.367006	SS28	-21.81526	27.248463
SS02	-21.769973	27.338492	SS29	-21.803202	27.261977
SS03	-21.781185	27.28316	SS30	-21.92497	27.304939
SS04	-21.879217	27.338602	SS31	-21.925998	27.304759
SS05	-21.905756	27.331044	SS32	-21.921653	27.306643
SS06	-21.919538	27.292518	SS33	-21.920232	27.306871
SS07	-21.856036	27.208388	SS34	-21.918973	27.307152
SS08	-21.860939	27.199292	SS35	-21.918891	27.308016
SS09	-21.873432	27.189761	SS36	-21.918733	27.30891
SS10	-21.809844	27.23632	SS37	-21.918573	27.309948
SS11	-21.863991	27.291873	SS38	-21.974726	27.296998
SS12	-21.924329	27.305764	SS39	-21.829271	27.479462
SS13	-21.673468	27.368295	SS40	-21.82524	27.483116
SS14	-21.769952	27.335715	SS41	-21.887942	27.465535
SS15	-21.779029	27.329497	SS42	-21.943812	27.466202
SS16	-21.770664	27.300265	SS43	-21.832978	27.480978
SS17	-21.919943	27.279227	SS44	-21.82659	27.486995
SS18	-21.911605	27.261232	SS45	-21.825394	27.487106
SS19	-21.895373	27.238067	SS46	-21.826435	27.485243
SS20	-21.879992	27.216101	SS47	-21.824704	27.483541
SS21	-21.860378	27.199634	SS48	-21.829363	27.479592
SS22	-21.860618	27.200199	SS49	-21.825208	27.483008
SS23	-21.860695	27.20093	SS50	-21.824566	27.482355
SS24	-21.87641	27.191241	SS51	-21.824101	27.481681
SS25	-21.849166	27.206406	SS52	-21.823616	27.480752
SS26	-21.842032	27.217397	SS53	-21.836466	27.474355
SS27	-21.827626	27.2279	SS54	-21.886261	27.465636

Table E1: Continued

Sample code	Latitude	Longitude	Sample code	Latitude	Longitude
SS55	-21.897787	27.462177	SS65	-21.863261	27.4143366
SS56	-21.820716	27.4773	SS66	-21.862503	27.412314
SS57	-21.820363	27.476291	SS67	-21.872451	27.387301
SS58	-21.819845	27.475301	SS68	-21.871890	27.386039
SS59	-21.832136	27.449692	SS69	-21.871543	27.385282
SS60	-21.832093	27.448541	SS70	-21.831721	27.663317
SS61	-21.832846	27.447433	SS71	-21.83198	27.662633
SS62	-21.833461	27.446385	SS72	-21.843643	27.649049
SS63	-21.861884	27.415618	SS73	-21.851342	27.654562
SS64	-21.863096	27.414922			

Table E2: The details of sources of sediments samples. (Sediments are coded SED)

Sample code	Latitude	Longitude
SED01	-21.840144	27.672666
SED02	-21.839326	27.671728
SED03	-21.838177	27.672657
SED04	-21.834015	27.671592
SED05	-21.834622	27.671699
SED06	-21.833644	27.670694
SED07	-21.832074	27.663723
SED08	-21.831919	27.664314
SED9	-21.831679	27.663300
SED10	-21.835937	27.672514
SED11	-21.835160	27.672184
SED12	-21.834477	27.671925
SED13	-21.834216	27.672291
SED14	-21.833915	27.672890
SED15	-21.834466	27.673252
SED16	-21.834894	27.673985
SED17	-21.835344	27.673155

Table E3: Water sampling points

Season	Sample code	Latitude	Longitude	Description of the sampling location
Cool	WS01	-21.846016	27.705563	Letsibogo Dam water (D1)
	WS02	-21.840144	27.672666	Letsibogo Dam water
	WS03	-21.825023	27.483362	Water taken from a Hand dug well in Mosokobale river (W1)
	WS04	-21.782979	27.279923	Borehole near Gojwane village (BH1)
	WS05	-21.850786	27.293424	Borehole at Lerotobole cattle post (BH 2)
	WS06	-21.856036	27.208388	Borehole water at Lerotobole cattle post
	WS07	-21.873432	27.189761	Borehole at Masokobale cattle post (BH 3)
	WS08	-21.846016	27.705563	Letsibogo Dam water
	WS09	-21.840144	27.672666	Letsibogo Dam water
Rainy	WS10	-21.834015	27.671592	Letsibogo Dam water (D1)
	WS11	-21.834015	27.671592	Letsibogo Dam water
	WS12	-21.834015	27.671592	Letsibogo Dam water
	WS13	-21.868498	27.728422	Pond water near Letsibogo dam
	WS14	-21.909736	27.464177	Hand dug well in Mosokobale river
	WS15	-21.826392	27.483739	Hand dug well in Mosokobale river
	WS16	-21.825023	27.483362	Hand dug well in Mosokobale river (W1)
	WS17	-21.826242	27.485422	Hand dug well in Mosokobale river
	WS18	-21.824873	27.483339	Mosokobale River water
	WS19	-21.909728	27.368295	Pond near Damochojenaa village (P1)
	WS20	-21.673468	27.368295	Mosokobale River water
	WS21	-21.770664	27.300265	Pond water, near Sese community
	WS22	-21.782979	27.279923	Borehole near Gojwane village (BH 1)
	WS23	-21.873432	27.189761	Borehole at Masokobale cattle post (BH 3)
	WS24	-21.87641	27.191241	Surface water, at Masokobale cattle post
	WS25	-21.850786	27.293424	Borehole at Lerotobole cattle post (BH 2)

Table E3: Continued

Season	Sample code	Latitude	Longitude	Description of the sampling location
Dry	WS26	-21.846016	27.705563	Letsibogo Dam water (D1)
	WS27	-21.834015	27.671592	Letsibogo Dam water
	WS28	-21.825023	27.483362	Hand dug well in Mosokobale river (W1)
	WS29	-21.861943	27.415542	Hand dug well in Mosokobale river
	WS30	-21.870899	27.385367	Borehole at Damochojenaa cattle post
	WS31	-21.782979	27.279923	Borehole near Gojwane village (BH1)
	WS32	-21.770302	27.315738	Borehole water near Gojwane village
	WS33	-21.763311	27.32853	Borehole water near Gojwane village
	WS34	-21.873432	27.189761	Borehole at Masokobale cattle post (BH 3)
	WS35	-21.876066	27.19113	Borehole water at Masokobale cattle post
	WS36	-21.850786	27.293424	Borehole at Lerotobole cattle post (BH2)

Note: D1, P1, W1 and BH 1, 2 and 3 represent dam, pond, well and different boreholes respectively. The denoted samples were used for the assessment of seasonal variation.

Table E4: Dust sampling points

Sample code	Latitude	Longitude	Location
D01	-21.882868	27.762741	Mmadinare
D02	-21.898029	27.461018	Damochojenaa
D03	-21.770599	27.338831	Sese
D04	-21.782979	27.279923	Gojwane
D05	-21.920906	27.297472	Serule

Annexure F: Equations used for calculating weighted average and error propagation (Bevington & Robinson, 2003)

Weighted average

The following rules apply when ($a \pm \sigma a$), ($b \pm \sigma b$) and ($c \pm \sigma c$) functions are given, then the weighted average (W_{ave}) is given by;

$$W_{ave} = \frac{\frac{a}{\sigma a^2}+\frac{b}{\sigma b^2}+\frac{c}{\sigma c^2}}{\frac{1}{\sigma a^2}+\frac{1}{\sigma b^2}+\frac{1}{\sigma c^2}},$$

and the corresponding standard error or uncertainty of the weighted average is given by;

$$\sigma W_{ave} = \frac{1}{\sqrt{\frac{1}{\sigma a^2}+\frac{1}{\sigma b^2}+\frac{1}{\sigma c^2}}}$$

Error propagation

The simplified equations used for propagation of errors are presented in the table below;

Manipulation	Function	Uncertainty
Addition or Subtraction	$y = a_1x_1 + a_2x_2$ or $y = a_1x_1 - a_2x_2$	$s_y = \sqrt{a_1^2 s_{x_1}^2 + a_2^2 s_{x_2}^2}$
Multiplication or Division	$y = a_1x_1x_2$ or $y = a_1\left(\frac{x_1}{x_2}\right)$	$\frac{s_y}{y} = \sqrt{\left(\frac{s_{x_1}}{x_1}\right)^2 + \left(\frac{s_{x_2}}{x_2}\right)^2}$
Power of *x*	$y = x^m$	$\frac{s_y}{y} = \frac{ms_x}{x}$
Power of *e*	$y = e^{-ax}$	$\frac{s_y}{y} = as_x$

Note: a, a_1, a_2 and m represent constants, x, x_1 and x_2 are functions of a, a_1 and a_2 (independent variables) and y is the dependent variable. s_i is the estimated standard deviation in variable x_i.

Annexure G: Decay details of ^{235}U, ^{238}U and ^{232}Th decay series.

Table G1: Decay details of ^{235}U decay series (Erdi-Krausz, et al., 2003; Martin, 2013).

Nuclides	Half-life	Major energies (MeV) and their associated intensities (%)		
		α	β	γ
^{235}U	7.04×10^{8} y	4.37 (17%)	–	0.143 (11%)
		4.4 (55%)		0.186 (57%)
		4.6 (5%)		0.205 (5%)
↓				
^{231}Th	25.5 h	–	0.08 (37%)	0.026 (14.5%)
				0.084 (6.6%)
↓				
^{231}Pa	3.28×10^{4} y	5.03 (20%)	–	0.027 (10%)
		5.01 (25.4%)		0.3 (2.5%)
		4.95 (22.8%)		
↓				
^{227}Ac	21.8 y	4.95 (0.66%)	–	0.16 (0.006%)
		4.94 (0.55%)		
		4.87 (0.09%)		
98.8% ↓ 1.2%				
^{227}Th		5.76 (20.4%)	–	0.050 (8%)
	18.7 d	6.04 (24.2%)		0.235 (12%)
		5.98 (23.5%)		0.256 (7%)
	^{223}Fr 21.8 m	–	0.35 (96%)	0.050 (36%)
				0.080 (9.1%)
				0.235 (3%)
↓				
^{223}Ra	11.4 d	5.61 (25.7%)	–	0.154 (5.6%)
		5.72 (52.6%)		0.269 (13%)
		5.54 (9.2%)		0.324 (3.9%)
↓				
^{219}Rn	3.96 s	6.43 (7%)	–	0.271 (10.8%)
		6.55 (12.9%)		0.401 (6.4%)
		6.82 (79.4%)		
↓				
^{215}Po	1.83 ms	7.38 (100%)	–	–
↓				
^{211}Pb	36.1 m	–	0.45 (100%)	0.404 (3.7%)
				0.832 (3.5%)
↓				
^{211}Bi	2.14 m	6.28 (16.2%)	0.18 (0.28%)	0.351 (12.9%)
		6.62 (83.5%)		
0.32% ↓ 98.68%				
^{211}Po	0.52 s	7.45 (98.9%)	–	0.90 (1.65%)
				0.897 (0.56%)
	^{207}Tl 4.77 m	–	0.5 (100%)	0.897 (0.26%)
↓				
^{207}Pb	Stable	–	–	–

– No relevant data

Table G2: Decay details of ^{238}U decay series (Erdi-Krausz, et al., 2003; Martin, 2013).

Nuclides	Half-life	Major energies (MeV) and their associated intensities (%)		
		α	β	γ
^{238}U	4.47×10^9 y	4.15 (21%) 4.2 (79%)	–	–
↓				
^{234}Th	24.1 d	–	0.04 (100%)	0.092 (2.8%) 0.063 (4.8%)
↓				
^{234}Pa	1.17 m	–	0.82 (98%)	1.0 (0.84%) 0.77 (0.29%)
↓				
^{234}U	2.46×105 y	4.72 (28%) 4.77 (71%)	–	0.053 (0.12%)
↓				
^{230}Th	7.54×104 y	4.62 (23%) 4.69 (76%)	–	0.068 (0.38%) 0.144 (0.05%)
↓				
^{226}Ra	1600 y	4.60 (5.5%) 4.78 (94.5%)	–	0.186 (3.6%)
↓				
^{222}Rn	3.82 d	5.49 (~100%)	–	–
↓				
^{218}Po	3.11 m	6.00 (100%)	–	–
99.98% ↓ 0.02%				
^{214}Pb	26.8 m	–	0.21 (49%)	0.295 (19%) 0.352 (37.6%)
	^{218}At 1.6 s	6.65 (6%) 6.69 (89.9%)	–	–
↓				
^{214}Bi	19.9 m	5.45(1%)	0.64(99%)	0.609 (46%) 1.120 (15.1%) 1.764 (15.4%)
99.96% ↓ 0.04%				
^{214}Po	164 μs	7.69 (100%)	–	0.799 (0.01%)
	^{210}Tl 1.3 m	–	1.18 (100%)	0.296 (79%) 0.799 (99%) 1.32 (21%)
↓				
^{210}Pb	22.3 y	3.72 (0%)	0.004 (84%) 0.016 (16%)	0.047 (4.3%)
↓				
^{210}Bi	5.01 d	–	0.39 (100%)	0.266 (50%) 0.305 (28%)
-100% ↓~.00001%				
^{210}Po	138.3 d	5.30 (100%)	–	–
	^{206}Tl 4.19 m	–	0.54 (100%)	0.453 (93%)
↓				
^{206}Pb	Stable	–	–	–

– No relevant data

Table G3: Decay details of ^{232}Th decay series (Erdi-Krausz, et al., 2003; Martin, 2013).

Nuclides	Half-life	Major energies (MeV) and their associated intensities (%)		
		α	β	γ
^{232}Th	1.41×10^{10} y	3.95 (21.7%) 4.01 (78.2%)	–	–
↓				
^{228}Ra	5.75 y	–	0.007 (100%)	–
↓				
^{228}Ac	6.15 h	–	0.38 (93%)	0.911 (25.8%)) 1.59 (3.2%)
↓				
^{228}Th	1.91 y	5.34 (27.2%) 5.42 (72.2%)	–	0.084 (1.2%) 0.216 (0.25%)
↓				
^{224}Ra	3.66 d	5.45 (5.05%) 5.69 (94.9%)	–	0.241 (4.1%)
↓				
^{220}Rn	55.6 s	6.29 (99.9%)	–	0.549 (0.12%)
↓				
^{216}Po	0.145 s	6.78 (100%)	–	–
↓				
^{212}Pb	10.64 h	–	0.1 (100%)	0.239 (43.3%) 0.300 (3.28%)
↓				
^{212}Bi	60.6 m	6.09 (9.75%) 6.05 (25%)	0.77 (64%)	0.727 (6.58%) 0.785 (1.1%) 1.620 (1.49%)
64.0% ↓ 36.0%				
^{212}Po	304 ns	8.78 (100%)	–	0.57 (2%) 2.61 (2.6%)
^{208}Tl	4.1 m	–	0.54 (100%)	0.511 (22.6%) 0.583 (84.5%) 0.860 (12.4%) 2.614 (99.2%)
↓				
^{208}Pb	Stable	–	–	–

– No relevant data

Annexure H: Instruments used to measure environmental samples

H.1 Gamma (γ) spectrometry

Figure D.1 shows the physical layout of the HPGe system setup used in this study. The HPGe system includes a Genie™ 2000 software program, which allows complete data processing and instrument control and a Dewar to cool the detector down to the temperature of liquid nitrogen.

Figure H.1: Physical layout of the HPGe system

H.2 Liquid scintillation counting (LSC)

Figure D.2 shows the physical layout of the LSC system setup. The LSC system includes a software program (Quantulus 1220^{TM}), which allows complete data processing and instrument control. It offers a number of parameter groups or protocols constrained by the hard disk size of the computer and also provides live display of selected spectra.

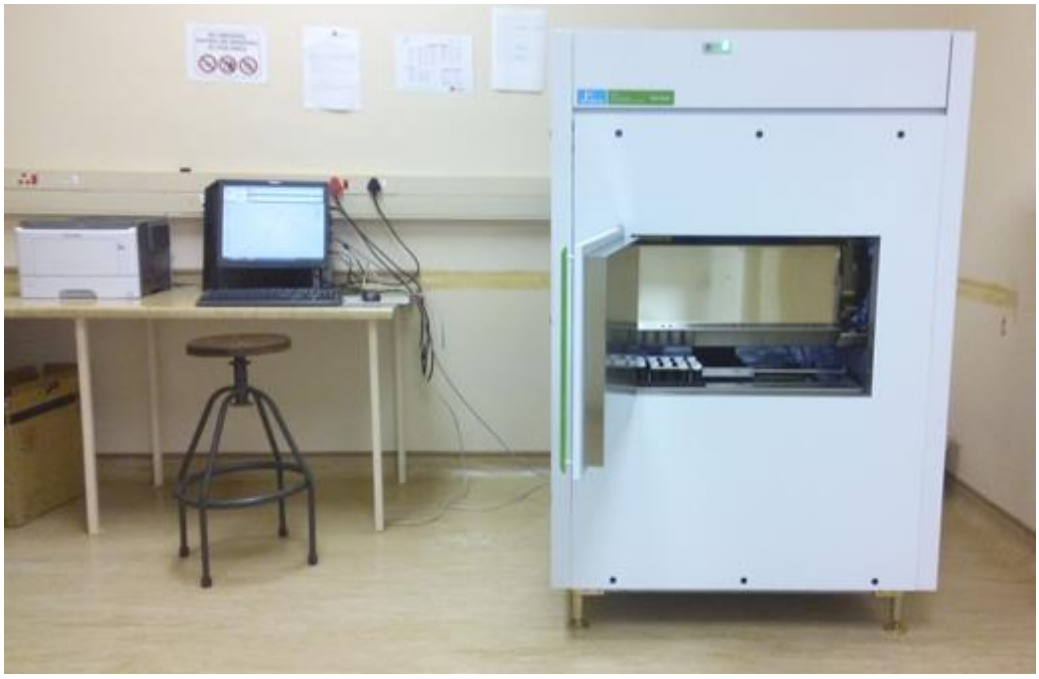

Figure H.2: The Wallac Quantulus 1220™ (PerkinElmer Life and Analytical Sciences) frontal view with open lid, showing the auto sampler trays

H.3 Inductively Coupled Plasma-Mass Spectrometry (ICP-MS)

The physical layout of the ICP-MS system setup, model NexION 300Q, manufactured by PerkinElmer, used in this study is shown in Figure D.3. The ICP-MS system includes a software program (NexION 300Q), which allows complete data processing and instrument control.

Figure H.3: The NexION 300Q Model ICP-MS system setup

Annexure I: List of Presentations & Publications

Oral Presentations

1. **Mashaba, M**., Kotze, D., Tshivhase, V.M., Faanhof, A. (2017). Gross Alpha - Beta Measurements of Water Samples from Wonderfonteinspruit Catchment Area in the Gauteng Province South Africa using LSC. International conference on advances in Liquid Scintillation Spectrometry, (LSC 2017), 1-5 May 2017, Copenhagen, Denmark.
2. **Mashaba, M**., Tshivhase, V.M., Faanhof, A. (2017). Measurement of Gross Alpha & Beta Activities in Environmental Water around a Proposed Uranium Mining Area in the Central District of Botswana. 18th WaterNet/WARFSA/GWPSA Symposium on Integrated Water Resources Development and Management: Innovative Technological Advances for Water Security in Eastern and Southern Africa – 25 to 27 October 2017, Swakopmund, Namibia.

Poster Presentations

1. **Mashaba, M**., Kotze, D., Tshivhase, V.M., Faanhof, A. (2016). Energy Calibration of Liquid Scintillation Counter to allow Semi-Qualitative Nuclide Identification in Water Samples. 14th International Congress of the International Radiation Protection Association (IRPA), Cape town International Convention Centre, South Africa; 9th – 13th May 2016.

Publications

1. **Mashaba, M**., Kotze, D., Tshivhase, V.M., Faanhof, A. (2016). Energy Calibration of Liquid Scintillation Counter to allow Semi-Qualitative Nuclide Identification in Water Samples. (9th – 14th May, 14th International Congress of the International Radiation Protection Association. IRPA 2016). Proceedings of the 14th International Congress of the International Radiation Protection Association http://www.irpa.net/page.asp?id=2

Papers still being reviewed

1. **Mashaba, M.,** Tshivhase, V.M., Dlamini, T., Faanhof, A. Determination of natural radioactivity content in riverbank soil samples along the Sidibe river basin in Central district of Botswana.